University of Alberta

In-situ Testing for Liquefaction Evaluation of Sandy Soils

by

Catherine Elizabeth Fear ©

A thesis submitted to the Faculty of Graduate Studies and Research
in partial fulfillment of the requirements for the degree of
Doctor of Philosophy

in

Geotechnical Engineering

Department of Civil Engineering

Edmonton, Alberta

Spring 1996

ISBN 0-612-10586-5

University of Alberta

Faculty of Graduate Studies and Research

The undersigned certify that they have read, and recommend to the Faculty of Graduate Studies and Research for acceptance, a thesis entitled **In-situ Testing for Liquefaction Evaluation of Sandy Soils** submitted by **Catherine Elizabeth Fear** in partial fulfillment of the requirements for the degree of Doctor of Philosophy in Geotechnical Engineering.

Dr. P.K. Robertson (Supervisor)

Dr. N.R. Morgenstern

Dr. D.C. Sego

Dr. F.E. Hicks

Dr. A.W. Lipsett

Dr. T.L. Youd (External Examiner)

April 11 1996

Date of Approval by Committee

University of Alberta
Edmonton

Canada T6G 2G7

Department of Civil Engineering

220 Civil Electrical Engineering Building
Telephone (403) 492-4235
Fax (403) 492-0249

To: Catherine Fear

From: Gerry Cyre

Date: April 19, 1996

As co-author, I give you my permission to use the following material in your Ph.D. thesis:

Fear, C.E., Cyre, G., Robertson, P.K., and Morgenstern, N.R. 1996. Proceedings of the 49th Canadian Geotechnical Conference, St. John's, Newfoundland, September 23-25.

Gerry Cyre

Gerry Cyre
Specialist Technologist (Geotechnical)

University of Alberta
Edmonton

Canada T6G 2G7

Department of Civil Engineering

220 Civil Electrical Engineering Building
Telephone (403) 492-4235
Fax (403) 492-0249

To: Catherine Fear

From: Dr. N.R. Morgenstern

Date: April 19, 1996

As co-author, I give you my permission to use the following material in your Ph.D. thesis:

Fear, C.E., Cyre, G., Robertson, P.K., and Morgenstern, N.R. 1996. Proceedings of the 49th Canadian Geotechnical Conference, St. John's, Newfoundland, September 23-25.

Dr. N.R. Morgenstern
University Professor

University of Alberta
Edmonton

Canada T6G 2G7

Department of Civil Engineering

220 Civil Electrical Engineering Building
Telephone (403) 492 4235
Fax (403) 492 0249

To: Catherine Fear

From: Dr. P.K. Robertson
(Thesis Supervisor)

Date: April 19, 1996

As co-author and Principal Investigator of the Canadian Liquefaction Experiment (CANLEX) Project, I give you my permission to use the following papers or CANLEX reports in your Ph.D. thesis:

Robertson, P.K. and Fear, C.E. 1995. Liquefaction of sands and its evaluation, Proceedings of IS Tokyo '95, First International Conference on Earthquake Geotechnical Engineering, Keynote Lecture.

Robertson, P.K. and Fear, C.E. 1995. Application of CPT to evaluate liquefaction potential, Proceedings of the International Symposium on Cone Penetration Testing, CPT'95, Linkoping, Sweden.

Robertson, P.K. and Fear, C.E. 1996. Soil liquefaction and its evaluation based on SPT and CPT, Proceedings of the 1996 NCEER Workshop on Liquefaction.

Fear, C.E., Robertson, P.K., Hofmann, B.A., Sego, D.C., Campanella, R.G., Byrne, P.M., Davies, M.P., Konrad, J.-M., Küpper, A., List, B.R., and Youd, L. 1995. Summary of CANLEX Phase I Site Characterization, Proc. of the 48th Canadian Geotechnical Conference, Vancouver, B.C., 331-340.

Fear, C.E. and Robertson, P.K. 1995. Estimating the undrained strength of sand: a theoretical framework. Canadian Geotechnical Journal, 32(5): 859-870.

Fear, C.E., Cyre, G., Robertson, P.K., and Morgenstern, N.R. 1996. Proceedings of the 49th Canadian Geotechnical Conference, St. John's, Newfoundland, September 23-25.

Fear, C.E. and Robertson, P.K. 1996. CANLEX Phase II data review report.

PK Robertson

Dr. P.K. Robertson
Professor and CANLEX Principal Investigator

AGRA Earth & Environmental Limited

FACSIMILE TRANSMITTAL

4810 - 93 Street
EDMONTON, ALBERTA T6E 5M4
Phone No. (403) 436-2152
Fax No. (403) 435-8425

TO: Dr. C. Fear

COMPANY: U. Of A. - Dept. Of Civil Eng.

FAX NO.: 492-8198

SENDER: Dr. E. McRoberts, Ph.D.,P.Eng. **FILE NO.:** 2210

NO. OF PAGES (INCLUDING THIS PAGE): 1 **DATE:** April 15, 1996

ORIGINAL TO BE SENT BY MAIL: YES NO x

RE: ASCE "A RECONSIDERATION OF THE INITIATION OF LIQUEFACTION IN SANDY SOILS" VOL. 121, ISSUE 3, PAGES 249-261; BY CATHERINE E. FEAR AND EDWARD C. McROBERTS

As co-author I give my permission to use this material in your thesis.

E.C. McRoberts, Ph.D., P. Eng.
Senior Vice President
Chief Technical Officer

University of Alberta

Library Release Form

Name of Author: Catherine Elizabeth Fear

Title of Thesis: In-situ Testing for Liquefaction Evaluation of Sandy Soils

Degree: Doctor of Philosophy

Year this Degree Granted: 1996

Catherine Fear.

20 Haddington Avenue
Toronto, Ontario
Canada, M5M 2N7

April 19, 1996

Date submitted to the Faculty of
Graduate Studies and Research

Dedicated to my mom,
Elizabeth Carlisle Fear,
for all her love and encouragement.

ABSTRACT

Liquefaction of sandy soils can have significant financial, environmental and human impacts, with observable ground surface features ranging from sand boils to catastrophic flow failures, depending on the type and extent of liquefaction that occurs. Liquefaction phenomena have been divided into two main types: cyclic softening and flow liquefaction. Cyclic softening (liquefaction) generally occurs in level to gently sloping ground in which shear stress reversal can occur, but may also occur in and around soil structures and buildings. Deformations associated with cyclic softening occur only during cyclic loading and accumulate with additional cycles of loading as a consequence of a loss in soil stiffness. Flow liquefaction occurs only in strain-softening soil, provided that a trigger mechanism (static or cyclic) causes the soil to strain-soften. Flow liquefaction generally occurs in sloping ground in which the driving stresses are larger than the resulting undrained shear strength of the soil. Deformations can be catastrophic if the soil structure contains sufficient strain-softening material and if the geometry is such that a kinematically admissible mechanism can develop. In-situ testing can provide a useful tool for evaluating liquefaction potential and any consequences. Conventional standard penetration test (SPT) based methods and cone penetration test (CPT) based methods for evaluating liquefaction potential and resulting undrained shear strengths are reviewed. An integrated CPT based method for evaluating cyclic softening (liquefaction) potential is proposed. In addition, a comprehensive framework for evaluating flow liquefaction potential, linking in-situ testing to undrained laboratory response is developed. Other methods for estimating the undrained strength of sand susceptible to flow liquefaction are investigated, including critical state soil mechanics concepts applied to in-situ testing results and an experimental program of rapid downhole plate load tests in loose sand. Finally, a family of solutions is recommended for evaluating either cyclic softening (liquefaction) or flow liquefaction potential in sandy soils from in-situ testing, based on the level of risk associated with a particular project.

ACKNOWLEDGEMENTS

To my supervisor, Dr. Peter K. Robertson, thank-you for your expert guid countless hours discussing various new ideas. Your never-ending enthusiasm pr with a constant source of motivation. The opportunities you provided me wit being an active participant in the CANLEX project, co-authoring various paper and presenting papers at conferences, have all benefitted me greatly. I could h picked a better supervisor!

To Dr. Ed McRoberts, Chief Technical Officer of AGRA Earth and Environm Edmonton, it was a privilege to be able to work with you and learn so mu practitioner's point of view. Your initial ideas for research projects (see Chapter and the great amounts of your own time that you spent working with me appreciated. You helped teach me to have a questioning mind and think a concepts to greater depths.

To other staff members in the Department of Civil Engineering, particularly Dr. Morgenstern and Dr. Dave C. Sego (both in the Geotechnical Group), thank-yo valuable input and review of my work as it progressed. To Gerry Cyre, Technologist (Geotechnical), thank-you for your ingenuity and inventiveness w to field testing and particularly for your assistance with Chapter 6. To Prof. Pe Dr. Sieman AbouRizk and Dr. A.E. Elwi, thank-you for recruiting me to the Un Alberta in the first place!

I gratefully appreciate the funding that I received from various organizations thro time at the University of Alberta, as follows: a 1967 Science and Engineering S (1991-1995) from the Natural Sciences and Engineering Research Council (NSERC), a Ralph Steinhauer Award of Distinction (1992-1994) from the Albert Fund, and a Karl A. Clark Memorial Scholarship (1995-1996) from the Albert Council. I am also grateful to the University of Alberta for providing me with a Johns Graduate Fellowship (1991-1995) and a J. Gordin Kaplan Graduate Stud (1994). In addition, in 1993, I was honoured to receive a Leonard E. Gads Assistant Award from the Faculty of Engineering and a Graduate Student Teach from University Teaching Services.

TABLE OF CONTENTS

Page

CHAPTER 2: REASSESSMENT OF CURRENT PRACTICE USED FOR EVALUATING CYCLIC LIQUEFACTION POTENTIAL BASED ON THE STANDARD PENETRATION TEST (SPT)

CHAPTER 5: A FRAMEWORK FOR ESTIMATING UNDRAINED SHEAR STRENGTH BASED ON IN-SITU TESTING

CHAPTER 6: EMPIRICAL ESTIMATION OF UNDRAINED SHEAR STRENGTH BASED ON DOWNHOLE PLATE LOAD TESTS

CHAPTER 7: A RECONSIDERATION OF CASE HISTORIES USED TO EMPIRICALLY ESTIMATE UNDRAINED SHEAR STRENGTH

CHAPTER 8: WORKED EXAMPLE

CHAPTER 9: GENERAL DISCUSSION AND CONCLUSIONS

LIST OF TABLES

CHAPTER 8

LIST OF FIGURES

CHAPTER 3

CHAPTER 4

task. There are many variable factors which serve to complicate the process. No matter how the study is performed or how consistent one tries to be in assigning a single valued combination of $(N_1)_{60}$ and CSR to a case record, one must always exercise a certain amount of judgement. It is clear that the original Berkeley interpretations involved judgement and were directed toward a conservative assessment of the database. In addition, $(N_1)_{60}$ and CSR are not the only factors affecting the potential for liquefaction at a particular site. Other factors such as fines content, gravel content, cementation, age, fabric, thickness of the liquefied layer, thickness or nature of any overlying non-liquefied layer, impeded seepage and topography may affect both the potential for liquefaction and the extent of the effects once liquefaction has been triggered. These factors and others likely add uncertainty to the database and may account for the transition zones that have been observed in this study. However, based on the available data, it was difficult to further distinguish between the data on the basis of any of these factors, except for fines content and possible impeded seepage. While an effect of fines content was found, the study does not support the broader range reported in the original work. Some trends have been suggested regarding the effects of impeded drainage; however, further investigation and research is needed to determine specific effects on liquefaction potential. The application of statistical techniques to the revised database using the methods and procedures followed by Liao (1986) would constitute a logical extension of this study.

Table 2-1: Composition of 125 case records in the original Berkeley catalogue

	Number of Case Records
A. Classification of the Original 125 Case Records	
(i) Berkeley catalogue	
Liquefied	67
Marginal Liquefaction	7
Non-liquefied	51
(ii) This study	
Liquefied	56
Pressure relief/marginal liquefaction	15
Non-liquefied	52
Liquefied or non-liquefied depending on location at the site	2
B. Case Records repeated twice in the Database (each pair of points reflects one site investigation, but two different earthquakes, usually one which did not cause liquefaction and a larger one which did)	21
C. Availability of Reference Papers	
Original reference papers were located	112
Related papers found when original reference was not found	12
No reference paper found	1
D. Site conditions	
Level ground	49
On or near sloping ground (dyke, dam, slope, river embankment, lakeside or riverside)	25
Under or near a structure (e.g. bridge, building)	22
Site conditions unknown	29
E. Re-evaluation of case records	
(i) No re-evaluation could be made	31
Original reference paper did not contain a BH log	18
Original reference paper was not found; any alternates that were found did not contain BH logs	13
(ii) A re-evaluation was made	94
Same $(N_1)_{60}$ selected as in the Berkeley catalogue	36
Lower $(N_1)_{60}$ selected than in the Berkeley catalogue	58

Table 2-2: Summary of changes in $(N_1)_{60}$ for critical liquefied case records in the original Berkeley study

	Case Record				Original Data					New Data					
	No.	Name	Earthquake	Reference	Liquefied?	$(N_1)_{60}$	Depth (m)	CSR	FC (%)	Liquefied?	$(N_1)_{60}$	Depth (m)	CSR	FC (%)	Comments
Case Records Originally in Clean Sands	1	Ogaki	1891 Mino-Owari	Kishida (1969)	yes	25.5	10.05	0.375	0	pressure relief pressure relief	6.7 10.7	5.00 17.00	0.371 0.362	0 8	• sand boils only • investigated in late sixties by Kishida (1969) • area in artesian condition (artesian wells used until 1940) • "not clear whether the eruptions of water resulted from a liquefied condition or from the artesian conditions" (Kishida, 1969) • located in what appears to be the same geological environment as case records 3 and 4
	3	Unuma	1891 Mino-Owari	Kishida (1969)	yes	25.0	6.10	0.330	3	pressure relief	20.0	9.35	0.339	4	• sand boils and some cracking • investigated in late sixties by Kishida (1969) • site investigation missed a pumice layer at shallow depth which may or may not be significant since a white mixture of sand and water was observed erupting from the ground • gravel contents greater than 20% • similar concerns re: artesian conditions as for case record 1
	4	Ogase	1891 Mino-Owari	Kishida (1969)	yes	17.0	5.18	0.290	4	pressure relief pressure relief	15.8 17.5	4.00 5.18	0.264 0.287	10 4	• sand boils and some cracking • investigated in late sixties by Kishida (1969) • gravel contents greater than 20% • similar concerns re: artesian conditions as for case record 1
	7	Arakawa 21	1923 Kanto	Kodera (1964)	yes	20.5	8.23	0.240	1	yes	3.9	8.25	0.237	10	• Pier 21 of the Arakawa Bridge • Piers 7 and 12 (case records 5 and 6) of the bridge which liquefied and Pier 49 which had marginal liquefaction were in the same geological environment and were re-assigned lower values of $(N_1)_{60}$ as well • site conditions may be considered to be other than truly level ground due to bridge piers and bridge loading
	8	Arakawa 30	1923 Kanto	Kodera (1964)	yes	16.5	5.18	0.230	5	yes	11.1	5.00	0.225	5	• Pier 30 of the Arakawa Bridge • same comments apply as for case record 7
	[illegible]	Takaya 45	1948 Fukui	Kishida (1969)	yes	24.0	7.01	0.280	4	yes yes	6.5 16.6	15.00 10.00	0.306 0.293	30 4	
	56	Luan Nan	1976 Tangshan	Shengcong et al. (1983)	yes	22.0	5.36	0.175	3	yes (56-L2) yes (56-L3) yes (56-L6) yes (56-L7) no (56-L1) no (56-L4) no (56-L5)	7.7 13.2 21.4 14.0 12.3 22.0 17.8	5.30 10.30 8.30 8.30 11.30 9.30 4.30	0.252 0.210 0.281 0.255 0.228 0.264 0.171	3 3 3 3 3 3 3	• apparently interpreted in the Berkeley catalogue using a "typical log" from Shengcong et al. (1983) • this study obtained additional logs from the Beijing Municipal Bureau of City Planning (1982), both liquefied and non-liquefied • failure modes not specified in either report
	87	Yuriagekami 2	June 1978 Miyagiken-Oki	Iwasaki et al (1978)	yes	15.0	4.27	0.250	0	yes	5.6	3.50	0.243	0	
Case Records Originally in Silty Sands	55	Qing Yin	1976 Tangshan	Shengcong et al. (1983)	yes	21.5	5.30	0.395	20	yes	6.2	11.75	0.394	clayey sand	• apparently interpreted in the Berkeley catalogue using a "typical log" from Shengcong et al. (1983) • no additional logs were obtained • clayey sand layer could be interbedded sand and clay • failure mode not specified in Shengcong et al. (1983)
	90	Yuriage Bridge 2	June 1978 Miyagiken-Oki	Iwasaki et al (1978)	yes	21.5	3.35	0.225	7	yes	20.1	3.35	0.216	7	• from the Yuriage Bridge (Iwasaki, 1978) • listed in the Berkeley catalogue, but not included in the Seed et al. (1984) plot for sand with fines, possibly because it had a gravel content > 20% • this same site did not liquefy in an smaller earlier EQ (case record 73 - also listed in the Berkeley catalogue, but not included in the plot for sand with fines) • another pier with a lower $(N_1)_{60}$ did not liquefy and lower $(N_1)_{60}$'s were found in other units which did liquefy
	111	River Park C	1979 Imperial Valley	Youd et al (1983)	yes	[illegible]	4.27	0.240	18	yes	10.6	3.50	0.239	18	• soil unit C at the site was said to have liquefied • Berkeley catalogue $(N_1)_{60}$ seems to be based on the average N in soil unit C for boreholes drilled at the site

Table 2-3: Summary of Berkeley case records for which the original assessment was the same as in this study

Response	Number of Case Records	(N1)60		
		Mean	Standard deviation	Range
A. 36 case records for which borehole logs were found				
liquefied	14	7.4	5.1	1.4 to 13.6 (1)
pressure relief	10	5.8	4.3	2.8 to 17.0
non-liquefied	12	10.6	5.7	2.4 to 20.1
B. 31 case records for which borehole logs were not found (2,3)				
liquefied	16	8.3	3.4	1.5 to 14.5
non-liquefied	15	13.0	5.4	8.0 to 26.5

Notes:

(1) Except for case record 90 (see Table 1) which liquefied with an (N1)60 of 20.1.
(2) Case records with no borehole logs in references cited by Seed et al. (1984) = 18.
(3) 10 case records are based on 5 sites, each affected by two earthquakes.

Table 2-4: Classification of drainage conditions for all case records

Case Record	Drainage Condition	Case Record	Drainage Condition	Case Record	Drainage Condition	Case Record	Drainage Condition	Case Record	Drainage Condition
1	3	29	2	56 (L7)	1*	68	2	101	1
1	1*	30	1*	57 (BH1)	3	69	2	102	1
2	1	31	4	57 (BH10)	1	70	2	103	4
2	1	32	2	57 (BH11)	1*	71	2	104	4
3	2	33	1	57 (BH12)	3	72	2	105	1*
4	3	34	1	57 (BH13)	3	73	4	106	1*
4	3	35	1	57 (BH14)	3	74	1	107	1
5	3	36	4	57 (BH15)	3	75	4	108	1
6	1	37	4	57 (BH19)	3	76	4	109	1
7	1	38	4	57 (BH2)	3	77	3	110	1
8	1	39	4	57 (BH21)	3	78	1	111	3
9	1*	40	4	57 (BH22)	3	79	1	112	3
10	4	41	4	57 (BH23)	3	80	1	113	3
11	4	42	4	57 (BH24)	3	81	1	114	1*
12	2	43	4	57 (BH25)	3	82	1	115	1*
13	2	44	3	57 (BH26)	3	83	4	116	3
14	2	45	3	57 (BH4)	3	84	2	117	2
15	1	46	3	57 (BH5)	3	85	2	118	2
15	1	47	3	57 (BH7)	3	86	2	119	1
16	2	48	1	57 (BH8)	3	87	2	120	3
17	1*	49	2	57 (BH9)	3	88	2	121	3
17	1*	50	2	58	3	89	2	122	3
18	2	51	3	59	4	90	4	123	1*
19	3	52	4	60	4	91	1		
20	1	53	4	61	4	92	4		
21	1*	54	3	62	3	93	4		
22	4	55	3	63	3	94	4		
23	4	56 (L1)	3	63	3	95	3		
24	4	56 (L2)	2	64	1*	96	3		
25	4	56 (L3)	3	64	3	97	1		
26	4	56 (L4)	3	65	2	98	1		
27	1	56 (L5)	2	66	3	99	1		
28	3	56 (L6)	1*	67	2	100	1		

Notes:
1 = open drainage = perm. above ≥ perm. of layer of interest (e.g. gravel over sand)
1* = indicates that open drainage exists for some thickness above the layer of interest, although there is a less permeable layer well above the layer of interest
2 = shut drainage A = perm. above slightly less than in layer of interest (e.g. silt over sand)
3 = shut drainage B = perm. above much less than in layer of interest (e.g. clay over sand)
4 = drainage conditions unknown

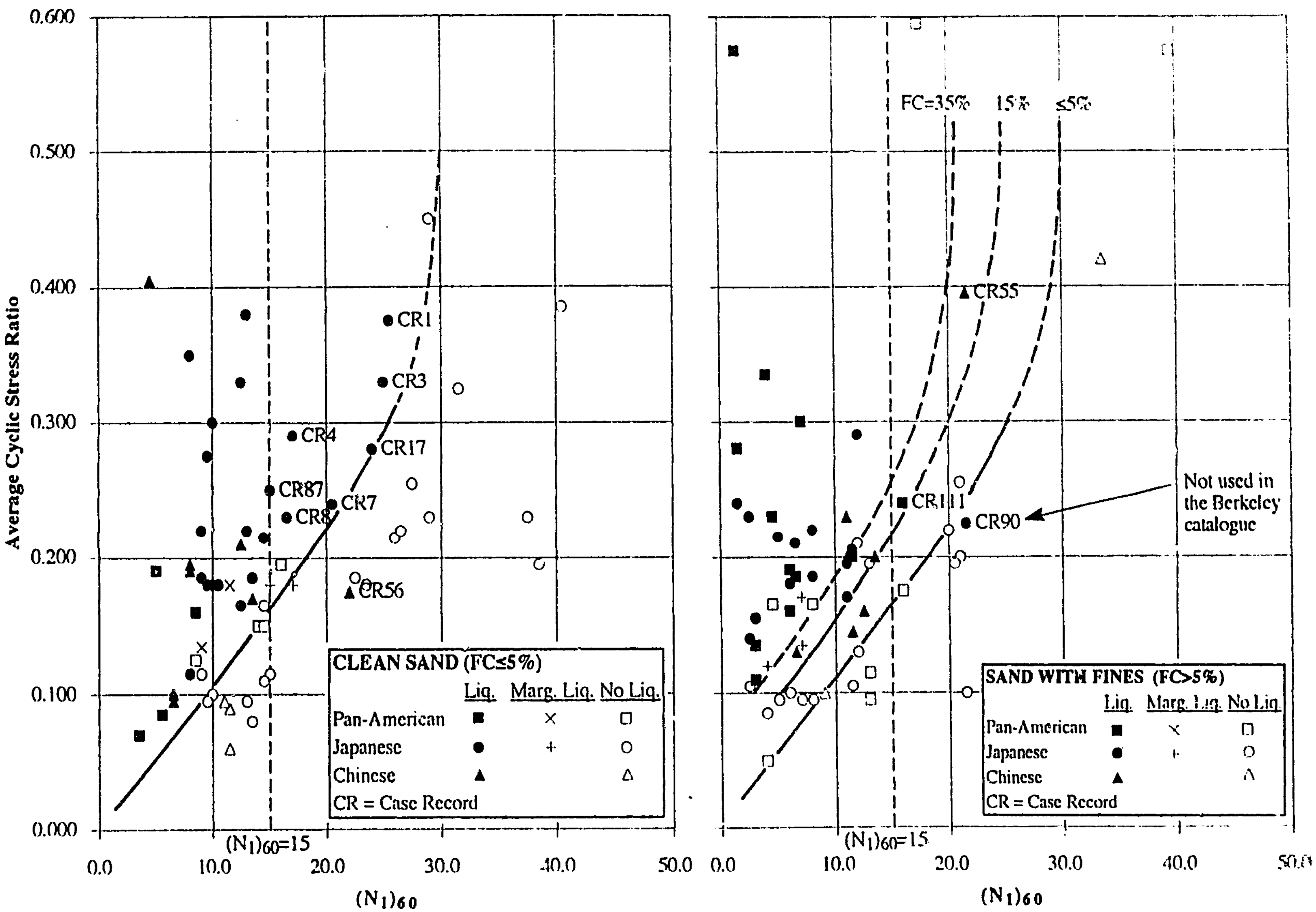

Figure 2-1 Plots of CSR versus $(N_1)_{60}$ in original Berkeley catalogue.

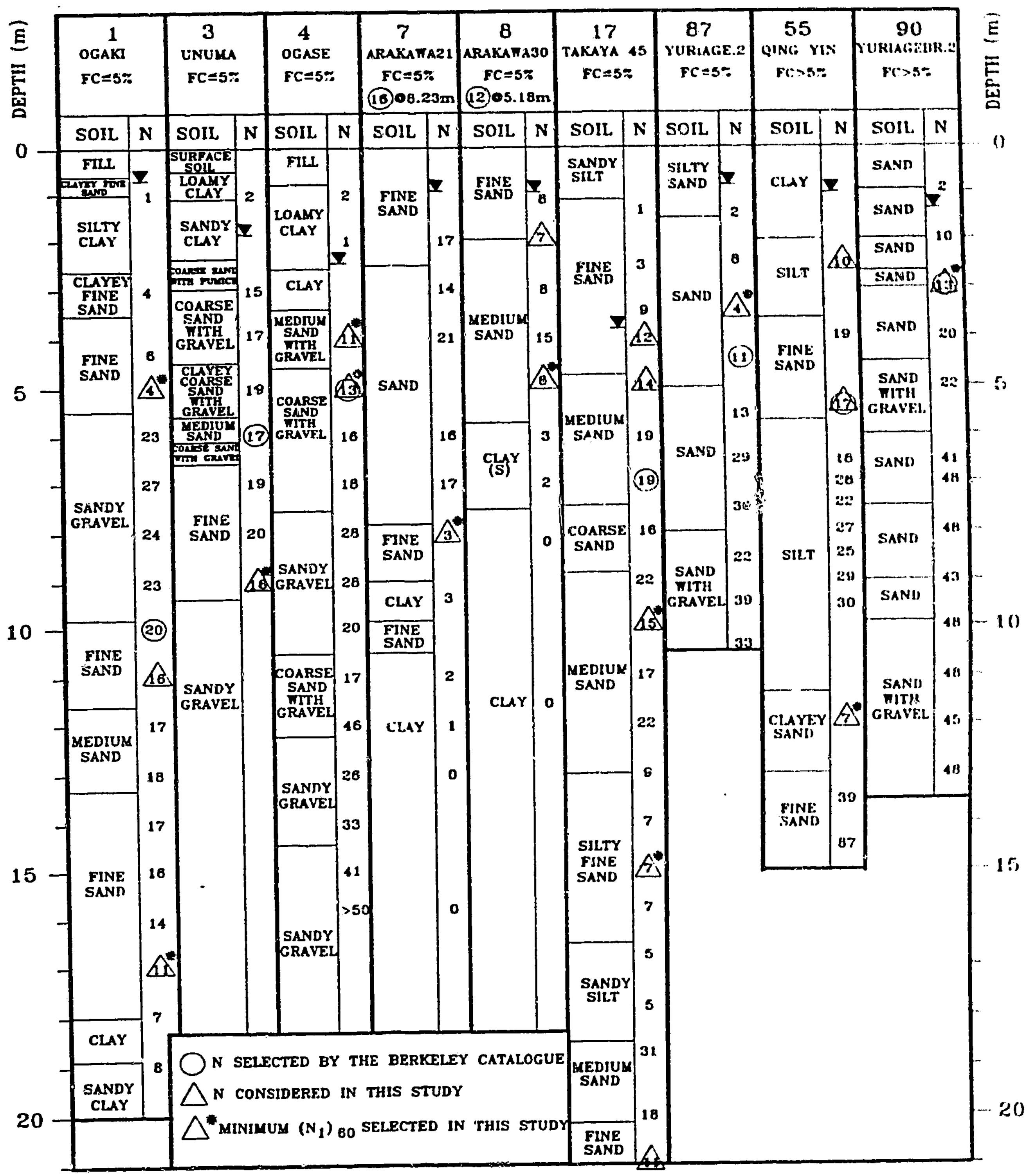

Figure 2-2 Summary strip logs for all critical liquefied case records except Luan Nan (case record 56).

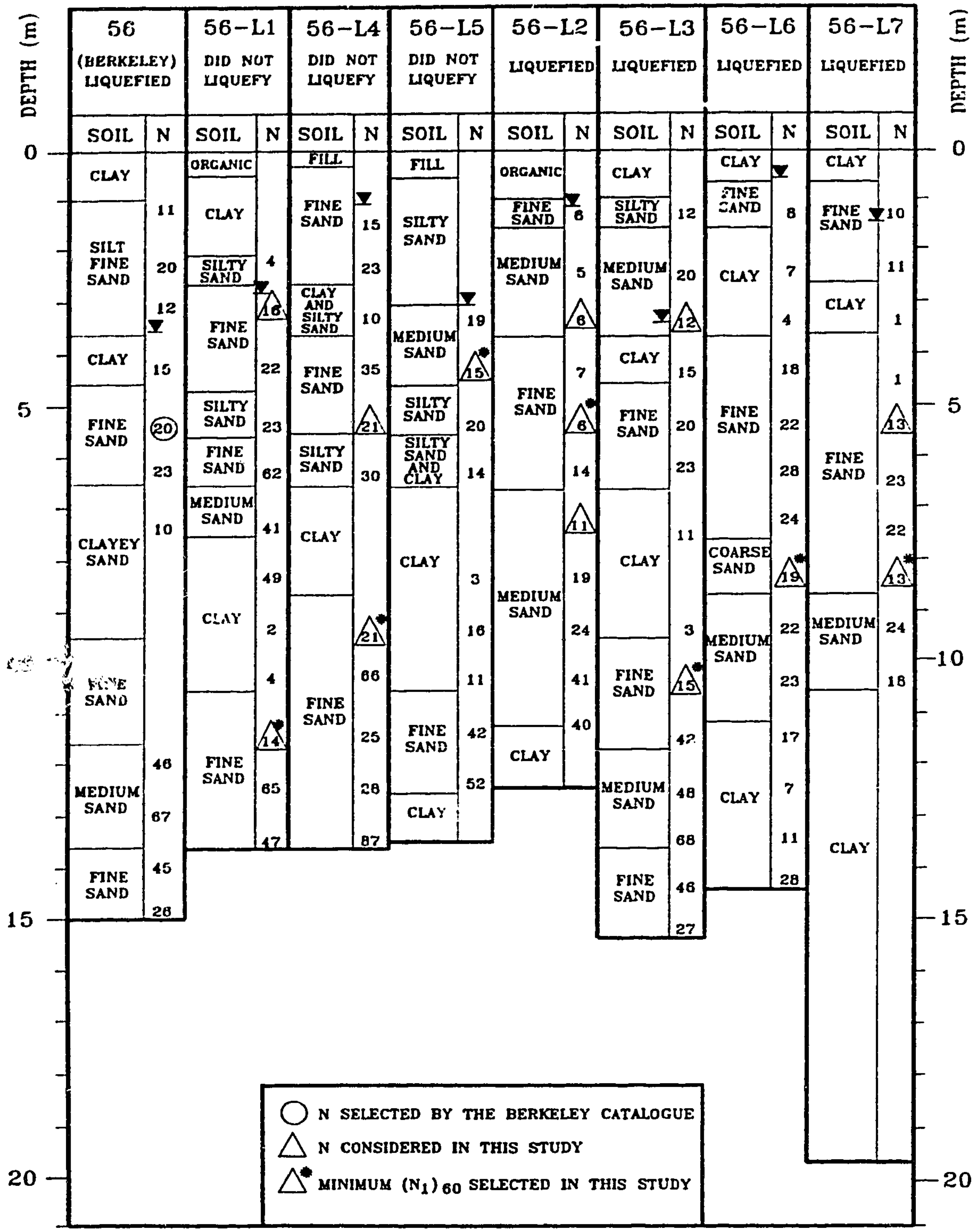

Figure 2-3 Comparison of original summary strip log for Luan Nan (case record 56) with additional logs obtained in this study.

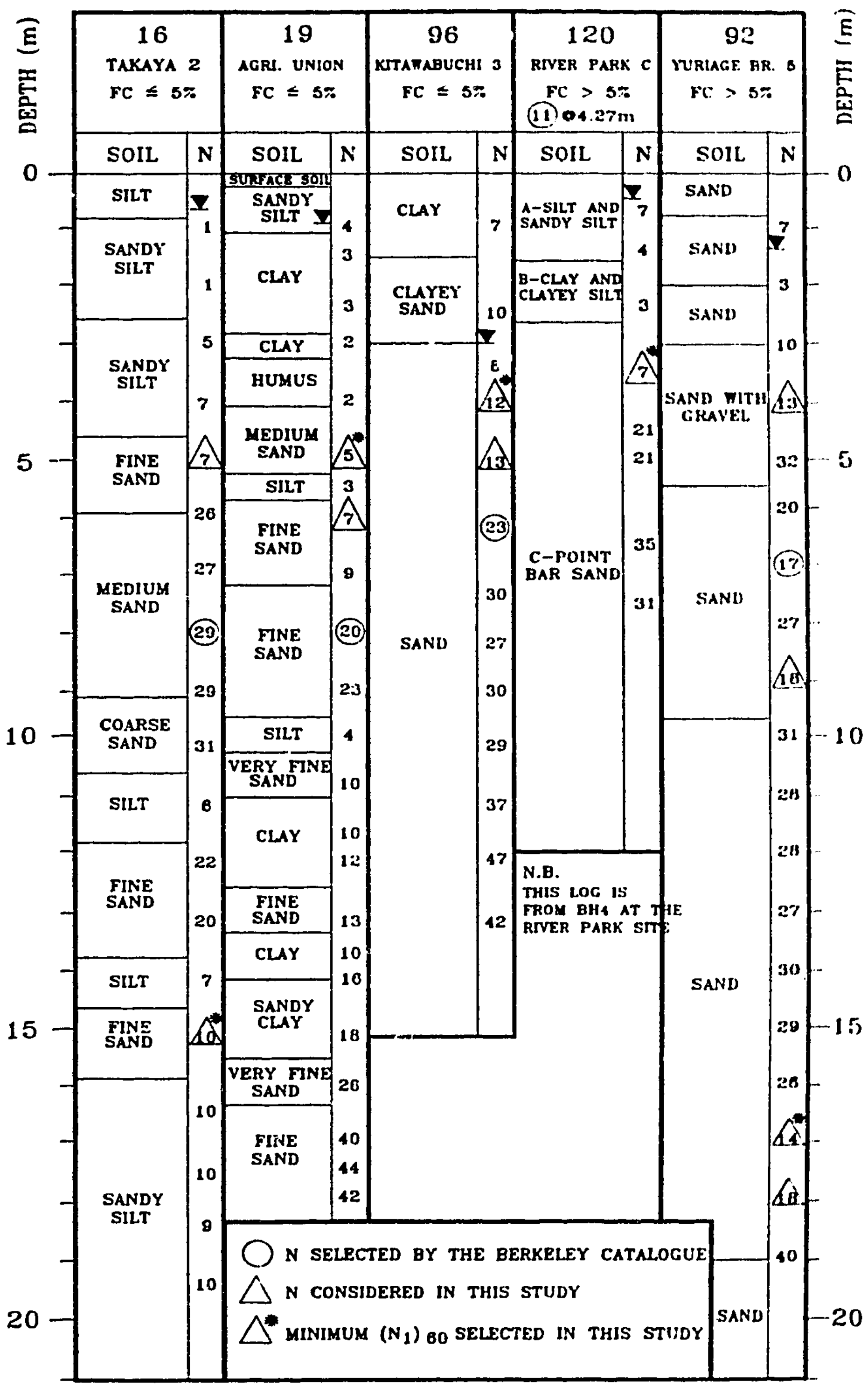

Figure 2-4 Summary strip logs for five sample nonliquefied case records.

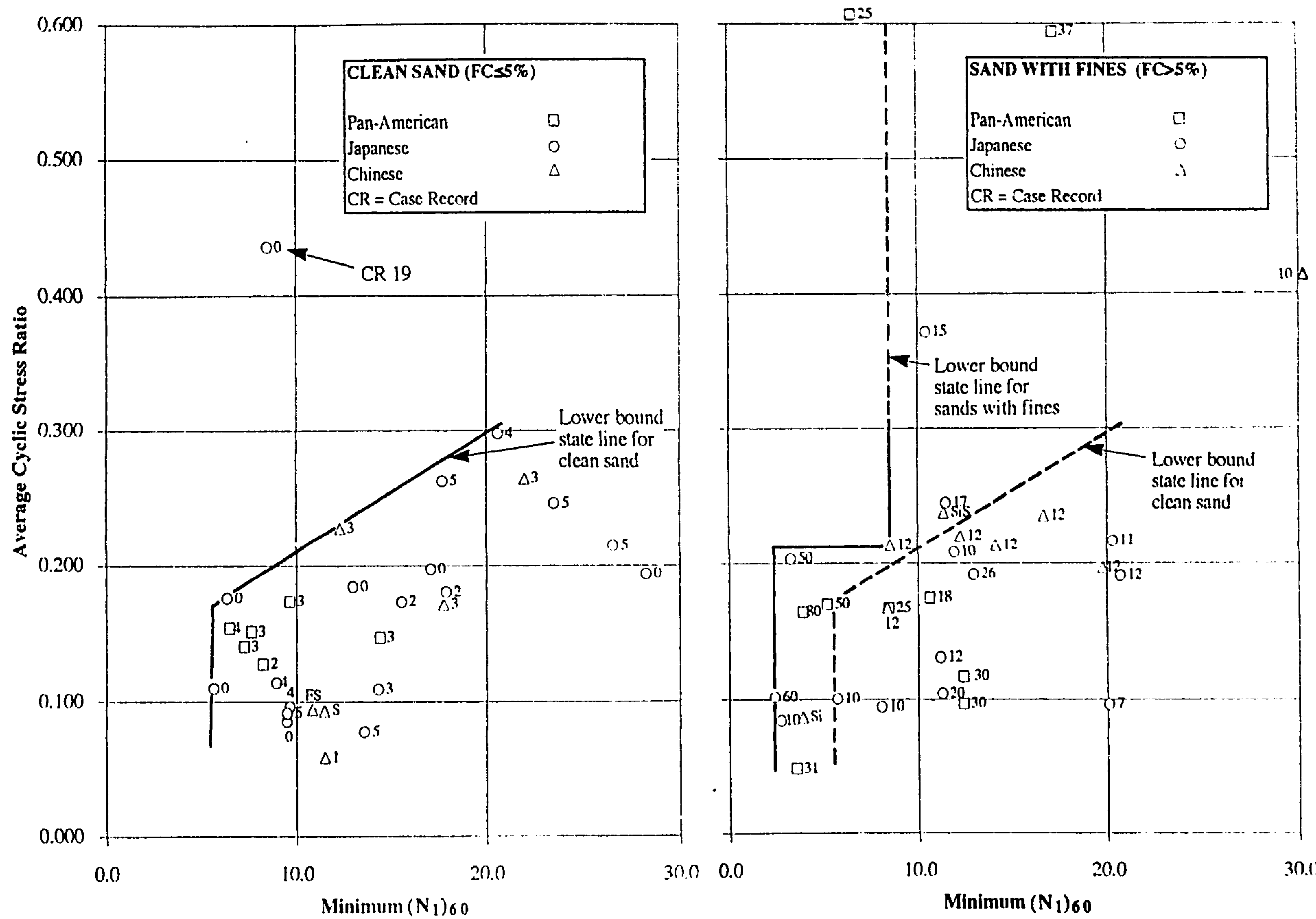

Figure 2-5 Plot of CSR versus $(N_1)_{60}$ from this study for nonliquefied case records.

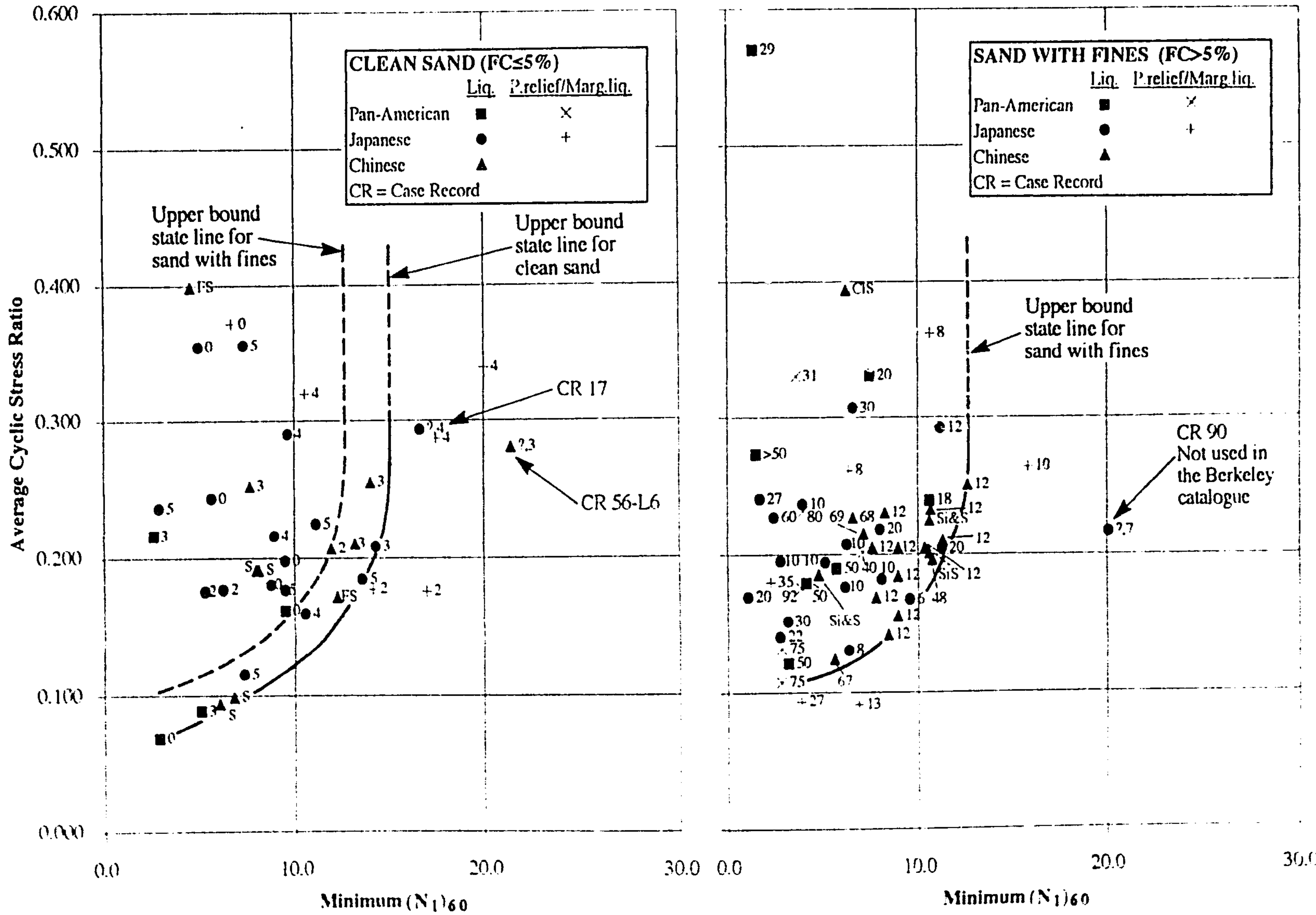

Figure 2-6 Plot of CSR versus $(N_1)_{60}$ from this study for liquefied and pressure relief case records.

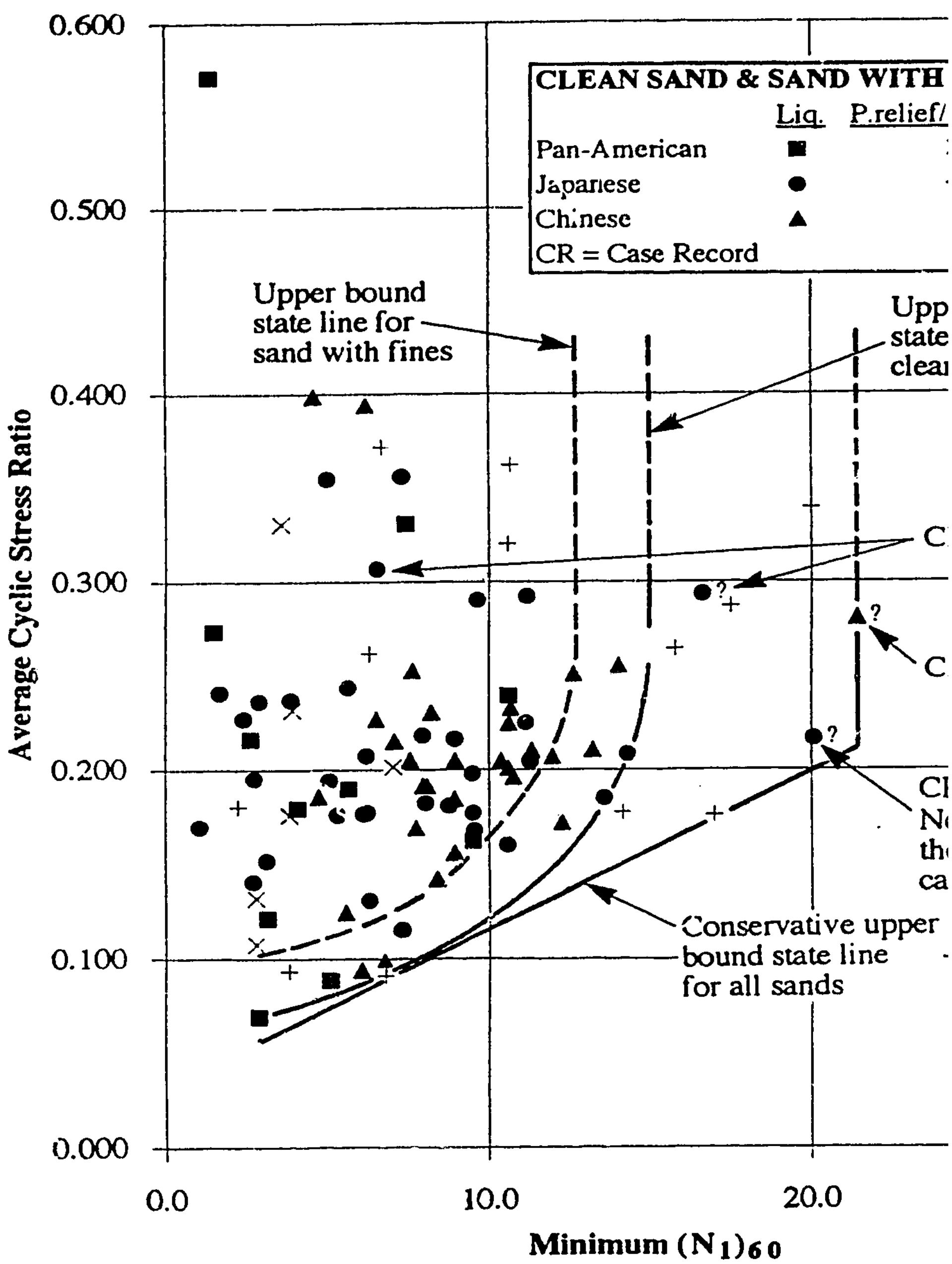

Figure 2-7 Plot of all liquefied and pressure relief case records showing upper bound state lines.

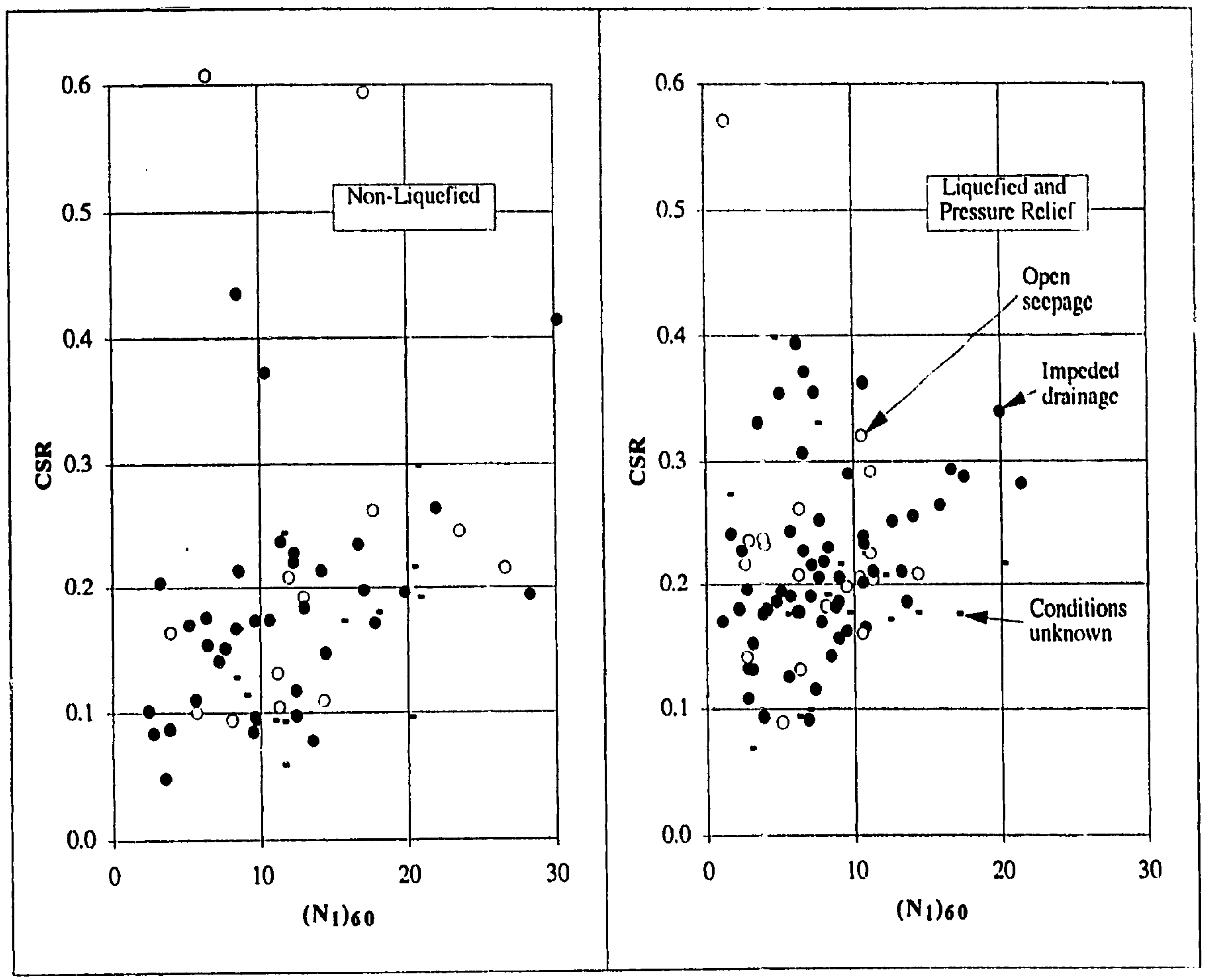

Figure 2-9 Plots of CSR versus $(N_1)_{60}$ to investigate effects of site drainage conditions.

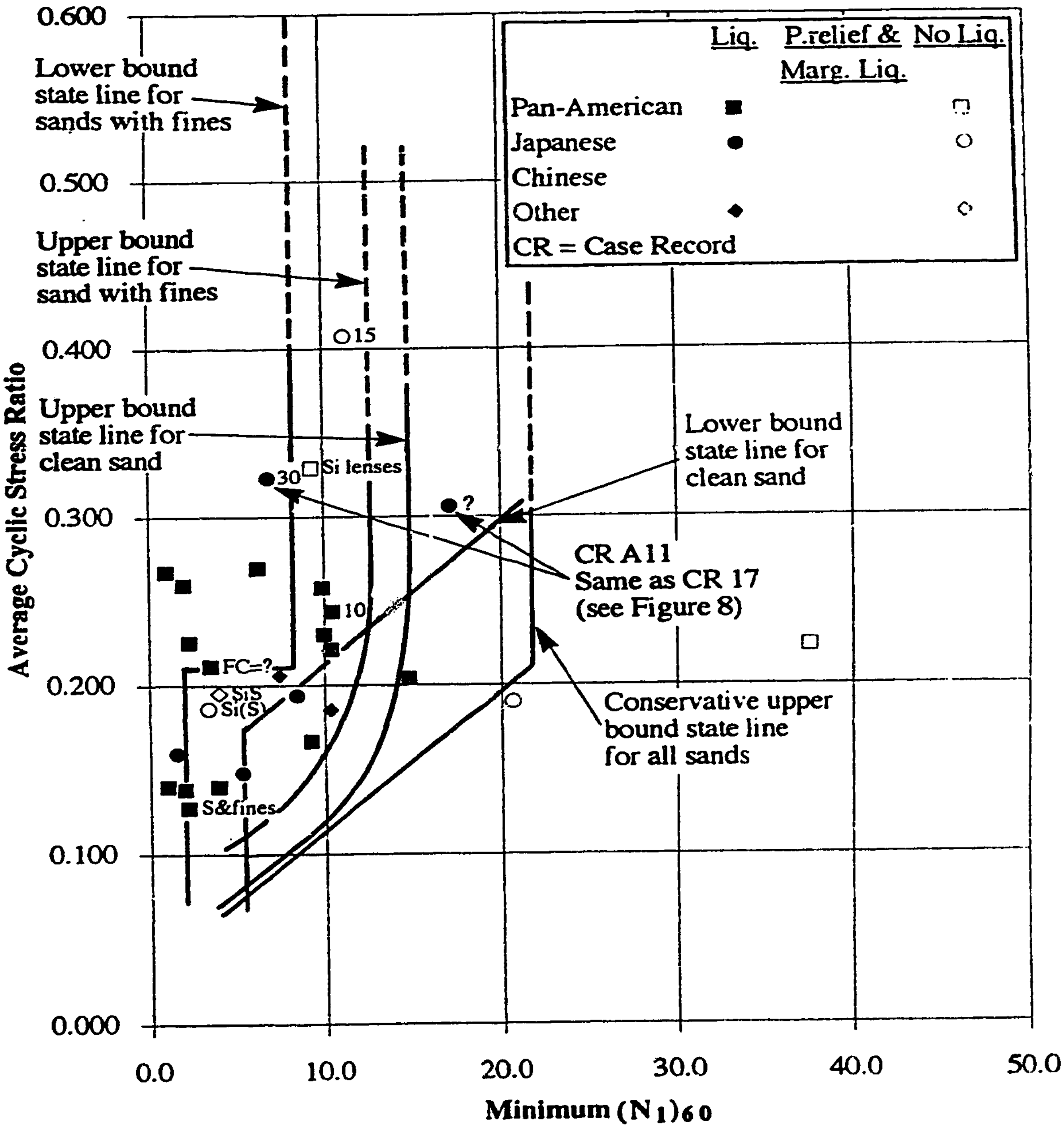

Figure 2-10 Comparison of recent data with the results of this study (labels refer to fines contents).

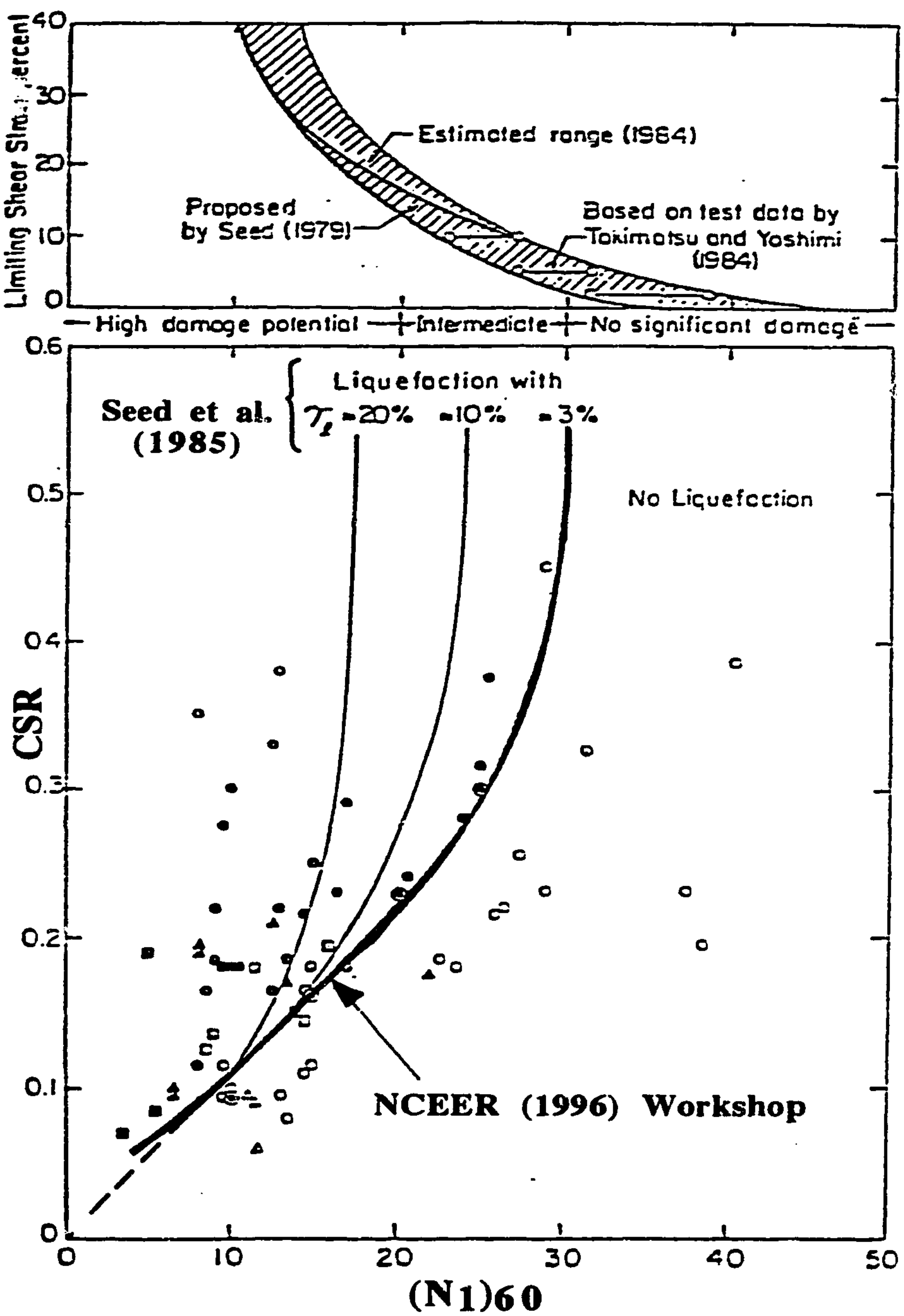

Figure 2-11 Plot of CSR versus $(N_1)_{60}$ with limiting strain lines for clean sand and line from NCEER (1996) Workshop (modified from Seed et al., 1985).

References

Ambraseys, N.N. 1992. Personal communication containing the list of references for the additional sites added to the Berkeley catalogue by Ambraseys (1988).

Ambraseys, N.N. 1988. Engineering seismology. *Earthquake Engineering and Structural Dynamics*, 17(1): 1-105.

Andrus, R.D., Stokoe, K.H., and Roesset, J.M. 1991. Liquefaction of gravelly soil at Pence Ranch during the 1983 Borah Peak earthquake. *Proc., Soil Dyn. and Earthq. Engrg.*, V, Computational Mech. Publ., Southampton, U.K., 251-262.

Bartlett, S.F. and Youd, T.L. 1992. Empirical analysis of horizontal ground displacements generated by liquefaction-induced lateral spreads. *National Center for Earthquake Engineering Research (NCEER), Technical Report NCEER-92-0021.*

Beijing Municipal Bureau of City Planning, Department of Geotechnical Exploration et al. 1982. *Research report of sand liquefaction during the Tangshan earthquake.* (in Chinese).

Byrne, P.M., Imrie, A.S., and Morgenstern, N.R. 1994. Results and implications of seismic performance studies for Duncan Dam. *Canadian Geotechnical Journal*, 31(6): 979-988.

Casagrande, A. 1976. Liquefaction and cyclic deformation of sands, a critical review. *Harvard Soil Mechanics Series No. 88*, Harvard University, Cambridge, Massachusetts.

Cluff, L.S. 1973. Personal communication cited by Seed et al. (1984).

Dames and Moore 1975. Offshore soils investigation, Los Angeles Harbor, LNG Ship Terminal. *Report to Western LNG Terminal Company.*

Fear, C.E., and McRoberts, E.C. 1993. Report on liquefaction potential and catalogue of case records, *Internal Research Report, Geotechnical Engineering Library*, Department of Civil Engineering, University of Alberta, Edmonton, Alberta, Canada.

Ishihara, K. 1993. Liquefaction and flow failure during earthquakes. *The 33rd Rankine Lecture, Géotechnique*, 43(3): 351-415.

Iwasaki, T. 1981. Studies on aseismic stability of river dykes considering ground liquefaction. *Proc. of the 16th Annual Meeting, JSSMFE*, 637-640 (in Japanese).

Iwasaki, T., Kawashima, K., and Tokida K. 1978. Report of the Miyagiken-Oki earthquake of June, 1978. *Public Works Research Institute, Ministry of Construction, Japan, Report No. 1422* (in Japanese).

Jamiolkowski, M., Baldi, G., Bellotti, R., Ghionna, V., and Pasqualini, E. 1986. Penetration resistance and liquefaction of sands. *Proceedings of the 11th International Conference of Soil Mechanics and Foundation Engineering*, San Francisco, 4: 1891-1896.

Kayen, R.E. 1993. Personal communication containing several borehole logs referred to, but not contained in Kayen et al. (1992).

Kayen, R.E., Mitchell, J.K., Lodge, A., Seed, R.B., Nishio, S., and Coutinho, R. 1992. Evaluation of SPT-, CPT-, and shear wave-based methods for liquefaction potential assessment using Loma Prieta data. *Proceedings of the Fourth Japan-U.S. Workshop on Earthquake Resistant Design of Lifeline Facilities and Countermeasures for Soil Liquefaction, Technical Report NCEER-92-0019*, 1, M. Hamada, and T. D. O'Rouke, eds., 177-204.

Kishida, H. 1969. Characteristics of liquefied sands during Mino-Owari, Tohnankai and Fukui earthquakes. *Soils Found.*, 9(1): 75-92.

Kodera, J. 1964. Earthquake damage and the ground of pier foundations, Part 1. *Tsuchi-To-Kiso*, 12(3): 11-18 (in Japanese).

Liao, S.S.C. 1986. Statistical modeling of earthquake-induced liquefaction. *Ph.D. Dissertation*, Department of Civil Engineering, Massachusetts Institute of Technology, 470 p.

Liao, S.S.C., and Whitman, R.V. 1986. A catalog of liquefaction and non-liquefaction occurrences during earthquakes. *Research Report*, Department of Civil Engineering, M.I.T., Cambridge, Massachusetts.

McRoberts, E.C., and Sladen, J.A. 1992. Observations on static and cyclic sand liquefaction methodologies. *Can. Geotech. J.*, 29(4): 650-665.

National Research Council 1985. Liquefaction of soils during earthquakes. Committee on Earthquake Engineering, Commission on Engineering and Technical Systems, G.W. Housner (Chairman), National Academy Press, 240 p.

NCEER Workshop 1996. Proceedings to be published at a subsequent date by Youd et al. (1996).

Robertson, P.K. 1994. Suggested terminology for liquefaction. *Proceedings of the 47th Canadian Geotechnical Conference, Halifax, Nova Scotia*, Canadian Geotechnical Society, Ottawa, Canada, 277-286.

Robertson, P.K., Woeller, D.J., and Finn, W.D.L. 1992. Seismic cone penetration test for evaluating liquefaction potential under cyclic loading. *Can. Geotech. J.*, 29(4): 686-695.

Rollins, K.M., and Seed, H.B. 1990. Influence of buildings on potential liquefaction damage. *J. Geotech. Engrg.*, ASCE 116(2): 165-185.

Seed, H.B. 1987. Design problems in soil liquefaction. *J. Geotech. Engrg.*, ASCE 113(8): 827-845.

Seed, H.B. 1983. Earthquake-resistant design of earth dams. *Proc. Symp. on Seismic Design of Embankments and Caverns*, ASCE, 41-64.

Seed, H.B. 1973. Cited in text, but missing from reference list in Seed et al. (1984).

Seed, H.B., Arango, I., and Chan, C. 1975. Evaluation of soil liquefaction potential during earthquakes. *Report No. EERC 75-28*, University of California, Berkeley.

Seed, H.B., and Idriss, I.M. 1971. Simplified procedure for evaluating soil liquefaction potential. *J. Soil Mech. Found. Div.*, ASCE 97(9): 1249-1273.

Seed, H.B., and Idriss, I.M. 1982. *Ground motions and soil liquefaction during earthquakes.* The Earthquake Engineering Research Institute, University of California, Berkeley.

Seed, H.B., and Peacock, W.H. 1971. Test procedures for measuring soil liquefaction characteristics. *J. Soil Mech. Found. Div.*, 97(8): 1099-1119.

Seed, H.B., Tokimatsu, K., Harder, L.F., and Chung, R.M. 1985. Influence of SPT procedures in soil liquefaction resistance evaluations. *J. Geotech. Engrg.*, ASCE 111(12): 1425-1445.

Seed H.B., Tokimatsu K., Harder L.F., and Chung R.M. 1984. The influence of SPT procedures in soil liquefaction resistance evaluations. *Earthquake Engineering Research Center Report No. UCB/EERC-84/15*, College of Engineering, University of California, Berkeley, California.

Shengcong, F., and Tatsuoka, F. 1983. *Report of Japan-China Cooperative Research on Engineering Lessons from Recent Chinese Earthquakes, Including the 1976 Tangshan Earthquake (Part 1).* C. Tamura, T. Katayama, and F. Tatsuoka, eds., Institute of Industrial Science, University of Tokyo.

Skempton, A. W. 1986. Standard penetration test procedures and the effects in sands of overburden pressure, relative density, particle size, ageing and overconsolidation." *Geotechnique*, 36(3): 425-447.

Tsuchida, H. 1979. The damage to port structures by the 1978 Miyagiken-Oki earthquake. *Technical Note, The Port and Harbour Research Institute, Ministry of Transport, Japan, No. 325* (in Japanese).

Yegian, M.K., Ghahraman, V.G., and Hrutiunyan, R.N. 1994. Liquefaction and embankment failure case histories, 1988 Armenian earthquake. *J. Geotech. Engrg. Div.*, ASCE 120(3): 581-596.

Youd, T.L. 1993. Liquefaction-induced lateral spread displacement. *Technical Note N-1862*, Naval Civil Engineering Laboratory, Port Hueneme, California.

Youd, T.L., and Bennett, M.J. 1983. Liquefaction Sites, Imperial Valley, California. *J. Geotech. Engrg. Div.*, ASCE 109(3): 440-457.

CHAPTER 3

AN INTEGRATED METHOD FOR EVALUATING CYCLIC LIQUEFACTION POTENTIAL BASED ON THE CONE PENETRATION TEST (CPT)[1,2,3]

3.1 Introduction

Cyclic softening commonly occurs in the field as a result of earthquake loading, resulting in observable features such as sand boils, lateral spreading, and ground cracks. The largest deformations occur when in-situ shear stresses are low and the earthquake causes shear stress reversal in the ground (see Figure 3-1). This process results in essentially zero effective stress and subsequent large reductions in soil stiffness leading to deformations which accumulate with additional cycles of loading. Cyclic softening potential is a function of the density of the soil as well as the duration and size of the cyclic loading.

The previous chapter dealt with the SPT-based method of evaluating cyclic softening (liquefaction) potential at a site. The SPT based method, although it is the most commonly used method in practice, has many problems, primarily due to the unreliable nature of the SPT. Many factors can affect the SPT, including inadequate cleaning of the hole, failure to maintain an adequate head of water in the borehole, careless measure of hammer drop, inaccurate weight of the hammer, hammer striking the drill rod collar eccentrically, lack of hammer free fall, sampler driven above the bottom of the casing, careless blow count, use of a non-standard sampler, coarse gravel or cobbles in the soil and the use of bent drill rods (Kulhawy and Mayne, 1990). However, the most important factor affecting SPT results is the energy delivered to the SPT sampler. It is extremely important to measure the rod energy ratio delivered to the sampler during the actual site investigation (rather than relying on global correction values) and correct the measured blowcount to a reference energy ratio (generally accepted as 60%), in order to improve the level of reliability of the SPT. In

---

[1] *A version of part of this chapter has been published. Robertson, P.K. and Fear, C.E. 1995. Application of CPT to evaluate liquefaction potential, Proceedings of the International Symposium on Cone Penetration Testing, CPT'95, Linkoping, Sweden.*

[2] *A version of part of this chapter has been published. Robertson, P.K. and Fear, C.E. 1995. Liquefaction of sands and its evaluation, Proceedings of IS Tokyo '95, First International Conference on Earthquake Geotechnical Engineering, Keynote Lecture.*

[3] *A version of part of this chapter is in the process of being published. Robertson, P.K. and Fear, C.E. 1996. Soil liquefaction and its evaluation based on SPT and CPT, Proceedings of the 1996 NCEER Workshop on Liquefaction.*

addition, the SPT is typically conducted at five foot depth intervals. It is therefore possible to miss important ground features. The cone penetration test (CPT), being continuous in nature, can provide a more detailed profile of the ground. In addition, the CPT is generally more repeatable and reliable.

3.2 Estimation of Cyclic Resistance Ratio (CRR)

Cyclic softening is predicted to occur when the cyclic stress ratio (CSR) induced by the earthquake exceeds the cyclic resistance ratio (CRR), τ_{cyc}/σ_{vo}', available in the ground. Seed et al. (1985) developed a simplified method to estimate CSR (see Chapter 2); this approach can be summarized as follows (after Tokimatsu and Yoshimi, 1983):

[3-1] $$CSR = \frac{\tau_{av}}{\sigma_{vo}'} = 0.1\,(M - 1)\left(\frac{a_{max}}{g}\right)\left(\frac{\sigma_{vo}}{\sigma_{vo}'}\right)(1 - 0.015z)$$

where:

τ_{av} = average cyclic shear stress
M = earthquake magnitude, commonly 7.5
a_{max} = maximum horizontal acceleration at ground surface
g = acceleration due to gravity = 9.81 m/s^2
σ_{vo} = total vertical overburden stress
σ_{vo}' = effective vertical overburden stress
z = depth in meters (for z < 25m).

CRR can be estimated in the field using the SPT (see Chapter 2), CPT or V_s measurements or estimated in the laboratory using cyclic triaxial or cyclic simple shear testing.

Correlations between CRR and CPT q_{c1} for both clean sand and silty sands were developed by Robertson and Campanella (1985), by converting the Seed et al. (1985) SPT-based correlation for clean sand (see Chapter 2) using general $q_{c1}/(N_1)_{60}$ ratios. Similar CPT-based charts were developed by Seed and de Alba (1986), Shibata and Teparaska (1988) and Mitchell and Tseng (1990). Figure 3-2 illustrates the differences between the most commonly used CPT-based charts. Based on recent discussions at the NCEER Workshop (1996), the curve by Robertson and Campanella (1985) has been modified slightly to be more consistent with the SPT curve (see Figure 3-3: solid line represents relationship proposed by Robertson and Campanella, 1985; dashed line represents modification based on NCEER Workshop, 1996). The resulting modified CPT clean sand correlation can be approximated by the following equation:

[3-2] $$CRR = 93 \left(\frac{(q_{c1})_{cs}}{100}\right)^3 + 0.08$$

where:
$(q_{c1})_{cs}$ is the equivalent clean sand q_{c1}, in MPa
3 MPa < $(q_{c1})_{cs}$ < 16 MPa.

Until recently, the database of cyclic softening (liquefaction) case histories having SPT data available (see Chapter 2) was much larger than the databases of case histories having CPT or shear wave velocity data available; consequently, the SPT-based method has been the most commonly used method in practice. However, the amount of available CPT field performance data is increasing (Ishihara, 1993; Kayen et al., 1992; Stark and Olson, 1995; Suzuki et al., 1995) and the combined database is now larger than the SPT database. The recent CPT data seem to confirm that the existing CPT-based correlations for estimating CRR are generally good for both clean sands and silty sands. Figure 3-3 compares the recent field performance data from Stark and Olson (1995) and Suzuki et al. (1995) for clean sands to the Robertson and Campanella (1985) clean sand correlation. In general, the correlation by Robertson and Campanella (1985) gives a dividing line between liquefaction case records and non-liquefaction case records that matches the field performance data well. The slight modification to the Robertson and Campanella (1985) correlation, based on the NCEER Workshop (1996) discussions and as approximated by Equation 3-2, is also shown in Figure 3-3.

The field observation data in the Stark and Olson (1995) and Suzuki et al. (1995) databases are apparently based on the following:

- Holocene age, clean sand deposits
- Level or gently sloping ground
- Magnitude M=7.5 earthquakes
- Depth range from 1 to 15 m (3 to 45 ft)
  (84% is for depths < 10 m (30 ft))
- Representative average CPT q_{c1} values for the layer that was considered to have experienced cyclic liquefaction.

Therefore, caution should be exercised when extrapolating the CPT correlation given in Equation 3-2 to conditions outside of the above range. Since this CPT method is based on the Seed methodology, similar limitations apply as to when the correlation is applicable and similar uncertainty exists over degree of conservatism contained within the correlation. An important feature to recognize is that the correlation appears to be based on average values for the liquefied layers. However, due to the continuous nature of the CPT, the correlation is often applied to all measured CPT values, including low values below the average. Having the continuous soil profile is useful, but caution should be taken when applying the average based CPT methodology to variable deposits in which a small part of the CPT data predicts that cyclic liquefaction could occur. The possible conservatism of the method when applied to such cases as well as the consequences of liquefaction of individual layers should be considered as part of the design process. A detailed review of the CPT data, similar to that carried out by Fear and McRoberts (1995) on SPT data (see Chapter 2) would be required to investigate the degree of conservatism contained in Figure 3-3.

The correlation given in Equation 3-2 is for clean sands. In general, for the same CRR, the penetration resistance in silty sands is smaller. This is likely due to the greater compressibility and decreased permeability of silty sands, which reduces penetration resistance and moves the penetration process toward an undrained penetration, respectively. Based on their database of 180 CPT case records (some in clean sands, as shown in Figure 3-3, and some in silty sands), Stark and Olson (1995) were able to develop a set of correlations between CRR and q_{c1} for various sandy soils, based on fines content and mean grain size, as shown in Figure 3-4.

Based on the work by Stark and Olson (1995), fines content based corrections to tip resistance can be estimated to allow measurements of q_{c1} in silty sands to be converted to clean sand equivalent values. The range in potential corrections (Δq_{c1}) are illustrated in Figure 3-5; the recommended correction can be expressed by the following:

[3-3] $\Delta q_{c1} = 6$ MPa if $FC \geq 35\%$

$\Delta q_{c1} = 0$ if $FC \leq 5\%$

$\Delta q_{c1} = 0.2\ (FC - 5)$ MPa if $5\% < FC < 35\%$

where:
FC = fines content, in percent.

Note that Figure 3-5 also indicates the corresponding suggested corrections, $\Delta(N_1)_{60}$, for the SPT, as a function of fines content. Although the corrections given by Figure 3-5 and Equation 3-3 are based on fines content, it is clear that the CRR of a soil is a function of many factors, including plasticity of the fines, grain characteristics (mineralogy, grain shape etc.) as well as fines content. Hence, the corrections should be applied with caution. When a soil is fine-grained or contains some amount of fines, some cohesion or adhesion can develop between the fine particles making the soil more resistant at essentially zero effective confining stress. A greater CRR is generally exhibited by sandy soils containing some fines. However, this tendency depends on the type of fines (Ishihara, 1993). Laboratory testing has shown that the most important index property distinguishing which type of fines have this effect is plasticity index, I_p (Ishihara and Koseki, 1989). Cyclic triaxial tests reported by Ishihara (1993) suggested that $I_p=10$ is the point below which the presence of fines has little effect on CRR, but above which, CRR increases with increasing values of I_p.

3.3 Estimation of Soil Behaviour Type

Since the corrections suggested in Equation 3-3 are based on fines content, a profile of fines content with depth must be determined. One reason for the continued use of the SPT has been the need to obtain a soil sample for determining the fines content of the soil in order to apply the Seed methodology (see Chapter 2). Although the CPT has the advantage that it produces a continuous profile, unlike the SPT, it does not provide samples for which grain size distributions can be produced. However, in recent years, various charts have been developed to estimate soil type from the CPT (Olsen and Malone, 1988; Robertson and Campanella, 1988; Robertson, 1990). Since fines content is obviously some function of soil type, it seems logical to try to estimate fines content from the CPT predictions of soil behaviour type. It is possible to combine the CPT results (cone tip resistance and sleeve friction) with soil classification charts, such as that by Robertson (1990) shown in Figure 3-6 to estimate soil behaviour type. The boundaries between soil behaviour type zones 2 to 7 can be approximated as concentric circles about a common point (Jefferies and Davies, 1993). The radius of each circle can then be used as a soil behaviour type index. This index, I_c, based on the CPT chart by Robertson (1990), is defined as follows:

[3-4] $$I_c = [\,(3.47 - \log Q)^2 + (\log F + 1.22)^2\,]^{0.5}$$

where:
Q = normalized CPT penetration resistance = $(q_c - \sigma_{vo})/\sigma_{vo}'$
F = normalized friction ratio, in percent = $[f_s/(q_c - \sigma_{vo})] \times 100\%$
f_s = CPT sleeve friction.

The boundaries of soil behaviour type are then given in terms of the index, Table 3-1. The soil behaviour type index does not apply to zones 1, 8 or 9

3.4 Estimation of Fines Content

Experience has shown that the CPT friction ratio (ratio of the CPT sleev cone tip resistance) increases with increasing fines content and soil plastic from Suzuki et al. (1995) illustrates the relationship between friction content. Many soils fall in the normally consolidated region of the soil beha shown in Figure 3-6. Therefore, as soil behaviour type changes from a sandy silt (I_c increases from 1.31 to 2.60), friction ratio increases and a content can be estimated according to the soil behaviour type index, Figure 3-8. The recommended relationship shown in Figure 3-8 can be a the following equation:

[3-5] $$\text{Fines Content, FC (\%)} = 1.75\, I_c^{3} - 3.7$$

In combination, Equations 3-2 to 3-5 provide an integrated CPT approach t potential for cyclic liquefaction in a sandy deposit. By considering this inte in terms of its individual components, it is possible to modify the equation site specific conditions. For example, the profile of estimated fines conten be compared with actual measured fines contents from samples and the Equation 3-5 can be modified to best fit the site specific data. The final pro CRR with depth can be compared with laboratory testing on undisturbed sa

3.5 Laboratory Methods for Estimating CRR

Resistance to cyclic loading (CRR) is a primarily a function of the state of ratio, effective confining stresses and soil structure) and the intensity and cyclic loading (i.e. cyclic shear stress and number of cycles), as we characteristics of the soil. Soil structure incorporates factors such as cementation. Grain characteristics incorporate factors such as grain size di shape and morphology. Void ratio (i.e. relative density) is recognized as a approximated by the following equation:

$$[3\text{-}6] \qquad \frac{1}{r_m} = \frac{0.1(M-1)}{0.65}$$

A best fit curve through the M and N data in Table 3-2, is shown in Figure 3-9 and indicates that M can be approximated from N using the following equation:

$$[3\text{-}7] \qquad M = -0.0038N^2 + 0.2442N + 4.7034 \qquad (R^2 = 0.9989)$$

Equations 3-6 and 3-7 can be combined in order to correct the applied CSR to an equivalent CSR at N=15 cycles. This can be taken as the CRR of the soil for a Magnitude M=7.5 earthquake with 15 cycles of equivalent uniform loading.

For high risk projects, a limited amount of laboratory testing on high quality undisturbed samples of sand should be considered. The method of in-situ ground freezing has been successful in obtaining undisturbed samples of sandy soils at several sites (Yoshimi et al., 1978; Yoshimi et al., 1989; Yoshimi et al., 1994; Sego et al., 1994; Hofmann et al., 1994 and 1995). In general, cyclic simple shear tests are the most appropriate tests to perform.

3.6 Linking the In-Situ Method to Laboratory Testing

On a site specific basis, predictions of CRR based on any of the three in-situ tests (SPT, CPT or V_s) and measurements of CRR by laboratory testing of undisturbed samples can be compared. The integrated CPT approach is the most straightforward and comprehensive method to apply. However, if data from more than one in-situ testing method are available, evaluating CRR based on each of the methods is useful for providing independent evaluations of cyclic softening (liquefaction) potential. The formulae given for the integrated CPT approach are general in nature and may not apply on a site specific basis. It is recommended that for low risk projects, the integrated CPT approach be applied directly. However, for moderate to high risk projects, a site specific approach with a link to laboratory testing should be taken in order to modify the individual components of the method if necessary. This will allow for estimates of CRR to be extrapolated beyond the zone of undisturbed sampling, based on the results of in-situ testing alone. Thus, laboratory testing and field testing can be linked in a framework for investigating the potential for cyclic softening. The profile of CRR can then be compared with the predicted CSR profile for the design earthquake in order to estimate liquefaction potential at the site in question.

The primary concern for cases of cyclic liquefaction is the amount of deformation that occurs during and after the earthquake. Catastrophic flowslides will generally not occur, since cyclic liquefaction tends to occur in level or gently sloping ground in which shear stress reversal occurs (although if cyclic liquefaction occurs at the toe of a slope, the slope may fail in a slumping fashion). However, cyclic liquefaction will result in horizontal displacements, lateral spreading and surface settlements. These movements can affect the integrity of structures if the deformations are significant. Post cyclic liquefaction shear strains (resulting in horizontal displacements) and post cyclic liquefaction volumetric strains (resulting in settlements) can be estimated using methods suggested by Ishihara (1993), as shown in Figure 3-10. These methods are suitable to the integrated CPT approach because they are based on the factor of safety against liquefaction (i.e. the ratio of CRR to CSR) and incorporate values of CPT q_{c1}. In the case of slightly sloping ground, methods such as those proposed by Bartlett and Youd (1995) can be used to estimate deformations associated with lateral spreading.

3.7 Application of the Integrated CPT Approach

Phase III of the Canadian Liquefaction Experiment (CANLEX) Project consisted of filling an old borrow pit (J-pit) at Syncrude, in Ft. McMurray, Alberta, with tailings to create a relatively loose sand deposit with a groundwater table at a depth of approximately 0.5 m. Figure 3-11 presents a plan of the area of detailed test site at which in-situ testing and in-situ freezing and sampling were performed. Both SPT and CPT testing was conducted in the detailed test site area.

Grain size distributions were performed on samples from the SPT sampler, giving estimates of fines content with depth at the site. Each SPT was paired up with the closest CPT in order to compare the measured fines contents with the fines content profiles predicted using the integrated CPT method. Thus, CPT-20 and SPT-1 were paired together, CPT-22 and SPT-2 were paired together, and CPT-23 and SPT-3 were paired together. Figure 3-12 compares the profiles of predicted fines content for each CPT with the measured fines contents from the corresponding SPT. In general, the predicted fines content is close to the measured values, although there is some scatter, which may be due, in part, to the averaging effect of the sampling as well as the approximate nature of the correlation. It appears that the method may overestimate fines content when the actual fines content is low (e.g. see the CPT22-SPT2 comparison). However, it is interesting to note the rapid variation in fines content with depth at this particular site and how the interpretations of fines content using the integrated CPT method appears to track this variation.

Figure 3-13 illustrates how each component of the integrated CPT approach can be applied to a CPT profile. In this case, the CPT profile is one of several CPTs performed in the detailed test site at the Massey Tunnel site (CPT M9406), as part of Phase II of the CANLEX project. Detailed testing and in-situ freezing and s[illegible]ing was concentrated in a target zone located from 8 m to 13 m. Additional details regarding the interpretation of the Massey Tunnel site are given in Chapter 8. Figure 3-13 first presents the profile of corrected cone tip resistance, q_{c1}, for the particular CPT. The profile of soil behaviour type index, I_c, was estimated by combining the cone tip resistance and sleeve friction from the CPT with Equation 3-4. The soil above 5 m depth is quite variable with the estimated I_c ranging from approximately 1 to 3. However, below 5 m, the soil becomes fairly uniform, with an average estimated I_c of approximately 1.8. Based on Table 3-1, this value of I_c corresponds to a sand, ranging from a clean sand to a silty sand.

The profile of fines content was estimated by combining the profile of I_c with Equation 3-5. The estimated fines content is quite variable above 5 m, but below 5 m, it is fairly constant with an average value of approximately 6%. Superimposed on the CPT estimated profile of fines content is a range of measured fines contents in the target zone (8 m to 13 m). The CPT estimated profile appears to overestimate fines content in this region; however, the indicated range of measured values are presently based on very limited data. Further testing is required at this site to produce a clear profile of measured fines contents with depth. The profile of the recommended correction to cone tip resistance, Δq_{c1}, was estimated by combining the profile of fines content with Equation 3-3. Above 5 m, Δq_{c1} is quite variable, ranging from zero to large values, corresponding to the variety in the estimated fines content. Below 5 m, Δq_{c1} is fairly uniform and rather small because the estimated fines content in this region is fairly constant and generally not much greater than 5% (see Equation 3-3).

Adding the Δq_{c1} profile to the measured q_{c1} profile and combining the resulting equivalent clean sand profile of corrected tip resistance, $(q_{c1})_{cs}$, with Equation 3-2 produces the final profile of CRR. As for the profiles of the individual components of the integrated CPT method, the estimated CRR is quite variable above 5 m. However, below 5 m, it is fairly constant with an average value of approximately 0.1. Superimposed on the CRR profile are the results of testing undisturbed samples of sand from the Massey site in the laboratory. Cyclic simple shear tests were performed and the measured cyclic resistance for each test was corrected to equivalent Magnitude M=7.5 (N=15 cycles) values of CRR using Equations 3-6 and 3-7. The CPT estimated profile of CRR compares well with the laboratory results. However, since the average fines content was generally less than 10% in the region in which the samples were tested, the corrections to CPT tip resistance for fines content were very small. Further laboratory testing of undisturbed samples from sites at which the fines content is greater and would lead to more significant corrections to cone tip resistance would be useful to confirm how well the integrated CPT method estimates CRR in siltier sands.

3.8 Other Methods of Estimating CRR

Olsen and Malone (1988), Olsen and Koester (1995) and Suzuki et al. (1995) have also suggested integrated methods to estimate the CRR of sandy soils directly from the CPT. The correlations are presented in the form of soil type behaviour charts with contours of CRR. The Olsen and Koester (1995) method (see Figure 3-14) is based on SPT-CPT conversions plus some laboratory CRR data. The Suzuki et al. (1995) method (see Figure 3-15) is based on field observation data. Note that the Olsen and Koester (1995) method has truly normalized the corrected q_{c1} by dividing it by atmospheric pressure (typically taken as 100 kPa = 0.1 MPa), resulting in a dimensionless term, whereas Suzuki et al (1995) presented results in MPa. When q_{c1} is expressed in units of MPa, the normalized value is therefore approximately ten times larger in magnitude.

The method described here is based on field observations and is similar to those of Olsen and Koester (1995) and Suzuki et al. (1995), but has the advantage that the process has been broken down into its individual components (see Equations 3-2 to 3-5). This allows for the incorporation of site specific correlations when applying the method. Figure 3-16 summarizes the components of the integrated CPT method recommended here by presenting contours of estimated CRR on the soil classification chart by Robertson (1990). Note that the cone tip resistance in Figure 3-16 is expressed as Q (see Equation 3-4); for vertical effective stresses close to 100 kPa, the value of Q is essentially the same as the normalized q_{c1} used by Olsen and Koester (1995). The contours of estimated CRR were determined by combining Equations 3-2 to 3-5. Note that the contours of estimated CRR are generally cut off in zone 4 (silt mixtures). Beyond this zone, soil plasticity can have a significant effect on cyclic resistance. For CPT data falling within zone 4, soil plasticity should be evaluated in order to determine its effect on CRR. The integrated CPT method proposed here does not incorporate the effects of soil plasticity. Consequently, it does not apply to zone 3 (clays) where the effects of soil plasticity can be significant. Contours of estimated fines content are also presented, based on combining Equations 3-4 and 3-5. Comparing Figure 3-16 to Figures 3-14 and 3-15 illustrates that, in general, the predictions of CRR using the method proposed here are more conservative than either the Olsen and Koester (1995) method or the Suzuki et al. (1995) method, particularly for sandy soils with fines. The chart in Figure 3-16 is primarily shown for illustrative purposes.

CRR can also be estimated from shear wave velocity measurements. Figure 3-17a presents a correlation between corrected shear wave velocity, V_{s1}, and CRR developed by Robertson et al. (1992), based on limited field performance data. Tokimatsu et al. (1991) suggested a similar chart based on laboratory results. Kayen et al. (1992) and Lodge (1994) modified the chart proposed by Robertson et al. (1992), based on additional field data. A comparison of the methods by Robertson et al. (1992), Kayen et al. (1992) and Lodge (1994) is presented in Figure 3-17b. Based on discussions at the recent NCEER Workshop (1996), use of a relationship between V_{s1} and CRR similar to that by Lodge (1994) has been recommended. Note that the correlations in Figure 3-17b have been shown down to a CRR of only about 0.1. It would be expected that below CRR=0.1, the relationships would become much flatter. The correlations are empirical and, again, there is uncertainty over the degree of conservatism that they contain because of the methods used to select the representative values of shear wave velocity for the various case histories. A detailed review of the shear wave velocity data, similar to that carried out by Fear and McRoberts (1995) on SPT data would be required to investigate the degree of conservatism contained in Figure 3-17. The same limitations as to the applicability of the correlation apply as for the SPT and CPT, due to the type of the case records contained in the database. At present, the integrated CPT approach is more reliable than the shear wave velocity method. The shear wave velocity database is limited and the profiles of shear wave velocity, although they are step functions, are not truly continuous in nature. Shear wave velocity intervals are typically in the order of 1 m which may average out some of the low shear wave velocity regions associated with looser sand.

3.9 Correction for Thin Sand Layers

Interpretation of the CPT tip resistance can be difficult in thin sand layers embedded in softer (e.g. clay) deposits. As the CPT cone penetrates the ground, it is influenced both by the soil ahead of it and behind it. Therefore, the measured cone resistance will start to change before it reaches a new soil, as the cone begins to sense a soil ahead of itself. The cone will also continue to sense the original soil for a certain distance into a new soil. The result is that, in thinly interbedded soils, the measured cone resistance may not reach the true value that would be measured in a given layer if the layer were thicker. The cone can respond more fully in thin soft layers than in thin stiff layers because, in soft soils, the diameter of the sphere of influence is as small as 2 to 3 cone diameters, whereas, in stiff soils, it can be up to 20 cone diameters. The measured cone resistance in thin sand layers embedded in soft clay may underpredict the true resistance of the sand. This can have a significant impact on the estimated CRR and, thus, the cyclic liquefaction potential of the layer.

Vreugdenhil et al. (1994) have shown that the error in the measured cone resistance in a thin stiff layer (soil A, a sand) is a function of the thickness of the layer as well as the stiffness of the layer relative to the surrounding softer soil (soil B, a fine grained soil). The relative stiffness of soil A to soil B is related to the relative measured cone resistance (q_{cA}/q_{cB}). Figure 3-18 presents a suggested correction factor to cone resistance (K_c) as a function of the layer thickness. The corrections have a reasonable trend, but are large. The recommended conservative correction indicated in Figure 3-18 corresponds to $q_{cA}/q_{cB}=2$ and is given by the following equation:

$$[3\text{-}8] \qquad K_c = 0.5\left(\frac{H}{1000} - 1.45\right)^2 + 1.0$$

where:

q_{cA}/q_{cB} =2

H = layer thickness, in mm

q_{cA} = tip resistance in the sand layer

q_{cB} = tip resistance in the fine grained soil surrounding the layer.

When CPT data are plotted on a soil classification chart such as that by Robertson (1990) shown in Figure 3-6, thin sand layers embedded in soft clay deposits are often incorrectly classified as silty sands as a result of the measured cone tip resistance being lower than the actual full value for the sand if it were a thicker layer. Classification of such soil layers can be improved if a correction such as K_c is applied to the cone resistance before the soil classification charts are applied.

It is interesting to note, however, that the drainage conditions for a thin sand layer embedded in a soft clay are quite different than a thicker deposit of the very same sand. Further studies could be conducted to investigate the effect of restricted drainage conditions on the CRR of a thin sand layer embedded in a soft clay, as compared to the CRR of similar, but thicker, sand deposits. Such studies could help investigate the applicability of the Robertson and Campanella (1985) correlation between CRR and $(q_{c1})_{cs}$, as given in Equation 3-2, to thin sand layers after the cone tip resistance is corrected as suggested in Equation 3-8.

3.10 Conclusions and Recommendations

A framework has been proposed for estimating the CRR directly from the CPT, by first estimating soil behaviour type (as represented by I_c), then estimating fines content, next estimating the required correction to tip resistance to obtain an equivalent clean sand tip resistance and finally, estimating CRR using the relationship proposed by Robertson and Campanella (1985). Recent field performance data summarized by Stark and Olson (1995) and Suzuki et al. (1995) have confirmed this relationship. Corrections should be made to thin sand layers embedded in thick surrounding clay layers. If undisturbed sampling and testing are within the scope of the project (i.e. for a high risk project), the test results can be compared with the estimated CRR profile for the site, in order to modify the individual components of the CPT method to suit site-specific conditions. If the project is low risk in nature, or for initial site screening of a high risk project site, the integrated CPT method, as proposed here, can be applied directly. For moderate risk projects, the correction for fines content can be modified on a site specific basis.

Cyclic softening (liquefaction) potential can then be estimated by comparing the CRR profile with the CSR profile corresponding to the design earthquake, estimated using Equation 3-1. Zones in which CRR<CSR are predicted to be susceptible to cyclic softening (liquefaction). As discussed above, the Robertson and Campanella (1985) may

contain some degree of conservatism, based on the methods used to select representative values of q_{c1} for the case records (i.e. generally average values). Therefore, if only limited thin layers (of minimum q_{c1}) are predicted to liquefy, the site should be investigated more carefully. Finally, in regions in which cyclic softening (liquefaction) is predicted, methods such as those proposed by Ishihara (1993), as shown in Figure 3-10, can be used to estimate volumetric and shear strains at the site. These can be integrated to estimate permanent post-liquefaction settlements and horizontal displacements. In the case of slightly sloping ground, methods such as those proposed by Bartlett and Youd (1995) can be used to estimate deformations associated with lateral spreading.

Table 3-1: Boundaries of soil behaviour type

Soil Behaviour Type Index, Ic	Zone	Soil Behaviour Type (see Figure I-27)
$Ic < 1.31$	7	Gravelly sand
$1.31 < Ic < 2.05$	6	Sands: clean sand to silty sand
$2.05 < Ic < 2.60$	5	Sand Mixtures: silty sand to sandy silt
$2.60 < Ic < 2.95$	4	Silt Mixtures: clayey silt to silty clay
$2.95 < Ic < 3.60$	3	Clays
$Ic > 3.60$	2	Organic soils: peats

Table 3-2: Correction factors for influence of earthquake magnitude on cyclic resistance ratio (after Seed et al., 1985)

Earthquake Magnitude, M	No. of representative cycles at 0.65 τ_{max}	$r_m = \frac{\text{CRR for M=M}}{\text{CRR for M=7.5}}$
8.5	26	0.89
7.5	15	1.0
6.75	10	1.13
6	5 to 6	1.32
5.25	2 to 3	1.5

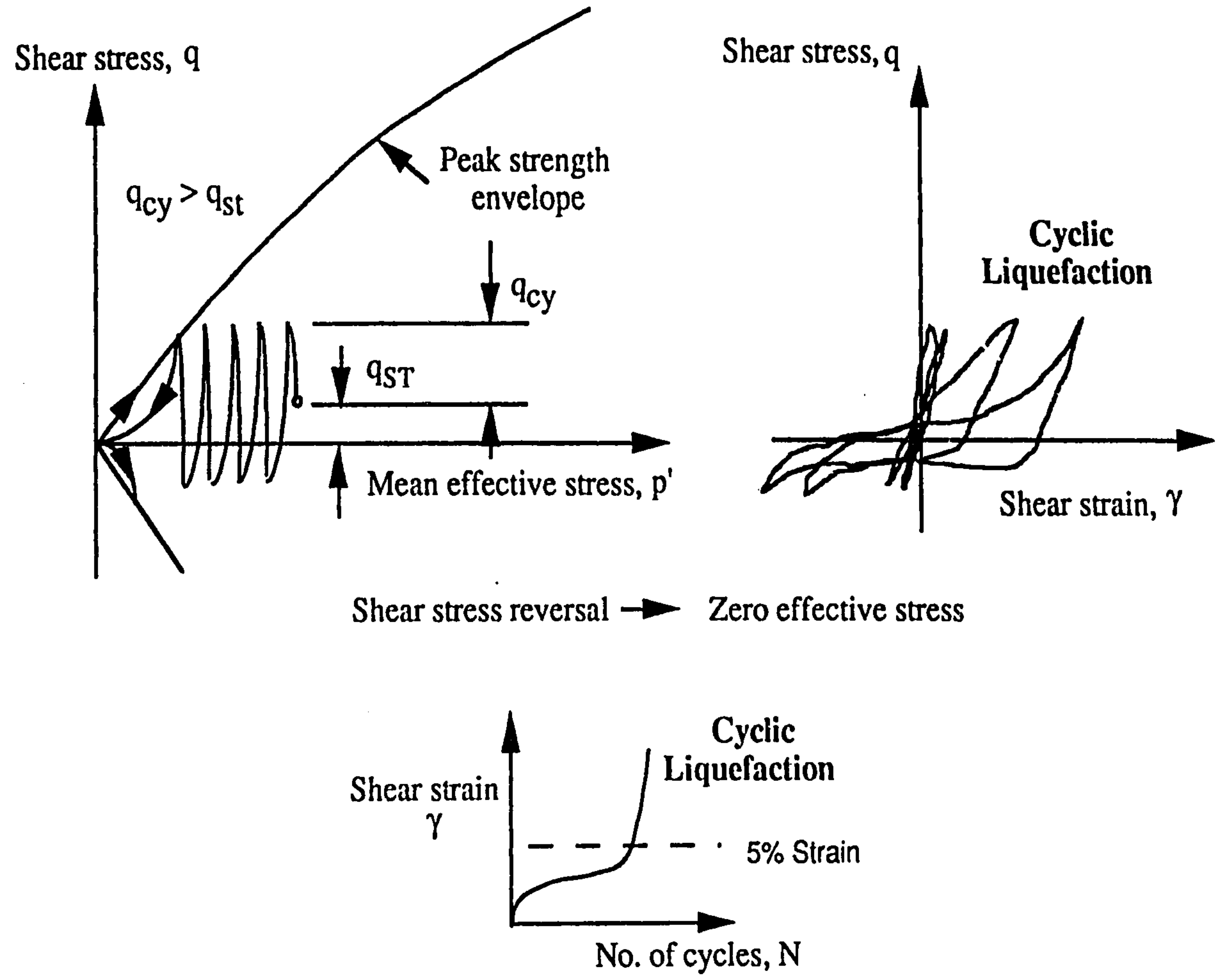

Figure 3-1 Schematic of undrained cyclic behaviour of sand illustrating cyclic liquefaction (modified from Robertson, 1994).

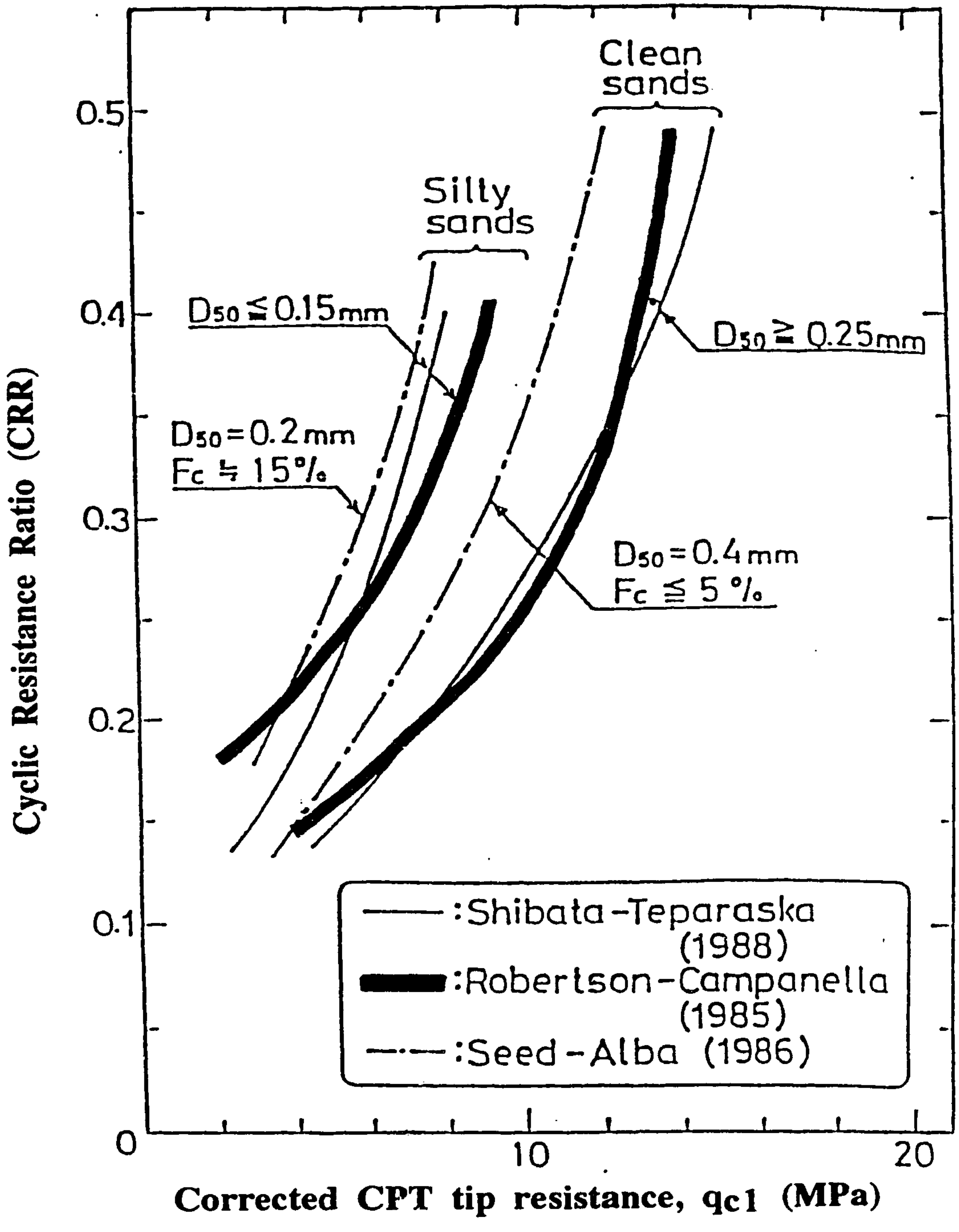

Figure 3-2 Comparison between various CPT based charts for estimating cyclic resistance ratio (CRR) for clean sands (modified from Robertson and Fear, 1995).

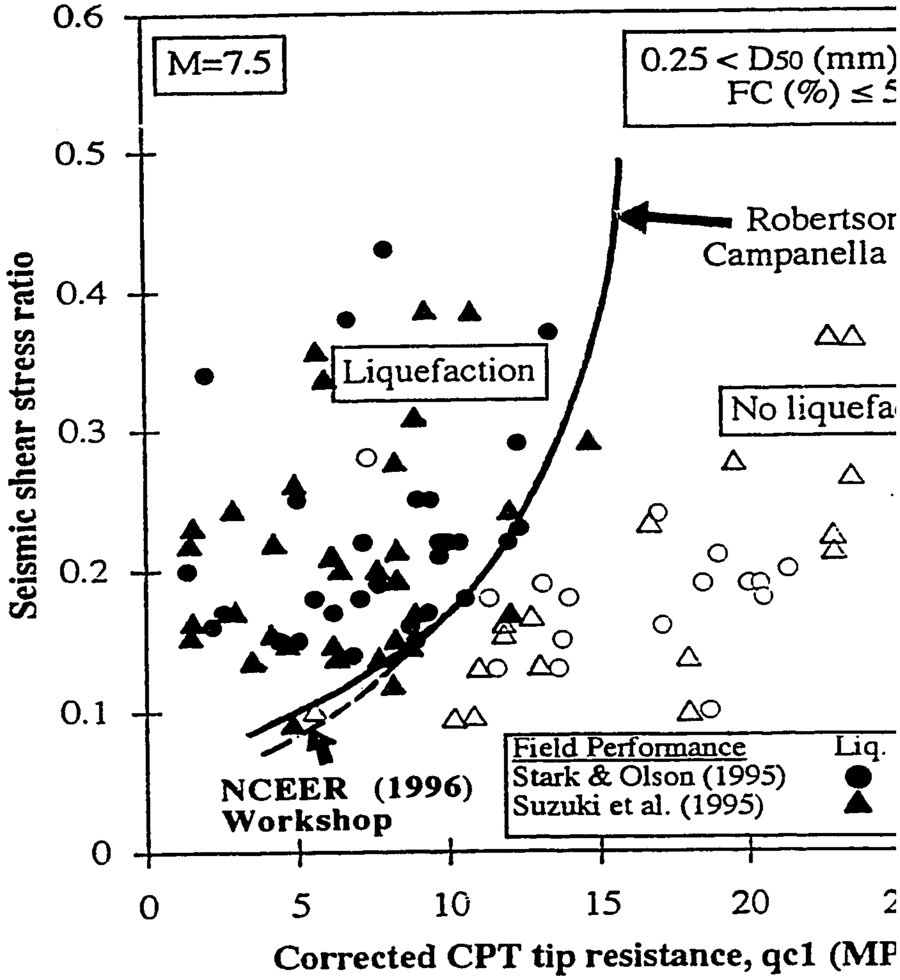

Figure 3-3 Comparison of CPT based methods for clean sands prop and Campanella (1985) and NCEER (1996) with recent data from Stark and Olson (1995) and Suzuki et al. (199

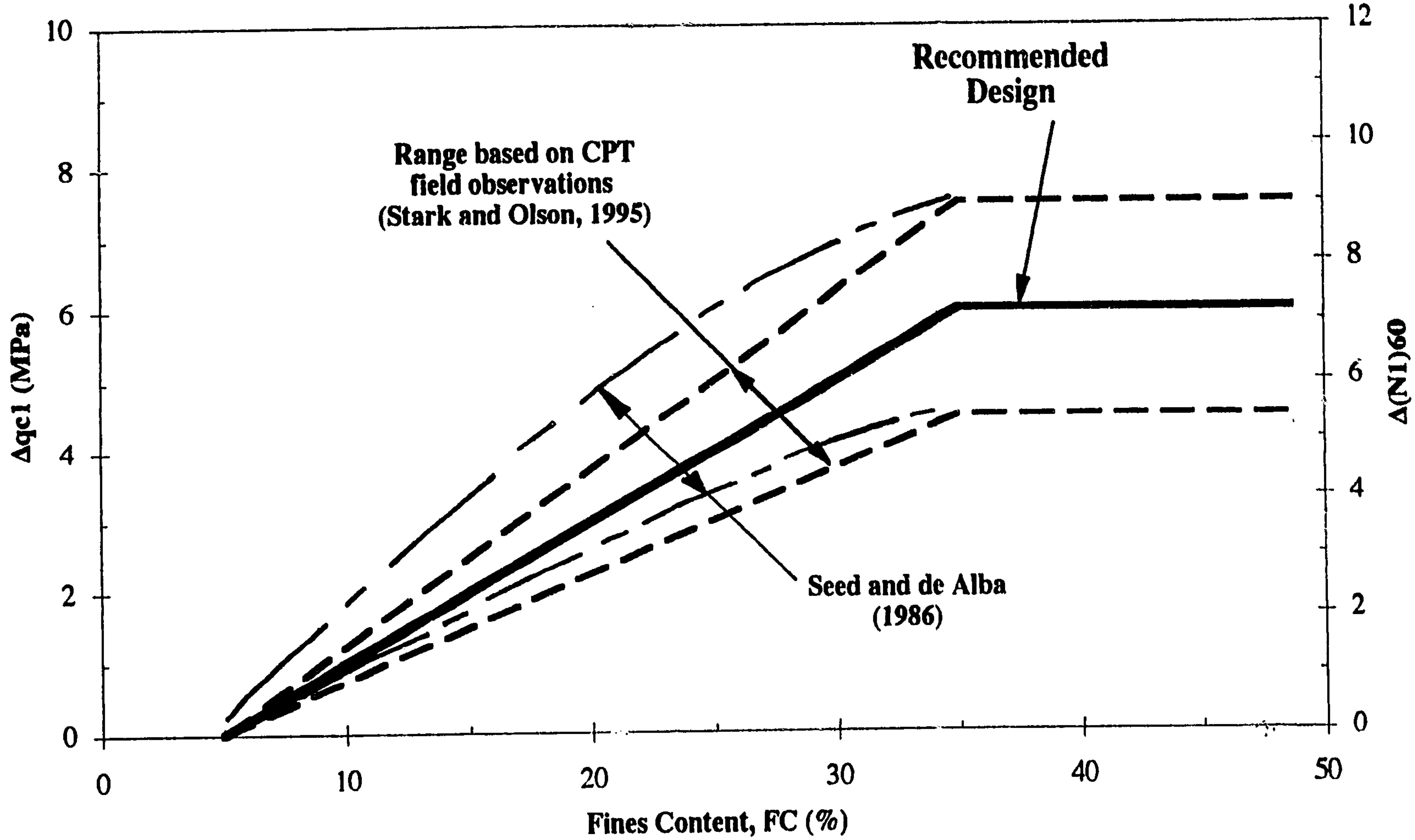

Figure 3-5 Suggested correction for fines content to corrected cone tip resistance based on field performance data.

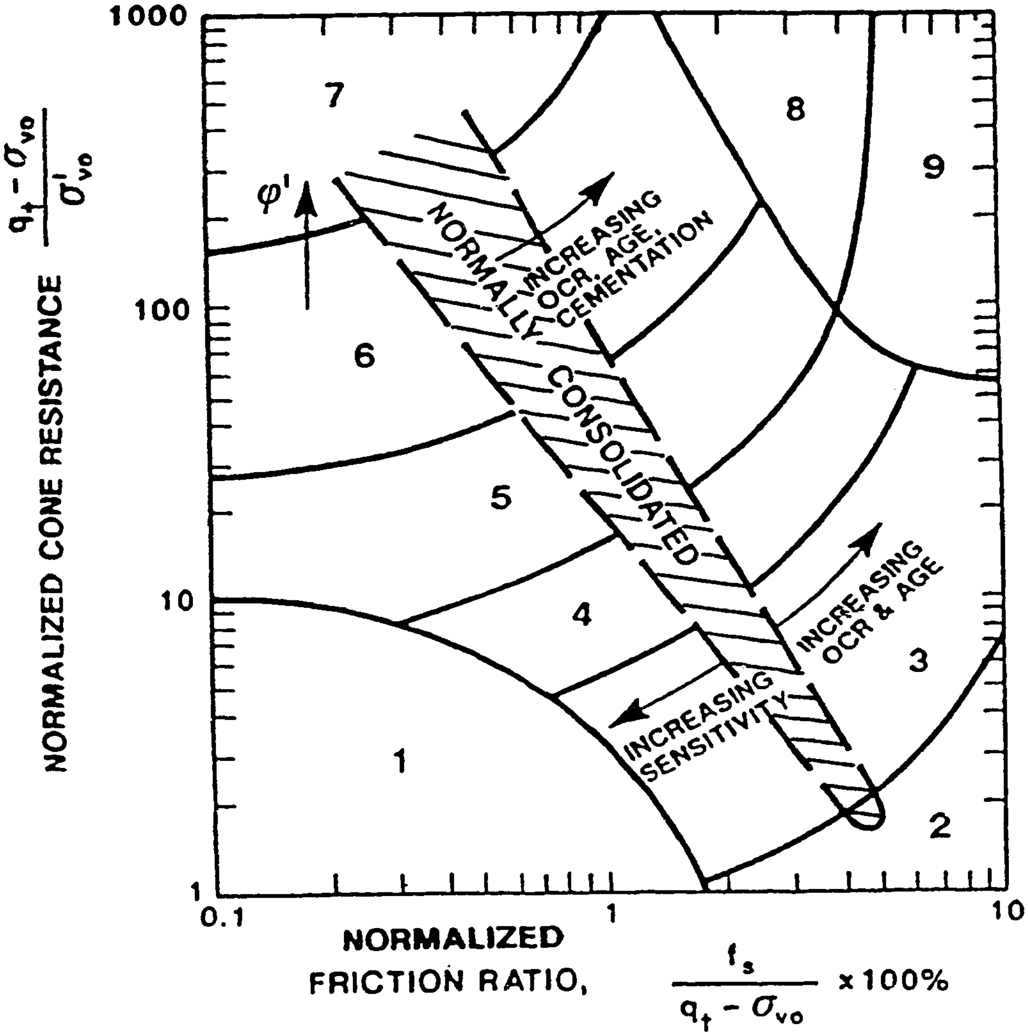

1. SENSITIVE, FINE GRAINED
2. ORGANIC SOILS – PEATS
3. CLAYS – CLAY TO SILTY CLAY
4. SILT MIXTURES – CLAYEY SILT TO SILTY CLAY
5. SAND MIXTURES – SILTY SAND TO SANDY SILT
6. SANDS – CLEAN SAND TO SILTY SAND
7. GRAVELLY SAND TO SAND
8. VERY STIFF SAND TO CLAYEY* SAND
9. VERY STIFF, FINE GRAINED*

(*) HEAVILY OVERCONSOLIDATED OR CEMENTED

Figure 3-6 CPT soil behaviour type chart (modified from Robertson, 1990).

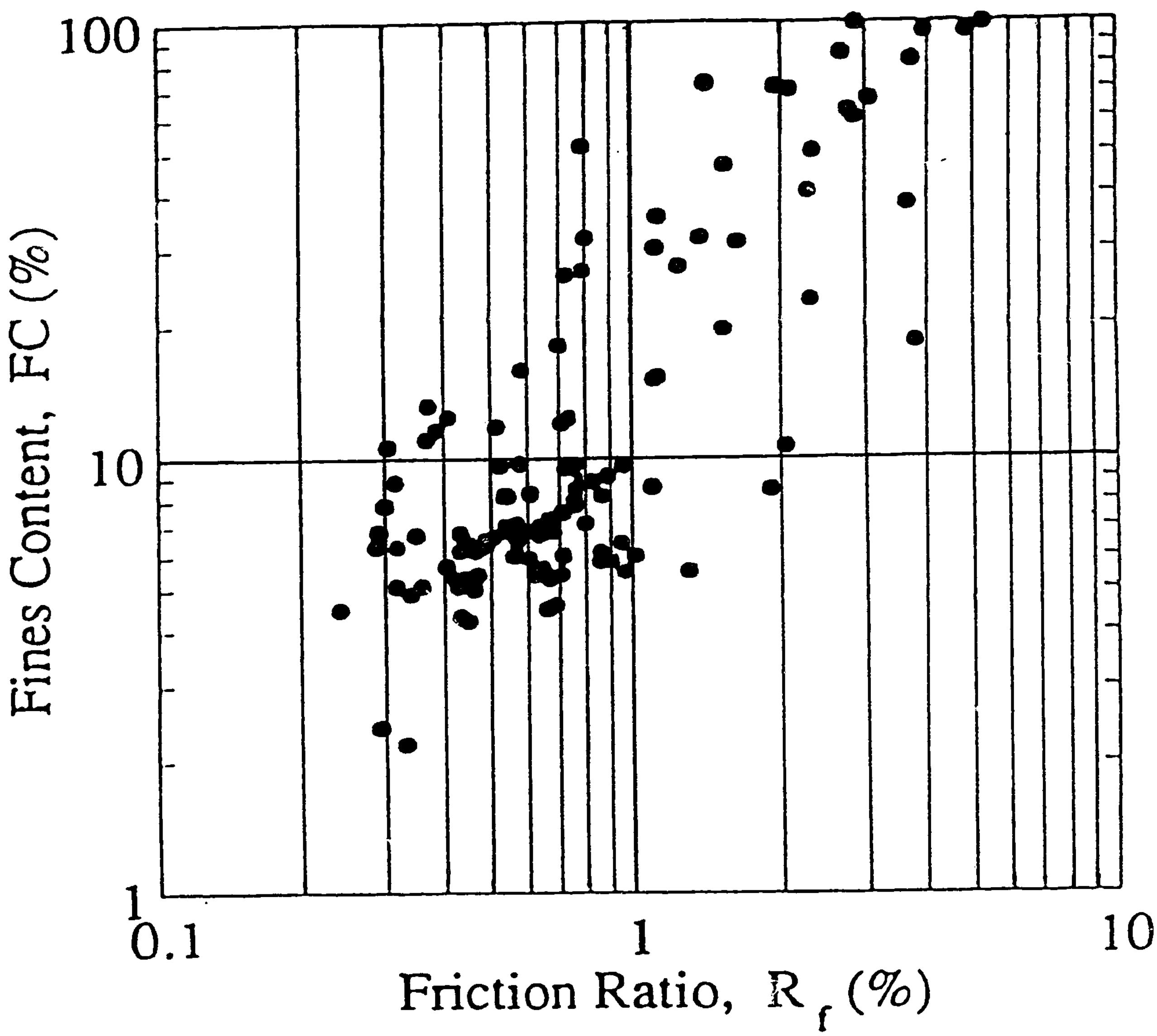

Figure 3-7 Variation of fines content with increasing CPT friction ratio (modified from Suzuki et al., 1995).

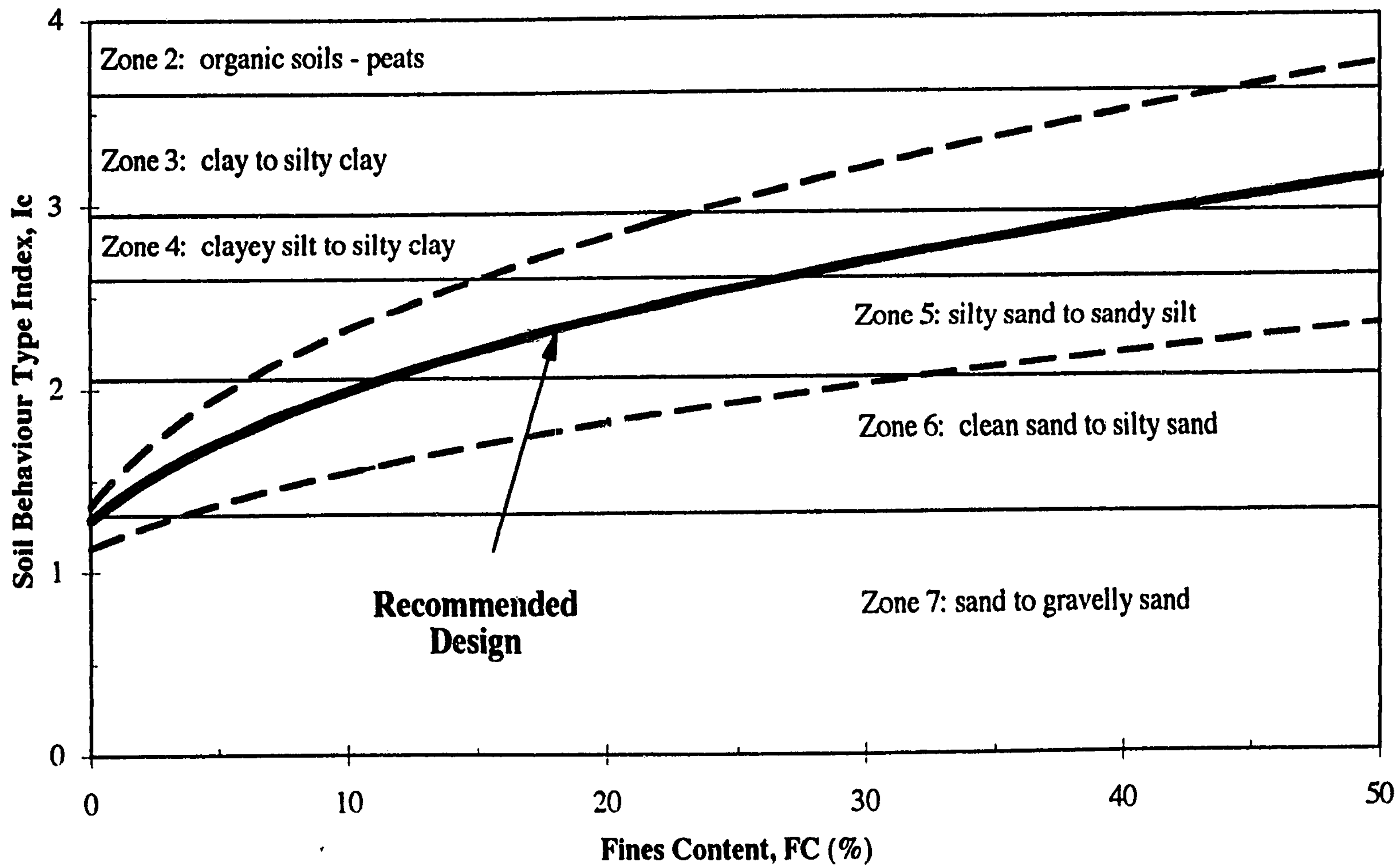

Figure 3-8 Variation of soil behaviour type index (I_c) with fines content.

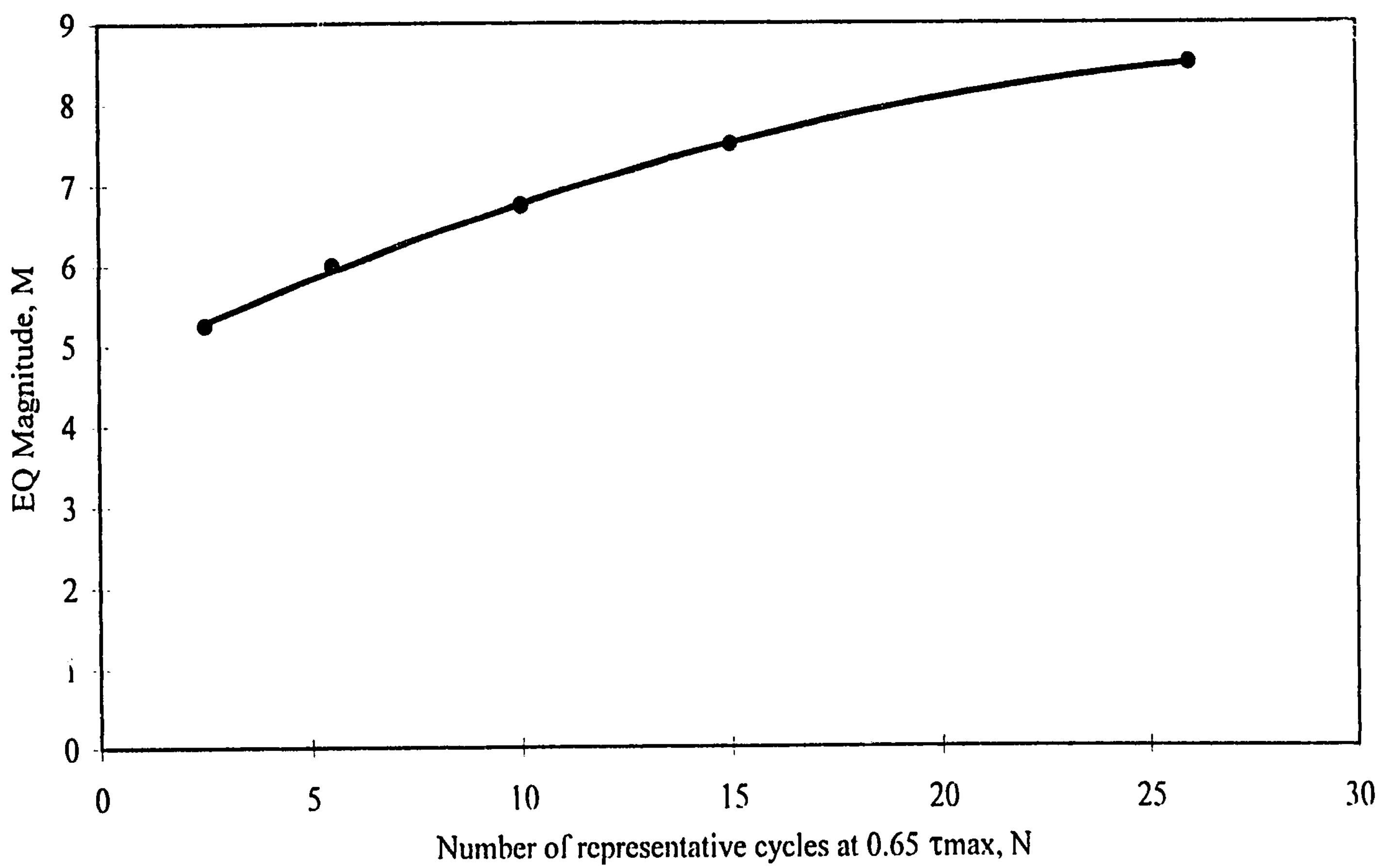

Figure 3-9 Correlation between earthquake magnitude (M) and number of representative cycles at $0.65\tau_{max}$ (N), based on recommendations by Seed et al. (1985).

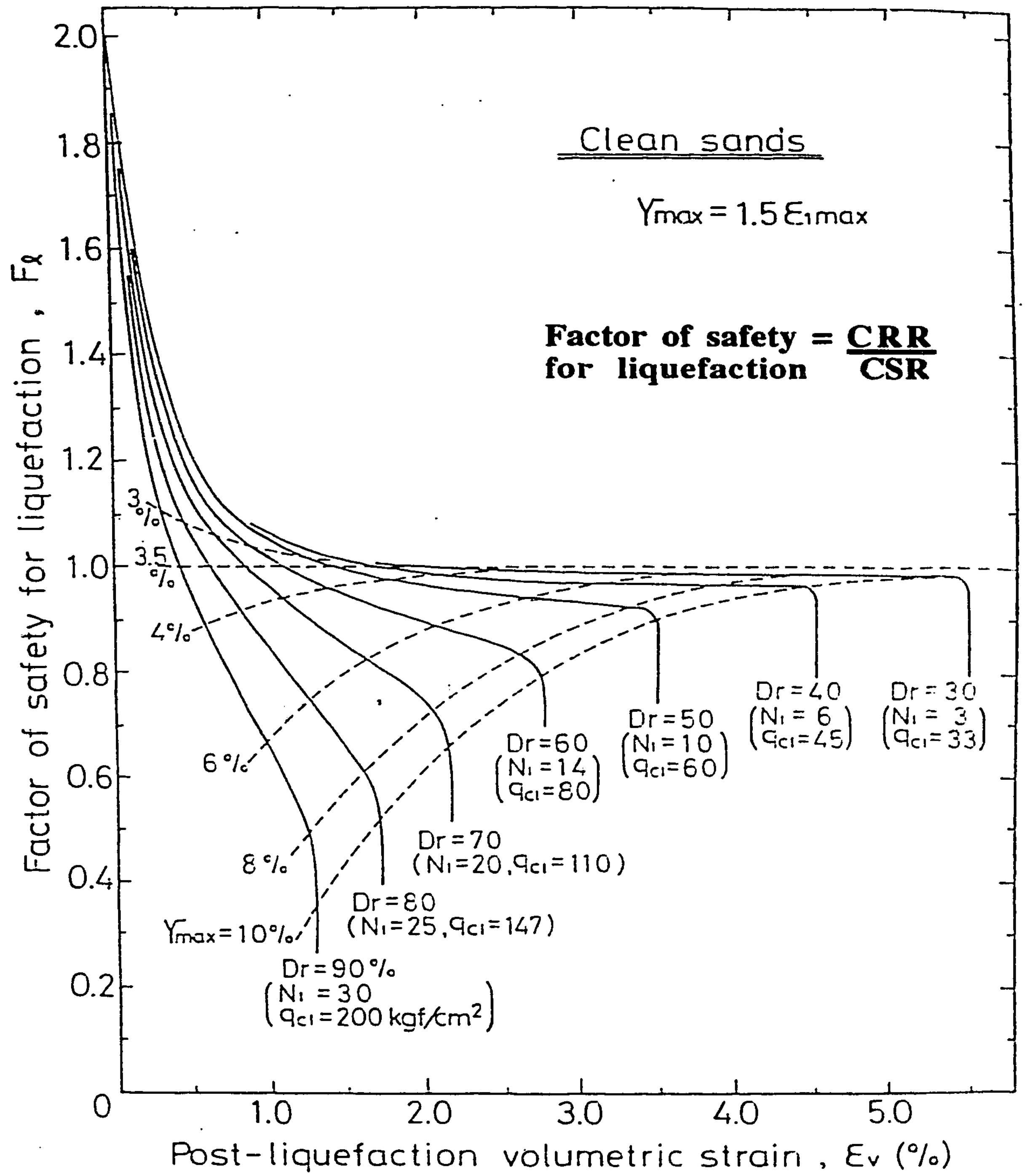

Figure 3-10 Post cyclic liquefaction volumetric and horizontal strain curves using CPT or SPT results (modified from Ishihara, 1993).

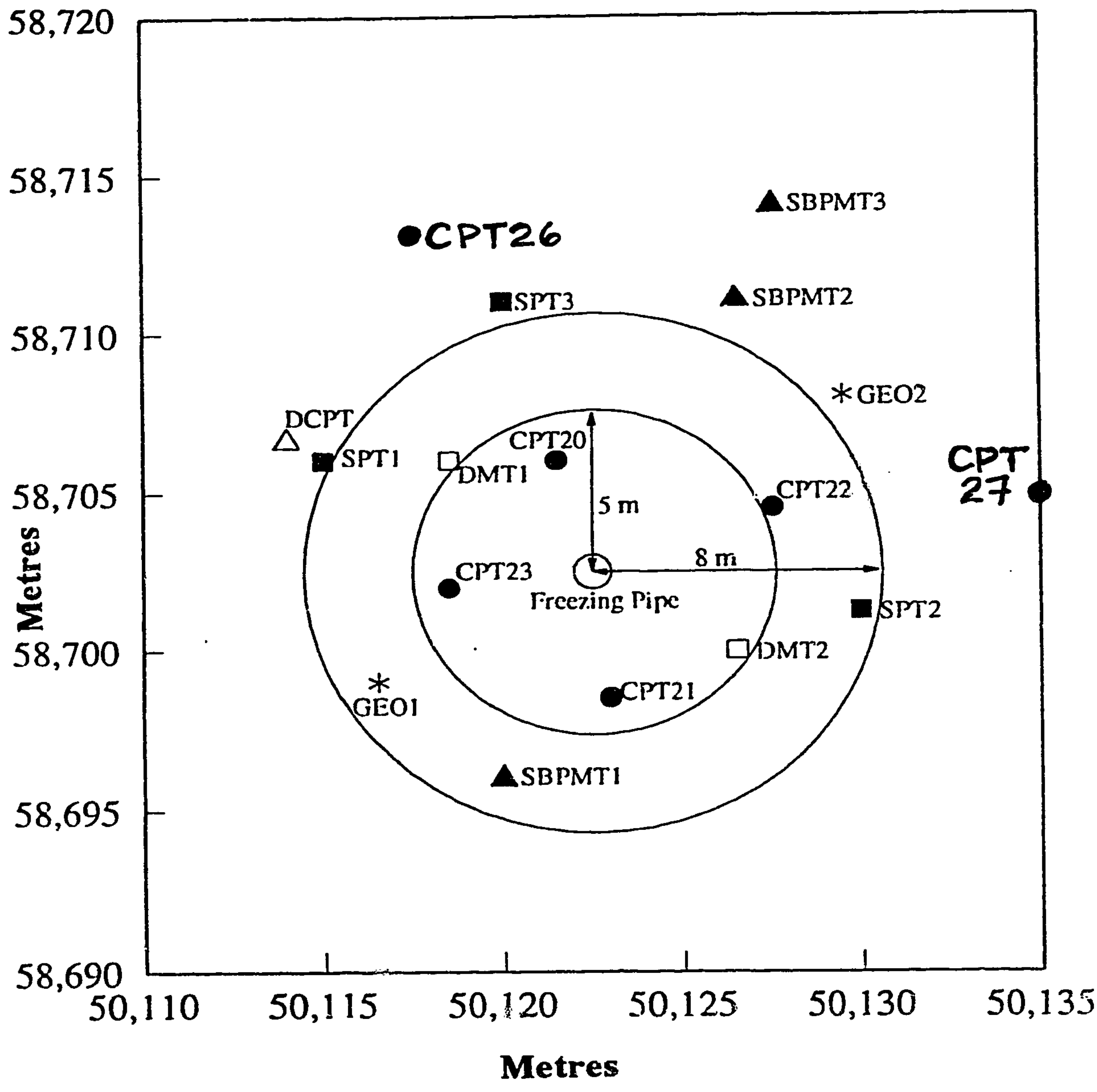

Figure 3-11 Plan of the detailed test site area at the CANLEX Phase III site (J-pit) (modified from Iravani et al., 1996).

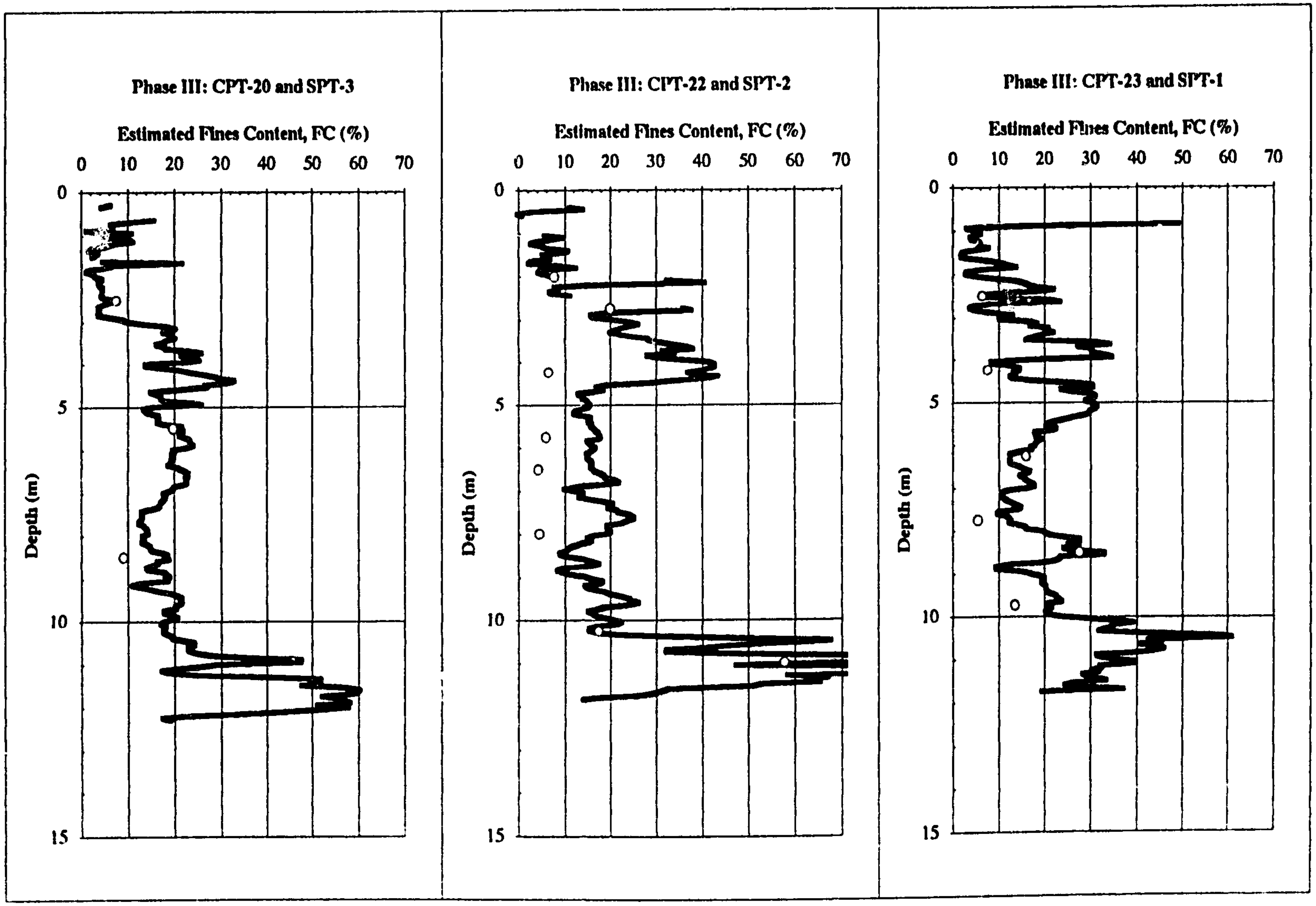

Figure 3-12 Comparison between measured fines contents (from SPT sampler) and those predicted using the CPT for three profiles at the CANLEX Phase III site (J-pit).

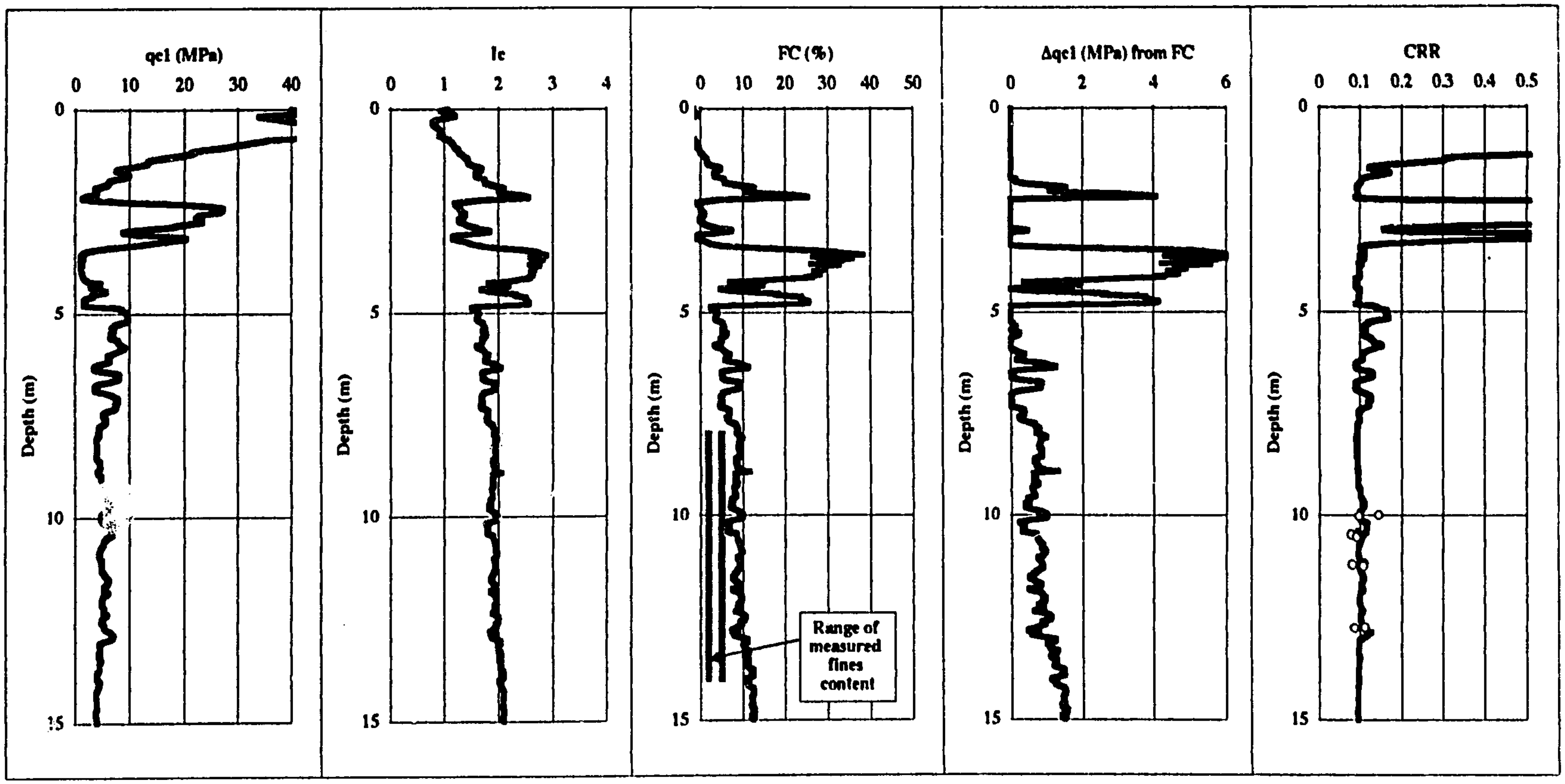

Figure 3-13 Example of applying the integrated CPT method to estimate cyclic resistance ratio (CRR) and comparison with the results of cyclic simple shear tests on in-situ frozen samples from the CANLEX Phase II Massey site.

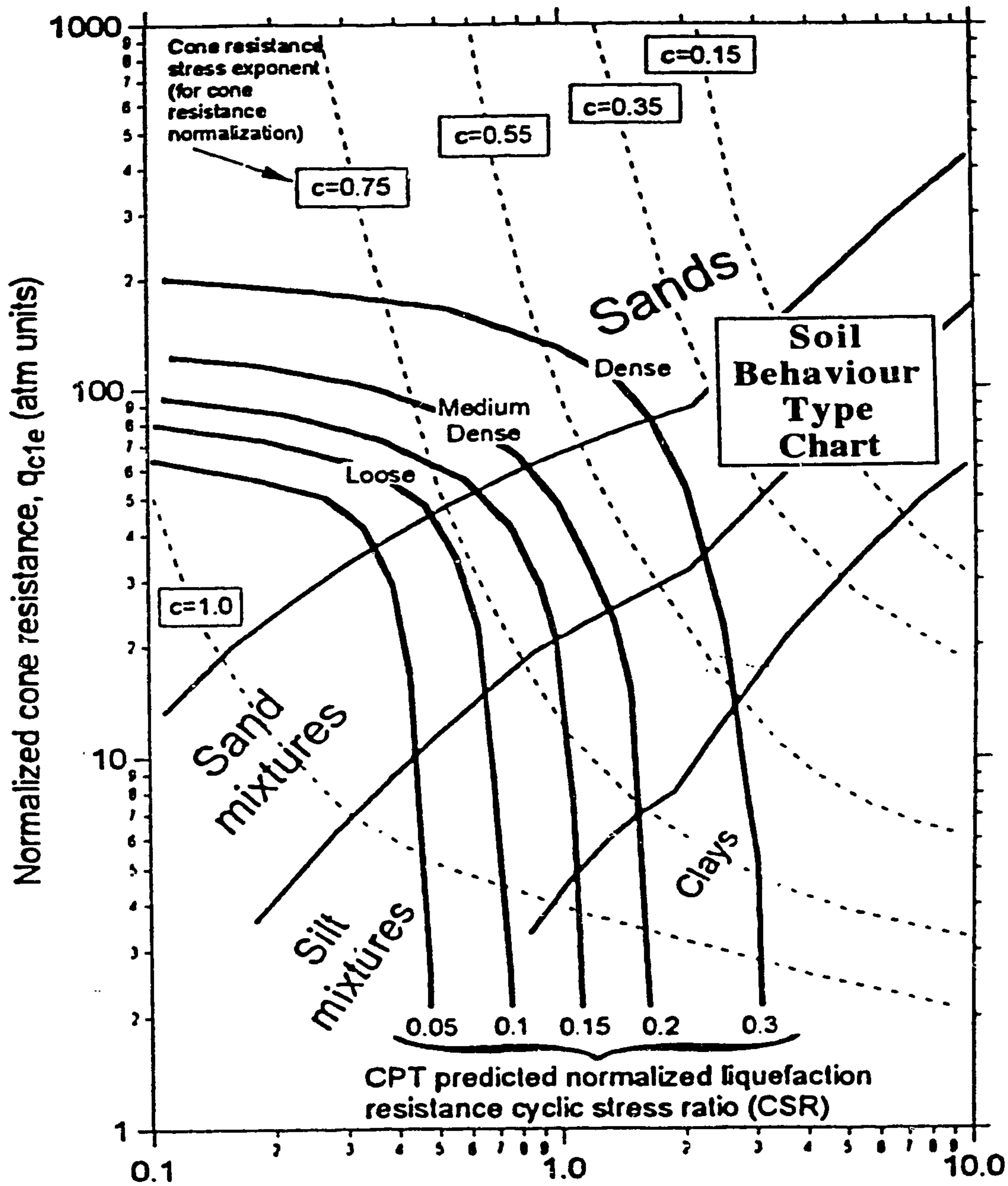

Figure 3-14 Soil behaviour type chart to estimate cyclic resistance ratio (CRR) (modified from Olsen and Koester, 1995).

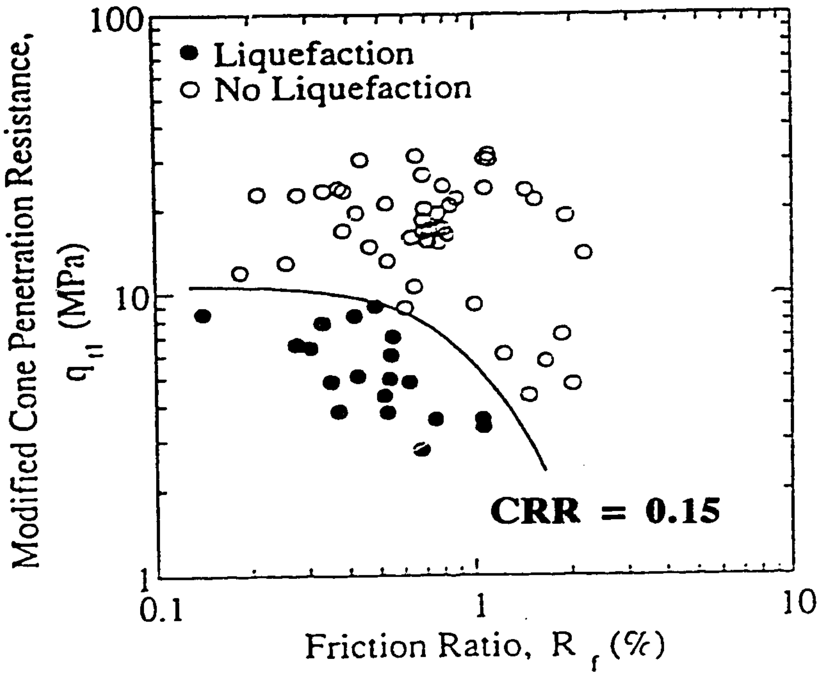

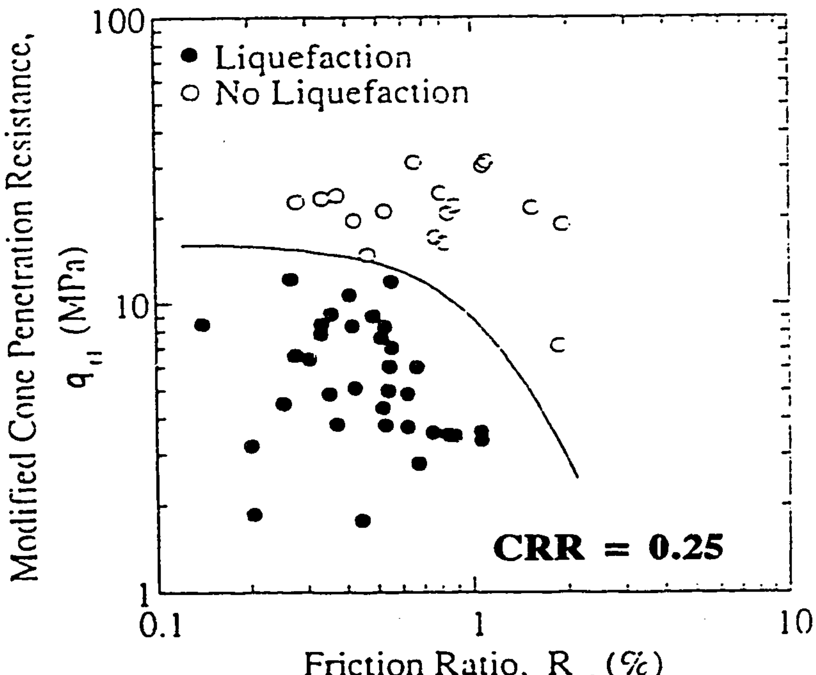

Figure 3-15 Soil behaviour type chart to estimate cyclic resistance ratio (CRR) (modified from Suzuki et al., 1995).

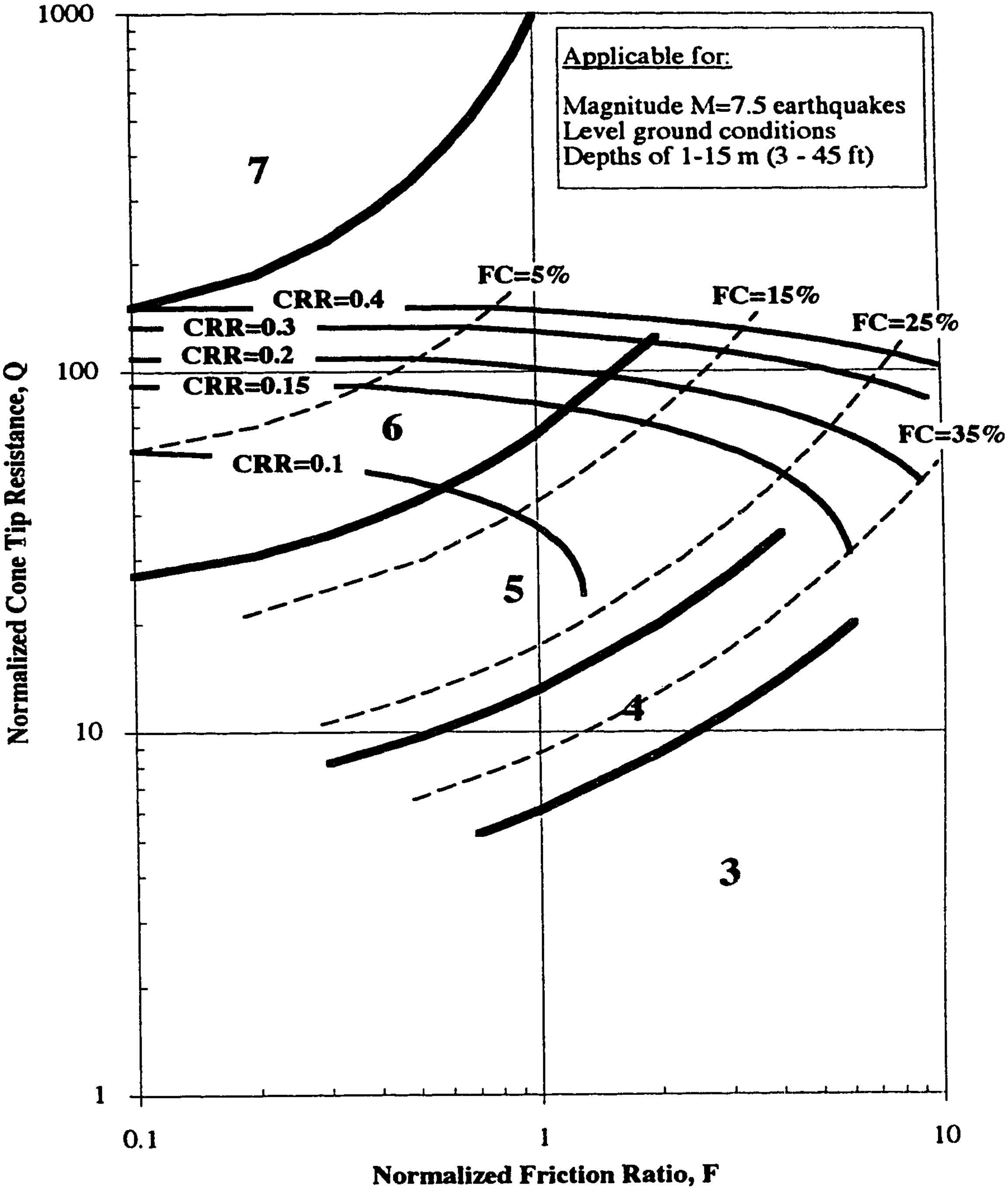

Figure 3-16 Cyclic resistance ratio predicted from Robertson's (1990) soil behaviour type chart based on the integrated CPT method.

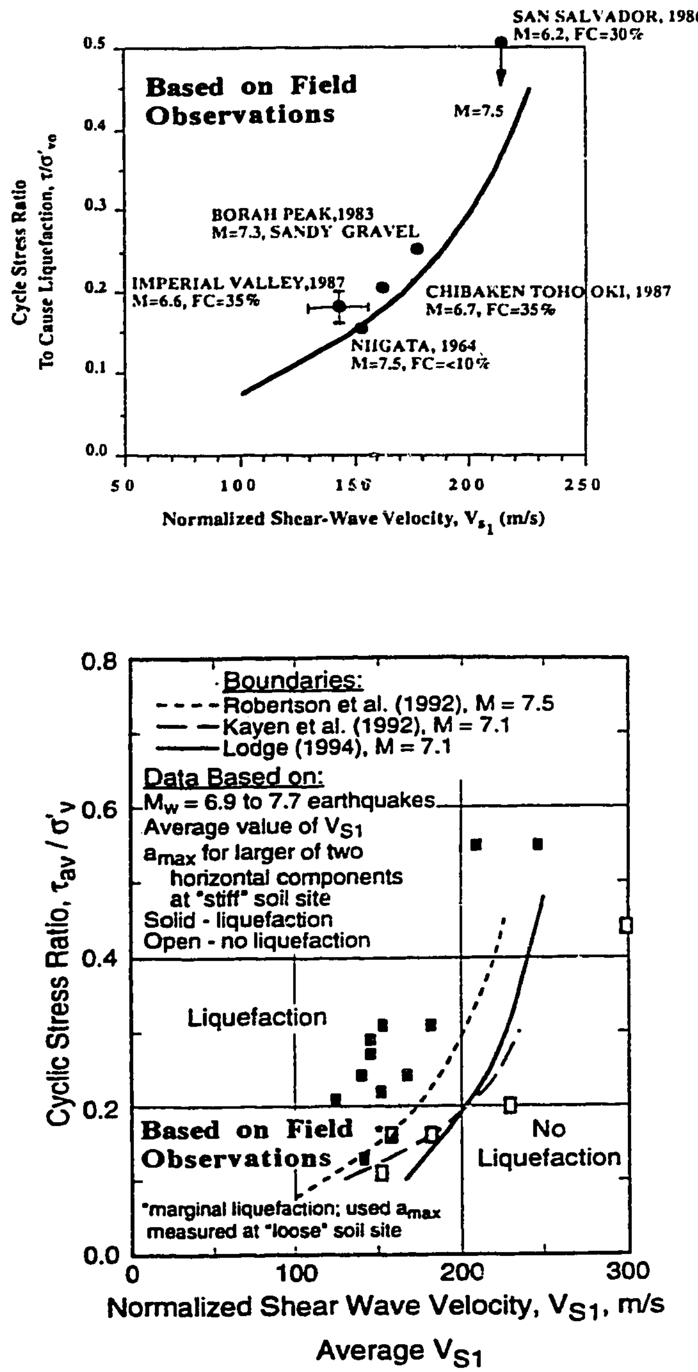

Figure 3-17 Predicting cyclic resistance ratio (CRR) from shear measurements: (a) modified from Robertson et al. (1992) ε Workshop (1996) (modified from Andrus and Stokoe, 1996

References

Andrus, R.D. and Stokoe, K.H. 1996. Guidelines for evaluation of liquefaction resistance using shear wave velocity. *Submission to 1996 NCEER Workshop.*

Bartlett S.F., and Youd, T.L. 1995. Empirical prediction of liquefaction induced lateral spread. *Journal of Geotechnical Engineering,* ASCE 121(4): 316-329.

Fear, C.E. and McRoberts, E.C. 1995. Reconsideration of Initiation of Liquefaction in Sandy Soils. *Journal of Geotechnical Engineering,* ASCE 121(3): 249-261.

Hofmann, B.A., Sego, D.C., and Robertson, P.K. 1994. Undisturbed sampling of a deep loose sand deposit using ground freezing. *Proceedings of the 47th Canadian Geotechnical Conference,* Halifax, Nova Scotia, 287-296.

Hofmann, B.A., and Sego, D.C. 1995. In-situ ground freezing for undisturbed samples of loose sand - Phase II. *Proceedings of the 48th Canadian Geotechnical Conference, Vancouver,* B.C., 197-212.

Iravani, S., Hofmann, B.A., Fear, C., Cyre, G., Lefebvre, M.E., Natarajan, S., Stahl, R., and Robertson, P.K. 1995. General Site Characterization of J-pit Site - Syncrude Canada Ltd., *CANLEX Phase III Activity 3A (General Site Characterization),* University of Alberta.

Ishihara, K. 1993. Liquefaction and flow failure during earthquakes. The 33rd Rankine Lecture, *Géotechnique,* 43(3), 351-415.

Ishihara, K., and Koseki, J. 1989. Cyclic shear strength of fines-containing sands. Earthquake Geotechnical Engineering. *Proceedings of the Discussion Session on Influence of Local Conditions on Seismic Response, 12th ICSMFE,* Rio de Janeiro, 101-106.

Jefferies M.G. and Davies, M.P. 1993. Use of CPTu to estimate equivalent SPT N_{60}. *ASTM Geotechnical Testing Journal,* 16(4): 458-467.

Kayen, R. E., Mitchell, J. K., Lodge, A., Seed, R. B., Nishio, S., and Coutinho, R. 1992. Evaluation of SPT-, CPT-, and shear wave-based methods for liquefaction potential assessment using Loma Prieta data. *Proceedings of the Fourth Japan-U.S. Workshop on Earthquake Resistant Design of Lifeline Facilities and Countermeasures for Soil Liquefaction, Technical Report NCEER-92-0019,* 1, M. Hamada, and T. D. O'Rouke, eds., 177-204.

Kulhawy, F.M., and Mayne, P.W. 1990. Manual on estimating soil properties for foundation design. Cornell University, EL-6800, *Research Project 1493-6,* prepared for Electric Power Research Institute.

Ladd, R.S. 1974. Specimen preparation and liquefaction of sands. *Journal of ASCE*, 110(GT10): 1180-1184.

Lodge, A.L. 1994. Shear wave velocity measurements for subsurface characterization. Ph.D. Dissertation, University of California at Berkeley.

Mitchell, J.K., and Tseng, D.-J. 1990. Assessment of liquefaction potential by cone penetration resistance. *Proceedings, H. Bolton Seed Memorial Symposium*, Berkeley, California, 2, J.M. Duncan (ed.), 335-350.

Mulilis, J.P., Seed, H.B., Chan, C.K., Mitchell, J.K., and Arulanandan, K. 1977. Effects of sample preparation on sand liquefaction. *Journal of ASCE*, 103(GT2): 99-108.

NCEER Workshop 1996. Proceedings to be published at a subsequent date by Youd et al. (1996).

Olsen, R.S., and Koester, J.P. 1995. Prediction of liquefaction resistance using the CPT. *Proceedings of the International Symposium on Cone Penetration Testing, CPT '95*, Linkoping, Sweden.

Olsen, R.S., and Malone, P.G. 1988. Soil classification and site characterization using the cone penetrometer test. *Penetration Testing 1988, ISOPT-1*, De Ruiter (ed.), Balkema, Rotterdam, 2: 887-893.

Robertson, P.K. 1990. Soil classification using the CPT. *Canadian Geotechnical Journal*, 27(1): 151-158.

Robertson, P.K. and Campanella, R.G. 1985. Liquefaction potential of sands using the cone penetration test. *Journal of Geotechnical Division of ASCE*, 22(3): 298-307.

Robertson, P.K. and Campanella, R.G. 1988. *Design manual for use of CPT and CPTu*. Pennsylvania Department of Transportation, (PennDot), 200 p.

Robertson, P.K. and Fear, C.E. 1995. Liquefaction of sands and its evaluation. *IS Tokyo '95, First International Conference on Earthquake Geotechnical Engineering*, Keynote Lecture, 3.

Robertson, P.K., Woeller, D.J., and Finn, W.D.L. 1992. Seismic cone penetration test for evaluating liquefaction potential under cyclic loading. *Canadian Geotechnical Journal*, 29: 686-695.

Seed, H.B., and de Alba, P. 1986. Use of SPT and CPT tests for evaluating the liquefaction resistance of sands. *Use of In-situ Tests in Geotechnical Engineering*, ASCE, Geotechnical Special Publication, 6: 281-302.

Seed, H. B., Tokimatsu, K., Harder, L. F., and Chung, R. 1985. Influence of SPT procedures in soil liquefaction resistance evaluations. *J. Geotech. Engrg.*, ASCE 111(12), 1425-1445.

Sego, D.C., Robertson, P.K., Sasitharan, S., Kilpatrick, B.L., and Pillai, V.S. 1994. Ground freezing and sampling of foundation soils at Duncan Dam. *Canadian Geotechnical Journal*, 31(6): 939-950.

Shibata, T., and Teparaska, W. 1988. Evaluation of liquefaction potentials of soils using cone penetration tests. *Soils and Foundations*, 28(2): 49-60.

Stark, T.D., and Olson, S.M. 1995. Liquefaction resistance using CPT and field case histories, *Journal of Geotechnical Engineering*, ASCE 121(12): 856-869.

Suzuki, Y., Tokimatsu, K., Taye, Y. and Kubota, Y. 1995. Correlation between CPT data and dynamic properties of in-situ frozen samples. *Proceedings of the 3rd International Conference on Recent Advances in Geotechnical Earthquake Engineering and Soil Dynamics*, 1, St. Louis, U.S.A..

Tatsuoka, F., Ochi, K., Fujii, S., and Okamoto, M. 1986. Cyclic undrained triaxial and torsional shear strength of sands for different sample preparation methods. *Soils and Foundations*, 26(3): 23-41.

Tokimatsu, K., and Hosaka, Y. 1986. Effects of sample disturbance on dynamic properties of sand. *Soils and Foundations*, 26(1): 53-64.

Tokimatsu, K., and Yoshimi, Y. 1983. Empirical correlation of soil liquefaction based on SPT N-value and fines content. *Soils and Foundations*, 23(4): 56-74.

Tokimatsu, K., Kuwayama, S., and Tamura, S. 1991. Liquefaction potential evaluation based on Rayleigh wave investigation and its comparison with field behaviour. *Proceedings of the 2nd International Conference on Recent Advances in Geotechnical Earthquake Engineering and Soil Dynamics*, St. Louis, Mo., 1: 357-364.

Vreugdenhil, R., Davis, R., and Berrill, J. 1994. Interpretation of cone penetration results in multilayered soils. *International Journal for Numerical Methods in Geomechanics*, 18: 585-599.

Yoshimi, Y., Hatanaka, M., and Oh-Oka, H. 1978. Undisturbed sampling of saturated sands by freezing. *Soils and Foundations*, 18(3): 105-111.

Yoshimi, Y., Tokimatsu, K., and Hosaka, Y. 1989. Evaluation of liquefaction resistance of clean sands based on high-quality undisturbed samples. *Soils and Foundations*, 29(1): 93-104.

Yoshimi, Y., Tokimatsu, K., and Ohara, J. 1994. In situ liquefaction resistance of clean sands over a wide density range. *Géotechnique*, 44(3): 479-494.

CHAPTER 4

A FRAMEWORK FOR EVALUATING FLOW LIQUEFACTION POTENTIAL AND UNDRAINED RESPONSE BASED ON BOTH LABORATORY AND IN-SITU TESTING[1,2]

4.1 Introduction

Flow liquefaction can occur only in strain-softening soils. If sufficient material strain-softens and the driving stresses are greater than the ultimate undrained strength, flow liquefaction can lead to large deformations. Figure 4-1 illustrates how the response of a sand under undrained monotonic loading is a function of the initial state of the material relative to the ultimate state line (USL). If the initial state of the sand is sufficiently loose, the material will strain-soften directly to ultimate state; this is the definition of flow liquefaction. If the initial state of the sand is sufficiently dense, the material will strain-harden directly to ultimate state; such material cannot experience flow liquefaction, but may be susceptible to cyclic softening (liquefaction) depending on the size and duration of cyclic loading. Limited strain-softening (LSS) can occur when the initial state of the sand is close to the ultimate state line. Such material will experience a temporary loss in strength as it strain-softens to a quasi-steady state (QSS) before strain-hardening to ultimate state. As long as the strains that occur while the material is passing through the QSS (minimum strength) point are small, this type of soil response would be expected to result in only limited deformations, not catastrophic flowslides. However, this is an area of continuing research; further studies are required to investigate the in-situ importance of the QSS point observed in the laboratory. From studies on Toyoura sand, Ishihara (1993) concluded that every type of sand has a unique ultimate state (in terms of void ratio and mean normal effective stress) at large strains, which is independent of drainage conditions and initial soil fabric, but that the QSS is a function of both the initial state and soil fabric.

Figure 4-1 illustrates how a strain-softening response can be triggered by monotonic undrained loading. However, this is only one type of trigger than can lead to such a

[1] *A version of part of this chapter has been published. Fear, C.E., Robertson, P.K., Hofmann, B.A., Sego, D.C., Campanella, R.G., Byrne, P.M., Davies, M.P., Konrad, J.-M., Küpper, A., List, B.R., and Youd, L. 1995. Summary of CANLEX Phase 1 Site Characterization, Proc. of the 48th Canadian Geotechnical Conference, Vancouver, B.C., 331-340.*

[2] *A version of part of this chapter has been published. Robertson, P.K. and Fear, C.E. 1995. Liquefaction of sands and its evaluation, Proceedings of IS Tokyo '95, First International Conference on Earthquake Geotechnical Engineering, Keynote Lecture.*

response if the state of the soil is sufficiently loose. A strain-softening response can also be triggered by undrained cyclic loading, a q=constant stress path and even drained loading, as long as the stress path leads to the collapse surface, as indicated in Figure 4-1. Once the collapse surface is reached, the material will strain-soften to ultimate state. This chapter examines methods for determining flow liquefaction potential based on in-situ testing and presents a framework for linking the in-situ state with the estimated response. Undrained monotonic loading is examined in particular, because undrained monotonic triaxial tests (compression and extension) were performed at each of the Canadian Liquefaction Experiment (CANLEX) sites. Additional details regarding one of the CANLEX sites illustrating the link between laboratory response and field predictions will be presented in Chapter 8.

4.2 Void Ratio Interpretations from In-Situ Testing

The first step in any liquefaction analysis should be to estimate the in-situ state of the soil to determine if flow liquefaction is possible (i.e. if the soil is strain-softening in undrained shear). Void ratio is an important component of soil state and is a key factor that affects the response of a sand to either undrained monotonic or cyclic loading. When truly undisturbed samples of sand are obtained from the field (e.g. using ground freezing techniques), it is possible to measure the total void ratio of each sample in the laboratory. However, it is not always possible to obtain undisturbed samples and interpreting void ratio profiles from in-situ testing provides an alternative approach. The CANLEX sites are unique in that the interpreted void ratio profiles can be compared directly with the measured void ratios of the frozen samples. Additional details will be given in Chapter 8.

4.2.1 Conventional methods

Figure 4-2 presents a flowchart outlining the various in-situ tests and the conventional methods of estimating in-situ void ratio from the CPT, SPT, V_s measurements and geophysical logging. Methods for interpreting the CPT and SPT are conventionally based on estimating relative density using empirical formulae and then estimating void ratio using e_{max} and e_{min}. The shear wave velocity and geophysical methods estimate void ratio directly.

a) CPT

The conventional interpretation of void ratio from the CPT for unaged, uncemented sands follows the work by Baldi et al. (1986), as shown in Figure 4-3. This method consists of first estimating profiles of relative density (D_r) using the following relationship:

$$[4\text{-}1] \qquad D_r = \left(\frac{1}{C_2}\right) \ln\left(\frac{q_c}{C_0(\sigma_v')^{C_1}}\right)$$

where:
q_c = measured cone tip resistance
σ_v'= vertical effective stress
C_0, C_1 and C_2 = material constants

The relationship given by Equation 4-1 was developed for Ticino sand, based on calibration chamber studies by Baldi et al. (1986). Ticino sand consists of approximately 95% quartz and 5% feldspar, with an average fines content of less than 5%. Index parameters for Ticino sand are as follows: e_{max}=0.89, e_{min}=0.52, G_s=2.67, and C_u = 1.13 (D_{60}/D_{10} = 0.65/0.40). If the sand to be analyzed has grain characteristics similar to those of Ticino sand, the values of material constants given in Figure 4-3 can be selected, as follows: C_0=157, C_1=0.55 and C_2=2.41 (applicable for K_o=0.45). Void ratio profiles can then be estimated, based on the estimated profiles of D_r, the values of e_{max} and e_{min}, and the following equation:

$$[4\text{-}2] \qquad e = e_{max} - D_r\,(e_{max} - e_{min})$$

b) SPT

The conventional interpretation of void ratio from the SPT for unaged, uncemented sands follows the work by Skempton (1986). This method consists of first estimating profiles of D_r using the following relationship:

$$[4\text{-}3] \qquad \frac{(N_1)_{60}}{D_r^{\,2}} = \text{constant}$$

Most sites at which flow liquefaction is an issue consist of loose young sands. When applying Equation 4-3 to such sites, a constant of 40 can be selected as being representative of loose, young sands. Void ratio profiles can then be estimated, based on the estimated profiles of D_r, the values of e_{max} and e_{min}, and Equation 4-2.

c) Shear wave velocity

Cunning et al. (1995) found that the primary factors controlling values of measured shear wave velocity for unaged, uncemented sands was void ratio and stress level. When shear wave velocity measurements were corrected for effective overburden pressure (i.e. V_{s1}), Cunning et al. (1995) found that V_{s1} and void ratio were related as illustrated in Figure 4-4 and given by the following equation:

[4-4] $$V_{s1} = (A - Be)\, K_o^{\,0.125}$$

where:
A and B = constants for a given sand
e = void ratio
K_o = coefficient of earth pressure at rest (from self-boring pressuremeter interpretation)
V_{s1} is in m/s and given by the following equation:

[4-5] $$V_{s1} = V_s \left(\frac{P_a}{\sigma_v'}\right)^{0.25}$$

where:
V_{s1} = corrected shear wave velocity
V_s = measured shear wave velocity
P_a = atmospheric pressure, typically 100 kPa
σ_v' = vertical effective stress, in kPa.

The shear wave velocity method is attractive because, for a given K_o, it estimates void ratio directly, rather than first estimating D_r; however, there is scatter in the correlation (see Figure 4-4) as the data tend to fall within a band. Global values of A and B can be used to describe this band; alternatively, specific values of A and B can be estimated for each individual sand. The D_r-based methods of interpreting the CPT and SPT depend on e_{min} and e_{max} to estimate void ratio. The validity of these terms are sometimes questionable, particularly in silty sands, which can result in difficulties in interpreting void ratio. In addition, the correlations based on penetration resistance from the SPT and CPT are affected by other factors such as soil compressibility. Shear wave velocity, on the other hand, is little influenced by factors such as soil compressibility.

Figure 4-4 was prepared by measuring shear wave velocity in the laboratory using bender elements during different stages of isotropic consolidation (i.e. K_o=1.0) of reconstituted samples. The data all fit within a band, suggesting that global values of A and B apply to all sands. However, for an individual sand, the parameters A and B are estimated by fitting a line to the data for the particular sand. It is important to note that because A and B are estimated from laboratory testing of reconstituted samples, the relationship given in Equation 4-4 is applicable only to young, recently deposited uncemented sands. However, many real deposits of sand are old and have experienced aging effects. Superimposed on Figure 4-4 are values of V_{s1}, as measured in the field, and corresponding average values of void ratio for the Phase I and Phase II CANLEX sites. It is not completely correct to directly compare the field ($K_o \approx 0.5$) and laboratory data (K_o=1) on the same plot because of the difference in K_o conditions (see Equation 4-4). However, the resulting error is typically less than 10%.

Based on Figure 4-4, Robertson et al. (1995) suggested that aging has the effect of increasing the measured shear wave velocity for a given void ratio and proposed a correlation between aging and the difference in V_{s1} measured in the field as compared to laboratory values for unaged sand. This correlation is shown in Figure 4-5; the relationship is tentative and, as additional data becomes available, could be modified. Since the relationship between V_{s1} and void ratio (as given in Equation 4-4) is approximately linear for a given K_o over typical ranges of void ratio, the change in measured V_{s1} in the field due to aging can be incorporated as a correction added to the parameter A (as determined in the laboratory) in Equation 4-4. This, in essence, shifts the relationship between V_{s1} and void ratio upwards on the plot in Figure 4-4, so that for a measured V_{s1}, void ratio in the field is not underpredicted. Aging also has a small effect on penetration resistance from the CPT and SPT (Skempton, 1986; Kulhawy and Mayne, 1990).

d) Geophysical logging

Geophysical logging can also be used to directly estimate void ratio. In simple terms, the following relationship can be used:

[4-6]
$$e = \frac{(G_s - \rho_b)}{(\rho_b - 1)}$$

where:
G_s = specific gravity of the soil
ρ_b = corrected bulk density of the soil.

The corrected bulk density of the soil can be determined from the results of geophysical logging using modified geophysical interpretations proposed by Plewes et al. (1988).

4.2.2 Correlations between in-situ tests

Comparisons between in-situ test methods are useful for examining for consistency between test signatures. Conversion factors between in-situ tests can also be used to convert one type of in-situ test signature to the equivalent signature of another type of in-situ test. This can allow for estimation of void ratios from the SPT or CPT using a direct void ratio method rather than a conventional D_r-method. Comparisons between the CPT, SPT and V_s profiles in the target zone were made and the appropriate conversion factors between in-situ tests were estimated.

In order to compare the various in-situ test signatures, the results should first be corrected for effective overburden pressure. The measured shear wave velocity, V_s, should be corrected to V_{s1} using Equation 4-5. The measured CPT tip resistance, q_c, should be corrected for effective overburden stress using the following equation:

[4-7] $$q_{c1} = q_c \left(\frac{P_a}{\sigma_v'}\right)^{0.5}$$

where:
q_{c1} = corrected tip resistance
q_c = measured tip resistance
P_a = atmospheric pressure, typically 100 kPa
σ_v' = vertical effective stress, in kPa.

The measured SPT N-value should be corrected for effective overburden stress and energy effects using the following equation:

[4-8] $$(N_1)_{60} = N \left(\frac{P_a}{\sigma_v'}\right)^{0.5} \left(\frac{ER}{60}\right)$$

where:
$(N_1)_{60}$ = corrected tip resistance
N = measured tip resistance
P_a = atmospheric pressure, typically 100 kPa
σ_v' = vertical effective stress, in kPa
ER = measured energy ratio, in percent.

The conventional conversion between corrected SPT and corrected CPT is in terms of the ratio $q_{c1}/(N_1)_{60}$. This ratio is a function of the soil type and typically has values ranging from 0.3 to 0.6 (when q_{c1} is in MPa), corresponding to soil types ranging from sandy silts to gravelly sands, respectively.

Based on earlier work by Robertson et al. (1992), the relationship between corrected shear wave velocity and corrected CPT tip resistance can be approximated by the following equation (see Chapter 5 as well):

[4-9] $$q_{c1} = \left(\frac{V_{s1}}{Y}\right)^4$$

where:
q_{c1} = corrected tip resistance, as given in Equation 4-7, in MPa
V_{s1} = corrected shear wave velocity, as given in Equation 4-5, in m/s
Y = conversion factor between CPT and V_s, in (m/s)/(MPa)$^{0.25}$.

Robertson et al. (1995) looked at various sands, including Fraser River sand, and investigated the effects of compressibility (represented by the slope of the ultimate state line (USL), λ_{ln}) on the value of Y, as indicated in Figure 4-6. There appears to be a relationship (which is influenced by aging) between Y and λ_{ln}. Increasing the compressibility of a sand decreases the measured q_{c1}, while having little effect on the measured V_{s1}. Values of Y appear to range from approximately 90 for relatively incompressible sands to 140 for compressible sands. Aging appears to have a greater effect on the measured V_{s1}, but little effect on the measured q_{c1}, with the result being that Y increases with age (Robertson et al., 1995).

Based on a modified version of the work by Yoshida et al (1988), a similar relationship can be developed between corrected shear wave velocity and corrected SPT blowcount as follows (see Chapter 5 as well):

[4-10] $$(N_1)_{60} = \left(\frac{V_{s1}}{X}\right)^4$$

where:
$(N_1)_{60}$ = corrected SPT blowcount, as given in Equation 4-8
V_{s1} = corrected shear wave velocity, as given in Equation 4-5, in m/s
X = conversion factor between SPT and V_s, in 1/(MPa)$^{0.25}$.

Note that, theoretically, the ratio $(X/Y)^4$ should equal to the ratio $q_{c1}/(N_1)_{60}$. Small differences between the field estimated average $(X/Y)^4$ and average $q_{c1}/(N_1)_{60}$ in a soil deposit at a given site would be expected due to the different intervals over which the various terms are estimated and averaged. Shear wave velocity measurements are typically step functions averaged over 1 m intervals, SPT measurements reflect a 1 foot (30 cm) interval and are usually measured at a depth of every 5 feet, while CPT measurements provide an essentially continuous profile, with measurements typically taken every few centimetres.

4.2.3 Shear wave velocity based method

As discussed previously, the shear wave velocity method provides a direct estimate of void ratio. The conventional CPT or SPT methods are indirect and are sensitive to the values of e_{min} and e_{max} as well as soil compressibility. However, combining Equation 4-4 (which links V_{s1} and void ratio) with the conversion factors Y and X (as defined in Equations 4-9 and 4-10) allows for more direct methods of interpreting void ratio from the CPT and SPT, respectively. The advantage of using the CPT is that its continuous nature allows for a more detailed profile of estimated void ratio within a given soil deposit.

Combining Equations 4-4 and 4-9 results in the following equation which allows for direct estimates of void ratio to be made based on profiles of CPT q_{c1} without having to first estimate D_r:

[4-11] $$q_{c1} = \left(\frac{(A - Be)\, K_o^{0.125}}{Y}\right)^4$$

Likewise, combining Equations 4-4 and 4-10 results in the following equation which allows for direct estimates of void ratio to be made based on profiles of SPT $(N_1)_{60}$ without having to first estimate D_r:

[4-12] $$(N_1)_{60} = \left(\frac{(A - Be)K_o^{0.125}}{X}\right)^4$$

Both the conventional and shear-wave velocity methods of interpreting void ratio from the CPT and SPT will be applied to one of the CANLEX sites and the results will be compared in Chapter 8. Void ratio can also be estimated from the CPT based on state parameter, Ψ (Been and Jefferies, 1992). However, a knowledge of the ultimate state line is required to convert state parameter to void ratio. Details of this approach are given in the next section.

4.3 General Concepts of the Proposed Framework

4.3.1 Critical state soil mechanics

Considerable evidence suggests that the response of sands can be described within a critical state framework similar to that applied to clay soils (e.g. Atkinson, 1993; Coop et al., 1995). The collapse surface approach (Sladen et al., 1985a) to flow liquefaction analysis resides within a critical state soil mechanics framework. The ultimate state line (USL) for a given sand and a given direction of loading (e.g. triaxial compression or triaxial extension) can be plotted in p'-q-e space (see Figure 4-7a), where e is void ratio and p' (mean normal effective stress) and q (deviator stress) are defined as follows:

[4-13] $$p' = \frac{1}{3}(\sigma_1' + 2\,\sigma_3')$$

[4-14] $$q = \sigma_1' - \sigma_3'$$

The USL is controlled by the grain characteristics of the soil. Along the USL, q and p' are related by M, which is a function of friction angle and direction of loading. Theoretical values of M for triaxial compression (M_C) and triaxial extension (M_E) are given by the following equations (Wood, 1990):

[4-15] $$M_C = (q_{us}/p'_{us})_C = \frac{6\sin\phi'_{us}}{3 - \sin\phi'_{us}}$$

[4-16] $$M_E = (q_{us}/p'_{us})_E = \frac{6\sin\phi'_{us}}{3 + \sin\phi'_{us}}$$

where:
ϕ'_{us} = ultimate state friction angle.

When the USL in p'-q-e space is projected onto the e-p' plane and the p' axis is plotted on a logarithmic scale, the USL can be approximated as a straight line over a given stress range (see Figure 4-7b). Been et al. (1991) showed that, in the e-p' plane critical state are the same condition and are independent of the stress path this ultimate state. Therefore, the various USLs in p'-q-e space project c in the e-p' plane. In theory, the USL in the e-p' plane can be defined o range by two parameters, Γ and λ_{ln}. Γ is the void ratio on the USL at p' the slope of the USL when the p' axis is plotted on a natural logarithm s the e-ln p' plane is therefore defined as follows:

[4-17] $$e = \Gamma - \lambda_{ln} \ln (p')$$

However, p' may not be the correct stress invariant to use. Eventually suitable to simply use the Mohr-Coulomb failure criterion (which is in intermediate principal stress), as previously suggested by Casagrande 1975). Nevertheless, proceeding with the use of p', in e-p' space, soils loose of the USL could strain soften at large strains, while soils dense strain harden at large strains. Soils that have initial void ratios close to th limited strain softening (LSS) response to monotonic loading, in that they to a quasi-steady-state (QSS) before eventually, at large strains, dilating (US) (see Figure 4-1). For some sands, very large strains are required to some cases, conventional triaxial equipment may not reach these large str

The response of a sand in undrained monotonic loading is a function Figure 4-8 illustrates that, in addition to void ratio (e) and initial mean stress (p'_i), several other factors will also influence the response of direction of loading (e.g. triaxial compression versus triaxial extension), fabric, aging, cementation), soil compressibility, and initial deviator desirable to eliminate one or more of the factors in order to observe the e major factors. Void ratio and p'_i can be combined in terms of state proposed by Been and Jefferies (1985), based on earlier work Bassett (1965), relative to a reference ultimate state line (USL) in e-ln difference between the initial void ratio of the sample and the void rati USL at the same value of p', e_{us} (see Figure 4-7b), as given by the follo

[4-18] $$\Psi = e - e_{us} = e - [\Gamma - \lambda_{ln} \ln (p')]$$

When Ψ=0, the initial state of the soil falls on the USL, in e-p' space. S

b) Been and Jefferies (1992)

Based on critical state soil mechanics theory outlined above, state parameter (Ψ) could be a useful indicator of flow liquefaction potential, provided there is a reliable method of predicting its value within a soil deposit. Been and Jefferies (1992) developed a method, based on earlier work by Been and Jefferies (1985) and Been et al. (1987), for estimating the state parameter of a soil deposit, directly from the CPT, based on calibration chamber testing. Some uncertainty exists over the corrections made for chamber size effects. In particular, since the correlations were determined mostly by testing relatively dense sand, for which large corrections had to be made, and the resulting correlations were extrapolated into the range of loose sands, there is uncertainty in the resulting correlations for loose sands. In addition, Sladen (1989) questioned the uniqueness of the relationship between Ψ and normalized CPT penetration resistance proposed by Been and Jefferies (1987) and suggested that stress effects had not been properly accounted for in the proposed relationship.

Nevertheless, different soil types were examined by Been and Jefferies (1992) and the estimation of Ψ was found to be a function of the friction angle (i.e. M) and the slope of the USL (λ_{log}) of the sand deposit, as shown in Figure 4-10. The following equation was proposed to estimate Ψ:

[4-20] $$q^* = k^* \exp(-m^* \Psi)$$

where:

[4-21] $$q^* = Q_p/(1 - B_q)$$

[4-22] $$Q_p = (q_c - p_o)/p'_o$$

[4-23] $$k^* = M\,(3 + 0.85/\lambda_{log})$$

[4-24] $$m^* = 11.9 - 13.3\lambda_{log}$$

Note that λ_{log} is the slope of the USL in e-p' space, when the p' axis is plotted on a logarithm base 10 scale; $\lambda_{log} = 2.302\lambda_{ln}$. It is very important, when comparing values of λ for various sands to be consistent in how λ is defined. The value of B_q is typically very close to zero in sandy soils. Therefore, q^* and Q_p can be considered to be equal in sandy soils, without significant error. The work was based on consideration of loading in triaxial compression; therefore M can be taken as equal to M_C.

In Chapter 8, this set of equations is applied to the CPT data at one of the CANLEX sites, for comparison with other methods of evaluating state. Been and Jefferies (1992) proposed that Ψ=0 represented the dividing line between material that could liquefy and that which could not.

c) Plewes et al. (1992)

Plewes et al. (1992) expanded upon the work by Been et al. (1987) by estimating contours of state parameter directly on the CPT soil classification chart as proposed by Jefferies and Davies (1991), as shown in Figure 4-11. Note that this soil classification chart normalizes cone tip resistance in a linear manner using mean normal stresses (p and p') rather than vertical stresses (σ_v and σ_v') as in the soil classification chart by Robertson (1990) that was used for the integrated CPT method in Chapter 3; i.e. Q_p (see Equation 4-22) rather than Q. CPT field data (in terms of normalized cone tip resistance and sleeve friction) can be superimposed on this figure in order to estimate the in-situ state of a sandy deposit. Soils with Ψ>0 are considered to be susceptible to liquefaction, given a suitable trigger mechanism.

4.3.3 Reference stress ratio (RSR) approach

State parameter, if estimated accurately, is one method for estimating the potential for flow liquefaction. However, the applicability of Ψ is limited predominantly to estimating the dividing line between states which are susceptible to flow liquefaction (i.e. Ψ>0) and those which are not (i.e. Ψ<0), over a limited stress range in a single sand deposit. The actual value of Ψ can not be correlated to response of a sand to monotonic undrained loading when dealing with either a large stress range in one sand or when trying to compare different sands. For a single straight reference USL in e-ln p' space (i.e. constant λ_{ln}), samples with constant values of Ψ would have similar undrained responses. However, in general, the USL for any given sand is curved (Ishihara, 1993; Sasitharan et al. 1994) and the slope, λ_{ln}, increases with increasing p'. Even in the same stress range, different sands have different USLs with different values of λ_{ln}. As shown in Figure 4-12, two sands may have the same state parameter relative to their individual USLs, but behave very differently in undrained shear, as a result of the different λ_{ln} value associated with each USL. The sand with the flatter USL will respond in a more brittle manner and will have a lower ultimate shear strength. Therefore, a constant value of Ψ does not imply similar responses in undrained loading for a given stress path due to the changing value of λ_{ln}.

An alternative measure of the initial state of a sample, which encompasses the effects of λ_{ln}, is the ratio p'_i/p'_{us} (see Figure 4-12) where p'_i is the initial mean normal effective stress of the sample and p'_{us} is the value of p' on the reference USL at the same void ratio. In e-ln p' space, Ψ and p'_i/p'_{us} are related by the slope of the USL, λ_{ln}, as follows:

$$[4\text{-}25] \qquad \frac{p'_i}{p'_{us}} = \exp\left(\frac{\Psi}{\lambda_{ln}}\right) = \text{Reference Stress Ratio (RSR)}$$

Note that when RSR=1, Ψ=0. The slope of the USL, λ_{ln}, is related to the grain characteristics of the material. The grain characteristics influence the compressibility of the sand skeleton. Thus, by combining e, p' and compressibility, the impact of the other factors such as direction of loading, structure and stress anisotropy can be examined more easily. Under a given direction of undrained monotonic loading, samples with the same soil structure and consolidation stress state and with the same value of RSR would be expected to respond in the same way (Sladen et al. 1985a). Identifying initial state by RSR relative to a selected reference USL provides a consistent framework that can be extended to other sands which have different USLs with different values of λ_{ln}. In Chapter 8, this ratio is used at one of the CANLEX sites to characterize Fraser River sand. In general, as RSR increases, a material is weaker and more brittle in response, when loaded undrained.

The concepts introduced here are not new, but rather, draw on the ideas of other researchers, as reported in the literature. Based on Mohr-Coulomb failure criteria, Casagrande (e.g. Casagrande, 1975) suggested characterizing a sand by a ratio between the initial effective confining pressure (σ'_3) and that at the liquefied state. Sladen et al. (1985a) proposed a relationship between brittleness index (one aspect of response) and RSR for Nerlerk sand with various fines contents and Leighton Buzzard sand, suggesting that "brittleness index is a reasonably unique function of initial p'/p'us for all sands and hence of state parameter for a given sand". McRoberts and Sladen (1992) suggested plotting laboratory stress path results in terms of q/p'_{us} and p'/p'_{us} to compare different tests. Cuccovillo and Coop (1993) plotted stress paths for triaxial compression tests on intact calcarenite in this manner. The ratio p'/p'_{us} represented a measure of the state of the soil relative to its ultimate state. Ishihara (1993) proposed a similar type of reference stress ratio, which he termed "initial state ratio" (r_c), relating the initial state of a soil to the quasi steady state (QSS) line in terms of the initial consolidation p' and the stress on the QSS line (p'_s), at the same void ratio. Ishihara (1993) noted that "this ratio is a parameter of prime importance for characterizing the undrained behaviour of sand".

It is interesting to note that the RSR concept for characterizing the state of sand is not unlike the method used to define state for clay. Overconsolidation ratio (OCR) can be expressed as the stress ratio relating the current p' to the maximum past p'. The only difference between RSR and OCR is that the latter is referenced to the virgin consolidation line, while the former is referenced to the USL because individual sands do not have unique consolidation lines. With increasing OCR, a clay becomes stronger and responds in a less brittle manner, when loaded undrained. Two samples of clay with the same OCR are expected to respond in a similar manner. OCR for a clay can be converted to RSR, based on the relationship between isotropic OCR and state parameter proposed by Plewes et al. (1992), as follows:

[4-26] $$\log(RSR) = \frac{\Psi}{\lambda_{log}} = \log(r) - \Lambda\log(OCR)$$

The term r represents the spacing between the USL and the virgin consolidation line and Λ is the critical state plastic hardening ratio. For most clays, $r \approx 2.3$ and $\Lambda = 0.8$ (Plewes et al., 1992). The RSR concept is, therefore, a global approach that could be applied to both sands and clays.

4.4 Application of the Proposed Framework

4.4.1 Field determination of RSR

Figure 4-13 (a modified version of Figure 4-2) outlines the various in-situ tests and the direct methods of estimating void ratio from the CPT, SPT, shear wave velocity measurements and geophysical logs, as explained earlier in this report. Note that the method of estimating void ratio for the SPT and CPT shown in Figure 4-13, is the V_s-based method. However, any reliable method of estimating void ratio from in-situ testing could be used. Once in-situ void ratios and stress conditions are estimated, in-situ profiles of RSR relative to the reference USL can be estimated. Following the flowchart in reverse, profiles of CPT, SPT, V_s or geophysical void ratios that represent an RSR of 1 could be back-calculated and superimposed over raw field logs. In-situ state (as estimated by in-situ testing) could then be compared to the reference USL (which, by definition, corresponds to RSR=1).

4.4.2 Laboratory determination of RSR

Figure 4-14 presents a flowchart outlining the various methods of preparing reconstituted samples and testing in the laboratory. Moist tamped samples tend to be looser for the same stress conditions and thus have higher values of RSR than water pluviated samples. Air pluviated samples have intermediate values of RSR. The magnitude of RSR, consolidation state (hydrostatic or K_o), soil structure and direction of loading govern the observed stress-strain response in terms of brittleness, strength, strain and stress ratio. The same factors govern the response of undisturbed samples. Triaxial and simple shear tests were performed at the CANLEX sites (further details for one of the sites are given in Chapter 8); only methods for interpreting triaxial data are presented here, due to the complexity and uncertainty of interpretation of simple shear test results. It is felt, based on the results of hollow cylinder testing on samples of Syncrude sand, that triaxial compression and triaxial extension represent the two loading condition extremes (Vaid et al., 1995). Vaid et al. (1995) concluded that the response in simple shear would therefore be predicted to fall between that in triaxial compression and that in triaxial extension.

Previous tests on Syncrude sand as part of Phase I of the CANLEX project (Vaid et al., 1995) have shown that anisotropically consolidated samples have a different stress-strain response to undrained loading than do isotropically consolidated samples. The results illustrated the importance of testing samples (reconstituted or undisturbed) under the in-situ K_o conditions. Studies reported by Georgiannou et al. (1990) resulted in similar conclusions. Anisotropic stress states that model in-situ conditions in loose sand ($Ko \approx 0.5$, based on the CANLEX test sites) have the effect of preloading a sample in compression. Therefore, less additional load is required for failure in compression that in extension. In extensional loading, the sample has to first be unloaded from the initial stress state before any strain-softening can possibly occur.

Reconstituted samples, even when tested anisotropically, may have different responses to undrained loading due to different methods of sample preparation. As a result, testing undisturbed samples that capture the in-situ state not only in terms of density and stress, but also in terms of soil structure is important. Direction of loading also has an effect on the response to undrained loading. Thus, it is also important to test samples under the direction(s) of loading appropriate to the in-situ conditions. Tests presented in Chapter 8 for one of the CANLEX sites are triaxial compression and extension tests predominantly on undisturbed samples under anisotropic initial stress conditions corresponding to K_o=0.5. However, a few tests were performed on reconstituted samples.

4.4.3 Laboratory response

In order to model in-situ sand behaviour, stress-strain relations are required. The undrained stress-strain response of any sample, when tested in the laboratory, can be characterized by various components. The key components identified here are: brittleness, minimum strength, strain that occurs while at minimum strength, strength at the end of the test (generally represents the ultimate strength), stress ratio (M=q/p') at peak and at the end of the test. Figures 4-15 and 4-16 illustrate the method of quantifying the various components of response for triaxial compression and extension, respectively.

Brittleness is defined in terms of the parameter termed brittleness index (I_B) which is defined as follows:

[4-27a] $$I_B = \frac{S_p - S_{min}}{S_p - S_i}$$ for triaxial compression

[4-27b] $$I_B = \frac{S_p - S_{min}}{S_p + S_i}$$ for triaxial extension

where:
S_p = magnitude of the peak shear strength
S_{min} = magnitude of the minimum shear strength
S_i = magnitude of the initial static shear stress.

Note that the formulae for brittleness index are slightly different for triaxial compression and extension for anisotropic samples ($S_i > 0$) and relate to the incremental stresses required to trigger failure from the initial stress state. For isotropic tests ($S_i = 0$), the two formulae become identical and simplify to the conventional definition of brittleness index (Bishop, 1971) which was based on isotropic testing. If sufficient straining occurs during the test, the end of the test represents the ultimate state (US) conditions. If the test does not experience a QSS, then the minimum strength and the end of test strength are assumed to be the same. A brittleness index of zero indicates a material that is strain-hardening.

Strain-hardening materials have equal peak, minimum and end-of-test strengths. A brittleness index greater than zero indicates a material that either strain-softens directly to US or experiences limited strain softening to a quasi-steady state (QSS) before dilating to US. The latter will generally have a smaller brittleness index than the former.

Based on critical state soil mechanics, a theoretical method for estimating the ultimate undrained shear strength for soils that are susceptible to flow liquefaction was proposed by Fear and Robertson (1995). Details are given in Chapter 5. However, the basic concept was that for a soil with a given void ratio, assuming no pore pressure redistribution and therefore no change in void ratio, the ultimate undrained shear strength (S_{us}) could be calculated within the critical state soil mechanics framework. An element of soil will travel along a stress path in an undrained plane with constant void ratio until it reaches the USL (see Figures 4-1 and 4-7). The value of p' on the USL (p'_{us}) at the given void ratio can be determined from the parameters Γ and λ_{ln}, using Equation 4-17. The ultimate undrained shear strength (S_{us}=0.5 q_{us}) at this point is related to p'_{us} by M. Fear and Robertson (1995) expressed the equation for S_{us} in terms of state parameter (Ψ) and λ_{ln}, assuming a single straight USL for a given sand over a given stress range (see Chapter 5). A more global approach, as explained previously, is to make use of RSR which is a function of Ψ and λ_{ln} (see Equation 4-25). Combining all of these relationships gives the following equation for theoretically estimating the ultimate undrained strength ratio of an element of soil:

[4-28] $$\frac{S_{us}}{p'_i} = \frac{M}{2} \bullet \frac{1}{RSR}$$

Note that M has different values in compression and extension (see Equations 4-15 and 4-16). Dividing Equation 4-15 by Equation 4-16, it can be concluded that for typical friction angles, ϕ'_{us}, ranging from 30° to 40°, the value of M_C ranges from 1.40 to 1.54 times the value of M_E. Therefore, this theoretical method would predict approximately 40% to 50% higher ultimate undrained shear strengths in compression than in extension, for the same RSR. Actual differences between the undrained response in triaxial compression and extension may also be partially due to the inherent material anisotropy of sands (Arthur and Menzies, 1972). If pore pressure redistribution occurs in the field, loosening a sand deposit from its original conditions, this method may overpredict the ultimate undrained strength.

For sands that are very loose and strain-soften immediately to ultimate state, the ultimate undrained strength is the key to estimating the consequences of flow liquefaction in terms of slope stability and predicting resulting deformations. However, it appears that many sandy soils, while not being sufficiently loose to be completely strain-softening, do demonstrate limited strain-softening. When loaded undrained, these soils strain-soften temporarily to a quasi-steady-state (QSS) before dilating to ultimate state. The undrained strength associated with the QSS point (S_{min}) can be significantly smaller than the ultimate undrained strength. Provided that the strains associated with passing through the point of QSS are small, it could be argued that it is only the final ultimate strength which is of concern and which is generally large for these soils relative to completely strain-softening soils. However, the issue of QSS and whether or how to incorporate it into design analysis are areas of continuing debate.

For the one CANLEX site given as a worked example in Chapter 8, both S_{min}/p'_o and S_f/p'_o are shown for all tests. S_f is the end-of-test strength, which is generally less than or equal to the ultimate strength (as the stress path may be still moving towards ultimate state at the end of the test). For tests with a QSS, S_{min} is less than S_f; for tests with no QSS, S_{min} and S_f are taken to be the same, the end-of-test strength. Based on limited laboratory results from Phase II of the CANLEX project, it was found that, on an e-ln p' plot, the QSS points appear to fall approximately along a parallel line to the USL (details are given in Chapter 8). As a result, assuming that q and p' are still related by M along the QSS line (QSSL), Equation 4-28 can be modified to theoretically estimate the undrained strength ratio at QSS (S_{min}/p'_i), as follows:

$$[4\text{-}29] \qquad \frac{S_{us}}{p'_i} = \frac{M}{2} \bullet \frac{1}{(RSR + \Delta RSR)}$$

The term ΔRSR corresponds to the horizontal shift on the e-ln p' plot between the USL and the QSSL. ΔRSR is computed as the ratio of p' on the USL to p' on the QSSL, at the same void ratio. Ishihara (1993), based on work on Toyoura sand, stated that a given sand will have a unique USL, because the soil is completely remoulded by the time US is reached, but may have several different QSSLs which are a function of soil fabric and which may or may not be completely parallel to the USL. Therefore, it can be expected that the QSS points for reconstituted samples of a given sand may plot differently than those for undisturbed samples. Conversely, if the QSS points for undisturbed samples from similar sands at different sites plot similarly, it could be concluded that the two sites have a similar soil fabric. It is logical that within any one uniform soil deposit, there could be one soil fabric and, hence, a unique QSSL.

The theoretical predictions of ultimate undrained strength and strength at QSS will be compared to the actual values measured in the laboratory on undisturbed and reconstituted samples at one of the CANLEX sites in Chapter 8.

4.4.4 Linking in-situ characterization and laboratory response

Figure 4-17 outlines the interaction between field characterization of a deposit and the response of samples of sand in the laboratory. Ideally, one would like to characterize a deposit using in-situ tests such as CPT, SPT, V_S, geophysical logging or pressuremeter testing, and be able to predict the in-situ response to loading. Undisturbed samples, when tested undrained in the laboratory, will produce a certain response, in terms of brittleness, strength, strain and stress ratio. The key to linking the observed laboratory response to the in-situ response is to be able to correlate a particular signature from an in-situ test with laboratory results for certain initial conditions and thus be able to estimate the in-situ response. It is postulated that this objective can be achieved by determining the RSR for each sample, relative to a reference USL in e-ln p' space, prior to subjecting the sample to undrained loading and observing its response. Likewise, the signatures from the CPT, SPT, V_S or geophysical logging can be converted into profiles of RSR relative to the same reference USL, using methods outlined in Cunning et al. (1995) and Fear and Robertson (1995). Therefore, RSR, defined relative to a reference USL, can serve to link field characterization to laboratory response, for a particular sand.

Chapter 8 compares the observed relationship between the minimum and end-of-test strength ratio components of response and RSR for undisturbed samples tested in the laboratory with the theoretical relationships presented in Equations 4-28 and 4-29. In addition, tentative relationships between the other components of response (brittleness, axial strain at minimum strength, etc.) and RSR are proposed in Chapter 8 for one of the CANLEX sites. When laboratory testing for all of the CANLEX sites is completed, it will be possible to confirm if these relationships between the various components of response and RSR are general in nature and applicable to a variety of sands. Careful selection of the reference USL is important if different sands are to be compared.

4.4.5 Selecting a reference ultimate state line (USL)

There may be significant scatter to data resulting from monotonic triaxial laboratory tests under different directions of loading (Vaid et al., 1990) and drawing a unique USL for all of the tested samples may be difficult. However, testing on both Syncrude sand and Fraser River sand, as part of the CANLEX project, has shown that the data at ultimate state for a given sand fall within a band. Therefore, the reference USL can be selected as any line parallel to this band. The critical issue is to use the same reference USL when interpreting both field and laboratory data in order to provide a consistent link between in-situ test signatures and response.

Generally, if monotonic tests on loose sands are taken to large enough strains, the end of each test represents the US condition; however, in some cases, tests may appear to have been stopped before they had strained sufficiently to reach US. Samples that do reach US in undrained loading are generally very loose and strain soften without experiencing a QSS (e.g. reconstituted samples prepared by moist tamping and therefore having high values of RSR). Samples that are denser and experience a QSS are ultimately dilating towards US when the tests are stopped. Samples that are dilating have a high propensity for pore water redistribution (i.e. changing void ratio) and/or shear band development. Hence, interpretation of stress, strains and void ratio become uncertain. In some cases, tests cannot be strained any further due to equipment limitations. The mixture of samples that reach US and those which are still moving towards US may partially explain the apparent observation of a band of data for the end-of-test conditions on an e-ln p' plot. It is advisable to select the reference USL based on the loosest samples which clearly reach US, in order to have a reference line that is as close as possible to the true USL (Castro, 1969).

Figure 4-18 presents USLs for a variety of sands as reported in the literature and tabulated by Sasitharan et al. (1994). It is clear from Figure 4-18 that the USL for most sands curves at high stresses. Ishihara (1993) also indicated that the USL is curved in nature. Approximating a curved USL by a bi-linear relationship is convenient in that the USL can be broken down into straight line portions over various stress ranges (corresponding to various void ratio ranges), with each portion having an associated Γ and λ_{ln}. In order to estimate RSR for a particular element of soil, the portion of the USL which has a void ratio range that includes the void ratio of the element must be used as the reference USL. In other words, the mean normal effective stress of the element, p'_i, must be divided by the mean normal effective stress at the same void ratio on this portion of the USL, p'_{us}, to estimate RSR. To determine p'_{us}, the value of Γ and λ_{ln} corresponding to the appropriate portion of the USL must be used.

4.5 Conclusions and Recommendations

This chapter has outlined both existing and new methods of estimating the void ratio and state of a sandy soil deposit. Conventional methods of estimating state (i.e the method by Sladen and Hewitt (1989) versus the method by Been and Jefferies (1992)) often give different conclusions regarding liquefaction potential. In addition, the conventional methods, although they may give reasonable dividing lines for liquefaction potential, are not good for estimating the response of a soil to undrained monotonic loading. The RSR-based framework suggested here allows for a direct estimation of soil response by linking in-situ characterization with the laboratory response of undisturbed samples. The framework can be applied on a site-specific basis, but as additional data becomes available, the ultimate goal of future studies would be to develop a global method of estimating in-situ response directly from in-situ testing without the need for undisturbed samples. This would be useful for low risk projects for which obtaining undisturbed samples is beyond the project scope and budget or for initial site screening of high risk projects.

Chapter 8 presents a worked example, based on detailed field and laboratory studies at one of the CANLEX sites, illustrating the step-by-step application of the framework outlined here and comparing the resulting predictions of void ratio and soil state with the predictions using existing methods. As will be seen in Chapter 8, the individual components of response clearly appear to be a function of the magnitude of RSR. Tentative relationships are given for the CANLEX site presented in the worked example and specific details regarding the proposed framework and how to apply it are discussed further.

The framework proposed here is capable of estimating flow liquefaction potential and the subsequent elements of response of a deposit of sand. However, whether a slope or soil structure will fail and slide depends on a number of factors, including the amount of strain-softening soil relative to strain-hardening soil, the brittleness of the strain-softening ground, drainage conditions and the geometry of the ground. Even if a catastrophic failure can not occur, the magnitude of any deformations that may occur depend on the same factors. Applying the framework proposed in this chapter is only the first step in a complete liquefaction analysis. If some material is found to be strain-softening with a brittle response to undrained loading, the slope or soil structure must be examined in detail as a whole, using numerical methods, for example, to estimate the overall stability and potential deformations that may occur. The most dangerous soils are those which have a sufficiently loose state to strain-soften directly to ultimate state in a brittle manner. In general, slope failures as a result of flow liquefaction are not common; however, when they do occur, they can take place rapidly, with little warning, and often catastrophic results. Consequently, it is important to proceed cautiously when designing against flow liquefaction, particularly in the case of high risk projects for which the consequences of failure can be enormous.

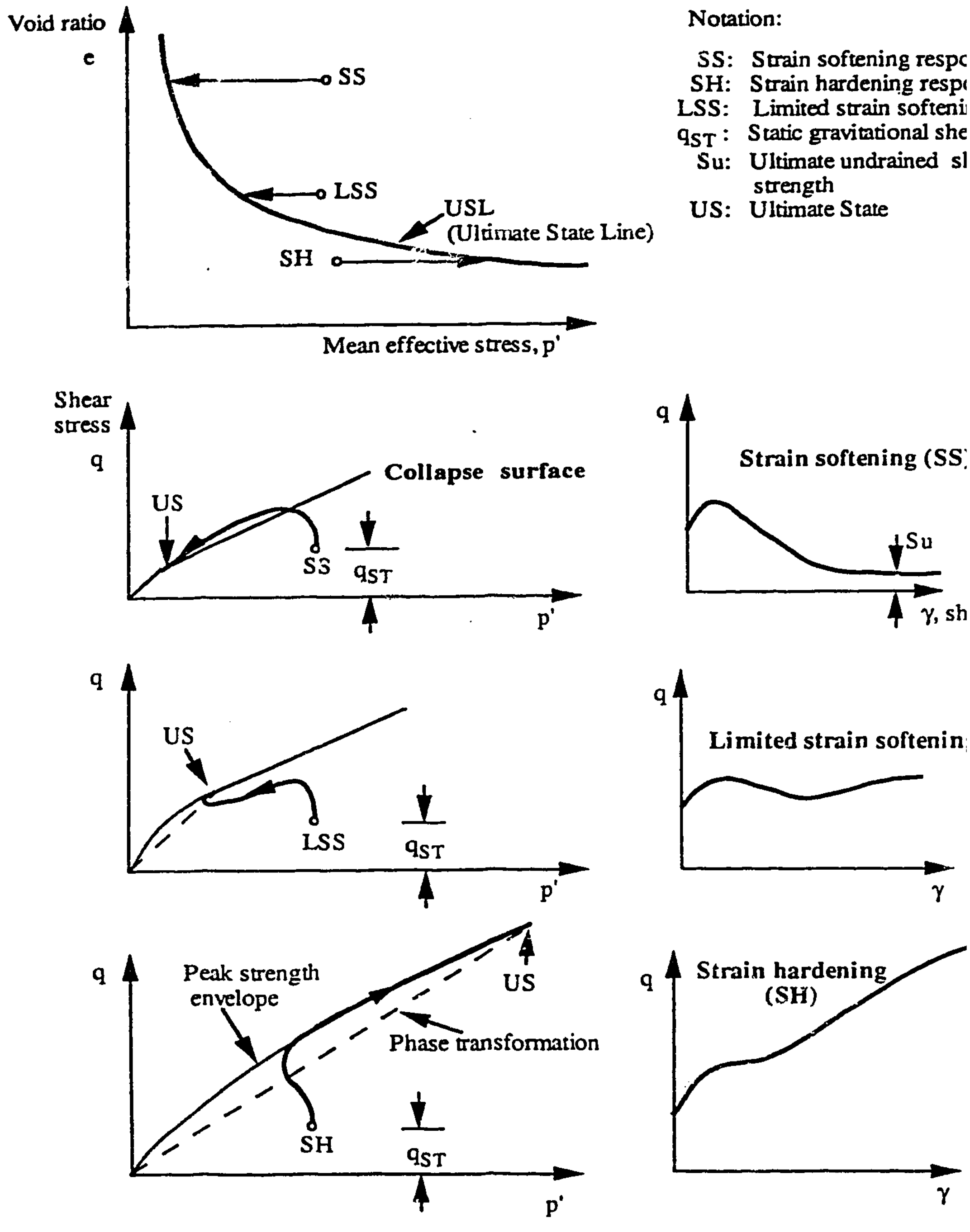

Figure 4-1 Schematic of undrained monotonic behaviour of sand compression (modified from Robertson, 1994).

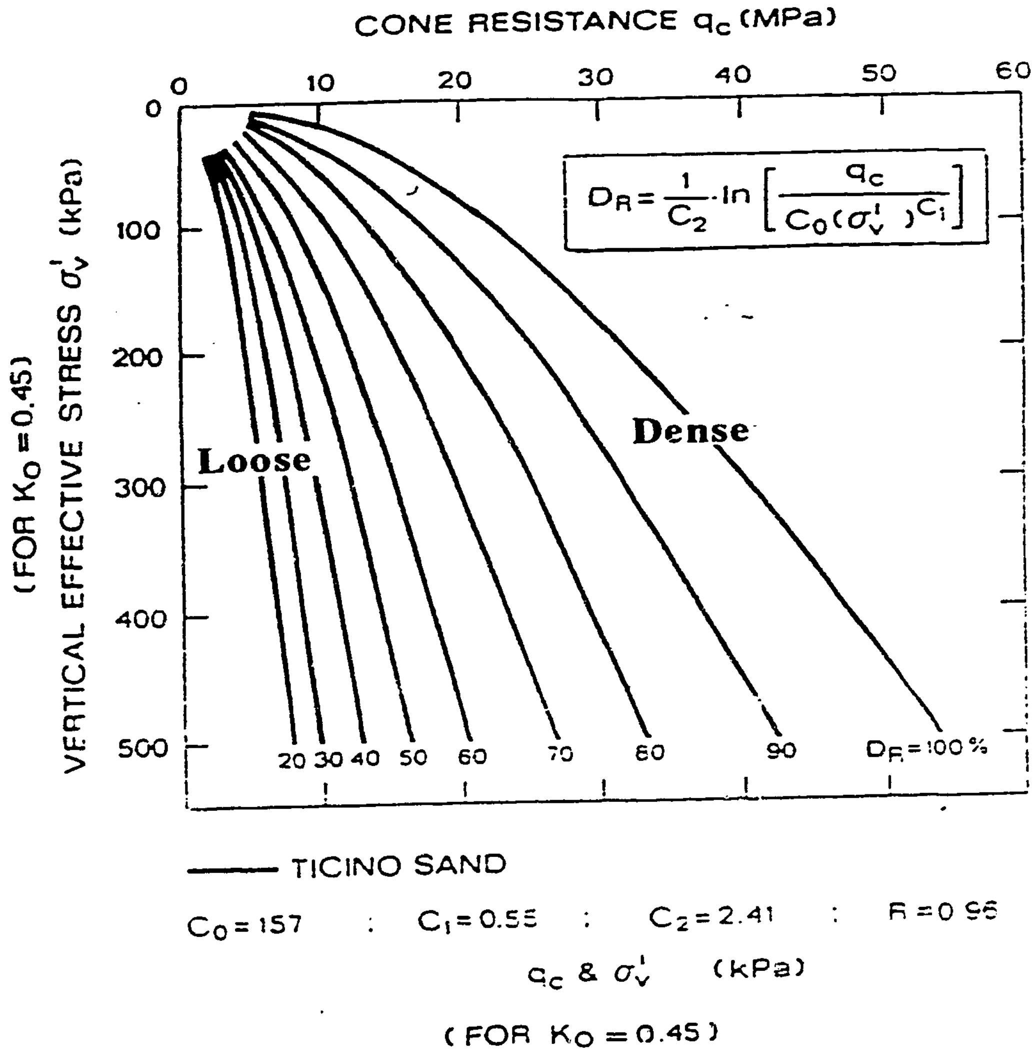

Figure 4-3 Conventional void ratio interpretation from CPT (modified from Baldi et al., 1986).

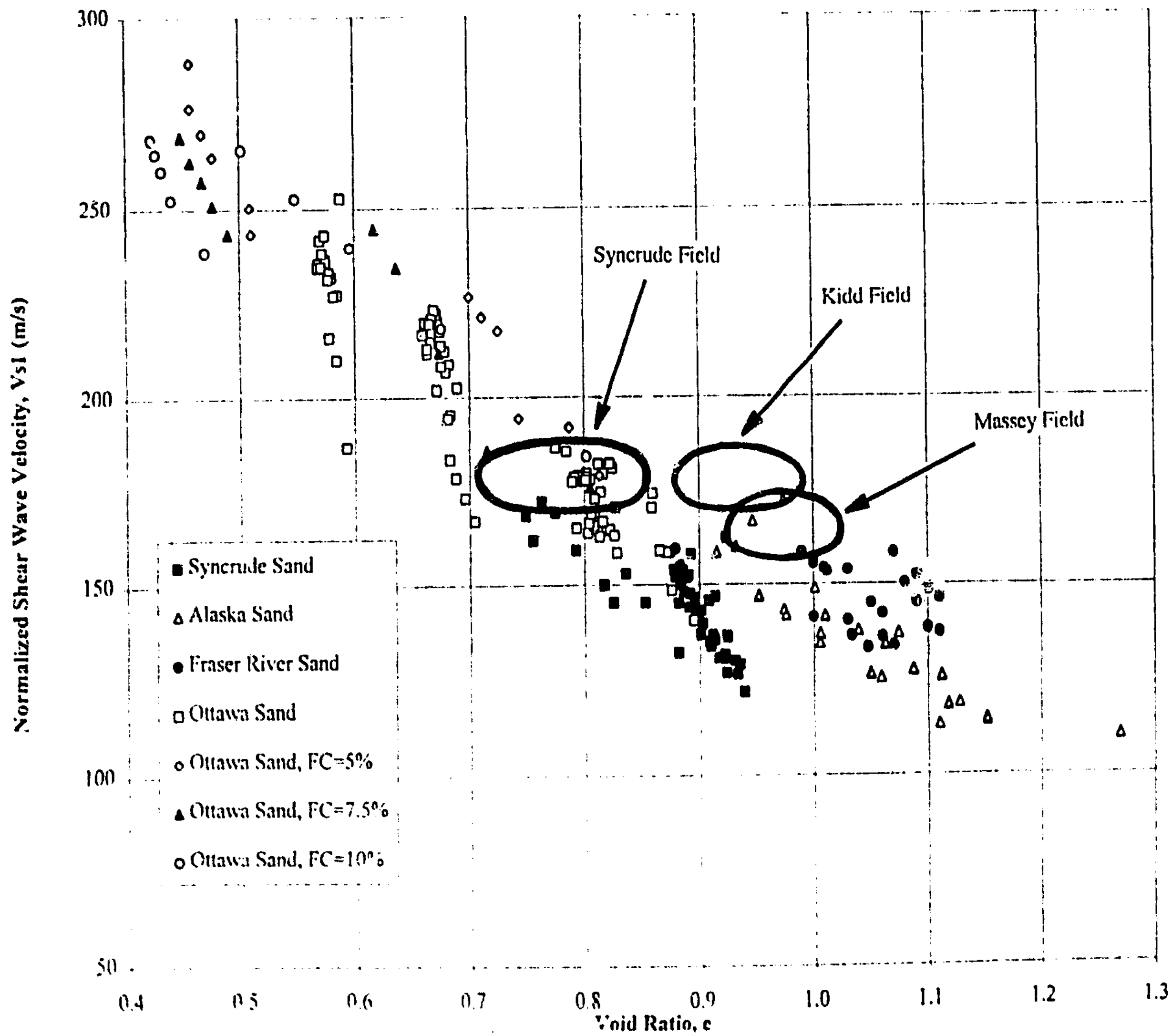

Figure 4-4 Variation of corrected shear wave velocity with void ratio for a range of sands (based on results from Sasitharan, 1994; Cunning, 1994; Chillarige, 1995; and Skirrow, 1996).

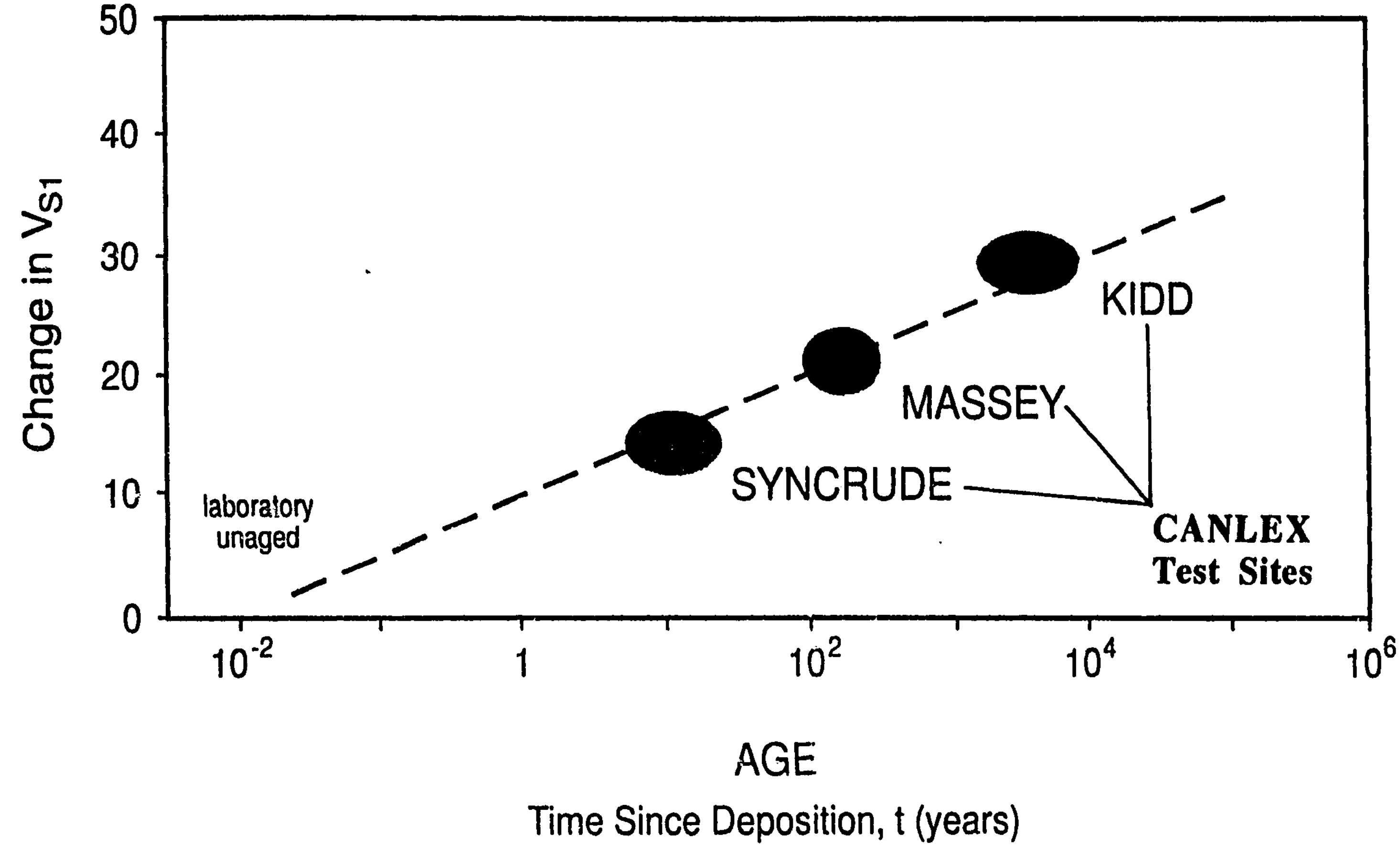

Figure 4-5 Change in corrected shear wave velocity with age for uncemented sands (modified from Robertson et al., 1995).

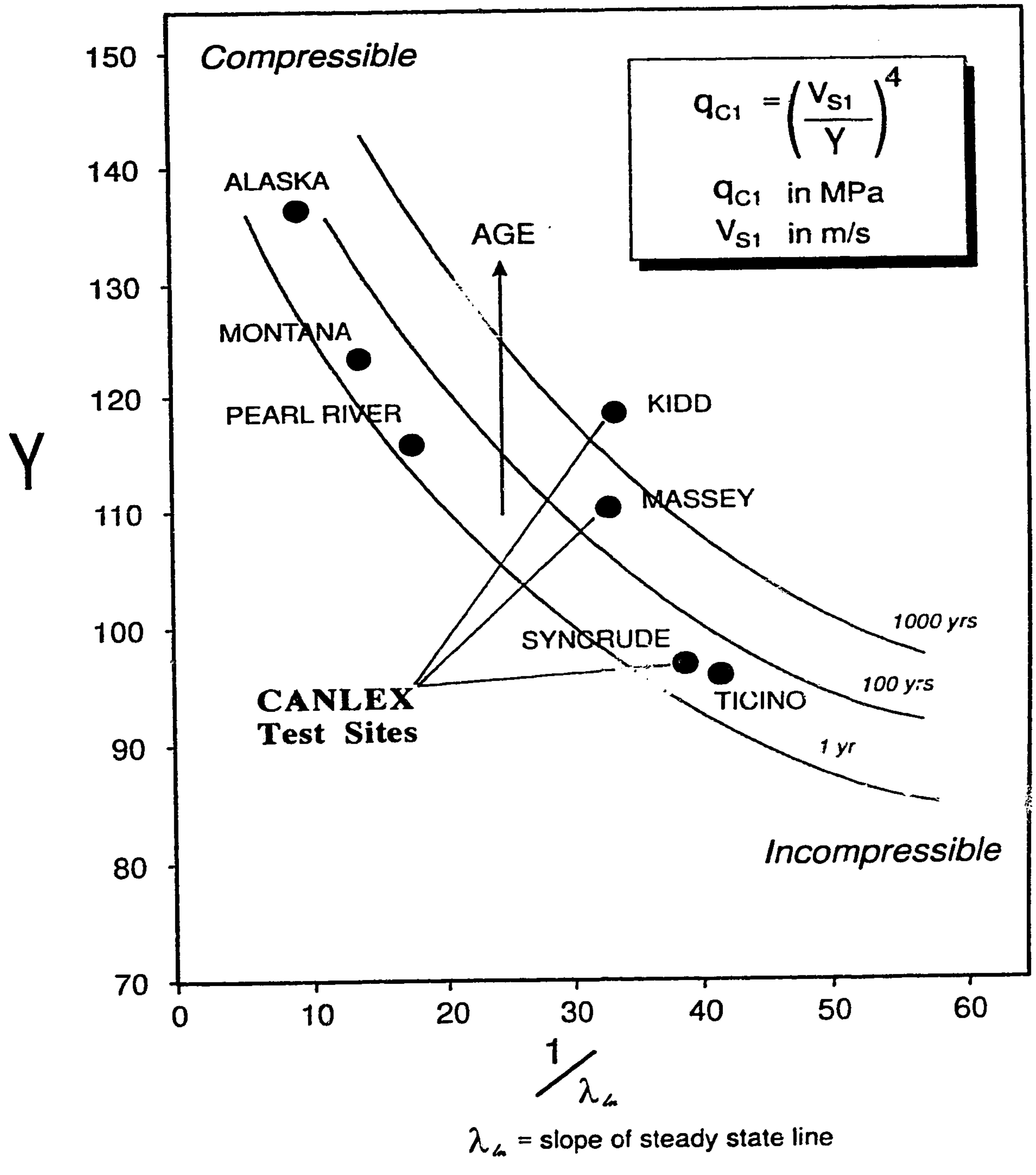

Figure 4-6 Proposed correlation between shear wave velocity and CPT tip resistance and slope (λ_{ln}) of the ultimate state line (USL) (modified from Robertson et al., 1995).

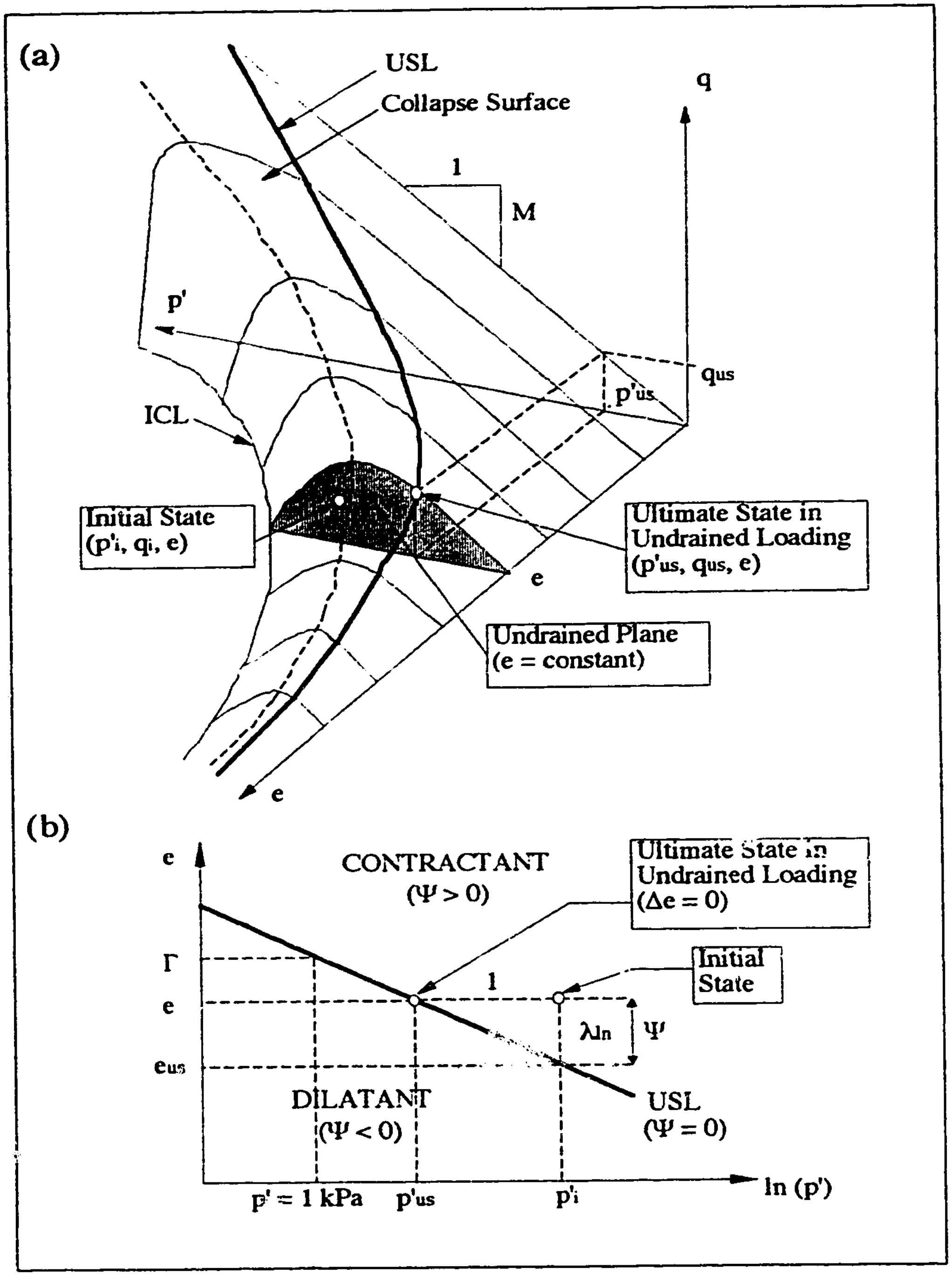

Figure 4-7 Critical state soil mechanics concepts illustrated by (a) an e-p'-q diagram with (b) projections onto the e-ln(p') plane.

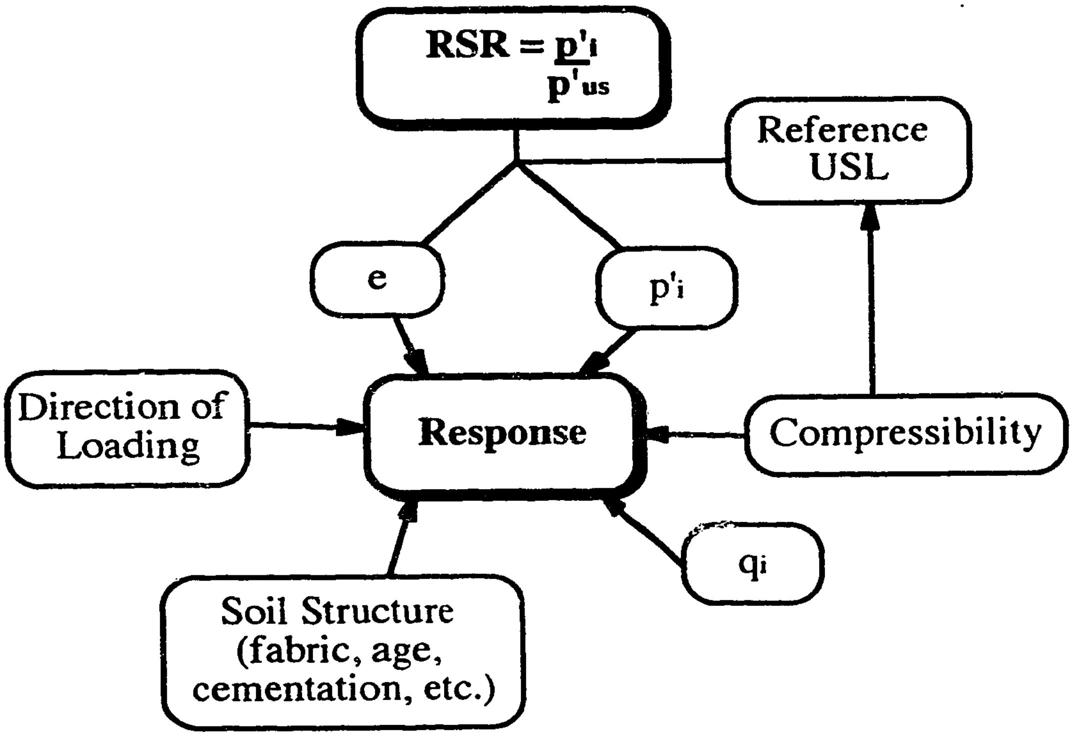

Figure 4-8 Factors influencing response of sandy soils in undrained monotonic testing.

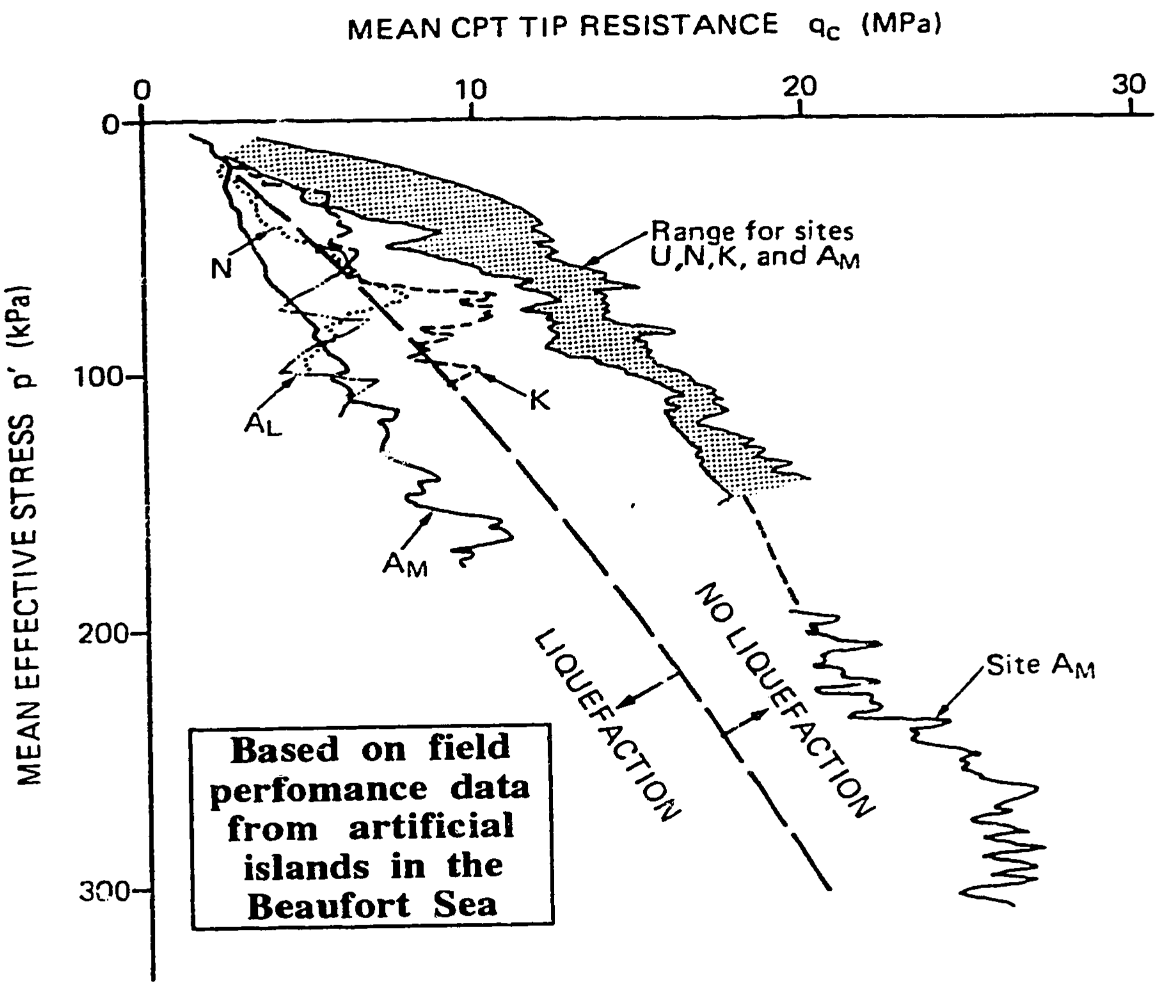

SYMBOL	SITES	PLACEMENT	LIQUEFACTION	SAND
	U,N,K,A_M	Hopper	No	Ukalerk
	K	Pipeline	No	Ukalerk
	N	Pipeline	Yes	Nerlerk
	A_M	Pipeline	Yes	Ukalerk
	A_L	Pipeline	Yes	Local Borrow

Figure 4-9 CPT liquefaction/nonliquefaction dividing line based on field observations (modified from Sladen and Hewitt, 1989).

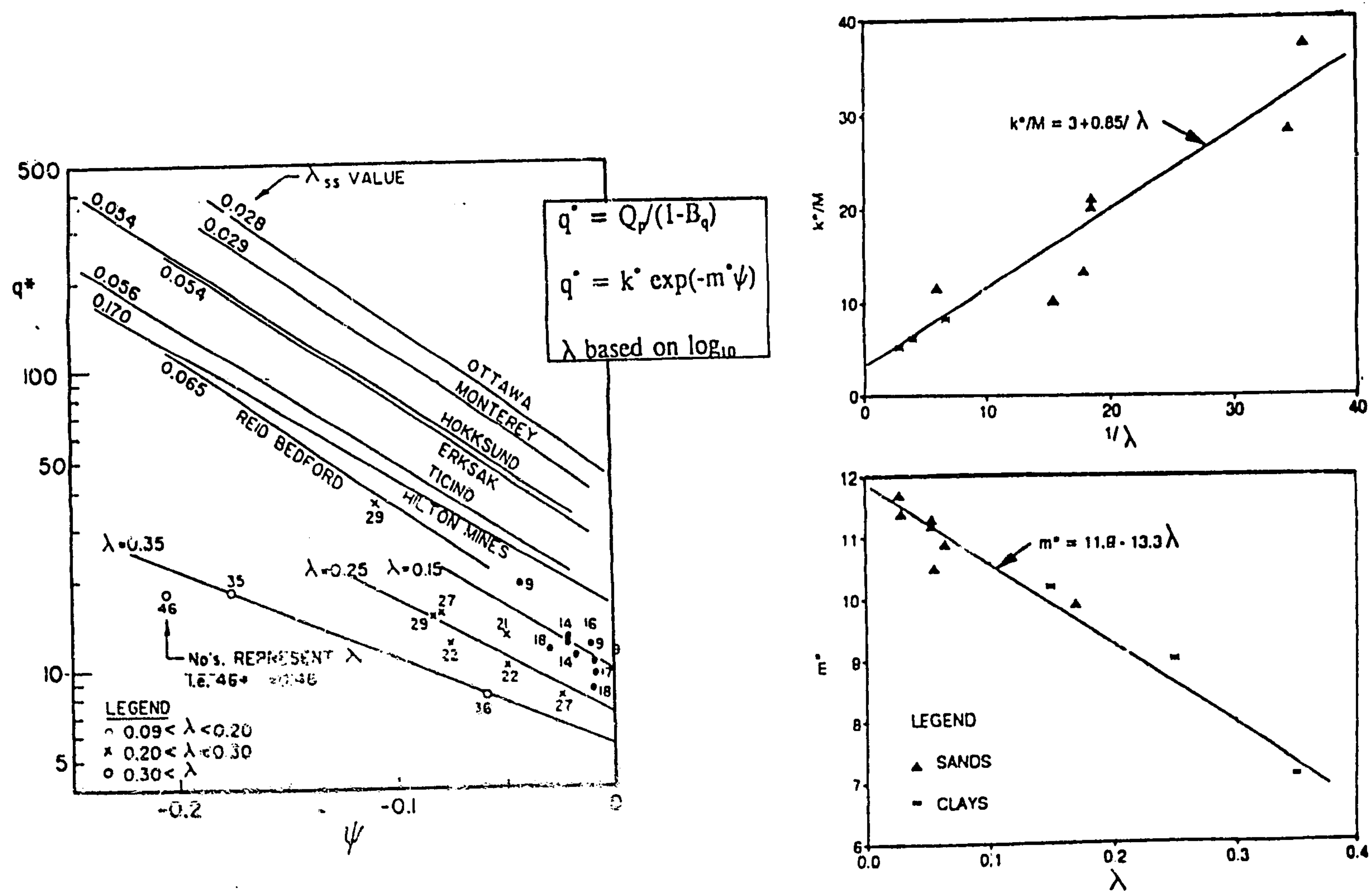

Figure 4-10 Unified relationship of $Q_p(1-B_q)$ to state parameter and critical state parameters M and λ_{log} (modified from Been and Jefferies, 1992).

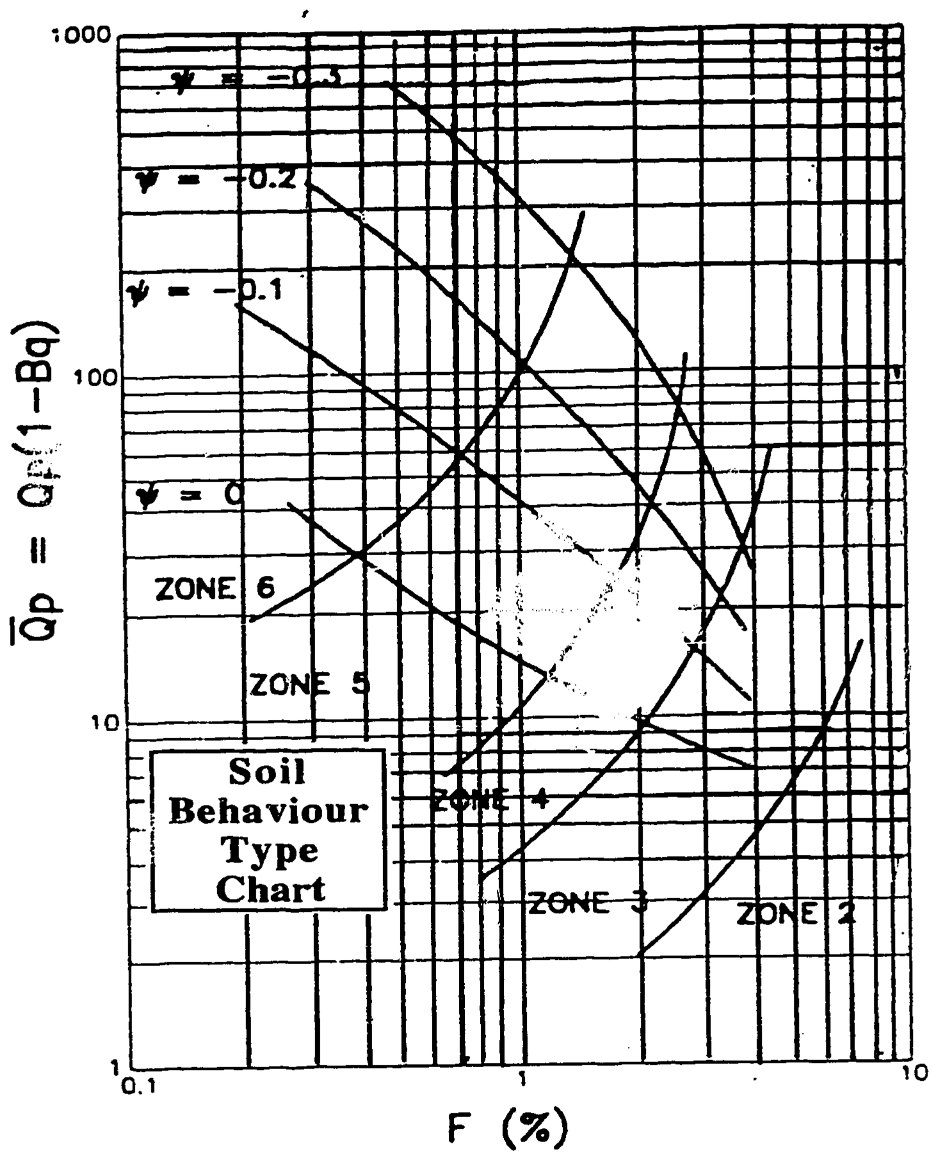

ZONE

2 ORGANIC SOILS-PEAT

3 CLAYS-CLAY TO SILTY CLAY

4 SILT MIXTURES-CLAYEY SILT TO SILTY CLAY

5 SAND MIXTURES-SILTY SAND TO SANDY SILT

6 SANDS-CLEAN SAND TO SILTY SAND

Figure 4-11 Contours of estimated state parameter on soil type behaviour classification chart (modified from Plewes et al., 1992).

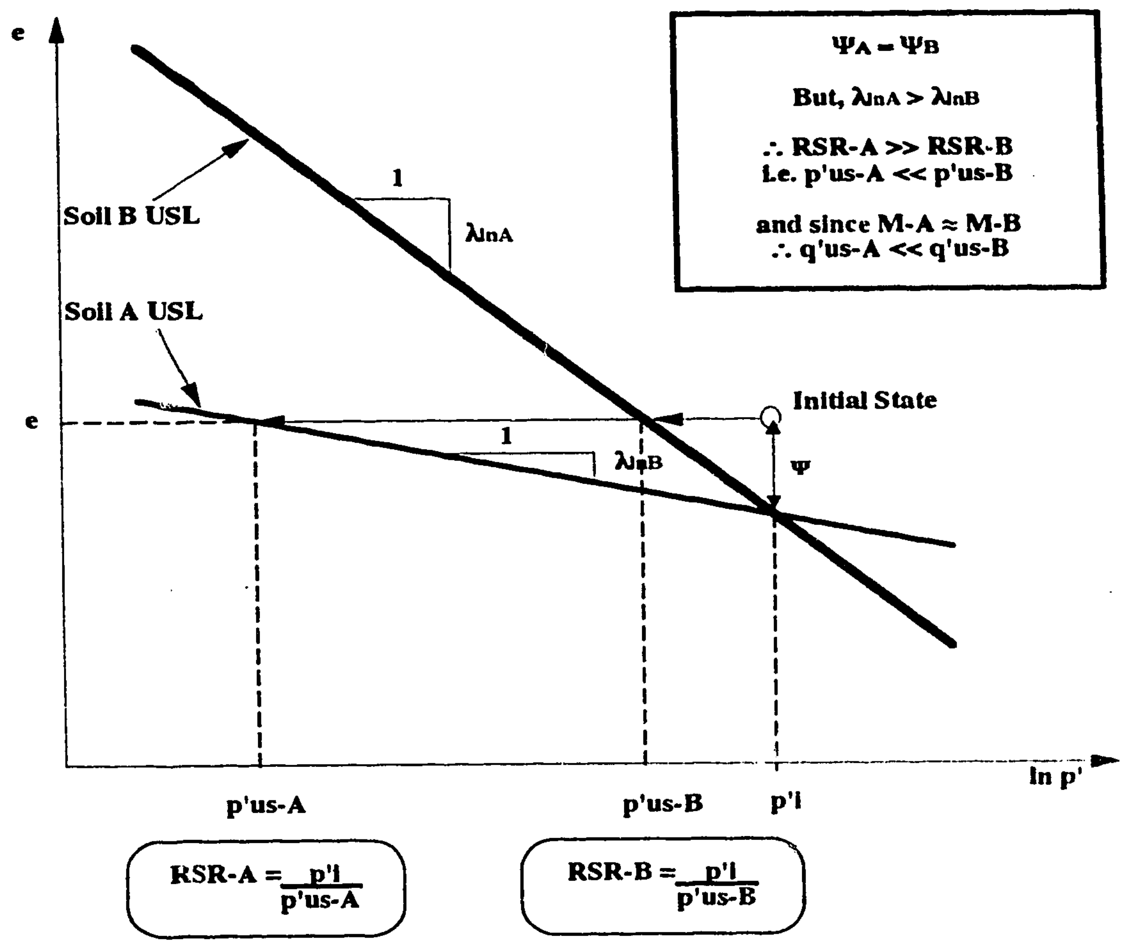

Figure 4-12 Effects of λ_{ln} on undrained response for the same value of state parameter.

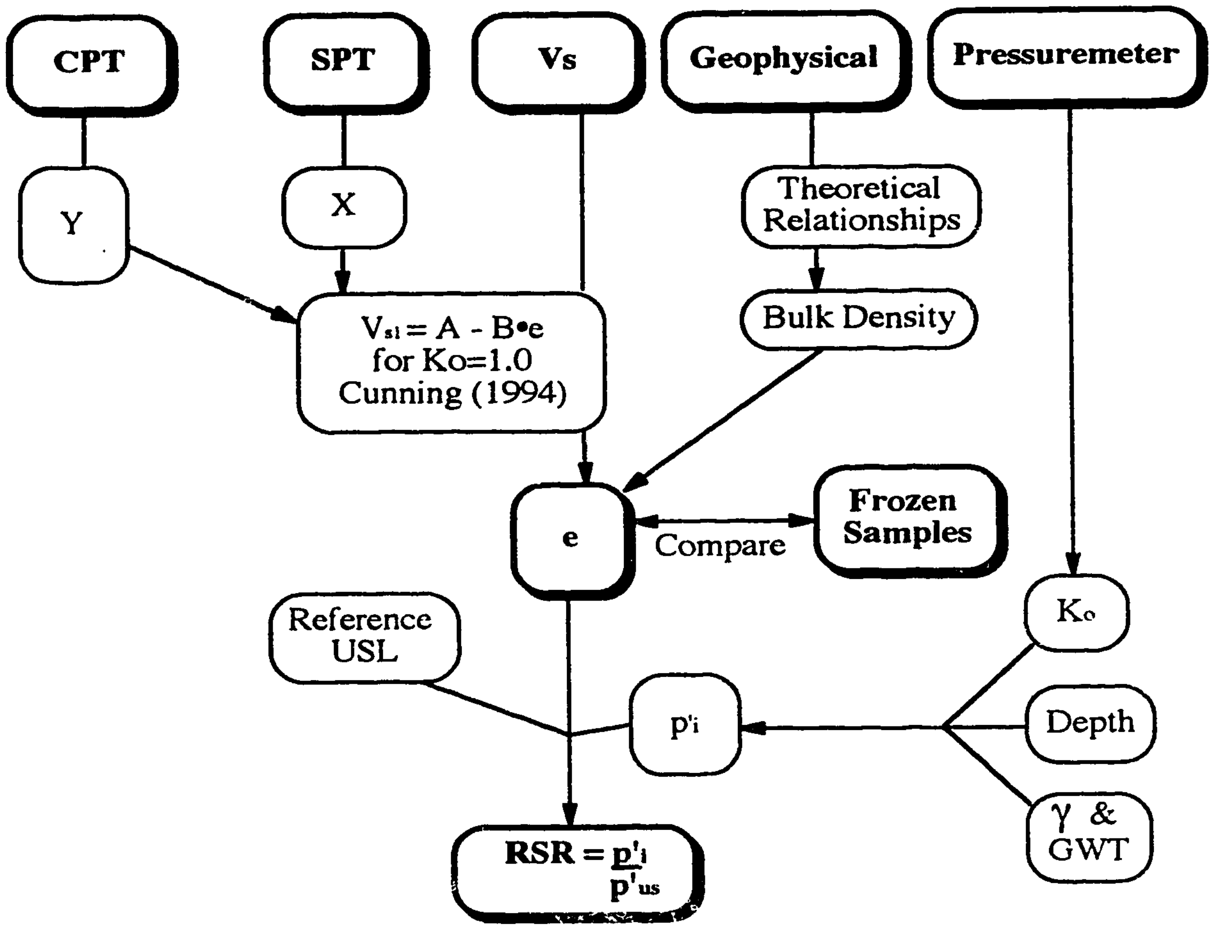

Figure 4-13 Flowchart for estimating RSR from in-situ testing.

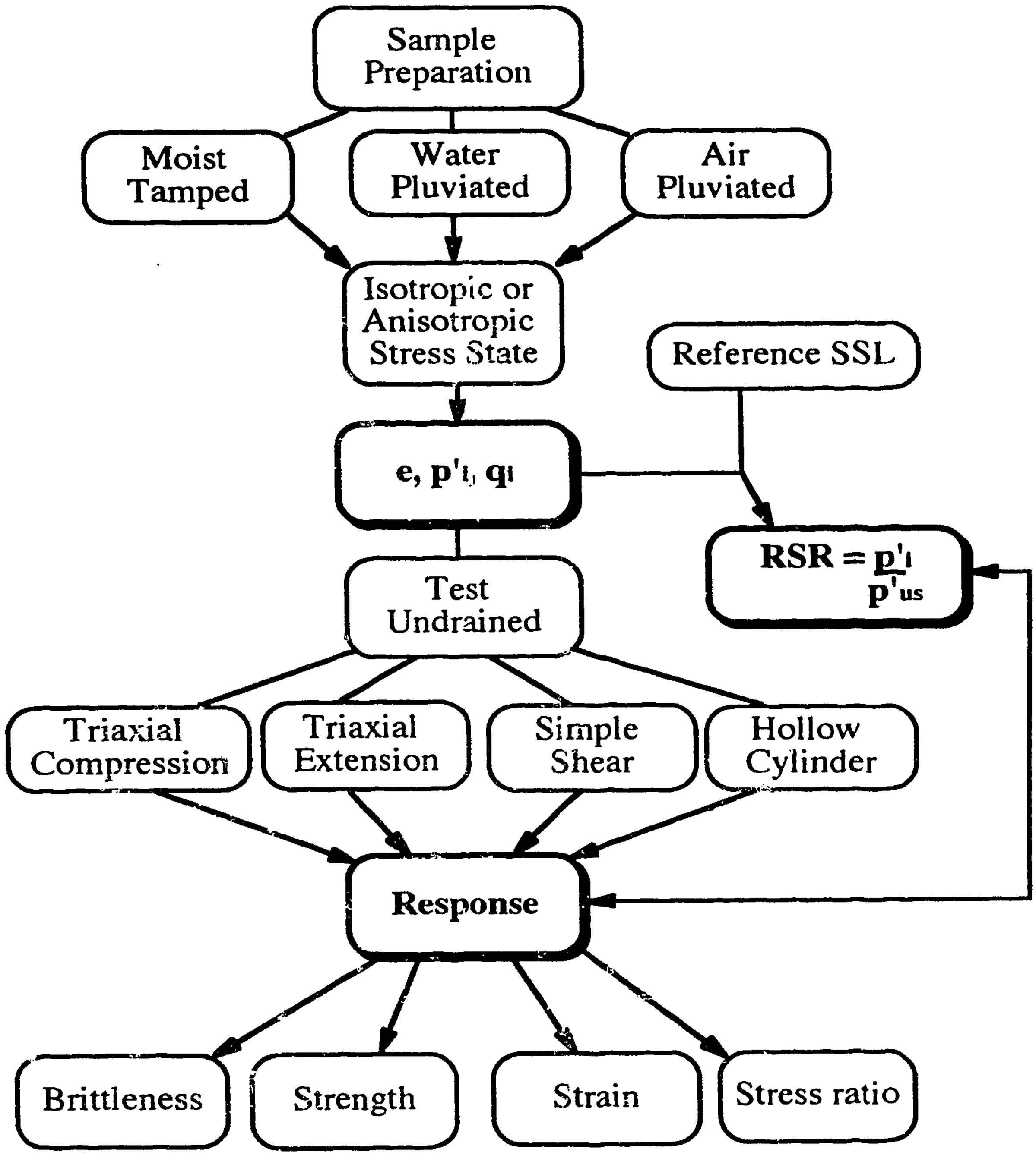

Figure 4-14 Flowchart for measuring undrained response from laboratory testing.

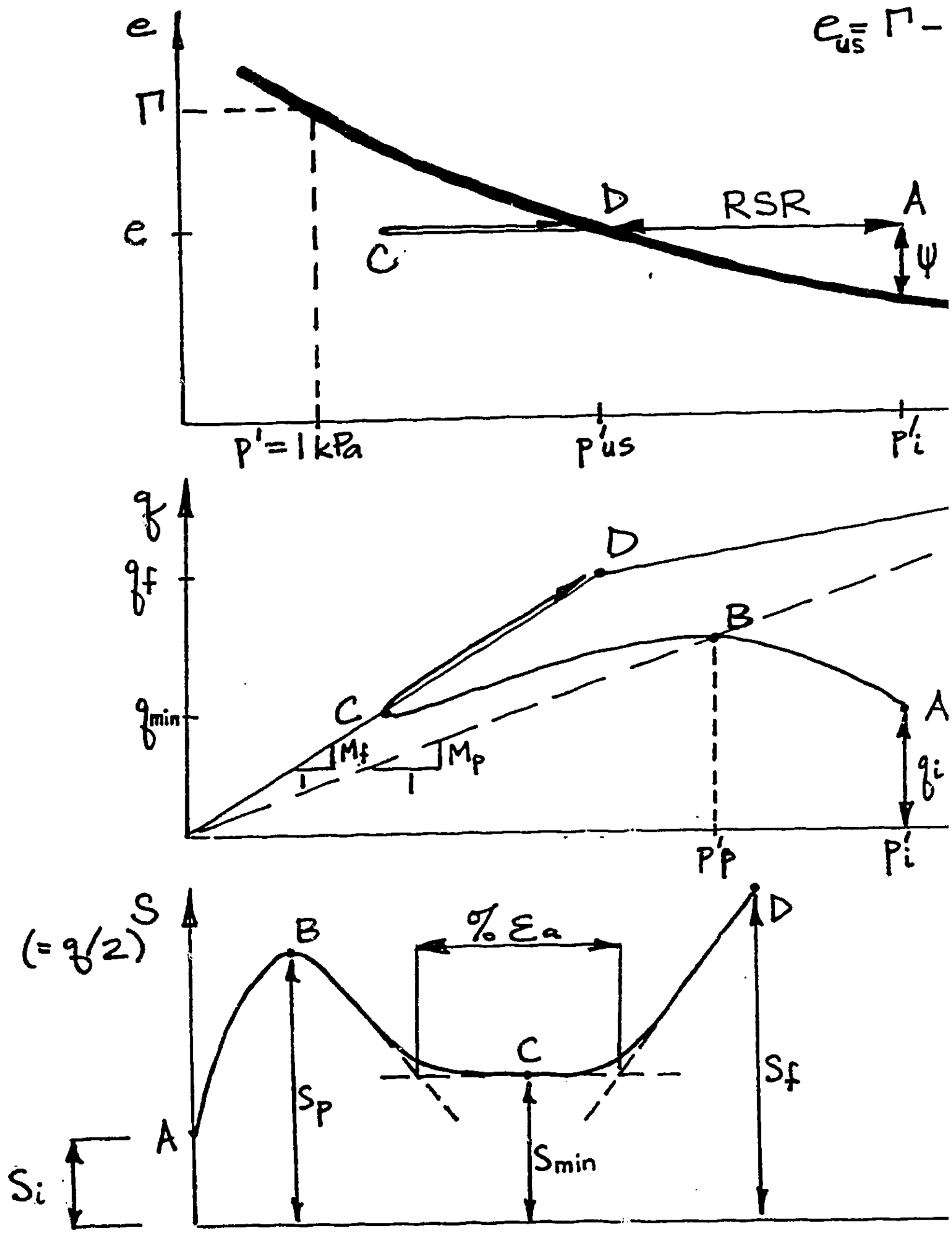

Figure 4-15 Components of undrained response for triaxial compressi

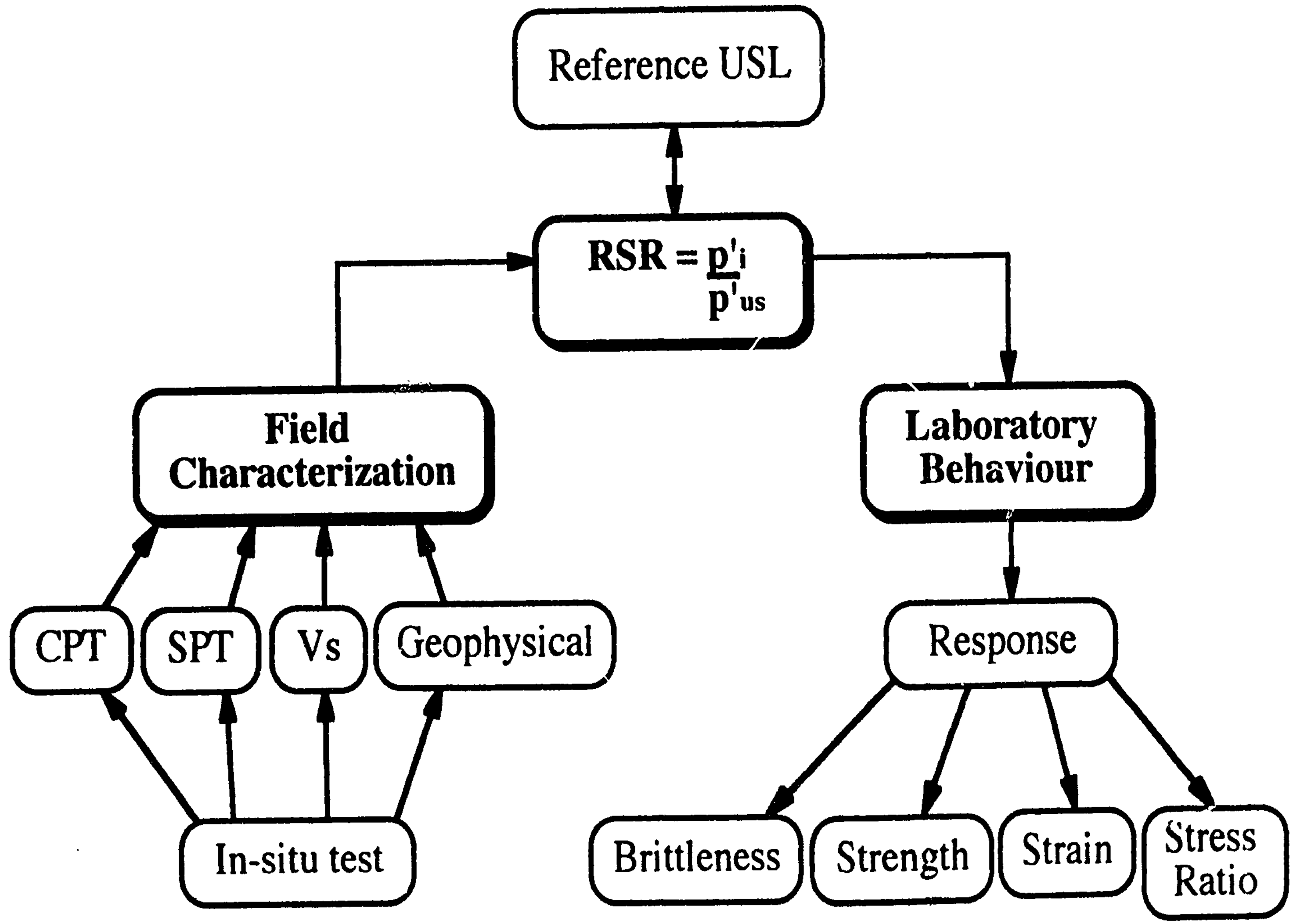

Figure 4-17 Suggested interaction between field characterization and in-situ response from laboratory testing.

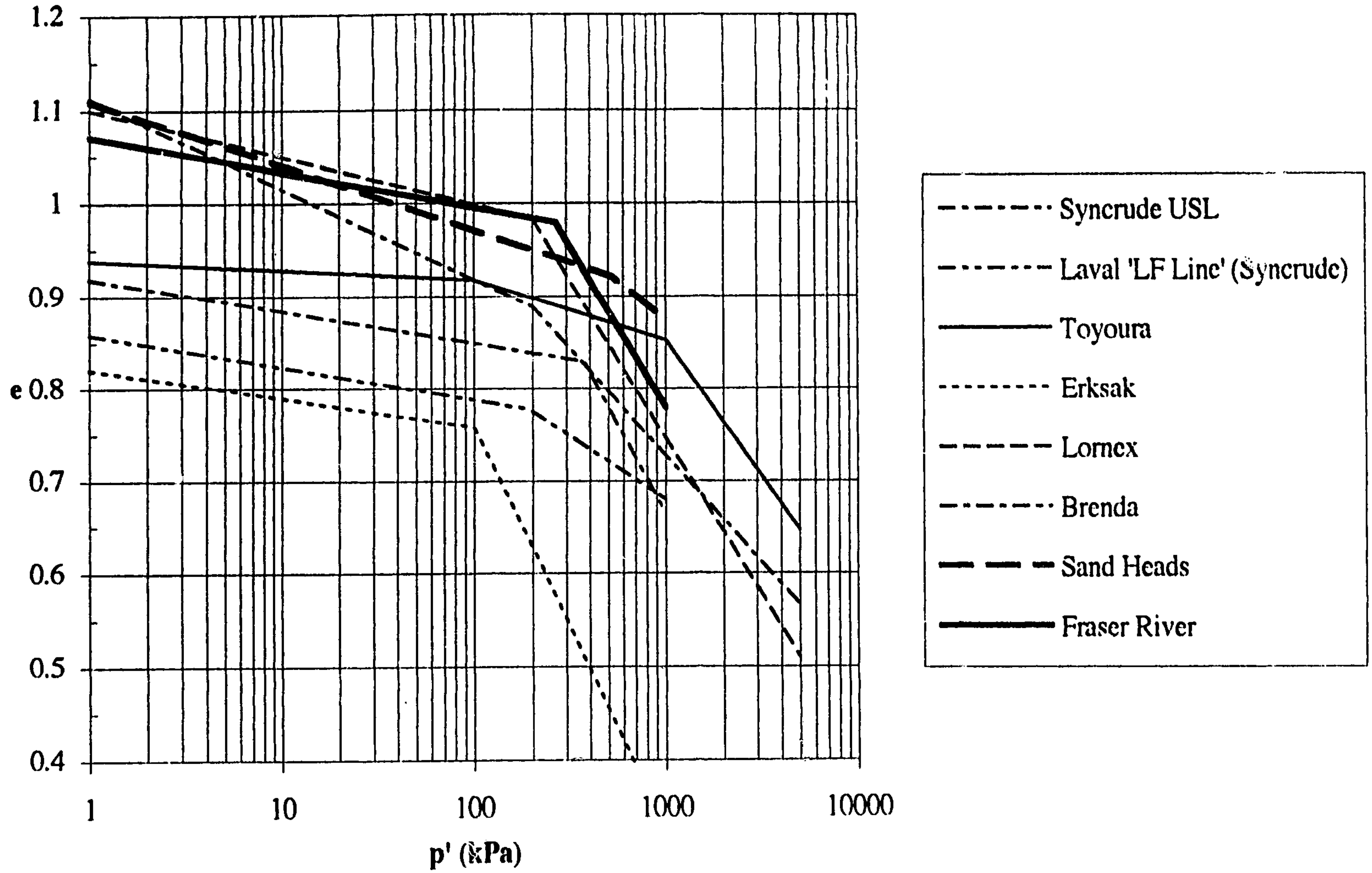

Figure 4-18 Ultimate state lines (USLs) for a variety of sands (based on data tabulated by Sasitharan et al., 1994); also shown are selected reference USLs for Sand Heads sand (after Chillarige et al., 1995) and Fraser River sand.

References

Arthur, J.R.F., and Menzies, B. 1972. Inherent anisotropy in a sand. *Géotechnique*, 22(1): 115-128.

Atkinson, J.H. 1993. *The mechanics of soils and foundations*, McGraw-Hill, London.

Baldi, G. et al. 1986. Interpretation of CPT's and CPTU's, II Part: Drained penetration on sands. *Proc. IV Int. Geotech. Seminar on Field Instrumentation and In Situ Measurements*, Nanyang Tech. Inst., Singapore.

Been, K., and Jefferies, M.G. 1985. A state parameter for sands. *Géotechnique*, 35(2): 99-112.

Been, K., and Jefferies, M.G. 1992. Towards systematic CPT interpretation. *Proceedings of the Wroth Symposium*, 44-55.

Been, K., Jefferies, M.B., Crooks, J.H.A., and Rothenburg, L. 1987. The cone penetration test in sands, Part 2: General inference of state. *Géotechnique*, 37(3): 285-299.

Been, K., Jefferies, M.G., and Hachey, J. 1991. The critical state of sands. *Géotechnique*, 41(3): 365-381.

Bishop, A.W. 1971. Shear strength parameters for undisturbed and remoulded soil specimens. *Roscoe Memorial Symposium*, Cambridge University, 3-58.

Casagrande, A. 1975. Liquefaction and cyclic deformation of sands, a critical review. *Proceedings of the 5th Pan American Conference on Soil Mechanics and Foundation Engineering*, Buenos Aires, 5, 80-133.

Castro, G. 1969. Liquefaction of sands, Harvard Soil Mechanics Series No. 81.

Chillarige, A.R.V. 1995. Liquefaction and seabed instability in the Fraser River Delta. *Ph.D. Thesis*, Department of Civil Engineering, University of Alberta, Edmonton, Alberta, Canada.

Coop, M.R., Atkinson, J.H., and Taylor, R.N. 1995. Strength and stiffness of structured and unstructured soils. *Proceedings of the 11th European Conference on Soil Mechanics and Foundation Engineering*, Copenhagen, 1: 1.55-1.62.

Cuccovillo, T., and Coop, M.R. 1993. The influence of band strength on the mechanics of carbonate soft rocks. *Geotechnical Engineering of Hard Soils - Soft Rocks*, Balkema, Rotterdam, 447-455.

Cunning, J.C. 1994. Shear wave velocity measurement of cohesionless soils for the evaluation of in-situ state. *M.Sc. Thesis*, Department of Civil Engineering, University of Alberta, Edmonton, Alberta, Canada.

Cunning, J.C., Robertson, P.K., and Sego, D.C. 1995. Shear wave velocity to evaluate in-situ state of cohesionless soils. *Canadian Geotechnical Journal*, 32(5): 848-858.

Fear, C.E., and Robertson, P.K. 1995. Estimating the undrained strength of sand: a theoretical framework. *Can. Geotech. J.*, 32(4).

Georgiannou, V.N., Burland, J.B. and Hight, D.W. 1990. The undrained behaviour of clayey sands in triaxial compression and extension, Géotechnique, 40(3): 431-449.

Ishihara, K. 1993. Liquefaction and flow failure during earthquakes. The 33rd Rankine Lecture, *Géotechnique*, 43(3): 351-415.

Jefferies, M.G. and Davies, M.P. 1991. Discussion on soil classification by the cone penetration test. *Canadian Geotechnical Journal*, 28(1): 173-176.

Kulhawy, F.M., and Mayne, P.W. 1990. Manual on estimating soil properties for foundation design. Cornell University, EL-6800, *Research Project 1493-6*, prepared for Electric Power Research Institute.

McRoberts, E.C., and Sladen, J.A. 1992. Observations on static and cyclic sand liquefaction methodologies. *Canadian Geotechnical Journal*, 29(4): 650-665.

Plewes, H.D., McRoberts, E.C., and Chan, W.K. 1988. Downhole nuclear density logging in sand tailings. *Proceedings of ASCE Specialty Conference on Hydraulic Fill Structures*, Fort Collins, Colorado, 290-309.

Plewes, H.D., Davies, M.P, and Jefferies, M.G. 1992. CPT based screening procedure for evaluating liquefaction susceptibility. *Proceedings of the 45th Canadian Geotechnical Conference*, Toronto, Ontario, 4:1-4:9.

Robertson, P.K. 1990. Soil classification using the CPT. *Canadian Geotechnical Journal*, 27(1): 151-158.

Robertson, P.K., Fear, C.E., Woeller, D.J., and Weemees, I. 1995. Estimation of sand compressibility from seismic CPT. *Proceedings of the 48th Canadian Geotechnical Conference*, Vancouver, 1, 441-448.

Robertson, P.K., Woeller, D.J., Kokan, M., Hunter, J., and Luternauer, J. 1992. Seismic techniques to evaluate liquefaction potential. *Proceedings of the 45th Canadian Geotechnical Conference*, 5:1-5:9.

Sasitharan, S. 1994. Collapse behaviour of very loose sand. *Ph.D. Thesis*, Department of Civil Engineering, University of Alberta, Edmonton, Alberta, Canada.

Sasitharan, S., Robertson, P.K., Sego, D.C., and Morgenstern, N.R. 1994. State boundary surface for very loose sand and its practical implications. *Can. Geotech. J.*, 31(3): 321-334.

Skempton, A.W. 1986. Standard penetration test procedures and the effects in sands of overburden pressure, relative density, particle size, ageing and overconsolidation. *Géotechnique*, 36(3): 425-447.

Skirrow, R. 1995. The effects of fines content on the monotonic triaxial testing of cohesionless soils for evaluation of in-situ state. *M.Sc. Thesis*, Department of Civil Engineering, University of Alberta, Edmonton, Alberta.

Sladen, J.A. 1989. Problems with interpretation of sand state from cone penetration test. *Géotechnique*, 39(2): 323-332.

Sladen, J.A., D'Hollander, R.D., and Krahn, J. 1985a. The liquefaction of sands, a collapse surface approach. *Can. Geotech. J.*, 22: 564-578.

Sladen, J.A., D'Hollander, R.D., Krahn, J., and Mitchell, D.E. 1985b. Back analysis of the Nerlerk berm liquefaction slides. *Canadian Geotechnical Journal*, 22: 579-588.

Sladen, J.A., and Hewitt, K.J. 1989. Influence of placement method on the in situ density of hydraulic sand fills. *Canadian Geotechnical Journal*, 26: 453-466.

Vaid, Y.P., Chung, E.K.F., and Kuerbis, R.H. 1990. Stress path and steady state. *Can. Geotech. J.*, 27: 1-7.

Vaid, Y.P., Sivathayalan, S., Uthayakumar, M., and Eliadorani, A. 1995. Liquefaction potential of reconstituted Syncrude sand. *Proceedings of the 48th Canadian Geotechnical Conference*, Vancouver, B.C., 1, 319-330.

Wood, D.M. 1990. *Soil behaviour and critical state soil mechanics*. Cambridge University Press, Cambridge, pp. 179-188.

Wroth, C.P., and Bassett, R.H. 1965. A stress-strain relationship for the shearing behaviour of a sand. *Géotechnique*, 15(1): 32-56.

Yoshida, Y., Ikemi, M., and Kokusho, T. 1988. Empirical formulas of SPT blow-counts for gravely soils. *Proceedings of Penetration Testing*, Balkema, Rotterdam, 1: 381-387.

CHAPTER 5

A FRAMEWORK FOR ESTIMATING UNDRAINED SHEAR STRENGTH BASED ON IN-SITU TESTING[1]

5.1 Introduction

As outlined in Chapter 4, one of the most important response parameters for flow liquefaction considerations is the undrained shear strength of the sand. Conducting an undrained stability analysis of sand, such as for post-liquefaction conditions, requires a knowledge of the undrained ultimate state shear strength (S_u). Provided that liquefaction will be triggered in a sandy slope, the great difficulty lies in deciding what value of S_u will best represent the particular conditions in the field. Current practice makes use of correlations between S_u and Standard Penetration Test (SPT) or Cone Penetration Test (CPT) resistance (Seed and Harder, 1990; Robertson, 1990; Stark and Mesri, 1992).

This study presents a framework for estimating S_u, combining critical state soil mechanics and shear wave velocity measurements, assuming undrained loading with no pore pressure redistribution. Shear wave velocity measurements are also converted to equivalent SPT and CPT penetration resistance. As a result, the uniqueness of each of the current empirical methods for estimating S_u using field penetration tests is critically examined and the factors that play a major role in the potential correlations between S_u and penetration resistance are investigated. In this chapter, S_u is estimated based on the ultimate state line (USL) for a given sand and undrained monotonic loading in triaxial compression; however, the same framework can be used to estimate quasi-steady-state (QSS) strengths or strengths under other directions of loading (e.g. triaxial extension), as already explained in Chapter 4. In addition, the same S_u will correspond to a given initial state of a soil if flow liquefaction is triggered by other means, such as by undrained cyclic loading. The term ultimate state is used in this study; this is synonymous with the terms critical state or steady state, which are interchangeable, after Been et al. (1991). Note that S_u is only applicable to the analysis of stability related to the phenomenon of flow liquefaction; it is not relevant to the analysis of deformations resulting from cyclic softening (liquefaction).

---

1 *A version of this chapter has been published. Fear, C.E. and Robertson, P.K. 1995. Estimating the undrained strength of sand: a theoretical framework. Canadian Geotechnical Journal, 32(5): 859-870.*

5.2 Current Methods for Estimating S_u using Penetration Tests

Figure 5-1 presents the empirical correlation proposed by Seed and Harder (1990), based on the original work by Seed (1987), which involved 17 case histories and provided a relationship between S_u and equivalent normalized Standard Penetration Test (SPT) resistance, $(N_1)_{60}$, in clean sand. As Figure 5-1 indicates, this relationship consists of upper and lower bound lines which present a dilemma to the geotechnical engineer. It is not uncommon to find that the upper bound line will suggest an apparently acceptable factor of safety whereas the lower bound line will suggest a potentially unstable condition. Conservative practice often leads engineers to use the lower bound line to assess overall slope stability which may result in unnecessary site remediation and expenditures.

Stark and Mesri (1992) provided an alternative approach to estimating S_u, and presented a relationship between undrained strength ratio and equivalent $(N_1)_{60}$ in clean sand, as shown in Figure 5-2. The undrained strength ratio is defined as the mobilized S_u, divided by the initial vertical effective stress, σ_v'. The idea was that expressing undrained strength in terms of the ratio S_u/σ_v' would lead to a method that would be easier to apply in practice. This relationship is based on the Seed and Harder (1990) case histories plus three additional ones. The Stark and Mesri (1992) relationship also consists of upper and lower bound lines. The work by Stark and Mesri (1992) followed the approach taken by Jefferies et al. (1990), which suggested that the shear strength ratio was a function of normalized CPT resistance. This idea was based on the view that shear strength ratio is a function of state parameter (Ψ) and the previous work by Been and Jefferies (1986 and 1987) which proposed that state parameter was a function of normalized CPT resistance.

Robertson (1990) presented a review of the relationship between S_u and normalized penetration resistance for four sands using relative density correlations with SPT $(N_1)_{60}$, correlations between normalized CPT q_{c1} and SPT $(N_1)_{60}$, published data on steady state relationships, field studies and large calibration chamber test results. The resulting relationships are presented in Figure 5-3. Robertson (1990) found that Ottawa sand appeared to provide the minimum steady state strength correlation and that the correlation by Seed (1987) represented a conservative lower bound correlation, especially at large values of $(N_1)_{60}$. The other sands that were studied (Monterey, Ticino and Hilton Mines) all possessed much higher values of S_u at a given penetration resistance than the Seed (1987) correlation would suggest, thus indicating that there appears to be no unique relationship between S_u and penetration resistance for all sands.

Figure 5-4 presents the results of Robertson's (1990) additional investigation into the correlation between normalized ultimate undrained strength (S_u/p') and normalized CPT resistance $(q_c-p)/p'$, based on state parameter, as suggested by Been and Jefferies (1985). Robertson (1990) recognized that these correlations were approximate in nature due to limited test data, but the results clearly suggested the lack of a unique relationship for all sands, with Ottawa sand representing the minimum relationship when compared with the other sands (Reid Bedford, Hilton Mines, Oilsand, Ticino and Monterey).

The approach used to estimate S_u at Duncan Dam (Byrne et al., 1994) was an alternative to the in-situ penetration methods discussed above. High quality undisturbed samples of sand were obtained at Duncan Dam using ground freezing and subsequent coring. These undisturbed samples were then tested in the laboratory to directly determine S_u of the sand. Although attractive, this approach can be expensive and is usually limited to high risk projects which have a sufficiently large scope and budget and for which the consequences of failure can be enormous.

5.3 Framework for Estimating S_u from Shear Wave Velocity Measurements

5.3.1 Determining S_u from critical state soil mechanics

As reviewed in Chapter 4, based on a critical state soil mechanics framework, the ultimate state line (USL) for a given sand and a given direction of loading (e.g. triaxial compression or triaxial extension) can be plotted in p'-q-e space (see Figure 5-5a), where e is void ratio and p' and q are defined as follows:

[5-1] $$p' = \frac{1}{3}(\sigma_1' + 2\,\sigma_3')$$

[5-2] $$q = \sigma_1' - \sigma_3'$$

The USL is controlled by the grain characteristics of the soil. Along the USL, q and p' are related by M, which is a function of friction angle and direction of loading. Theoretical values of M for triaxial compression (M_C) and triaxial extension (M_E) are given by the following equations (Wood, 1990):

[5-3] $$M_C = (q_{us}/p'_{us})_C = \frac{6\sin\phi'_{us}}{3 - \sin\phi'_{us}}$$

[5-4] $$M_E = (q_{us}/p'_{us})_E = \frac{6\sin\phi'_{us}}{3 + \sin\phi'_{us}}$$

In theory, these lines in p'-q-e space project onto a single USL in e-p' space, since ultimate state is independent of the stress path followed to reach it (Been et al., 1991). When the p' axis is plotted on a logarithmic scale, the true USL is curved, as explained in Chapter 4. However, the USL can be approximated as a bi-linear relationship; i.e. as a straight line over a given stress range (see straight line shown in Figure 5-5b for a particular stress range). The USL in the e-p' plane can therefore be defined over a given stress range by two parameters, Γ and λ_{ln}. Γ is the void ratio of the portion of the USL at p'=1 kPa and λ_{ln} is the slope of the portion of the USL when the p' axis is plotted on a natural logarithm scale. Each straight line portion of the USL in e-ln p' space is therefore defined as follows:

[5-5] $$e = \Gamma - \lambda_{ln} \ln (p')$$

Within the critical state soil mechanics framework, it is possible to calculate S_u for a soil with a given void ratio when loaded in undrained shear, assuming no pore pressure redistribution and therefore no change in void ratio. The concept (shown in Figure 5-5) is that a sand which has an initial state given by (p'_i, q_i, e) and is loaded in undrained shear will reach the same S_u as the point on its USL with the same void ratio (p'_{us}, q_{us}, e). Therefore, S_u can be determined as follows:

[5-6] $$S_u = \frac{1}{2} M \left(\frac{p'_i}{\exp \left(\frac{\Psi}{\lambda_{ln}}\right)} \right)$$

where:

M = M_C or M_E, depending on the direction of loading (see Equations 5-3 and 5-4)

[5-7] Ψ= initial state parameter = $e - e_{us}$ (Been and Jefferies, 1985)

e = initial void ratio

e_{us} = void ratio of the point on the USL with the same p' as the initial state

Each straight line portion of the USL is defined by both a range in stress (p') and a range in void ratio. Over the applicable range in void ratio, Ψ is related to the reference stress ratio

(RSR, as defined in Chapter 4) by the slope of that portion of the USL, λ_{ln}, as follows:

$$[5\text{-}8] \quad \text{Reference Stress Ratio (RSR)} = \frac{p'_i}{p'_{us}} = \exp\left(\frac{\Psi}{\lambda_{ln}}\right)$$

RSR is a better measure of initial state because it incorporates the effects of an USL that has a changing slope. It can therefore be used to estimate S_u over a wider range of void ratio (or stress). RSR is also a better parameter for comparing sands of different compressibilities, and which, therefore, have different values of λ_{ln}. Combining Equation 5-6 and Equation 5-8 gives the following equation for determining S_u:

$$[5\text{-}9] \qquad S_u = \frac{1}{2} M \left(\frac{p'_i}{RSR}\right)$$

For a given sand (i.e. constant M and λ_{ln}), S_u is a function of both RSR and p'_i because defining these two parameters for a given USL determines the void ratio of the sand. Rearranging Equation 5-6 produces the following equation for the strength ratio S_u/p'_i in terms of Ψ:

$$[5\text{-}10] \qquad \frac{S_u}{p'_i} = \frac{1}{2} M \exp\left(-\frac{\Psi}{\lambda_{ln}}\right)$$

In terms of RSR, Equation 5-10 can be expressed as follows:

$$[5\text{-}11] \qquad \frac{S_u}{p'_i} = \frac{1}{2} \frac{M}{RSR}$$

For a given sand under a particular direction of undrained loading, S_u/p'_i is solely a function of RSR. The maximum value of S_u/p'_i for a contractant soil (i.e. RSR $\geq$ 1) occurs when RSR=1 and has a value equal to 0.5 M. On a site-specific basis, a constant S_u/p'_i ratio applies only if the in-situ consolidation line for the deposit is parallel to the USL on an e-ln p' plot, resulting in constant RSR. In this sense, sand differs from clay. For clay, it is reasonable to assume that the virgin compression line (i.e. normally consolidated clay) and the USL are relatively straight and parallel in e-ln p' space (Wood, 1990). As a result, all points on the virgin compression line have the same OCR (related to RSR, as explained in Chapter 4) and, therefore, a constant value of S_u/p'_i can be used for a particular normally consolidated clay. Sand, on the other hand, can be deposited in numerous ways, each producing a different consolidation line which may or may not be parallel to the USL. However, experience with reconstituted sand samples in the laboratory indicates that the consolidation line for very loose sands can be approximately parallel to the USL (Cunning, 1994). Therefore, a constant value of S_u/p'_i may be reasonable for very loose sands.

5.3.2 Estimating soil state from shear wave velocity measurements

Drawing on the work by Robertson et al. (1995), Cunning et al. (1995) demonstrated that soil state can be estimated from shear wave velocity measurements over a given range in void ratio using the following formula:

[5-12] $$\Psi = \left(\frac{A}{B} - \Gamma\right) - \left(\frac{V_{s1}}{B\ (K_o)^{na}} - \lambda_{ln} \ln \left|\frac{\sigma_{vi}'}{3}(1 + 2K_o)\right|\right)$$

where:

V_{s1} = normalized shear wave velocity, in m/s

[5-13] $$= V_s \left(\frac{P_a}{\sigma_v'}\right)^{na+nb}$$

P_a = 100 kPa and na=nb=0.125, typically
A and B = constants for a given sand, both in m/s
K_o = ratio of horizontal to vertical stresses
σ_{vi}' = initial vertical effective stress

State parameter is therefore a function of soil type (A, B, Γ and λ_{ln}), K_o, σ_{vi}', and V_{s1}. Over a given void ratio, this estimated Ψ can be converted to RSR using the corresponding value of λ_{ln} and Equation 5-8. This results in the following equation to estimate RSR:

[5-14] $$RSR = \frac{\frac{\sigma_{vi}'}{3}(1 + 2K_o)}{\exp\left(\frac{\Gamma - \frac{A}{B} + \frac{V_{s1}}{BK_o^{na}}}{\lambda_{ln}}\right)}$$

5.3.3 Estimating S_u from shear wave velocity measurements

Combining Equations 5-9 and 5-14 results in the following equation relating S_u to V_{s1}:

[5-15] $$S_u = \frac{M}{2}\exp\left[\frac{1}{\lambda_{ln}}\left(\frac{V_{s1}}{B\ (K_o)^{na}} - \left(\frac{A}{B} - \Gamma\right)\right)\right] \qquad \text{(kPa)}$$

where V_{s1} is in m/s.

Similarly, combining Equations 5-11 and 5-14 results in the following equation relating S_u/p'_i to V_{s1}:

$$[5\text{-}16] \qquad \frac{S_u}{p'_i} = \frac{M}{2} \frac{\exp\left[\frac{V_{s1}}{B\,(K_o)^{na}} - \lambda_{ln} \ln\left(\frac{\sigma_{vi}'}{3}(1+2K_o)\right)\right]}{\exp\left(\frac{A}{B} - \Gamma\right)}$$

Replacing p'_i in the left side of Equation 5-16 by the expression given in Equation 5-1 (substituting σ_{vi}' and $K_o \bullet \sigma_{vi}'$ for σ_1' and σ_3', respectively) results in a similar equation relating S_u/σ_{vi}' to V_{s1}:

$$[5\text{-}17] \qquad \frac{S_u}{\sigma_{vi}'} = \frac{M}{6} \left(\frac{\exp\left[\frac{V_{s1}}{B\,(K_o)^{na}} - \lambda_{ln} \ln\left(\frac{\sigma_{vi}'}{3}(1+2K_o)\right)\right]}{\exp\left(\frac{A}{B} - \Gamma\right)} \right) (1 + 2K_o)$$

Examining Equation 5-15, it is clear that for a given material under a particular direction of undrained loading (constant A, B, na, M, Γ and λ_{ln}) and for a given K_o, S_u is uniquely a function of V_{s1}. However, Equations 5-16 and 5-17 show that neither S_u/p'_i nor S_u/σ_{vi}' is a unique function of V_{s1}, even for a given material and K_o. Rather, S_u/p'_i and S_u/σ_{vi}' remain a function of σ_{vi}' as well.

5.4 Application of the Proposed Approach to Two Sands

5.4.1 Test program

Ottawa sand and a compressible tailings sand from Alaska (herein referred to as Alaska sand) were selected for use in this study as they appeared to represent two extremes encompassing most sands that could be encountered in practice. Laboratory data were available for both sands (Sasitharan, 1994; Cunning, 1994) and field data (SPT, CPT and V_s logs) were available for Alaska sand. Ottawa sand is a clean, uniform, subrounded quartz sand that is relatively incompressible. Alaska sand contains approximately 30% fines (passing the No. 200 sieve), composed of a large amount of carbonate shell material

The values of Γ and λ_{ln} given in Table 5-1 for each sand are for the flatter portion of the USL (i.e. $p' < 200$ kPa). The figures presented in the remainder of this chapter are determined using these values of Γ and λ_{ln}. Consequently, the values of S_u in subsequent figures correspond to the flatter portion of each USL. Sands that have an initial void ratio less than the USL breakpoint void ratio will reach an ultimate state on the steeper portion of the USL and will possess higher ultimate undrained strengths. Since the breakpoint in each USL occurs at approximately $p'=200$ kPa and typical values of M_C for sands range from 1.2 to 1.5 (see Table 5-1), these sands will have values of S_u greater than approximately 120 to 150 kPa (based on Equation 5-9 using RSR=1). Although not shown here, for sands having an initial void ratio in the appropriate range (i.e. less than the USL breakpoint void ratio), the same framework as is presented here could be combined with Γ and λ_{ln} associated with the steeper portion of each USL to estimate the corresponding values of S_u. Note that the USL breakpoint void ratio can be converted to a breakpoint V_{s1}, based on A and B for a particular sand. Only soils with measured values of V_{s1} greater than the breakpoint V_{s1} will have ultimate states along the steeper portion of the USL.

When testing the two sands, Cunning (1994) found that the best fit values for (na+nb) were 0.266 for Ottawa sand and 0.260 for Alaska sand. Although it appears that the stress exponents are dependent on the type of sand, this study adopted the historical value for (na+nb) of 0.25 as representing a generalized value that could be applied to all sands. This was divided equally with na and nb assigned equal values of 0.125. The values of A and B for Ottawa and Alaska sand given in Table 5-1 are based on this assumption and therefore differ from the values given by Cunning et al. (1995) which were based on the sand-specific values of (na+nb). Specific values of A and B were not available for the various sands tabulated by Sasitharan et al. (1994), Ottawa sand with added fines, or kaolin. However, global values of A and B were used for these sands (see Table 5-1) since Cunning (1994) showed that most sands tend to fall within a certain band on a V_{s1}-e plot. These global values are also based on the assumption that (na+nb) has a value of 0.25.

5.4.2 Results

Figure 5-7a presents the relationship between S_u/p'_i and state parameter in triaxial compression for both sands, based on Equation 5-10. This is a unique relationship for a given sand and is independent of both stress level and K_o. The curve for Ottawa sand is much steeper, due to the flatness of the USL. Alaska sand, on the other hand, exhibits a more gradual decrease in shear strength ratio with increasing state parameter. Figure 5-7a indicates that S_u/p'_i decreases with increasing Ψ. However, for each type of sand, there is likely a maximum value of Ψ beyond which the sand cannot exist. This would correspond to a minimum possible value of S_u/p'_i.

For comparison, Figure 5-7b presents the relationship between S_u/p'_i and RSR, based on Equation 5-11. The relationship is still unique for a given sand, because it is dependent on the value of M_C. However, M_C for most sands falls within a small range; consequently, the relationships between S_u/p'_i and RSR for both Ottawa and Alaska sands are much more similar than the relationships between S_u/p'_i and Ψ, despite the wide range in soil behaviour type. Figure 5-7b indicates that S_u/p'_i decreases with increasing RSR. However, for each type of sand, there is likely a maximum value of RSR beyond which the sand cannot exist. This would correspond to a minimum possible value of S_u/p'_i.

Figures 5-8(a) and (b) present plots of V_s versus σ_v' at a K_o of 0.4 for Ottawa sand and Alaska sand, respectively. Also shown on these plots are contours of V_{s1} and, hence, contours of S_u in triaxial compression. These figures clearly indicate that the value of V_{s1} that acts as a dividing line between contractant and dilatant behaviour (i.e. RSR = 1) is not constant with σ_v' (or depth). Rather, the dividing value of V_{s1} increases with depth for either sand. Except at low values of σ_v', the dividing values, especially for Ottawa sand, agree well with the values of 140 m/s to 160 m/s suggested by Robertson et al. (1992a). Shear wave velocity profiles from the field could be superimposed over Figures 5-8(a) and (b) in order to evaluate the in-situ state and estimate the range of S_u that could be expected in-situ.

Figure 5-9 presents a plot of S_u versus V_{s1} in triaxial compression for both Ottawa and Alaska sand. For a given sand and a given K_o, S_u is a unique function of V_{s1}. As K_o increases, the S_u-V_{s1} line moves to the right as higher values of K_o will result in higher values of measured shear wave velocity. The shapes and locations of the lines for Ottawa sand and Alaska sand are quite different. This is due to the differences between the USLs, reflected in λ_{ln} and Γ. For a given state (Ψ), a soil with a flat USL (i.e. low value of λ_{ln}) will have a lower value of S_u and be more brittle in undrained shear since RSR will be higher. The S_u-V_{s1} relationship for Ottawa sand is sharper and divides more distinctly between sand with very little undrained strength and sand with high strength. The relationship for Alaska sand is more gradual, indicating a slower, steadier increase in strength as V_{s1} increases. Thus, λ_{ln}, Γ, and K_o are three major factors affecting the S_u-V_{s1}

relationship.

Figure 5-10 compares the S_u-V_{s1} relationships in triaxial compression for Ottawa and Alaska sand to the other sands tabulated by Sasitharan et al. (1994), for K_o equal to 0.4. These figures illustrate that Ottawa and Alaska sand encompass most of the other sands on a plot of S_u versus V_{s1}. In addition, it is clear that most of the other sands have sharp S_u-V_{s1} relationships, similar to or sharper than that for Ottawa sand. Alaska sand has a more gradual relationship than any of the other sands. This is because most of the other sands plotted here have λ_{ln} values similar to that for Ottawa sand whereas the value for Alaska sand is an order of magnitude greater. Comparing Leighton Buzzard and Ottawa sand, which have similar values of λ_{ln} and ϕ'_{us} (see Table 5-1), it can be seen that Leighton Buzzard sand, which has a higher value of Γ, plots to the left of Ottawa sand, although the lines for both sands have similar shapes. The relative shapes and positions of the S_u-V_{s1} relationships for the various sands parallels the relative slopes and positions of the USLs in e-p' space for the various sands (see Figure 5-5a).

Figure 5-11 illustrates the effect of adding fines to clean Ottawa sand on the relationship between S_u and V_{s1} in triaxial compression, relative to clean Ottawa sand and Alaska sand for Ko equal to 0.4. Also included in Figure 5-11 is the relationship for kaolin. It can be seen that increasing the percent kaolinite from 0% to 10% moves the S_u-V_{s1} relationship to the right of the line for clean Ottawa sand. However, if larger percentages of kaolinite were added (greater than 20%) the USL moves upward to higher void ratios (Pitman, 1993) and it would be reasonable to expect that the S_u-V_{s1} relationship would move back to the left and eventually, at 100% kaolinite, to approximately the location of the relationship for kaolin. This would be consistent with the observation made earlier that the S_u-V_{s1} plot parallels the USL plot in e-p' space (see Figure 5-5b).

5.4.3 Conversion of V_{s1} to SPT $(N_1)_{60}$ and CPT q_{c1}

In order to compare the proposed shear wave velocity method of estimating S_u, S_u/p'_i and S_u/σ_{vi}' with existing methods, V_{s1} must be converted to equivalent values of SPT $(N_1)_{60}$ and equivalent CPT q_{c1}. As outlined in Chapter 4, the following equations can be used:

[5-18] $$(N_1)_{60} = \left(\frac{V_{s1}}{X}\right)^4$$

[5-19] $$q_{c1} = \left(\frac{V_{s1}}{Y}\right)^{4.35}$$

where:
V_{s1} is in units of m/s and q_{c1} is in MPa.

Note that in Chapter 4, the exponent in Equation 5-19 was approximated as a value of 4, for ease of calculation. However, the work in this chapter was completed previously and used an exponent of 4.35 to determine the value of Y.

For clean, unaged, uncemented, relatively incompressible, predominantly silica sands (of which Ottawa sand is one), $X \approx 89.8$ (based on a modification of work by Yoshida (1988)) and $Y \approx 102$ (Robertson et al., 1992b). Equations 5-18 and 5-19 can be combined with Equation 5-15 to produce equations for estimating S_u from $(N_1)_{60}$ and q_{c1} for such sands, as follows:

[5-20] $$S_u = \frac{M}{2} \exp\left[\frac{1}{\lambda_{ln}}\left(\frac{X\,(N_1)_{60}{}^{0.25}}{B\,(K_o)^{na}} - \left(\frac{A}{B} - \Gamma\right)\right)\right] \qquad \text{(kPa)}$$

and:

[5-21] $$S_u = \frac{M}{2} \exp\left[\frac{1}{\lambda_{ln}}\left(\frac{Y\,q_{c1}{}^{0.23}}{B\,(K_o)^{na}} - \left(\frac{A}{B} - \Gamma\right)\right)\right] \qquad \text{(kPa)}$$

where q_{c1} is in MPa.

Similarly, the relationships can be combined with Equations 5-16 or 5-17 to produce equations for estimating S_u/p'_i or S_u/σ_v' from $(N_1)_{60}$ and q_{c1}.

5.4.4 The effect of compressibility on V_{s1}-$(N_1)_{60}$ and V_{s1}-q_{c1} correlations

Compressibility will have little effect on the measured shear wave velocity since shear waves do not compress the sand, but it can greatly affect the SPT and CPT penetration resistance since the more compressible the sand, the lower the penetration resistance, even at the same relative density (Robertson and Campanella, 1983). Shear wave velocity, SPT and CPT profiles were available from the tailings sand site in Alaska. Examining these profiles, it was found that $X \approx 113$ and $Y \approx 135$ were more appropriate value for linking shear wave velocity to SPT and CPT penetration resistance in Alaska sand. The increased values of these constants, as compared to the values for Ottawa sand, reflect the higher compressibility of the sand. Examining Equations 5-18 and 5-19, it is clear that the values of X and Y for Alaska sand will give lower values of penetration resistance than for Ottawa sand for the same value of V_{s1}. Using the Alaska site-specific values of X and Y in Equations 5-20 and 5-21 allows S_u to be predicted from $(N_1)_{60}$ and q_{c1}, respectively, in Alaska sand.

5.4.5 Sensitivity of the proposed method to the input parameters

The discussion presented thus far revolves around the assumption that K_o and the soil parameters ϕ'_{us}, Γ, λ_{ln}, A and B can be determined with certainty. However, in reality, although each parameter will have a "best-fit" value, it will also have a possible range of values due to the uncertainty associated with estimating its true value. Careful laboratory testing and good field estimates of K_o can minimize uncertainties. All of the graphs presented thus far have only shown the results based on the "best-fit" values of ϕ'_{us}, Γ, λ_{ln}, A and B for the two particular sands. However, the possible degrees of inaccuracy associated with these parameters will translate into bands rather than unique lines on the various plots relating S_u to shear wave velocity and penetration resistance. As an example, Figure 5-12 presents the bands of uncertainty in the correlation between S_u and V_{s1} associated with the parameter A for both Ottawa and Alaska sand. The average, upper bound and lower bound relationships between S_u and V_{s1} are shown for each sand, corresponding to the average and potential range in the value of A (see Table 5-1).

As shown in Figure 5-9, for sands with flat USLs, such as Ottawa sand, the S_u-V_{s1} relationship based on the best-fit values is already relatively sensitive. As shown in Figure Figure 5-12 for the parameter A, any degree of uncertainty associated with the input parameters will only serve to accentuate this sensitivity. Clearly, the upper and lower bound lines shown in Figure 5-12 give very different estimates of S_u for sands such as Ottawa sand. The best that can be achieved for these sands is to determine whether the field profiles fall below or above the band (in terms of V_{s1}) in order to determine whether or not undrained stability will be an issue. The effects will be less significant for sands with steep USLs, such as Alaska sand, which have a less sensitive S_u-V_{s1} relationship in the first place. A significant range in S_u (which increases as V_{s1} increases) is still predicted, using the upper and lower bound lines shown in Figure 5-12 for Alaska sand, but the range is generally smaller than for Ottawa sand.

5.5 Other Considerations

This study has considered S_u for triaxial compression loading and has presented a framework to estimate the magnitude of S_u from the USL using shear wave velocity measurements. The USL and S_u in triaxial compression are independent of initial fabric since the soil is remoulded by the time steady state is reached. Some argue that the quasi-steady state (QSS) strength is more critical for stability analyses than the steady state strength (Ishihara, 1993). Some research has also suggested that the USL may be lower and hence S_u would be significantly smaller in triaxial extension than triaxial compression (Vaid et al., 1990; Negussey and Islam, 1994).

Nevertheless, the framework presented here is still valid. If one were interested in QSS or S_u in extensional loading, the same procedure could be used to estimate the undrained strength, given that the parameters Γ, λ_{ln}, and ϕ'_{us} were determined for the quasi steady state line (QSSL) in compression or either the USL or QSSL in extension. Note that the value of M is a function of the direction of loading and that lower ultimate strengths will be predicted for loading in extension than in compression even for the same USL in e-p' space. As indicated in Chapter 4, for typical values of ϕ', the value of M_C is typically 1.4 to 1.5 times the value of M_E. This translates into theoretical ultimate strengths in triaxial compression being generally about 40% to 50% higher than theoretical ultimate strengths in triaxial extension. Chapter 4 also presented a method for estimating the minimum undrained strength at QSS in a particular sand deposit having a uniform soil fabric, based on estimated ΔRSR between the USL and the (approximately parallel) QSSL. This method is applied to one of the CANLEX sites in Chapter 8. Ishihara (1993) demonstrated that the QSS is a function of soil fabric, while ultimate state is not.

5.6 Comparison with the Current Methods of Estimating S_u

Figure 5-13 presents the results of S_u in triaxial compression versus equivalent $(N_1)_{60}$ determined using the results of Figure 5-9 together with X=89.8 for clean Ottawa sand and both X=89.8 (the incompressible correlation, referred to as Alaska (I)) and X=113 (accounting for compressibility, referred to as Alaska (C)) for Alaska sand. The other sands tabulated by Sasitharan et al. (1994) and Ottawa sand with the various percentages of kaolinite cannot be included here since no data are available to allow for a conversion from V_{s1} to $(N_1)_{60}$ in such materials. However, it would seem reasonable to hypothesize that the S_u-$(N_1)_{60}$ lines for Ottawa sand plus kaolinite would plot to the left of clean Ottawa sand since one would expect to record lower blowcounts in soil with a higher fines content.

Results from the investigation into the stability of Duncan Dam are also shown in Figure 5-13. The site investigation results for Duncan Dam indicated an increase in $(N_1)_{60}$ with increasing vertical effective stress in the sand zone in which liquefaction was predicted to be triggered by the design earthquake (Pillai and Stewart, 1994). Post-cyclic undrained monotonic simple shear testing of frozen undisturbed samples of this sand indicated that a constant ratio of S_u/σ_{vi}' of 0.21 was applicable (Pillai and Salgado, 1994). Combining the field and lab results allowed for the relationship between S_u and $(N_1)_{60}$ to be plotted as shown in Figure 5-13. Although the testing involved a different direction of loading than is considered here, the relationship for Duncan Dam is clearly similar to the results of this study, having a similar shape and location on the plot and, in particular, showing S_u to increase with increasing $(N_1)_{60}$ at a similar rate as the triaxial compression relationships for Ottawa and Alaska sand.

Superimposed on Figure 5-13, for purpose of comparison, are the upper and lower bound lines relating S_u to $(N_1)_{60}$ from Seed and Harder (1990), as shown in Figure 5-1. There is a relationship between S_u and $(N_1)_{60}$, as Seed and Harder were suggesting; however, this relationship is unique only for a given sand and a given K_o-condition. This study has shown that K_o plays an important role in the S_u-$(N_1)_{60}$ relationship for any given sand and that the differences in compressibility and fabric between Ottawa sand and Alaska sand result in very different relationships. The empirical plot by Seed and Harder (1990) incorporates 17 case histories involving different types of sand and likely involving different conditions of K_o. Hence, the framework presented in this study can account for the scatter in the Seed and Harder (1990) plot by attributing it in part to variations in compressibility, fabric and K_o amongst the various case histories. The Seed and Harder (1990) lines appear much flatter than both the results from this study and those for Duncan Dam, thereby predicting much lower strengths for high values of $(N_1)_{60}$. It is possible that other factors which have not been taken into account in this study, such as pore pressure redistribution or the effects of other directions of loading, may be responsible for the differences between the Seed and Harder (1990) lines derived from case histories and the results of this study. The case histories forming the Seed and Harder (1990) empirical chart may have actually suffered failures due to a combination of undrained strengths in different directions of loading (e.g. triaxial compression, triaxial extension and simple shear). The single back-calculated value of S_u for each case history likely represents the overall average slope behaviour. In addition, some of the case histories in the Seed and Harder (1990) database appear to be cases of cyclic softening for which an estimate of S_u is not applicable (see Chapter 7).

The plot by Seed and Harder (1990) is for the equivalent SPT $(N_1)_{60}$ in clean sand. Thus, for the case histories in sand with fines, a fines content correction was applied to increase the value of the measured $(N_1)_{60}$ to reflect what the equivalent $(N_1)_{60}$ would be in clean sand. The fines content corrections (ΔN_1) suggested by Seed (1987) were $\Delta N_1 = 1, 2, 4$ and 5 for fines contents of 10%, 25%, 50% and 75%, respectively. Seed (1987) explained that these were tentative values, but that judgement should be exercised in applying the corrections due to differences between different soils. Although not explained as such by Seed (1987), it is felt by the authors that these correction factors were an attempt to account for the increased compressibility of sand with fines relative to clean sand. Looking at the results of this study for Alaska sand which has a fines content of about 31%, it can be seen that the difference between the Alaska (I) results and the Alaska (C) results varies with $(N_1)_{60}$ and K_o, but has an average $\Delta(N_1)_{60}$ of approximately 3. This is consistent with the correction factors suggested by Seed (1987). Note that, although fines content may be an indirect measure of compressibility, clean sands may also be compressible. For these sands, such as clean carbonate sands, Seed (1987) would not recommend a correction factor, whereas the method followed here would directly incorporate the compressibility of the sand into the relationship between S_u and $(N_1)_{60}$.

Figure 5-14 presents the results of S_u/σ_{vi}' in triaxial compression versus equivalent $(N_1)_{60}$ determined by combining Equation 5-17 with Equation 5-18, using X=89.8 for clean Ottawa sand and both X=89.8 (the incompressible correlation, referred to as Alaska (I)) and X=113 (accounting for compressibility, referred to as Alaska (C)) for Alaska sand. For the reasons explained above, the other sands from Sasitharan et al. (1994) and Ottawa sand plus kaolinite are not included on this figure. Superimposed on Figure 5-14, for purpose of comparison, are the upper bound, lower bound and average lines relating S_u/σ_{vi}' to $(N_1)_{60}$ from Stark and Mesri (1992), as shown in Figure 5-2. It can be seen that, contrary to the suggestion by Stark and Mesri, there is no unique relationship between S_u/σ_{vi}' and $(N_1)_{60}$. Although the 20 case histories in Stark and Mesri's plot appear to follow a trend, there is a lot of scatter. This is likely due to differences in compressibility, fabric and K_o between case histories, as in the Seed and Harder plot, but is also compounded by the fact that S_u/σ_{vi}' and $(N_1)_{60}$ are not related by a unique relationship, even for a given sand and K_o-condition. Two case histories involving similar types of sands and K_o-conditions, would not plot in the same place on the plot if the stress levels were different. As for the Seed and Harder (1990) plot, Stark and Mesri's (1992) plot is for the equivalent $(N_1)_{60}$ in clean sand. The same comments, outlined above, regarding the relationship between compressibility and fines content also apply here.

Figure 5-15 presents the results of S_u in triaxial compression versus equivalent q_{c1} using the results of Figure 5-9 and Y=102 for clean Ottawa sand and Y=135 for Alaska sand. The other sands from Sasitharan et al. (1994) and Ottawa sand with the various percentages of kaolinite cannot be included here since no data are available to allow for conversions from V_{s1} to q_{c1} in such materials. However, it would seem reasonable to hypothesize that the S_u-q_{c1} lines for Ottawa sand plus kaolinite would plot to the left of clean Ottawa sand since one would expect to record lower cone tip resistances in a material with a higher fines content. Superimposed on Figure 5-15 are the results from Robertson (1990), as shown in Figure 5-3, which he suggested were approximate in nature due to the limited test data and the complex series of assumptions required. The results of this study and from Robertson (1990) both indicate that there is a unique relationship between S_u and q_{c1} for a given sand at a given Ko. The lines for Ottawa sand from this study and from Robertson (1990) are both lower bounds for the given sands; however, there is some difference. The line for Alaska sand falls in the range of other compressible sands such as Hilton Mines tailings.

Figure 5-16 presents S_u/p'_i in triaxial compression versus normalized CPT penetration resistance, $(q_c\text{-}p)/p'$ for both Ottawa sand and Alaska sand calculated for K_o=0.5, since Robertson's (1990) results which are superimposed on this figure were for a K_o of 0.5 (see Figure 5-4). In general, Ottawa sand and Alaska sand encompass several other types of sands and therefore represent two extremes of the types of sands that are likely to be encountered in practice. Robertson's (1990) unique lines for each sand are based on the proposal by Been and Jefferies (1987) that there is a unique relationship between state parameter and normalized CPT penetration resistance. The fact that the results of this study indicate a dependency on stress for the relationship between S_u/p'_i and normalized CPT suggests that the relationship between state parameter and normalized CPT resistance is not unique. Sladen (1989) also questioned the uniqueness of the relationship proposed by Been and Jefferies (1987).

Figure 5-17 compares the results of this study with those by Baziar and Dobry (1995).

Baziar and Dobry (1995) compiled a database of liquefaction case histories consisting of lateral spreads and failures of slopes or embankments in saturated silty sands and sandy silts. These case histories are shown as points on a plot of $(N_1)_{60}$ versus vertical effective stress in Figure 5-17. Also shown in Figure 5-17 is the upper boundary for large deformation potential in saturated silt-sand deposits that Baziar and Dobry (1995) drew based on these case histories. This line is essentially a dividing line between contractant and dilatant behaviour. Superimposed on Figure 5-12 are the dividing lines (i.e. RSR=1) that would be predicted for Ottawa sand (using X=89.8) and Alaska sand (using X=113) for a K_o of 0.5, based on the framework presented earlier. The results of this study appear to be consistent with the findings by Baziar and Dobry (1995), as their upper boundary line (for silt-sands) falls between the lines for Ottawa sand (with no fines) and Alaska sand (very compressible with approximately 30% fines), at $\sigma_{vi}' < 100$ kPa.

At higher stresses, the Baziar and Dobry (1995) line is controlled by one case history (the Upper San Fernando Dam) which had an average in-situ measured $(N_1)_{60}$ of 13, as reported by Seed and Harder (1990). In fact, this case record did not represent a slope failure, as did most of the other slope or embankment case records. Rather, the dam suffered only limited deformations which were relatively small compared to the overall size of the dam. Therefore, if this case record is disregarded or if a lower $(N_1)_{60}$ (closer to the minimum measured value) controlled the observed deformations (see Chapter 7), the Baziar and Dobry (1995) line would remain between the lines for Alaska and Ottawa sand up to approximately 200 kPa.

5.7 Comparison with Laboratory Testing Results

The predictions of S_u based on in-situ testing using the framework proposed here can be compared to laboratory testing results on undisturbed samples of sand from deposits which have been characterized using in-situ testing. The earlier discussion regarding Duncan Dam provided a comparison between the framework suggested here and the combination of available SPT data and laboratory results. A comparison between laboratory test results and undrained strengths predicted using the framework suggested here and CPT data is illustrated in Chapter 8 for one of the CANLEX sites.

5.8 Conclusions

This study has combined critical state soil mechanics and shear wave velocity measurements in order to develop a framework which can be used to estimate the in-situ undrained ultimate state shear strength of a sand. In the process, the range of values that can be expected to encompass most sands on plots of S_u in triaxial compression versus V_{s1}, q_{c1} or $(N_1)_{60}$ has been shown and has been attributed primarily to the location of the USL in terms of Γ and λ_{ln} as well as K_o. More compressible sands tend to have larger values of λ_{ln}. In this chapter, S_u was estimated based on the ultimate state line for very loose samples tested in triaxial compression for each sand; however, the framework developed here can also be used to estimate undrained strengths at quasi-steady-state or in other directions of loading (see Chapter 4). The plot of S_u versus $(N_1)_{60}$ by Seed and Harder (1990) appears conservative when compared with the results of this study, especially for compressible sands with high values of λ_{ln} and Γ and for site conditions producing low values of K_o. However, other factors such as other directions of loading and pore pressure redistribution may have affected some of the case histories used to produce the Seed and Harder (1990) correlation. In addition, some of the case histories in the Seed and Harder (1990) database appear to be cases of cyclic softening for which an estimate of S_u is not applicable (see Chapter 7).

This study has also demonstrated that it is unlikely to have a unique relationship between S_u/σ_{vi}' and $(N_1)_{60}$, as suggested by Stark and Mesri (1992) or between S_u/p'_i and normalized CPT resistance, as suggested by Jefferies et al. (1990). The empirical case histories do suggest such a relationship, in that the general trend is an increase in S_u/σ_{vi}' or S_u/p'_i as $(N_1)_{60}$ or normalized CPT resistance increases. However, encompassed in the empirical case histories is the fact that the relationships are stress level dependent for a given sand, in addition to being dependent on compressibility and differences in K_o between sands. A constant S_u/p'_i or S_u/σ_{vi}' ratio can only be used on a site-specific basis for a particular direction of loading when RSR is a constant.

Finally, the application of the proposed method relies on laboratory work to determine the parameters of the USL (ϕ'_{us}, Γ, λ_{ln}) and the parameters relating V_{s1} to e for a particular sand (A and B). Although the method appears quite promising, it is not without drawbacks. The level of accuracy in estimating S_u using shear-wave velocity may present significant problems and should be considered when applying the method. If the USL of a sand is relatively flat ($\lambda_{ln} < 0.035$), it will not be possible to accurately determine S_u using shear wave velocity measurements or in-situ penetration testing. Note that this is the case for the flat portion of the USL for most of the uniform, clean silica sands included in this study. In fact, one of the most important findings of this study is that for most sands, S_u appears to be a very sensitive parameter and, therefore, very difficult to accurately estimate using any method, including the one investigated here. However, for such sands, it will be possible to estimate the dividing line, in terms of V_{s1}, $(N_1)_{60}$, or q_{c1}, between soil conditions that will exhibit essentially little or no strength when loaded undrained and soil conditions that will be able to fully mobilize the steady state drained friction angle. A further complication when estimating S_u from in-situ tests is the possible effects of pore pressure redistribution after cyclic (earthquake) loading.

Table 5-1: Material properties for (a) Ottawa and Alaska sand (Cunning, 1994); Ottawa sand with added kaolinite fines (Skirrow, 1995) and (b) other sands (Sasitharan et al., 1994)

(a) Sand	ϕ'_{us}	M_C	M_E	Γ^*	λ_{ln}^*	A	B
Ottawa	30.5	1.22	0.87	0.926	0.032	385.5[a]	261.8
Alaska	36.5	1.48	0.99	1.485	0.117	319.5[b]	178.7
Ottawa+5% fines	29.5	1.18	0.84	0.809	0.029	*c*	*c*
Ottawa+7.5% fines	29.6	1.18	0.85	0.835	0.052	*c*	*c*
Ottawa+10% fines	29.4	1.17	0.84	0.930	0.103	*c*	*c*
Kaolin[d]	25	0.98	0.74	1.92	0.181	*c*	*c*

(b) Sand	ϕ'_{us}	M_C	M_E	Γ^*	λ_{ln}^*	A	B
Erksak	30.9	1.24	0.88	0.82	0.013	*c*	*c*
Toyoura(p'us<100kPa)	30.9	1.24	0.88	0.938	0.004	*c*	*c*
Lornex	35	1.42	0.96	1.1	0.022	*c*	*c*
Brenda	35.9	1.46	0.98	1.112	0.042	*c*	*c*
Syncrude	29.8	1.19	0.85	0.847	0.017	*c*	*c*
Nerlerk	30	1.20	0.86	0.885	0.014	*c*	*c*
Leighton Buzzard	29.8	1.19	0.85	1	0.035	*c*	*c*

Notes:

* Γ and λ_{ln} apply to the flat portion of the USL for each soil (i.e. p'<200 kPa, unless noted otherwise)

a range = 371 to 397 m/s

b range = 314 to 326 m/s

c use global values of A = 363 m/s (range = 340 to 380 m/s) and B = 235 m/s

d ϕ'_{us} cited by Atkinson (1993); λ_{ln} & Γ based on PI=32%, Gs=2.70, and formulae in Atkinson (1993)

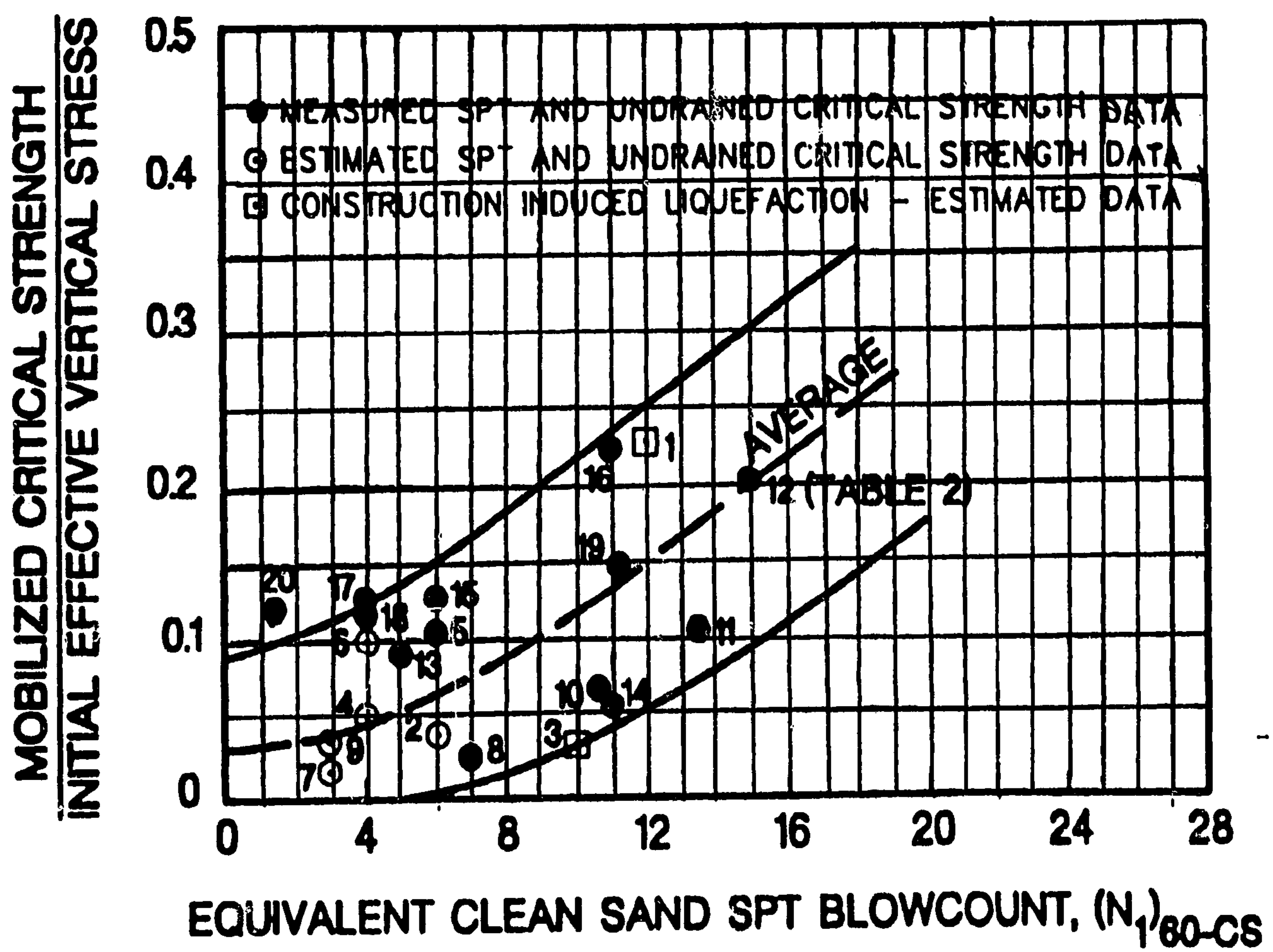

Figure 5-2 Relationship between clean sand equivalent SPT blowcount, $(N_1)_{60\text{-}cs}$ and undrained strength ratio, S_u/σ_v' (modified from Stark and Mesri, 1992).

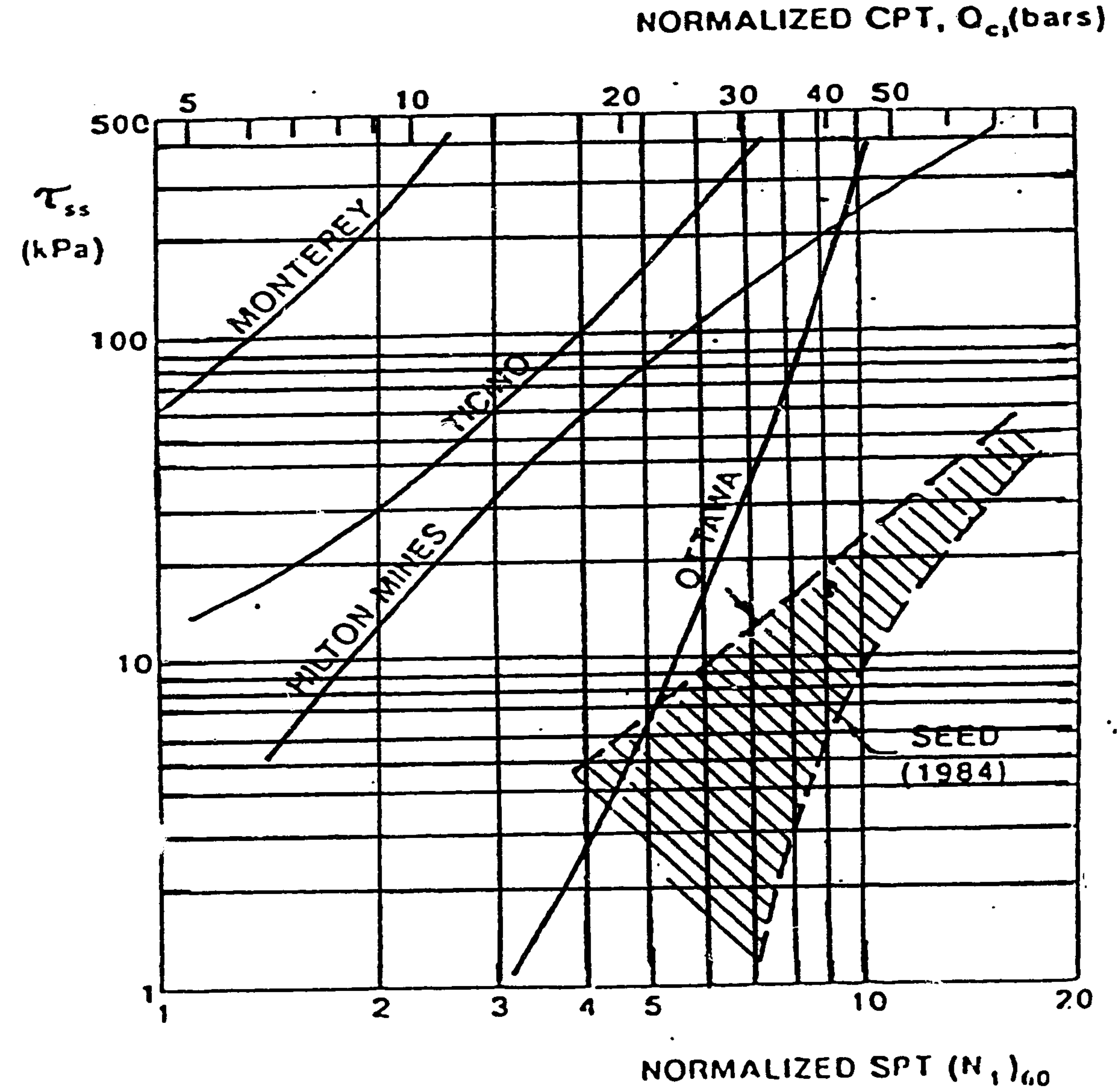

Figure 5-3 Correlations between residual strength and normalized CPT penetration resistance based on relative density (modified from Robertson, 1990).

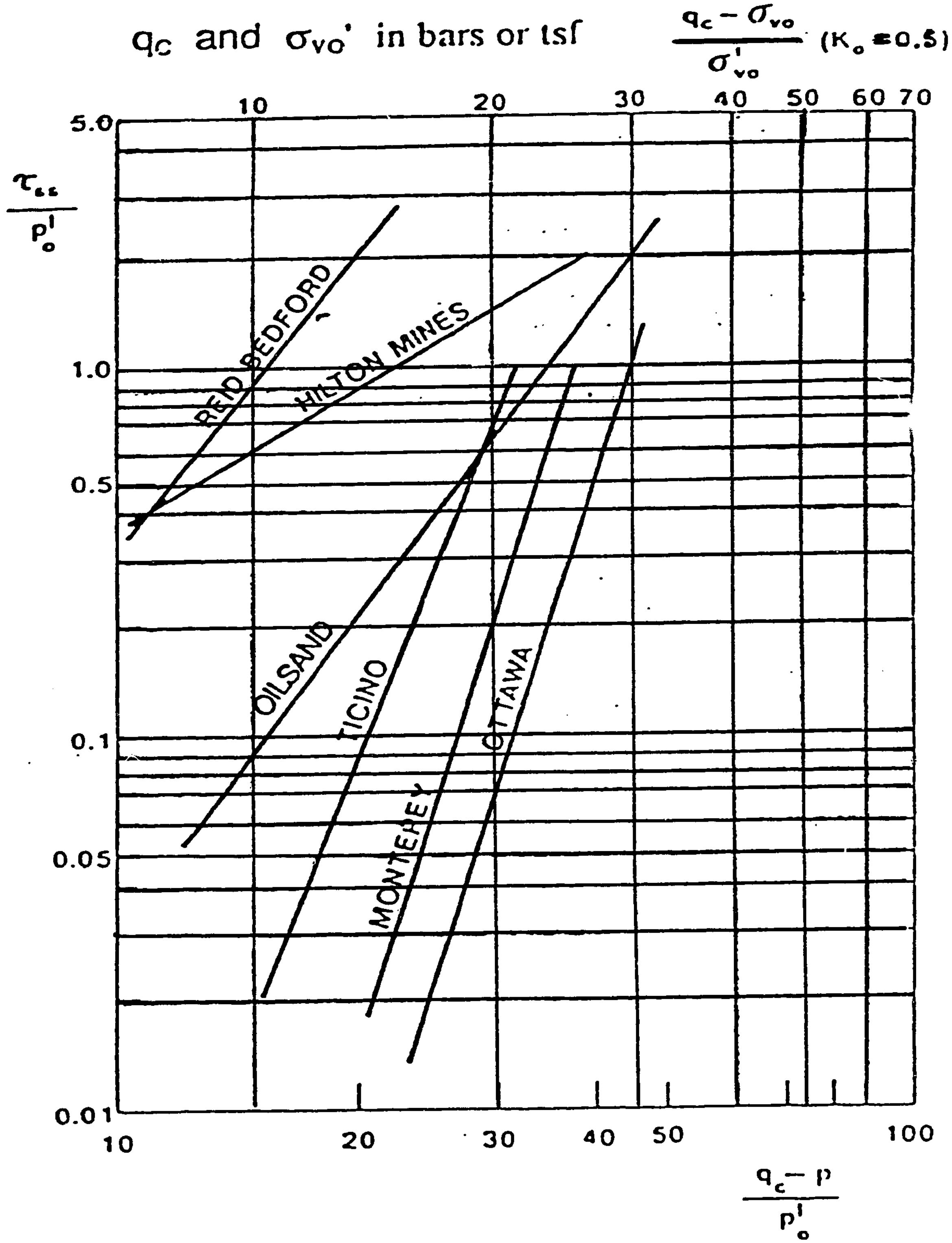

Figure 5-4 Correlations between residual strength ratio and normalized CPT penetration resistance based on state parameter (modified from Robertson, 1990).

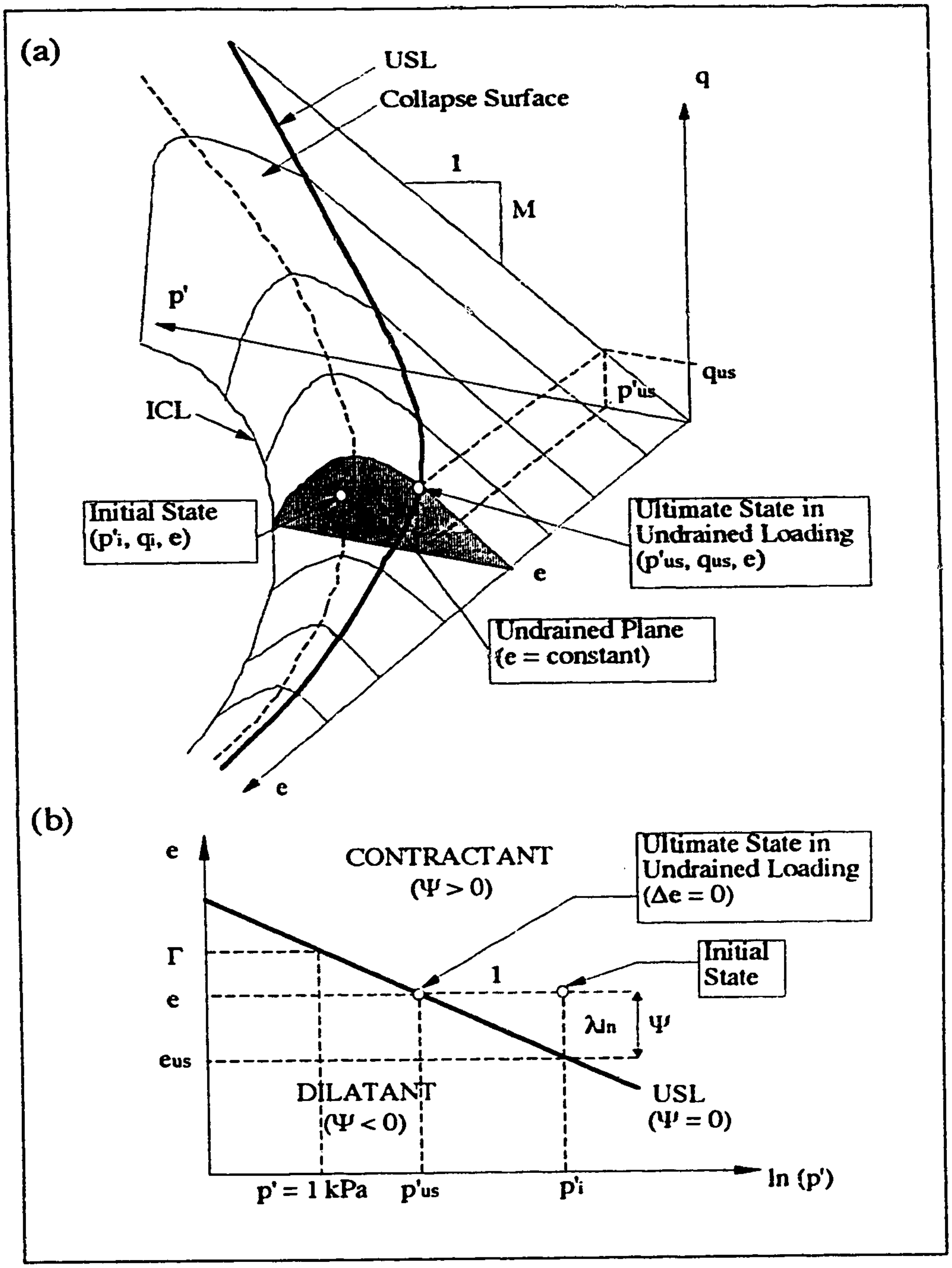

Figure 5-5 Critical state soil mechanics concepts illustrated by (a) e-p'-q diagram with (b) projections onto the e-ln(p') plane.

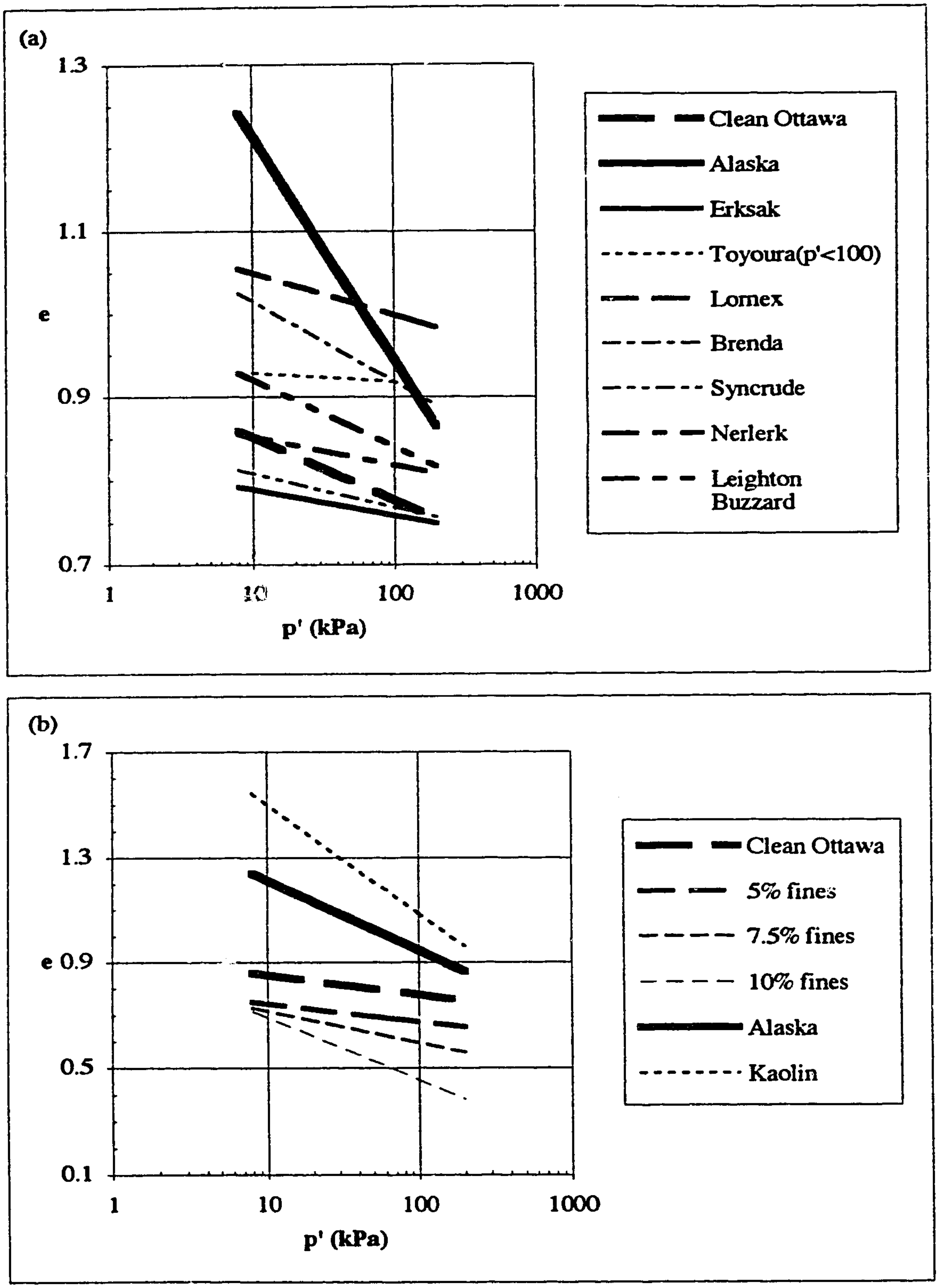

Figure 5-6 Steady state lines for Ottawa sand and Alaska sand compared with (a) other sands and (b) Ottawa sand with fines and kaolin.

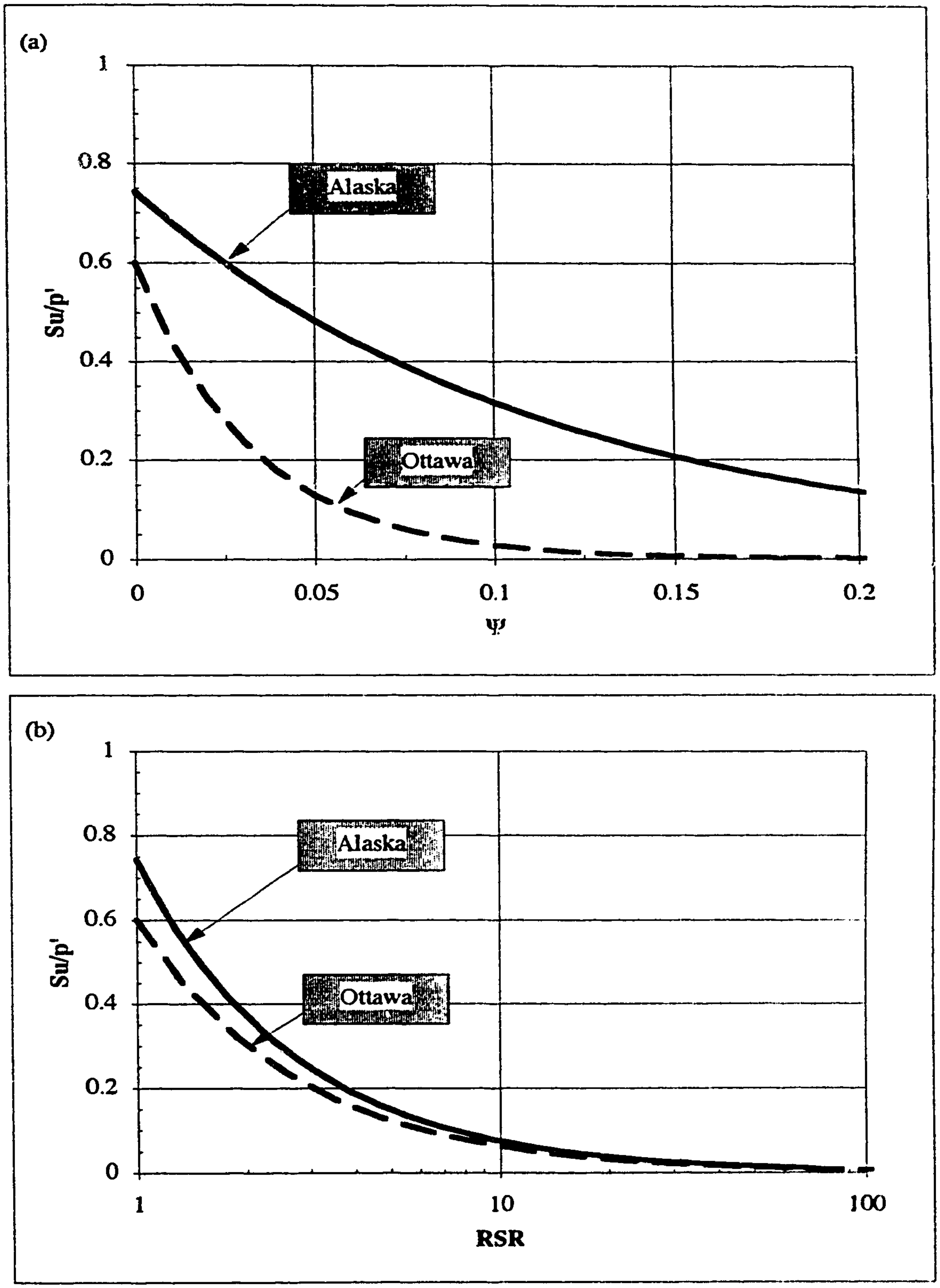

Figure 5-7 Relationship between S_u/p' and (a) state parameter (Ψ) and (b) reference stress ratio (RSR) in triaxial compression for Ottawa sand and Alaska sand.

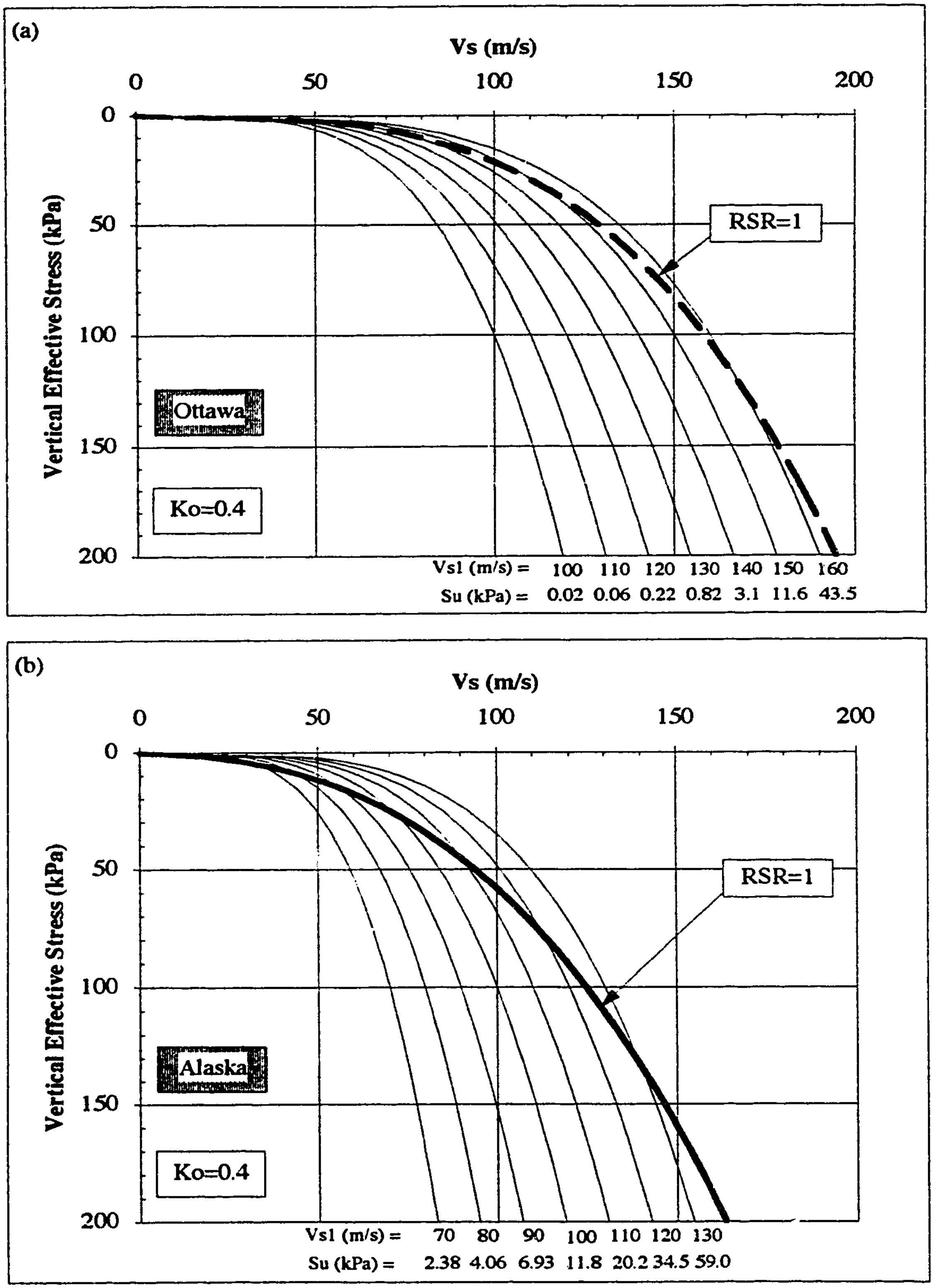

Figure 5-8 Contractant-dilatant boundary (RSR=1 or Ψ=0) compared with contours of V_{s1} (or S_u in triaxial compression) for (a) Ottawa sand and (b) Alaska sand.

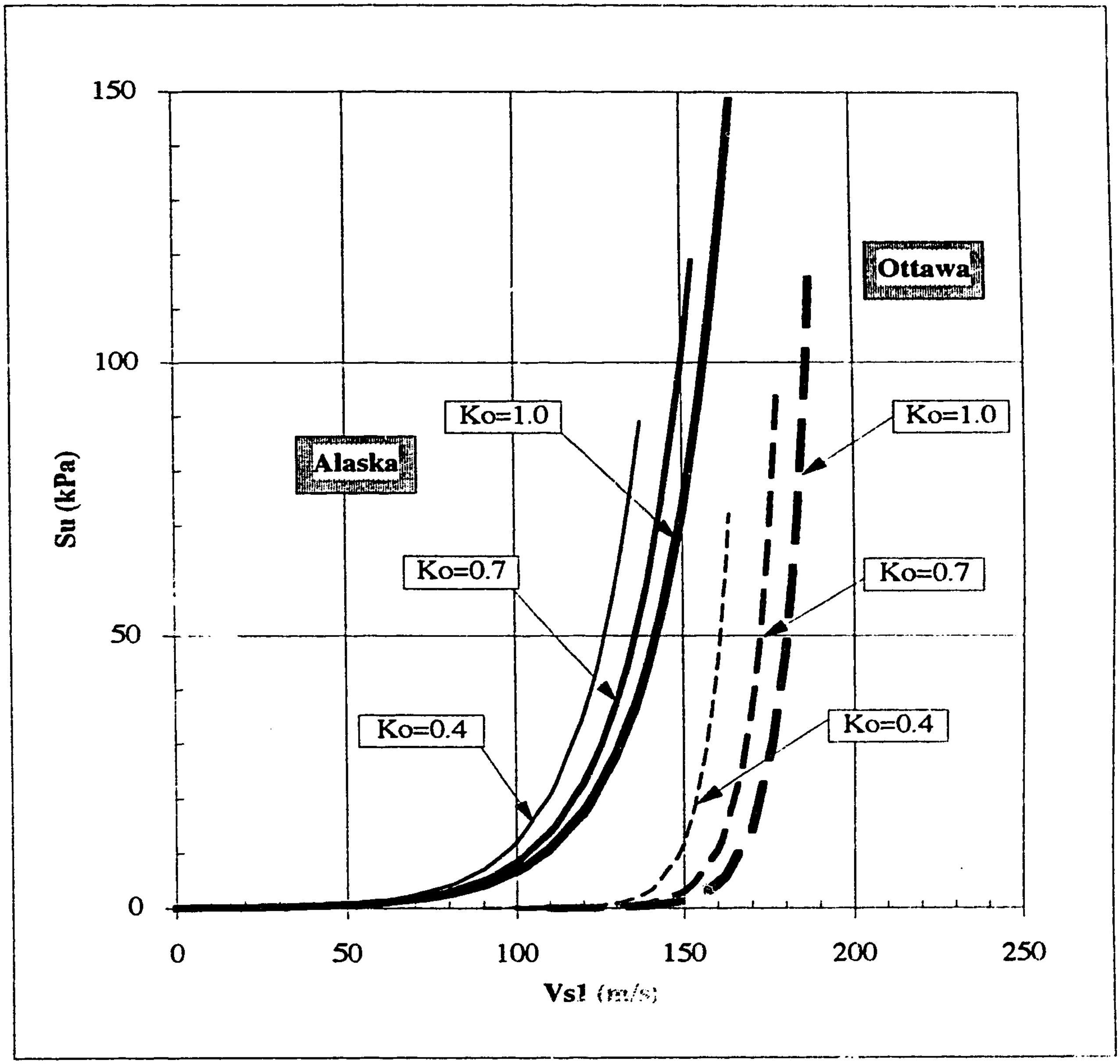

Figure 5-9 Relationship between S_u in triaxial compression and V_{s1} for Ottawa sand and Alaska sand for a range in K_o.

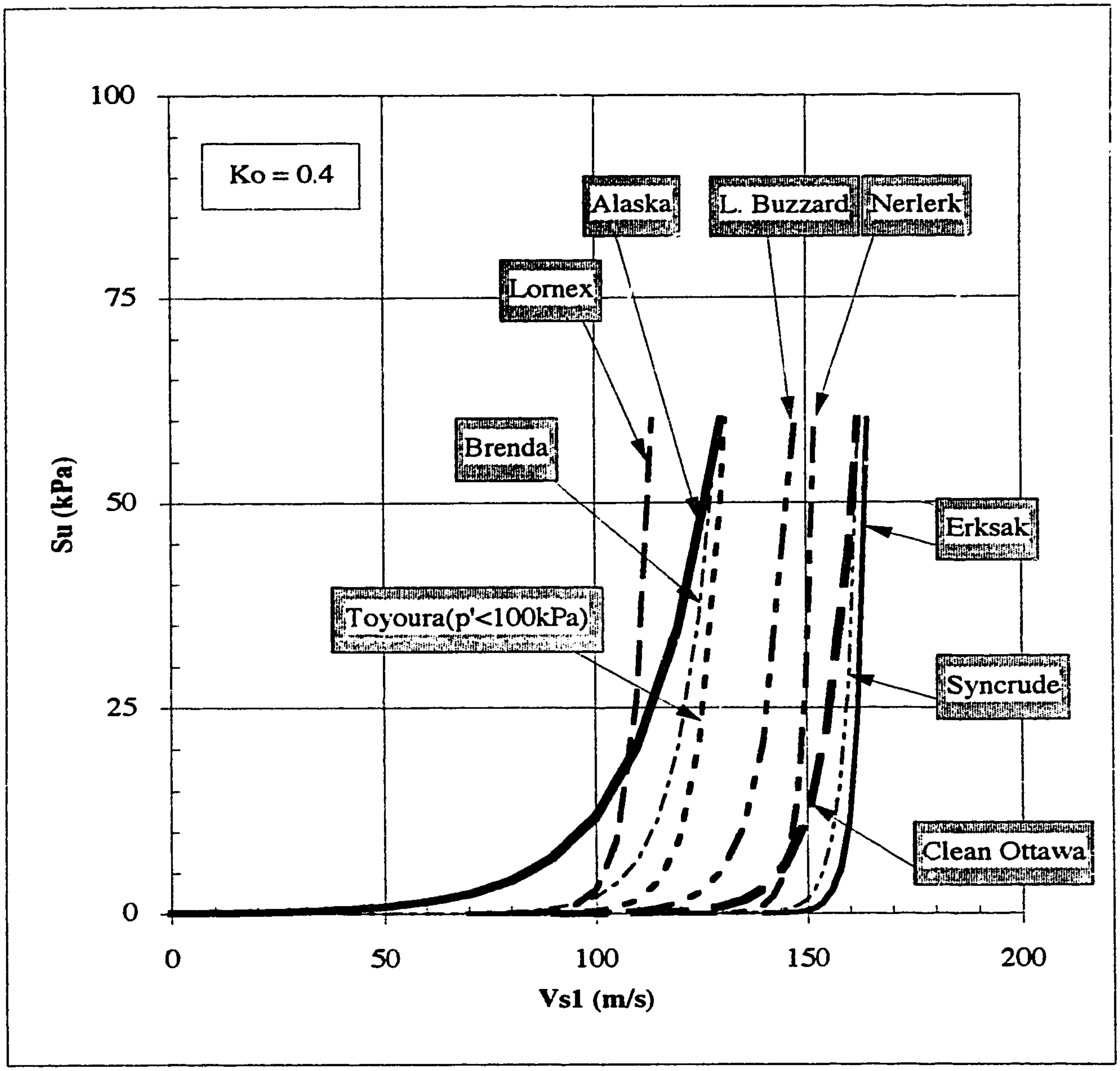

Figure 5-10 Relationship between S_u in triaxial compression and V_{s1} for other sands compared with Ottawa sand and Alaska sand.

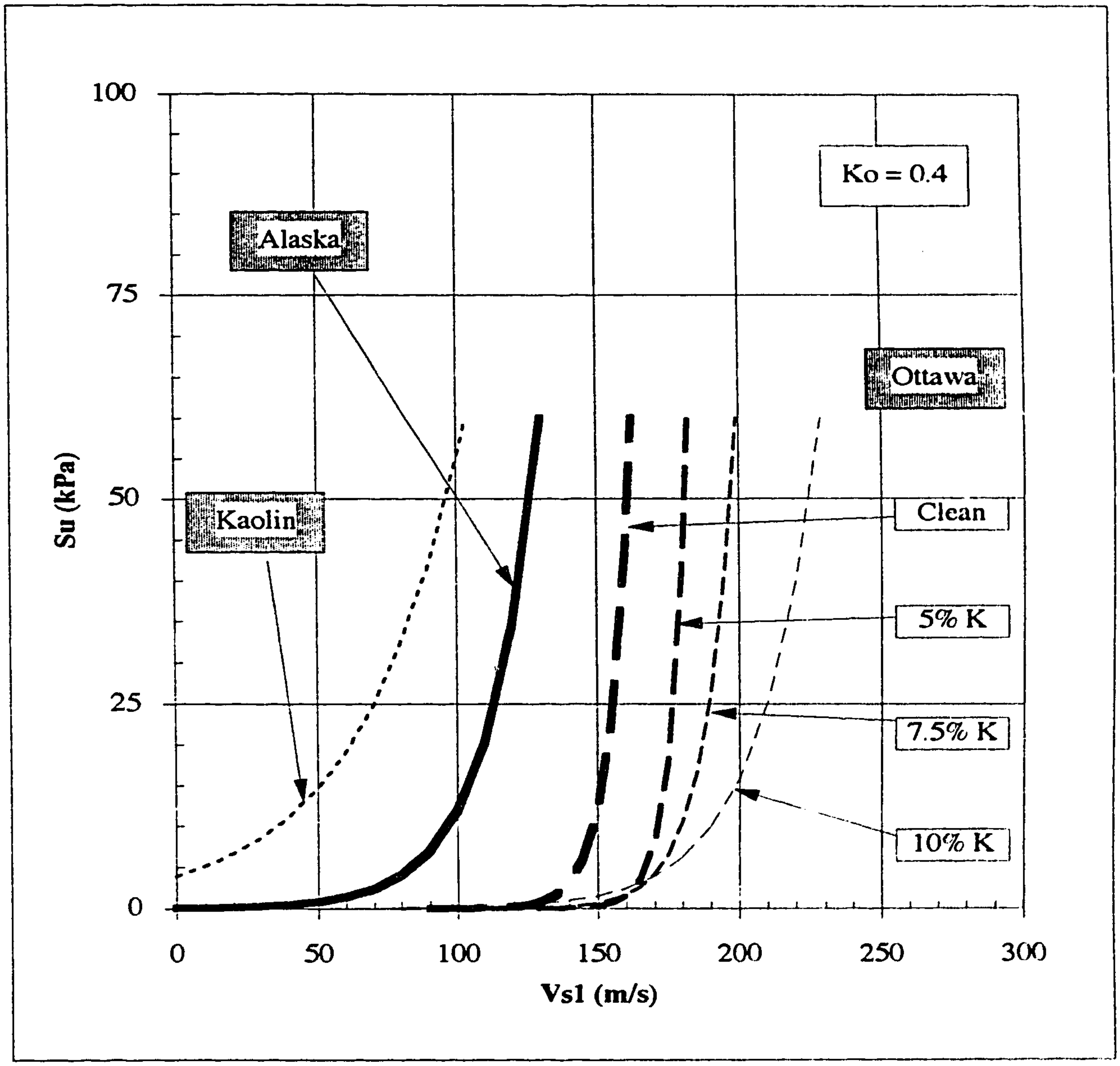

Figure 5-11 Relationship between S_u in triaxial compression and V_{s1} for Ottawa sand with fines and kaolin compared with Ottawa sand and Alaska sand.

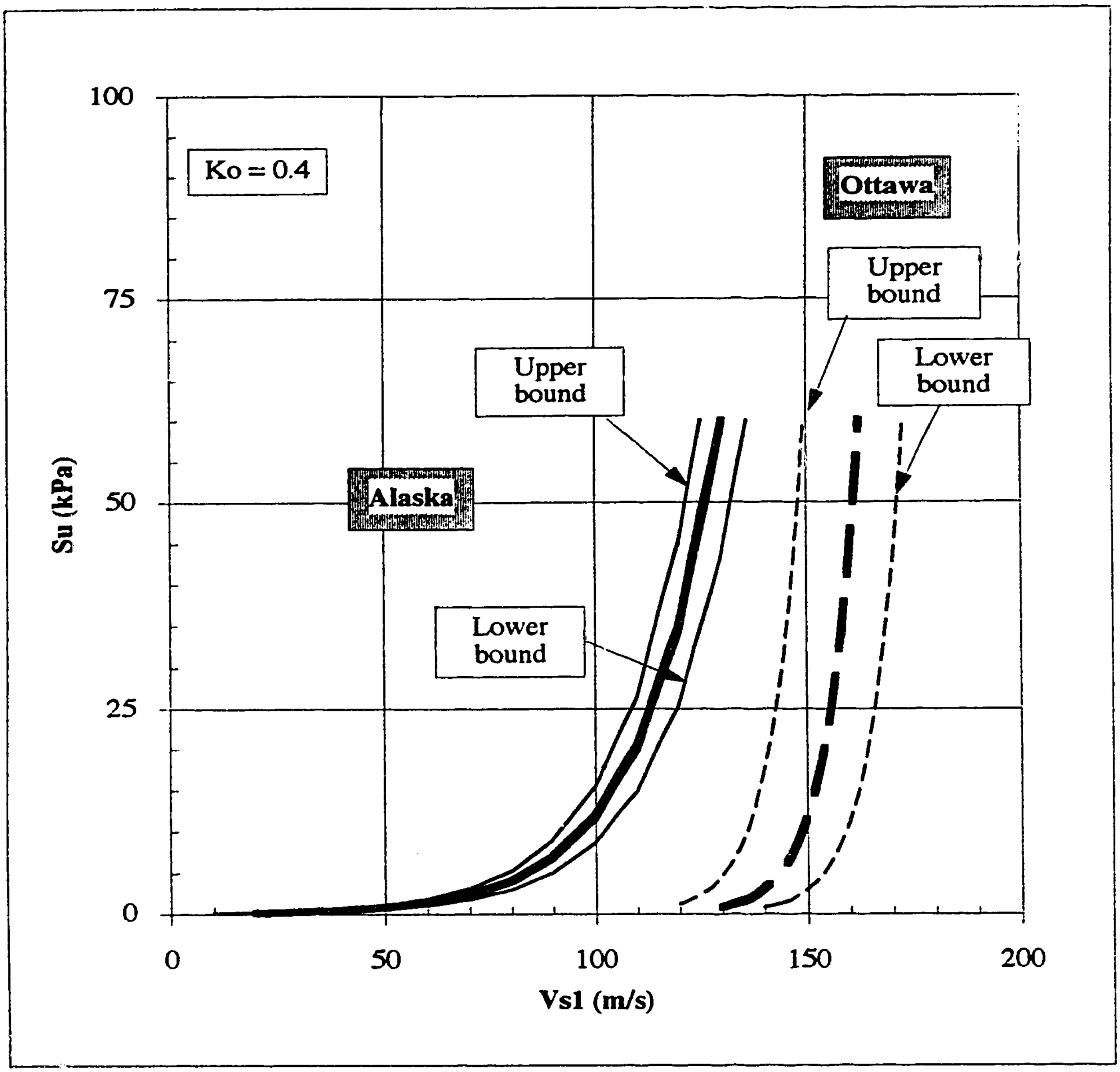

Figure 5-12 Illustration of the sensitivity of S_u-V_{s1} relationship in triaxial compression associated with the range in possible values for the parameter A for Ottawa sand and Alaska sand and K_o=0.4.

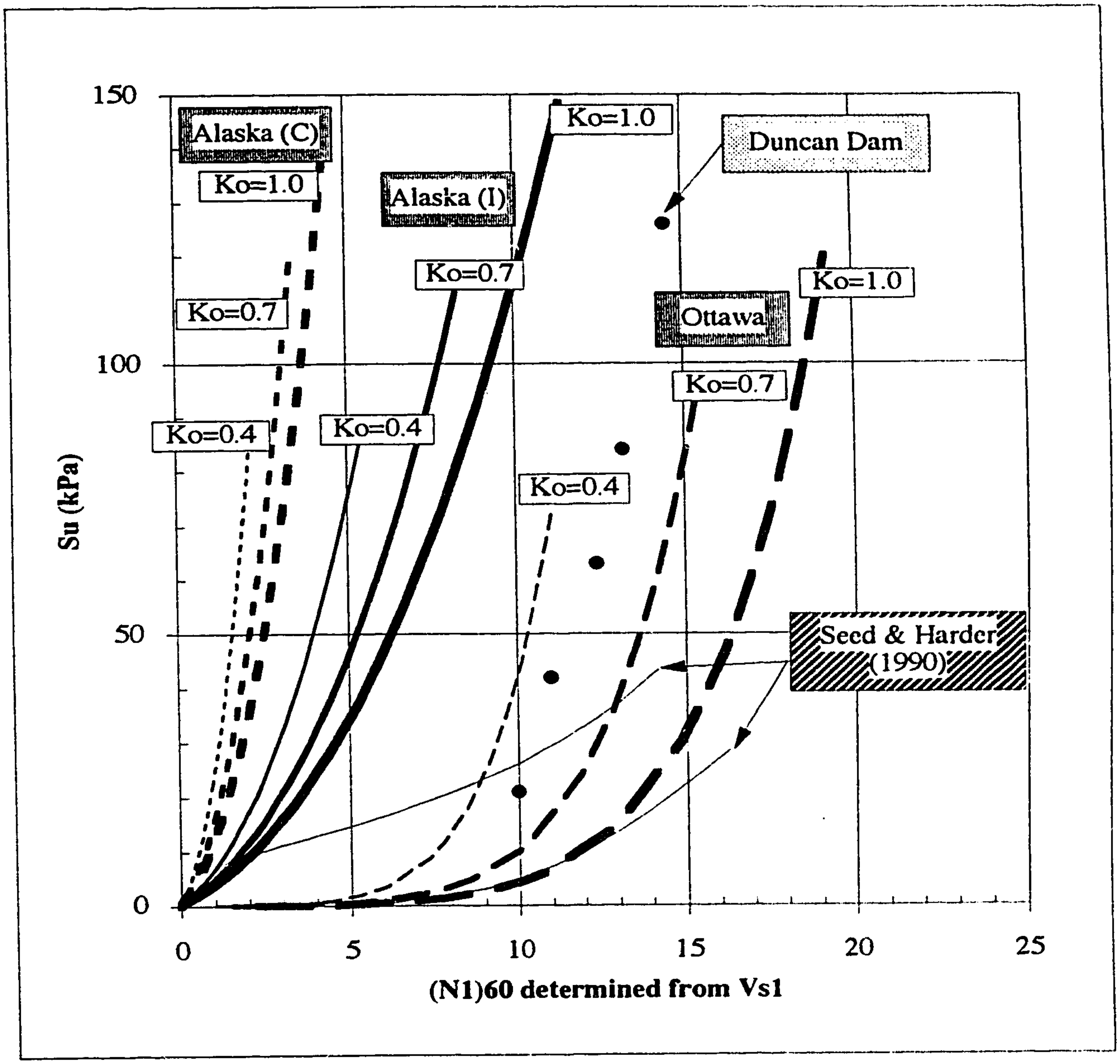

Figure 5-13 Relationship between S_u in triaxial compression and $(N_1)_{60}$ for Ottawa sand and Alaska sand compared with data from Duncan Dam and results from Seed and Harder (1990).

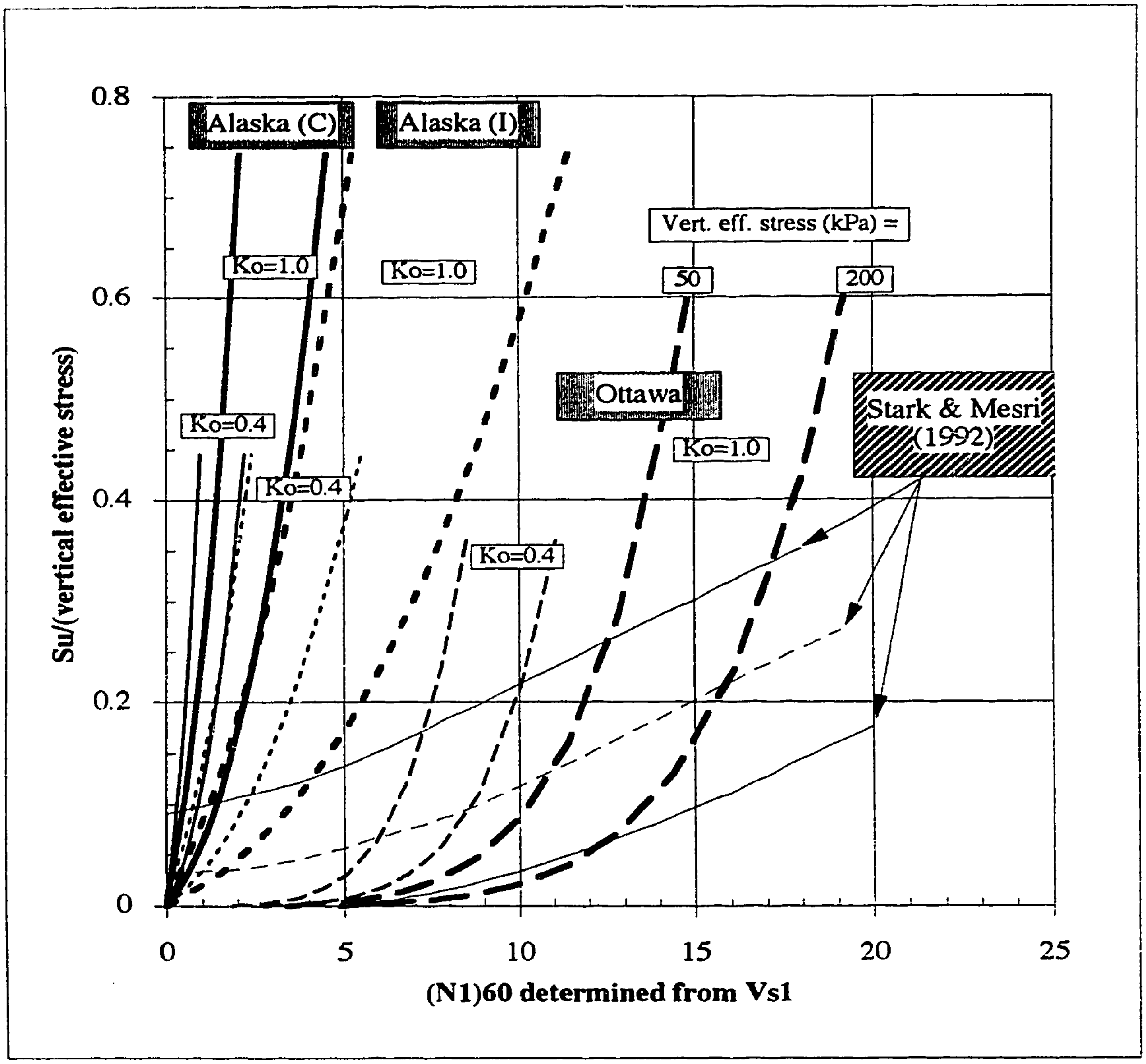

Figure 5-14 Relationship between S_u/σ_v' in triaxial compression and $(N_1)_{60}$ for Ottawa sand and Alaska sand compared with results from Stark and Mesri (1992).

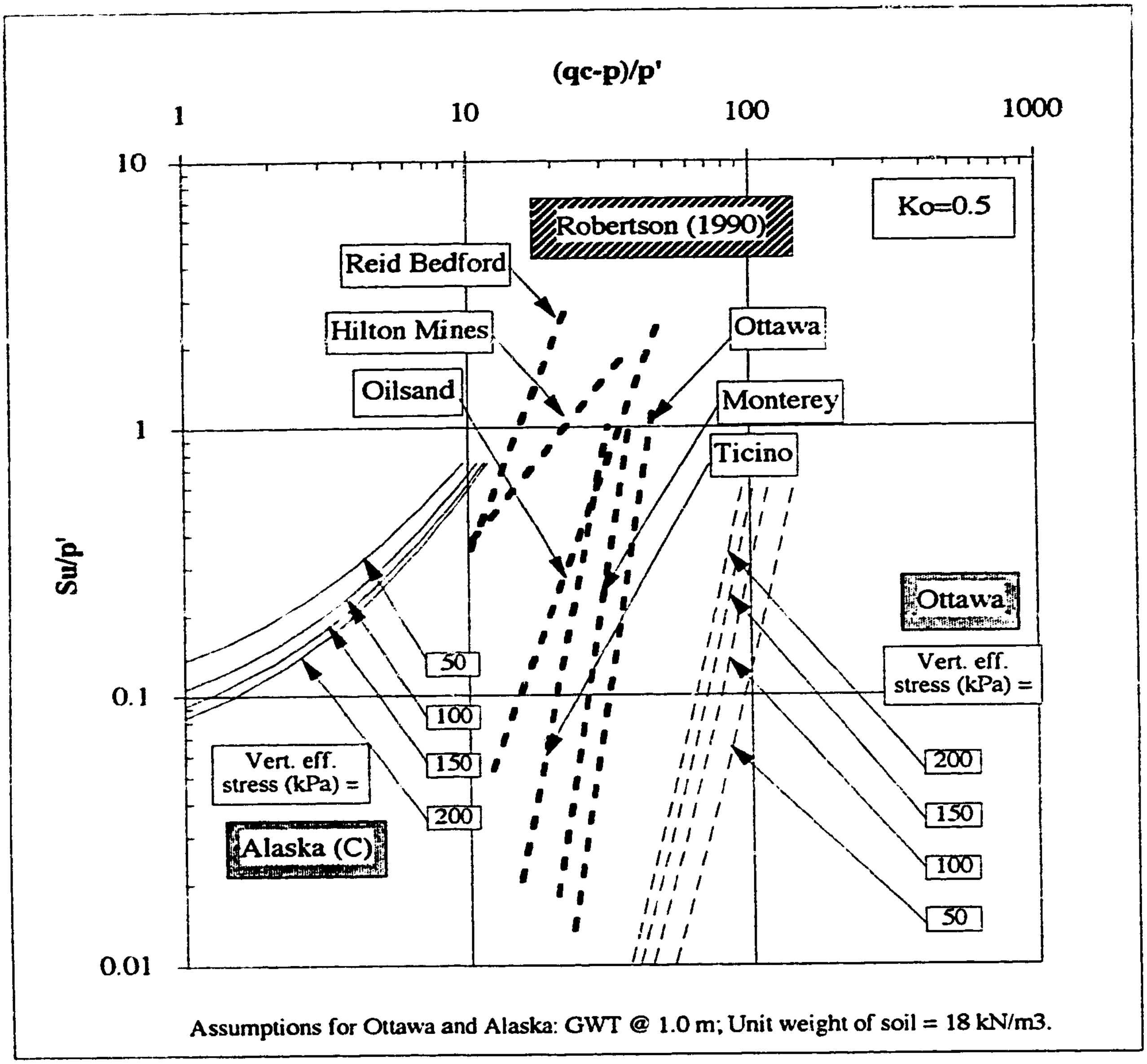

Figure 5-16 Relationship between S_u/p' in triaxial compression and $(q_c\text{-}p)/p'$ for Ottawa sand and Alaska sand compared with results from Robertson (1990).

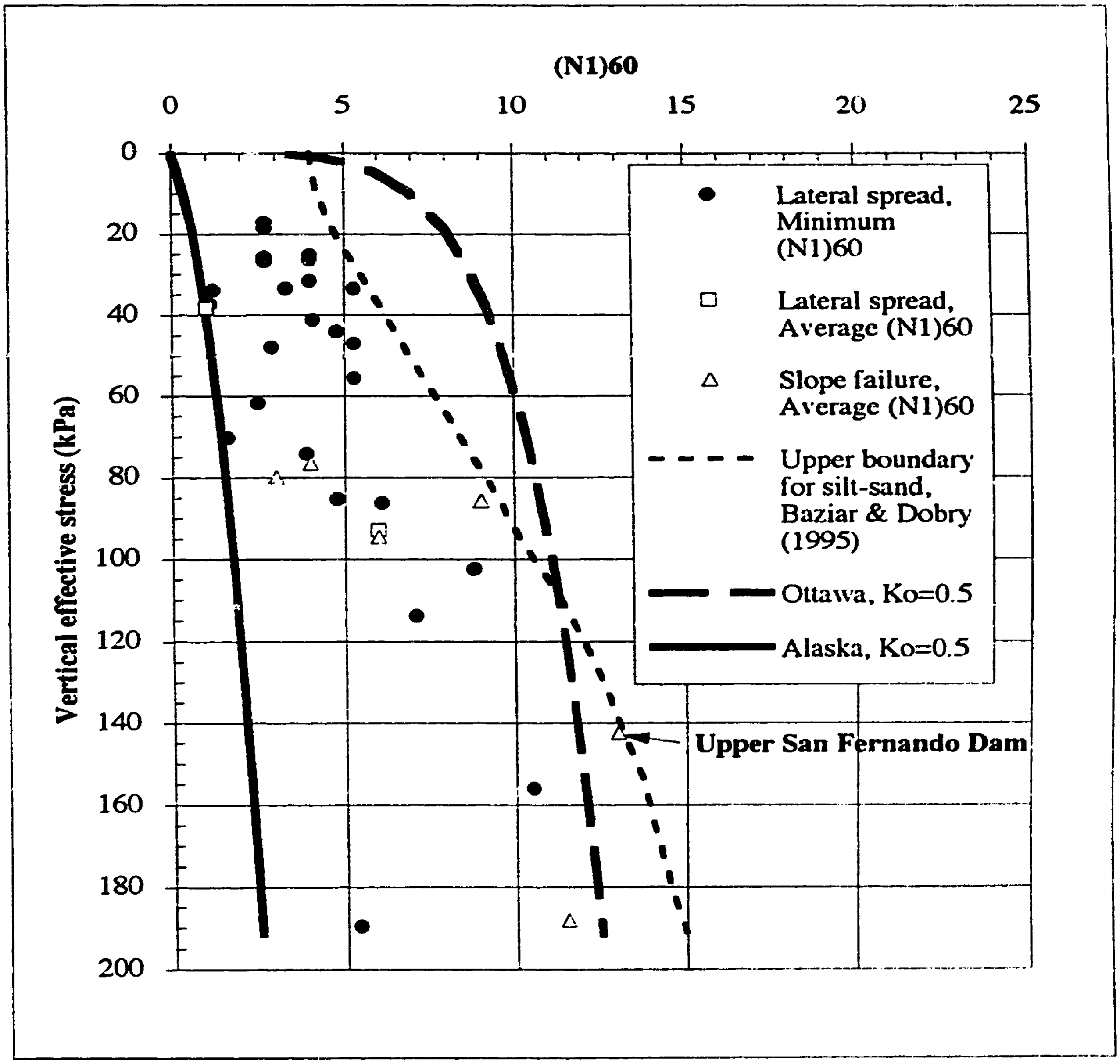

Figure 5-17 Contractant-dilatant boundary lines for Ottawa sand and Alaska sand compared with results from Baziar and Dobry (1995).

References

Atkinson, J. 1993. *An introduction to the mechanics of soils and foundations*, McGraw-Hill, London, pp. 103-123.

Baziar, M.H., and Dobry, R. 1995. Residual strength and large-deformation potential of loose silty sands. *Journal of Geotechnical Engineering*, ASCE 121(12): 896-907.

Been, K., and Jefferies, M.G. 1985. A state parameter for sands. *Géotechnique*, 35(2): 99-112.

Been, K., Crooks, J.H.A., Becker, D.E., and Jefferies, M.G. 1986. The cone penetration test in sands: part I, state parameter interpretation. *Géotechnique*, 36(2): 239-249.

Been, K., Jefferies, M.G., Crooks J.H.A., and Rothenburg, L. 1987. The cone penetration test in sands: part II, general inference of state. *Géotechnique*, 37(3): 285-299.

Been, K., Jefferies, M.G., and Hachey, J. 1991. The critical state of sands. *Géotechnique*, 41(3): 365-381.

Byrne, P.M., Imrie, A.S., and Morgenstern, N.R. 1994. Results and implications of seismic performance studies for Duncan Dam. *Canadian Geotechnical Journal*, 31(6): 979-988.

Cunning J.C. 1994. Shear wave velocity measurement of cohesionless soils for evaluation of in-situ state, *M.Sc. Thesis*, Department of Civil Engineering, University of Alberta at Edmonton, Alberta.

Cunning, J.C., Robertson, P.K., and Sego, D.C. 1995. Shear wave velocity to evaluate in-situ state of cohesionless soils, *Canadian Geotechnical Journal*, 32(5): 848-858.

Ishihara, K. 1993. Liquefaction and flow failure during earthquakes. The 33rd Rankine Lecture, *Géotechnique*, 43(3): 351-415.

Jefferies, M.G., Been, K., and Hachey, J.E. 1990. Influence of scale on the constitutive behaviour of sand. *Proceedings of the 43rd Canadian Geotechnical Conference*, Laval University, 1: 263-273.

Negussey D. and Islam, M.S. 1994. Uniqueness of steady state and liquefaction potential. *Canadian Geotechnical Journal*, 31(1): 132-139.

Pillai, V.S. and Salgado, F.M. 1994. Post-liquefaction stability and deformation analysis of Duncan Dam. *Canadian Geotechnical Journal*, 31(6): 967-978.

Pillai, V.S. and Stewart, R.A. 1994. Evaluation of liquefaction potential of foundation soils at Duncan Dam. *Canadian Geotechnical Journal*, 31(6): 951-966.

Pitman, T.D. 1993. Effect of fines and gradation of the collapse surface of a loose saturated soil. *M.Sc. thesis*, Department of Civil Engineering, University of Alberta, Edmonton, Alberta.

Robertson, P.K. 1990. Evaluation of residual shear strength of sands during liquefaction from penetration tests. *Proceedings of the 43rd Canadian Geotechnical Conference*, Laval University, 1: 257-262.

Robertson, P.K., and Campanella, R.G. 1983. Interpretation of cone penetration tests. Part I: sand. *Canadian Geotechnical Journal*, 20(4): 718-733.

Robertson, P.K., Woeller, D.J., and Finn, W.D.L. 1992a. Seismic cone penetration test for evaluation liquefaction potential under cyclic loading. *Canadian Geotechnical Journal*, 29: 686-695.

Robertson, P.K., Woeller, D.J., Kokan, M., Hunter, J., and Luternauer, J. 1992b. Seismic techniques to evaluate liquefaction potential. *Proceedings of the 45th Canadian Geotechnical Conference*, 5:1-5:9.

Robertson, P.K., Sasitharan, S., Cunning, J.C., and Sego, D.C. 1995. Shear wave velocity to evaluate in-situ state of Ottawa sand. *Journal of Geotechnical Engineering*, ASCE, 121(3): 249-261.

Sasitharan, S. 1994. Collapse behaviour of very loose sand. *Ph.D. Thesis*, Department of Civil Engineering, University of Alberta, Edmonton, Alberta.

Sasitharan, S., Robertson, P.K., Sego, D.C., and Morgenstern, N.R. 1994. State boundary surface for very loose sand and its practical implications. *Canadian Geotechnical Journal*, 31(3): 321-334.

Seed, H.B. 1987. Design problems in soil liquefaction. *Journal of Geotechnical Engineering*, 113(8): 827-845.

Seed, R.B., and Harder, L.F. 1990. SPT-based analysis of cyclic pore pressure generation and undrained residual strength. *Proceedings of the H. Bolton Seed Memorial Symposium*, 2: 351-376.

Skirrow, R. 1995. The effects of fines content on the monotonic triaxial testing of cohesionless soils for evaluation of in-situ state. *M.Sc. Thesis*, Department of Civil Engineering, University of Alberta, Edmonton, Alberta.

Sladen, J.A. 1989. Problems with interpretation of sand state from cone penetration test. *Géotechnique*, 39(2): 323-332.

Stark, T.D., and Mesri, G. 1992. Undrained shear strength of liquefied sands for stability analysis. *Journal of Geotechnical Engineering*, ASCE 118(11): 1727-1747.

Vaid, Y.P., Chung, E.K.F., and Kuerbis, R.H. 1990. Stress path and steady state. *Canadian Geotechnical Journal*, 27: 1-7.

Wood, D.M. 1990. *Soil Behaviour and Critical State Soil Mechanics.* Cambridge University Press, pp. 179-188.

Yoshida, Y., Ikemi, M., and Kokusho, T. 1988. Empirical formulas of SPT blow-counts for gravely soils. *Proceedings of Penetration Testing*, Balkema, Rotterdam, 1: 381-387.

CHAPTER 6

EMPIRICAL ESTIMATION OF UNDRAINED SHEAR STRENGTH BASED ON DOWNHOLE PLATE LOAD TESTS[1]

6.1 Introduction

The previous chapter has illustrated the difficulty in estimating undrained shear strengths from conventional penetration testing in sand. In clay, plate load testing is a method that is often used to estimate undrained shear strengths. This chapter reports on an experimental program that was developed to investigate the potential of using rapid downhole plate load testing as an alternative method for estimating undrained shear strengths in sand. The goal of the plate load testing was to push the plates as rapidly as possible in an attempt to load the sand in an undrained manner and, therefore, to be able to estimate the undrained shear strength of the loose sand from the measured bearing stress on the plate.

The experimental program consisted of a series of downhole plate load tests that were conducted at radii of approximately 5 to 9 m (in plan) from the location of in-situ freezing and sampling in J-pit at Syncrude, in conjunction with the Canadian Liquefaction Experiment (CANLEX) Phase III site investigation activity. This phase of the CANLEX project consisted of filling an old borrow pit (J-pit) at Syncrude, in Ft. McMurray, Alberta, with tailings to create a relatively loose sand deposit with a groundwater table at a depth of approximately 0.5 m.

The experimental program was preliminary in nature; however the results appear promising. This chapter describes the test program, presents the measured results from testing using both 4" (10 cm) and 6" (15 cm) diameter plates, provides a basic interpretation of the results and makes recommendations for future studies. Ideally, it would be desirable to compare the undrained strengths predicted using the plate load tests with undrained strengths measured in the laboratory by testing undisturbed samples. However, to date only very limited testing on undisturbed samples of Phase III sand has been conducted by the CANLEX project. Therefore, comparisons of the results of the

---

[1] *An abstract for a version of this chapter has been accepted for publication. Fear, C.E., Cyre, G., Robertson, P.K., and Morgenstern, N.R. 1996. Proceedings of the 49th Canadian Geotechnical Conference, St. John's, Newfoundland, September 23-25.*

plate load testing with the results of laboratory testing on undisturbed samples from the site will be possible at a future date once additional laboratory testing is performed and the overall Phase III data review activity is completed.

6.2 Test Program and Equipment[2]

Figure 6-1 presents a plan view of the detailed test site at J-pit. Indicated on Figure 6-1 are the locations of in-situ freezing and sampling, locations of conventional in-situ testing (SPT, CPT, geophysical logging) and the approximate locations of the plate load tests that were conducted at the site. 4" diameter plates were used in boreholes PL1, PL2, FS5 and FS52. Note that the abbreviation FS indicates a frozen sampling borehole; testing in these boreholes was conducted in the unfrozen soil beneath the frozen target zone after sampling of the frozen soil was completed. 6" diameter plates were used in boreholes PL4, PL5 and PL6, with the exception of one test using a seven inch diameter plate (the first test in borehole PL4).

6.2.1 Basic equipment for initial 4" diameter plate load tests

From June 27 to 29, 1995, a total of sixteen plate load tests were carried out using a 4" diameter steel plate (3/4 inch thick) that could be screwed onto the end of a drill stem. A load cell was constructed to fit between the drill head and the top of the drill stem and a displacement transducer that could measure the displacement of the drill head was mounted on the drill rig. Figure 6-2 illustrates the configuration of the overall test setup. Figure 6-3 illustrates the details of the plate system, the load cell and the displacement transducer. The data acquisition system that was in place to monitor the instrumentation for the planned CANLEX static liquefaction event was used to take and record readings from both the load cell and the displacement cell every tenth of a second. The average rate of penetration was approximately 30 cm/s, using a hydraulic drill rig from Mobile Augers.

Table 6-1 summarizes the details of each individual 4" diameter plate load test. The tests were carried out at a variety of depths in four boreholes, two of which were sampling holes through the frozen target zone (plate load tests in these holes were carried out in the

---

[2] *The plate load test equipment was all designed and built by Gerry Cyre of the University of Alberta. The detailed figures illustrating the specifics of the equipment configuration in the following section were also produced by Gerry Cyre.*

unfrozen soil below the frozen target zone). The plate was displaced anywhere from 20 cm to 120 cm during a given test.

The data acquisition system was turned on before each test was started and was kept running until the test was completed. The load cell and displacement cell readings were recorded automatically on a continuous basis. It was therefore very important to correctly identify the start of the test within a large data file and "zero" the initial readings accordingly. Figure 6-4 presents calibration charts for the load cell and the displacement cell that were used in this stage of plate load testing. Both of these charts were determined in the laboratory prior to conducting the plate load tests in the field.

The start of each test was identified as the point at which the displacement cell readings began to quickly change. At this point, the initial displacement was set equal to zero. Subsequent displacements were determined from the change in voltage and the displacement cell calibration chart given in Figure 6-4. The corresponding load measured by the load cell was set equal to zero. Additional loads were determined by the change in voltage and the load cell calibration chart given in Figure 6-4. The total initial load on the plate was determined by adding the weight of the rods and plate system to the load measured by the load cell, accounting for the correct number of rods that were added as the borehole advanced. The bearing stress on the plate was then determined by dividing the total load by the plate area.

6.2.2 Advanced equipment for 6", 7" or 8" diameter plate load tests

As will be explained in subsequent sections of this chapter, it appeared that the 4" diameter plate load testing did not create undrained conditions in the sand. Therefore, from August 21 to 22, 1995, a second stage of testing was conducted. This consisted of five plate load tests in 3 boreholes using larger diameter plates (i.e. with longer drainage paths), to try to ensure undrained conditions. Three of these tests were carried out continuously over several metres, stopping only to attach additional lengths of drillstem. A more sophisticated system consisting of a downhole load cell and a steel plate with a built-in pore pressure transducer was designed and built. The advantages of this system were that more reliable measurements of bearing stress on the downhole plate and an indication of the effects of loading on pore pressures could be obtained. If undrained conditions could be produced with sufficiently rapid loading, one would expect to see increases in pore pressure measured by the pore pressure transducer. Figure 6-5 illustrates the configuration of the overall test setup for the second stage of plate load testing.

Three plates of different diameters (6", 7" and 8") were constructed, each with a pore pressure transducer. Figure 6-6 illustrates the details of the downhole plate, load cell and pore pressure transducer configuration. The location of the pore pressure transducer is such that it may not correctly measure the actual pore pressures; however, the relative increase or decrease in observed pore pressure response can be meaningful. The same displacement transducer was used as for the 4" plate load tests. Again, readings were taken and recorded every tenth of a second, using the on-site data acquisition system. The average rate of penetration was slower, at approximately 5 to 7 cm/s, using a hydraulic drill rig from Elgin.

Table 6-2 summarizes the details of each individual 6" diameter plate load tests. The 8" plate would have been difficult to use because it would have been too tight a fit in the 8" borehole that the rig could drill. The first test was carried out starting at a depth of 10 ft (3 m) using the 7" diameter plate, but could not be pushed more than 10 inches because the bearing stress exceeded the capacity of the drill rig. The set-up was therefore switched to the 6" plate, which was used for the rest of the tests in this second stage of plate load testing. The first 6" plate load test at a depth of 15 ft (4.6 m) also exceeded the capacity of the drill rig after a small displacement. However, at a greater depth (starting at 20 ft (6.1 m)), the 6" plate advanced easily and a continuous plate load test was performed with a total displacement of approximately 6 m, at which point the drill rig's capacity was exceeded. Subsequently, in two other boreholes, continuous plate load tests were also performed using the 6" plate, starting at depths of 20 ft (6.1 m) and 17 ft (5.2 m), respectively, with each test advancing a total of 5 to 6 m before refusal.

As for the 4" diameter plate load tests, the data acquisition system was turned on before each test was started and was kept running until the test was completed and the load cell and displacement cell readings were recorded automatically on a continuous basis. Again, it was very important to correctly identify the start of the test within a large data file and "zero" the initial readings accordingly. Figure 6-7 presents the calibration charts for the load cell and displacement cell that were used during this stage of plate load testing. The load cell calibration was carried out in the laboratory after completion of the fieldwork. The displacement cell calibration was carried out while in the field. Figure 6-8 presents the calibration chart for the pore pressure transducer that was built into the downhole plate system. The pore pressure calibration was performed in the laboratory prior to conducting the plate load tests.

The start of the test was identified as the point at which the displacement cell readings began to quickly change. At this point, the initial displacement was set equal to zero. Subsequent displacements were determined from the change in voltage and the displacement cell calibration chart given in Figure 6-7. Since the load cell in this configuration was a downhole load cell, it essentially measures the total load on the plate. The total initial load measured by the load cell corresponding to zero displacement was set equal to the weight of the rods acting on the load cell before plate was advanced. Additional loads were determined by the change in voltage and the load cell calibration chart given in Figure 6-7. Since the load cell was part of the downhole plate system, any additional rods that were added as the plate was advanced would be felt by the load cell and be incorporated into the observed change in voltage relative to the initial zero value. The bearing stress on the plate was then determined by dividing the total load by the plate area. It was difficult to zero the pore pressure readings since no reference pressure was available. Pore pressure was therefore calculated directly by combining the measured voltage from the pore pressure transducer with the pore pressure calibration chart presented in Figure 6-8.

6.3 General Plate Load Test Theory

Conventional bearing capacity theory used to estimate the undrained strength of clay from plate load tests can be used to interpret undrained strengths in sand if the plate load test is performed with a big enough diameter plate and occurs rapidly enough to promote undrained conditions. The following section outlines conventional theory for estimating the undrained strength of a soil from plate load tests.

Assuming that undrained conditions apply, and that the soil is rigid, perfectly plastic in nature, the ultimate bearing capacity (q_f) of an infinite strip footing located on the ground surface is related to the undrained strength of the soil (S_u) by the following exact solution based on classical plasticity theory:

[6-1] $$q_f = (2 + \pi)\, S_u$$

Skempton (1951) modified this equation to account for the effects of footing shape (e.g. circular or square versus strip) and the depth below ground surface, provided that locating the plate at depth provides a confining effect to the soil beneath the plate. The resulting equation is:

[6-2] $$q_f = N_c S_u + \gamma D$$

where:
N_c = bearing capacity factor
γ = unit weight of soil
B = width of plate
L = length of footing
D = depth of footing

The bearing capacity factor, N_c, is a function of both the shape of the footing (defined by the ratio B/L) and the depth of the footing (defined by the ratio D/B). The chart proposed by Skempton (1951) for estimating N_c is given in Figure 6-9 and applies to soils that are rigid, perfectly plastic, as indicated. For infinite strip footings (i.e. B/L=0) located at the ground surface (i.e. D/B=0) the chart in Figure 6-9 gives an N_c of 5.14 corresponding to the value given in Equation 6-1 (i.e. $2 + \pi$).

The plate load tests conducted in this study were all circular plates; therefore the ratio B/L has a value of 1. In addition, the plate diameter (B) ranged from 4" to 6" (10 cm to 15 cm) and the depths that the tests were conducted at ranged from approximately 2.5 ft to 25 ft (0.8 to 8 m), giving ratios of D/B greater than 5 (the maximum value shown in Figure 6-9). For most of the tests, D/B was much greater than 5 since many of the tests were conducted at depths of more than 10 ft (3.3 m). Therefore, based on Skempton's (1951) chart shown in Figure 6-9, an N_c of 9 is appropriate for an initial interpretation of the downhole plate load tests, assuming that the soil is rigid, perfectly plastic in nature and that locating the plate at depth provides confinement.

Rearranging Equation 6-2 gives the following equation to theoretically estimate undrained shear strengths (S_u) in sand from the measured bearing stress (q_f) during rapid downhole circular plate load tests, assuming undrained conditions are induced:

[6-3] $$S_u = \frac{q_f - \sigma_v}{N_c}$$

where:
σ_v = total overburden stress at the depth of the test = γD
N_c = 9 for a test at depth (with confinement) in a rigid, perfectly plastic material

This formula is based on classical plasticity theory for a general shear model. However, many of the plate load tests that were conducted as part of this study (particularly during the second stage of testing) were continuous tests over a range in depth of up to several metres. The only pauses were to attach additional lengths of drillstem. Therefore, many of the tests were somewhat like a large CPT test. Note that the conventional CPT has a tip area of approximately 10 cm^2, while the 4" and 6" diameter plates used in this study had much larger areas of approximately 80 cm^2 and 180 cm^2, respectively. An additional complicating factor with the plate load tests, as compared to the CPT, is the geometry of the plate and rod system being pushed continuously into the soil. Since the plate diameter is larger than the drillstem diameter (see Figures 6-3 and 6-6) soil will be pushed around the plate and behind it as the plate is advanced into the soil. This may decrease the measured bearing stress on the plate, due to the lack of confinement of the soil.

CPT testing in fine grained soil has been used to estimate the undrained strength of the soil (Robertson and Campanella, 1988/89). The same formula as given by Equation 6-3 can been used, except that the term N_c is replaced by an empirical cone bearing factor, N_k. Various studies comparing the estimated undrained shear strengths with other methods of estimating undrained strengths in clay (e.g. the field vane test), as summarized by Robertson and Campanella (1988/89) have shown that N_k is in the order of 15 ± 5. In clay, the factor N_k is a function of OCR, sensitivity and soil stiffness; studies also show that in sensitive clays, N_k may have a value less than 10 (Robertson and Campanella, 1988/89).

In this study, N_c was assigned a value of 9 for an initial interpretation of the downhole plate load tests. Based on the earlier discussion, this value may not be appropriate if the soil is strain-softening in nature (i.e. not rigid, perfectly plastic) or if there is a lack of confinement at depth. Studies (e.g. Chan, 1986) indicate that Skempton's (1951) N_c values may underpredict the peak undrained strength in strain-softening soil from the measured bearing stress on the plate (particularly if the rate of strain-softening is high), while providing a reasonable estimate of the residual undrained strength. When the soil is at residual strength, it is closer to a rigid, perfectly plastic material. The soil beneath the plate may actually consist of a combination of elements at peak strength and elements at residual strength. Lack of confinement at depth (e.g. as soil squeezes around the advancing plate) may create a condition closer to a plate load test at the ground surface. Hence N_c values lower than 9 should be used, even in a rigid, perfectly plastic material.

6.4 Interpretation of Results

In the following section, the results of each stage of downhole plate load testing are compared with the results of adjacent CPT testing at the site (see Figure 6-1). Four CPTs were conducted at a 5 m radius from the zone of frozen sampling: CPT-20, CPT-21, CPT-22 and CPT-23. In addition, two nearby CPTs (CPT-26 and CPT-27) which were seismic CPTs were included in the CPT results.

Figure 6-10 presents the complete set of results for one CPT (CPT-21), which is typical for all six of the CPTs in the vicinity. Pore pressure measurements during CPT penetration indicate that the local groundwater table was located at approximately 0.5 m depth and that, relative to the hydrostatic line, some excess pore pressures were noted as each additional length of cone push rod was added. However, this excess was generally small relative to the hydrostatic pressure and the CPTs can be considered to be essentially drained penetration tests. Slightly larger pore pressures during cone penetration were observed for CPT-23 (see Figure 6-1) than for the other CPTs in the area.

Figure 6-11 compares the profiles of CPT cone tip resistance from the six CPTs in the vicinity of the plate load testing. The thick horizontal lines at 3 m and 7 m indicate the extent of the target zone for freezing, sampling and other in-situ testing at the site. With the exception of two denser zones within the target zone indicated by CPT-21, the six CPTs all give reasonably consistent results over the depth range, particularly below 3 m. Figure 6-12 plots the CPT results in the target zone on the soil classification chart proposed by Robertson (1990) which was presented in Chapter 3 (see Figure 3-6). Most of the data fall within zone 5, classifying the soil as a sand mixture, ranging from a silty sand to a sandy silt. Some of the data fall into zone 6 (sands: clean sand to silty sand) and zone 4 (silt mixtures: clayey silt to silty clay). A few datapoints fall into zone 3 (clays). In addition, the data generally fall within the normally consolidated region (see Chapter 3, Figure 3-6), which is to be expected for such a young deposit (approximately one month old).

For each plate load test, loads and displacements were recorded. The measured load during each test was converted to bearing stress on the plate. The measured displacement was converted to an actual depth, using the starting depth of each test as a reference. Put together, the stress and depth measurements result in a profile of bearing stress with depth through the soil deposit. These profiles of measured bearing stress for the plate load tests size and rate of penetration was not sufficient to create undrained conditions. It would, therefore, not be appropriate to estimate undrained strengths from the profile of bearing stress on the plate using Equation 6-3 which requires undrained conditions to be present. Although it is possible that portions of one or two tests which had lower bearing stresses than the CPT profiles (e.g. the last test in borehole PL1; see Figure 6-13) caused at least partially undrained conditions, there was no independent means of confirming this, such as having pore pressure measurements indicating excess pore pressures.

An interesting feature to note is the results of the first test in borehole FS52 which are not shown in Figure 6-15. As indicated in Table 6-1, a lot of slough (drill cuttings) was present in the borehole; although the borehole had been advanced to a depth of 18 ft (5.5 m), the top of the slough was at about 14.5 ft (4.4 m). The drillers moved the rods up and down to break through the slough, but the result was that the rods sank under their own weight from about 18 ft (5.5 m), eventually stopping at a depth of almost 25' (7.6 m). Perhaps some cyclic softening was induced in the sand.

6.4.2 Six inch diameter plate load tests

The second stage of plate load testing involved the more sophisticated system of a downhole load cell and a plate with a built-in pore pressure transducer (see Figure 6-5).

a) Raw field data versus time

Figures 6-17 and 6-18 present the measured displacements, pore pressures and bearing stress versus time for the first two tests in borehole PL4. The first test was performed starting at a depth of 10 ft (3.0 m) with a 7" diameter plate (see Figure 6-17). Figure 6-18 presents the results of the second test in borehole PL4, the first test with the 6" diameter plate, which started at a depth of 15 ft (4.6 m). Again, the drill rig reached its load capacity without pushing the plate very far. This test was done in two stages (hence the pause in the profiles versus time); the test was stopped momentarily as the rods were bending. Figures 6-17 and 6-18 indicate that the pore pressures in these first two tests decreased while the plate was being advanced (i.e. the observed excess pore pressure was negative). This could be indicative of a dense sand.

The borehole was then advanced to a depth of 19.5 ft (5.9 m) and the third test in borehole PL4 was performed (see Figure 6-19). This time, the plate advanced easily. The test was therefore continued for several metres, stopping only to attach additional lengths of drillstem. The plate was pushed for three complete intervals of approximately 150 cm before finally reaching the load capacity of the drill rig towards the end of the fourth interval. Figure 6-19 clearly indicates that the average rate of penetration for each interval was approximately 5 cm/s and that with each interval of pushing the plate, pore pressures measured by the built-in pore pressure transducer increased. In addition, in between intervals of advancing the plate, the pore pressures clearly dissipated.

Figures 6-20 and 6-21 present similar results as Figure 6-19, but for continuous plate load tests conducted in boreholes PL5 and PL6, respectively. As a result of the high bearing stresses measured at depths less than 15 ft (4.6 m) in borehole PL4 (see Figures 6-17 and 6-18), the tests in boreholes PL5 and PL6 were started at depths of 20 ft (6.1 m) and 17 ft (5.2 m) respectively. Again, four intervals of advancing the plate were conducted in each borehole with the load capacity of the drill rig being reached at some point in the last interval. Slightly higher average penetration rates of approximately 6 cm/s were reached in both boreholes PL5 and PL6. Again, clear increases in pore pressures were measured by the built-in pore pressure transducer. The excess pore pressures in borehole PL6 were similar to those in borehole PL4 (see Figure 6-19), increasing as the plate was advanced and dissipating while the plate was stopped and additional lengths of drillstem were attached. However, in borehole PL5, the pore pressures appeared to rapidly reach a peak and then dissipate very rapidly while the plate was still being advanced. In fact, the trends of the pore pressure profile in PL5 are somewhat similar to the trends of the bearing stress profile, whereas in PL4 and PL6 the pore pressure profiles had trends opposite to the bearing stress profiles. Therefore, it is possible that the pore pressure transducer was not correctly measuring pore pressures during this test. However, the measured pore pressure profiles in boreholes PL4 and PL6 seem reasonable; this is shown more clearly in subsequent figures (Figures 6-26 to 6-28) which compare the measured pore pressures to the estimated hydrostatic line.

In Figures 6-19 to 6-21, it is interesting to note that although the bearing stress was set equal to the initial weight of the rods in each borehole, such that the initial value was slightly greater than zero on the scale shown, the measured bearing stress appears to go slightly negative in the intervals of time in which additional rods were being added and the plate was stationary. While there may be some small errors in the "zeroing" of the load on the plate or the calibration of the load cell, a more likely explanation for this observation may be the method used by the drillers to attach additional lengths of drillstem. The drillstem is often lifted up slightly and clamped before the next rod is added. This may result in a slight tension on the drillstem because of the displaced soil around the plate and the portion of the drillstem below the bottom of the augered borehole. A slight tension would translate to a negative load on the load cell and, would appear as a negative bearing stress when divided by the plate area.

b) Bearing stress profiles

Figures 6-22 to 6-24 present the profiles of measured bearing stress with depth in the individual boreholes PL4, PL5 and PL6, respectively. Superimposed on each of these figures are the measured average and range (minimum and maximum) of the six adjacent CPT profiles of cone tip resistance. The thick horizontal lines at 3 m and 7 m indicate the extent of the target zone for freezing, sampling and other in-situ testing at the site.

Clearly the first two tests in borehole PL4 had bearing stresses in the range of the minimum to average CPT cone tip resistance (see Figure 6-22). However, much of the continuous third test had bearing stresses that were smaller than the range in CPT cone tip resistance. In particular, low bearing stresses were measured in the region of 7 m depth and 9.5 m depth. Similar observations could be made in both boreholes PL5 and PL6 (see Figures 6-23 and 6-24, respectively). It appears likely that the plate load tests may be at least partially undrained, particularly in the two zones of low measured bearing stresses.

Figure 6-25 summarizes the measured bearing stresses from the three boreholes, PL4, PL5 and PL6 and compares the results to the CPT profiles of cone tip resistance. The zones of low bearing stress appear to coincide in all three plate load test boreholes and have values significantly lower than the measured CPT cone tip resistance. Borehole PL4 extends to a greater depth than the other two boreholes. At depths greater than 11 m, the bearing stress on the plate in PL4 appears to be within the range of measured CPT values, as both the plate load test and the CPT detected the layer of clay shale at the base of J-pit.

c) Processed field data versus depth

Figures 6-26 to 6-28 present profiles of bearing stress versus depth, pore pressure versus depth, time versus depth and estimated undrained shear strength versus depth for the 6" plate load tests in boreholes PL4, PL5 and PL6, respectively. The profiles of bearing stress are identical to those in Figures 6-22 to 6-24. Superimposed over the pore pressure profiles for each test as a reference line is the approximate hydrostatic line based on a groundwater table located at a depth of 0.5 m. The profiles of estimated undrained shear strength were calculated by combining the profiles of bearing stress with Equation 6-3 (based on an N_c of 9). Although this equation is only applicable to undrained conditions, it was applied to the entire profile from each test to see what the results would be. Clearly the most likely areas to be considered as possibly undrained during testing are the two zones of low measured bearing stress as indicated in the previous section.

As explained earlier, the first (7" diameter plate) and second tests in borehole PL4 caused the load capacity of the drill rig to be met without much displacement of the plate. The pore pressures during these two tests decreased to values less than the hydrostatic reference line while the plate was being pushed (see Figure 6-26).

As outlined previously, the third test in PL4 (Figure 6-26) and the tests in PL5 (Figure 6-27) and PL6 (Figure 6-28) were continuous over several metres. As discussed previously, the pore pressure measurements in PL4 and PL6 demonstrated similar trends, while in PL5, the pore pressures behaved somewhat differently. In PL4 and PL6, pore pressures increased in excess of the hydrostatic reference line every time the plate was advanced and dissipated while the plate was stopped. The points of lowest measured bearing stress coincided with the highest measured excess pore pressures in both profiles. Towards the bottom of PL4, the excess pore pressures are a function of encountering fine-grained material (clay shale). At depths of 6 m to 11 m, however, it is likely that the high pore pressures are a result of at least partially undrained conditions being created in the sand. This is probably a combination of plate size, rate of loading and amount of fines in the sand. As discussed earlier, in PL5, the measured pore pressure profile appear to be inconsistent with the bearing stress profile, as compared to the results in PL4 and PL6. It is unclear whether the pore pressure measurements truly reflect the pore pressures in the ground during the test in this borehole or whether they are partially linked with the bearing stress on the plate.

d) Estimated undrained strength profiles

Figures 6-26 to 6-28 also present the estimated profiles of undrained strength based on combining the profiles of measured bearing stress with Equation 6-3. A groundwater table located at approximately 0.5 m and average unit weights of 18.5 kN/m^3 and 19.5 kN/m^3 for the soil above and below the groundwater table, respectively, were used to compute the total stress term in Equation 6-3. Zones of low estimated undrained strength occurred when the measured bearing stress was low, which as explained above, generally occurred when excess pore pressures were high. Based on an N_c of 9, undrained strengths less than 50 kPa are predicted in these zones. However, for reasons outlined earlier, an N_c less than 9 may be more appropriate; this would result in higher estimated undrained strengths.

In a couple of locations, slightly negative undrained shear strengths were calculated when Equation 6-3 was used to interpret the bearing stress data. This can not be correct and would only result if the estimated total stress was larger than the measured bearing stress (see Equation 6-3). Some uncertainty in either term may be the cause of this error in the calculated undrained shear strength. The likely lack of confinement as some soil squeezed around the advancing plate may have decreased the measured bearing stress on the plate in these regions. In addition, if there were a lack of confinement, the plate load test should have been interpreted as if it were at the ground surface (i.e. with lower N_c values and without subtracting the total stress term). In general, in the regions of low strength, the values of estimated undrained shear strength using an N_c of 9 are within the range conventionally applied to liquefied sand (see the plot by Seed and Harder (1990) for estimating undrained shear strengths from the SPT; Chapter 5, Figure 5-1). However, for reasons explained above, the actual undrained strengths may be significantly larger.

Figure 6-29 summarizes the estimated undrained strengths from PL4, PL5 and PL6 over a depth range of 6 m to 12 m. The lowest undrained strengths are predicted to occur from 6.5 m to 8 m , 9 to 10 m and in the region of 11 m. Using an Nc of 9, the lowest strengths are generally estimated to be in the order of 10 kPa; however, the actual values may be significantly higher. The variation in estimated undrained strengths may reflect the fact that the plate load testing appeared to be a mixture of undrained and drained penetration, as indicated by the increase and decrease of measured pore pressures relative to the hydrostatic reference line. However, the natural variability of the deposit (as reflected by the CPT testing) is likely another contributing factor. Even if the plate load tests were all completely undrained, variability in the estimated undrained strength profile would be expected as a result of the inherent variability of the sand deposit. Chapter 5 illustrated that undrained strength of a sandy soil can be very sensitive to its in-situ state. Consequently, it would not be surprising to find that the profile of undrained strength in a sandy deposit would be variable in nature. In addition, pre-peak estimates of strength are likely not reliable.

All of the estimated undrained strength profiles in Figure 6-29 were estimated using

Equation 6-3. This involved assuming an N_c of 9. Traditionally, the undrained shear strengths associated with N_c=9 have been in rigid, perfectly plastic materials. However, if a sand has a sufficiently loose state and is susceptible to flow liquefaction, it will be strain-softening in its response to undrained loading. Insufficient testing and analysis has been carried out at the Phase III site to investigate whether or not the sand is indeed strain-softening. If it is strain-softening, the simple interpretation used here may not be applicable.

Figures 6-30 and 6-31 present the profiles of S_u/σ_v' and S_u/p', respectively. In the zones of low estimated undrained strength, the ratio S_u/σ_v' has a typical value of about 0.2, based on an N_c of 9. The profile of S_u/p' was determined from the profile of S_u/σ_v' assuming that K_o at the site has a value of 0.5. Therefore, the zones of minimum $S_u/\sigma_v' \approx 0.2$ correspond to values of $S_u/p' \approx 0.3$. Chapter 5 explained that, based on critical state soil mechanics, the theoretical maximum Su/p' for a sand that strain-softens to ultimate state is given by 0.5M. For typical soils M_C can range from 1.2 to 1.5 and M_E can range from 0.9 to 1.0. These ranges correspond to a range in maximum S_u/p' of 0.6 to 0.75 in triaxial compression and 0.45 to 0.5 in triaxial extension. Therefore, the low points in the estimated undrained strength profiles give strength ratios in the range typically considered to apply to potentially liquefiable soils once they are triggered in flow liquefaction. However, as discussed above, the interpretation applied here (using N_c=9) may not be appropriate if the material is strain-softening or if a lack of confinement arises during the plate load test.

6.5 Comparison with Other Measures of Undrained Shear Strength

Unfortunately, it is not possible at this time to compare the estimates of undrained shear strength from the second stage of rapid downhole plate load tests with other measures of undrained shear strength at the site. Once the CANLEX project laboratory work and analysis of the Phase III site is completed, such a comparison will be made. This may help establish the appropriate N_c values for the sand deposit.

To date, only limited testing of undisturbed (frozen) samples of sand from the site has been performed. The few samples that have been tested strain-hardened in triaxial compression and demonstrated limited strain-softening (to a QSS) in triaxial extension before strain-hardening to ultimate state. Even when the testing of Phase III undisturbed samples is complete, a direct comparison with the second stage of plate load tests will not be possible. The frozen samples were all obtained in the 3 m to 7 m target zone (see Figure 6-11), while the region in which the second stage of plate load testing appeared to be possibly undrained was from 6 m to 12 m.

The flow liquefaction framework described in Chapter 4 will eventually be applied to the laboratory and field data from the Phase III site. The results can then be compared with the estimated undrained shear strengths from the second stage of downhole plate load testing. However, an added complication at the Phase III site is that the results of the data review for the Phase III site so far suggest that this sand is unusual, as compared to the other CANLEX sites. The average values of $(N_1)_{60}$, q_{c1} and V_{s1} are all significantly smaller than the values at the Phase I and Phase II sites. The integrated CPT method outlined in Chapter 3 predicts a higher fines content at the Phase III site than at the other sites. Limited laboratory testing to date supports this conclusion. Conventional or shear wave velocity based interpretations of the $(N_1)_{60}$, q_{c1} or V_{s1} profiles would predict significantly higher void ratios than suggested by the undisturbed samples available to date. However, geophysical logging predicts an average void ratio similar to the average void ratio of the undisturbed samples available to date.

A possible explanation for the discrepancy in results at the Phase III site is that the SPT, CPT and shear wave velocity measurements were strongly influenced by the high fines content and, hence, were controlled more by the skeletal void ratio at the Phase III site. The void ratios estimated for the undisturbed samples and predicted by the geophysical logging are total void ratios. When the undisturbed sample total void ratios were corrected to approximate equivalent skeletal void ratios based on the average fines content in the target zone, the void ratio interpretations of the SPT, CPT and shear wave velocity measurements had much better agreement with the undisturbed samples. The results seem to indicate that skeletal void ratio may be a factor for sands with a high fines content. Scanning electron microscopy has also shown that at least some of the undisturbed samples from the Phase III site appear to have an unusual fabric due to the high fines content (Hofmann, 1996). It will be interesting to carefully examine the results of testing undisturbed samples to see if their response appears to be linked to skeletal or total void ratios. It is unclear at this point whether skeletal or total void ratios would affect the results of the plate load tests.

6.6 Conclusions and Recommendations

The experimental program described in this chapter was clearly preliminary in nature. The above discussion indicates that interpreting results and estimating undrained shear strengths from downhole plate load tests can be complicated, particularly if, as for this study, the tests are not conventional plate load tests, but continuous penetration tests. If the soil is strain-softening in nature and/or a lack of confinement arises during the plate load test, the interpretation procedure becomes more challenging. However, a simple analysis of the results using Skempton's bearing capacity formula indicates that the downhole plate load test appears promising as a potential in-situ test for estimating undrained strengths in sandy soils. However, the undrained strengths can only be estimated using this formula when the combination of rate of loading and the size of the plate is sufficient to produce undrained loading and the soil behaves as a rigid, perfectly plastic material. Pore pressure measurements are useful as an independent means of assessing whether a given plate load test was drained or undrained. Studies by Charlie et al. (1993) investigating the potential of the Piezovane™ for identifying sands that are susceptible to liquefaction have led to similar conclusions; i.e. estimating the undrained strength of the sand is difficult, but the type of soil (susceptible to liquefaction or not) can be identified based on an observed increase or decrease in pore pressure during shear.

It would be interesting to conduct additional plate load tests in sandy deposits for which other methods of estimating or directly measuring the undrained strength have been applied; e.g. any of the CANLEX sites. However, based on the conclusions of Chapter 5, undrained strength is a response parameter that can be very sensitive to variability within a deposit. Consequently, the resulting estimates of undrained strength from rapid downhole plate load tests may be no better than estimates of undrained strength from other in-situ tests using methods described in Chapter 5. What might be the most worthwhile test to investigate in future studies is a large diameter CPT that can create undrained loading in a sandy deposit. The effects of sand squeezing around the plate in a plate load test would not be a factor in such a test. However, the loads required to push such a probe into the ground may pose difficulties to conventional drill rigs.

Table 6-1: Summary of 4" (10 cm) plate load testing

Borehole	Test No.	No. Rods*	Start Depth (ft)	Total Displacement (cm)	Total Time (s)	Comments
PL1	1	1	2.5	≈60	< 5	•no data available§
	2	2	7.5	≈60	< 5	•no data available§
	3	3	12.5	≈60	2.67	•no data available§
	4	4	17.5	≈65	1.91	
	5	5	22.5	≈60	1.86	
	6	6	24.5	≈60	--	•plate was advanced for about 2', then unloaded
		7		≈60	--	•plate was reloaded and advanced another 2'
	7	8	28.5	≈120	≈ 3.8	•plate was advanced continuously for about 4'
PL2	1	1	2.5	≈50	≈2	
	2	2	5	--	--	•system buckled out and load cell was dislodged; test was restarted 8" deeper (see test no. 3)
	3	2	5.67	≈40	1.81	
	4	3	10	≈65	≈2	
	5	4	15	≈20	≈2	•; iate advanced 8"; then test stopped to prevent buckling and restarted
		4	15.67	≈45	--	
	6	5	20	≈20	2.1	•plate was loaded and advanced for about 8", then unloaded
		5	20.67	≈45	--	•plate was reloaded and advanced about 1.5'
FS52	1	5	18	≈208	--	•slough into borehole; depth to top of slough was about 14.5'; moved rods up and down to break through slough; rods sank under their own weight from about 18' to 24'; rods continued to slowly sink to a depth of 24'10"
	2	6	25	≈55	1.89	•added another rod, loaded and advanced the plate; slough in borehole; depth to top of slough was about 15'
FS5	1	6	24.17	≈30	1.14	•plate was advanced for about 1', then unloaded
		6	25.17	≈120	≈ 2 or 3	•plate was reloaded and advanced about 4'

Notes:

* Weight of one rod ≈ 13.64 kg
Weight of 4" plate + short attachment rod + screws = 6.4 kg

§ Data for these tests were lost because the data acquisition system was not recording information from the load and displacement cells at a sufficiently frequent rate; this was corrected for subsequent tests

Table 6-2: Summary of 6" (15 cm) plate load testing

Borehole	Test No.	No. Rods*	Start Depth (ft)	Total Displacement (cm)	Total Time (s)	Comments
PL4	1**	4	10	≈25	--	•hollow stem auger to depth; pulled auger out and filled hole with water •approx. 2' of slough below 10' depth; advanced plate about 10" before meeting load capacity of drill rig
	2	5	15	≈25	--	•hollow stem auger to depth; pulled auger out and filled hole with mud •advanced plate a bit, but seemed to be bending rods; stopped and then pushed a bit more; met load capacity of drill rig
	3					•hollow stem auger to depth; pulled auger out and filled borehole with mud
		6	19.5	≈150	--	
		7		≈150	32.25	
		8		≈150	20.5	
		9		≈150	25	•load capacity of drill rig reached during last interval
PL5	1					•hollow stem auger to depth; pulled auger out and filled borehole with mud
		5	19.6	≈25	12	
		6		≈150	23.75	
		7		≈150	28.6	
		8		≈50	--	•load capacity of drill rig reached during last interval
PL6	1					•hollow stem auger to depth; pulled auger out and filled borehole with mud
		5	17.2	≈60	22.79	
		6		≈150	19.75	
		7		≈150	18.57	
		8		≈125	≈22	•load capacity of drill rig reached during last interval

Notes:
* Weight of one rod ≈ 13.64 kg
** Test performed with 7" (18 cm) diameter plate

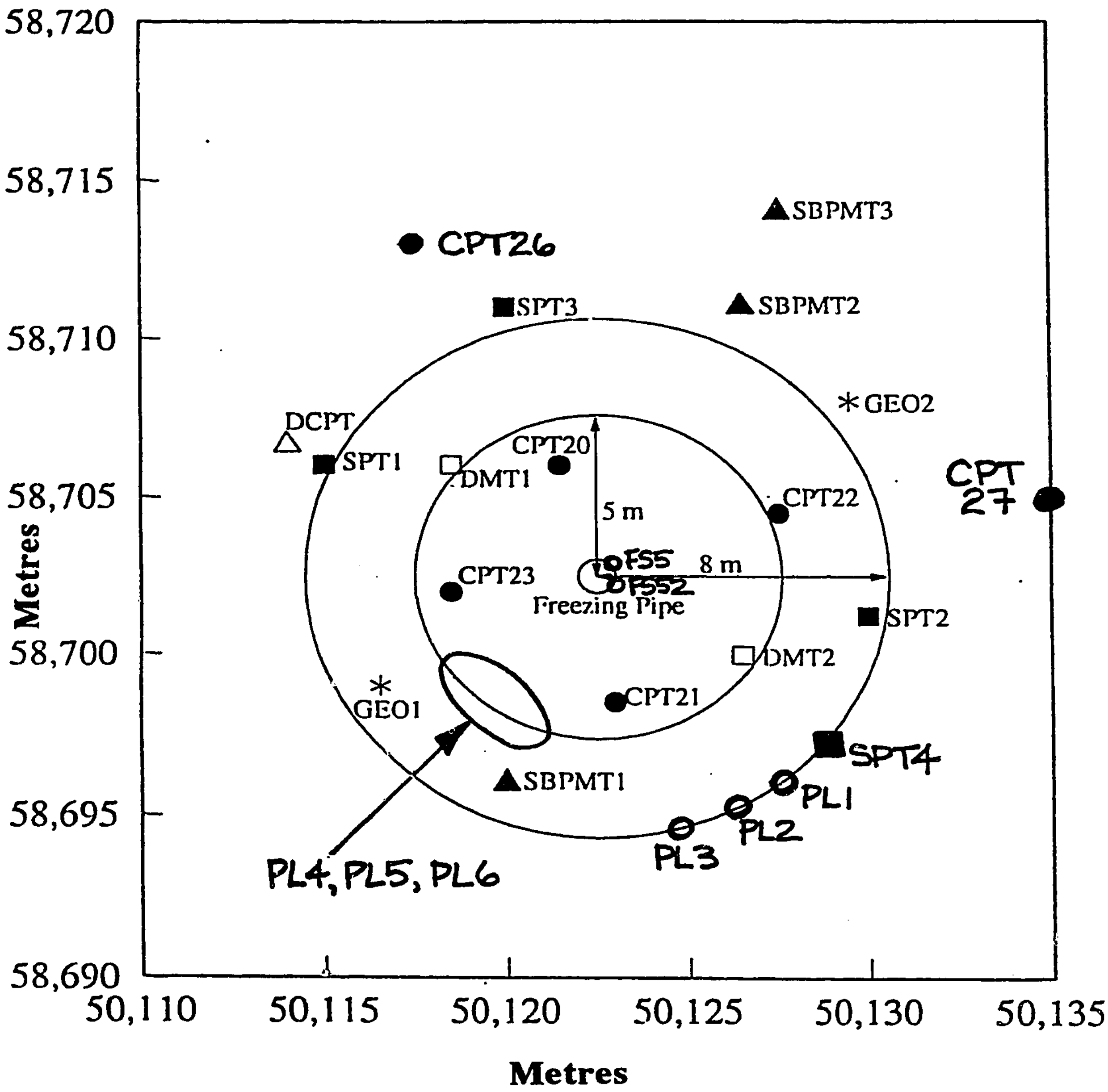

Figure 6-1 Plan of the detailed test site area at the CANLEX Phase III site (J-pit) (modified from Iravani et al., 1996).

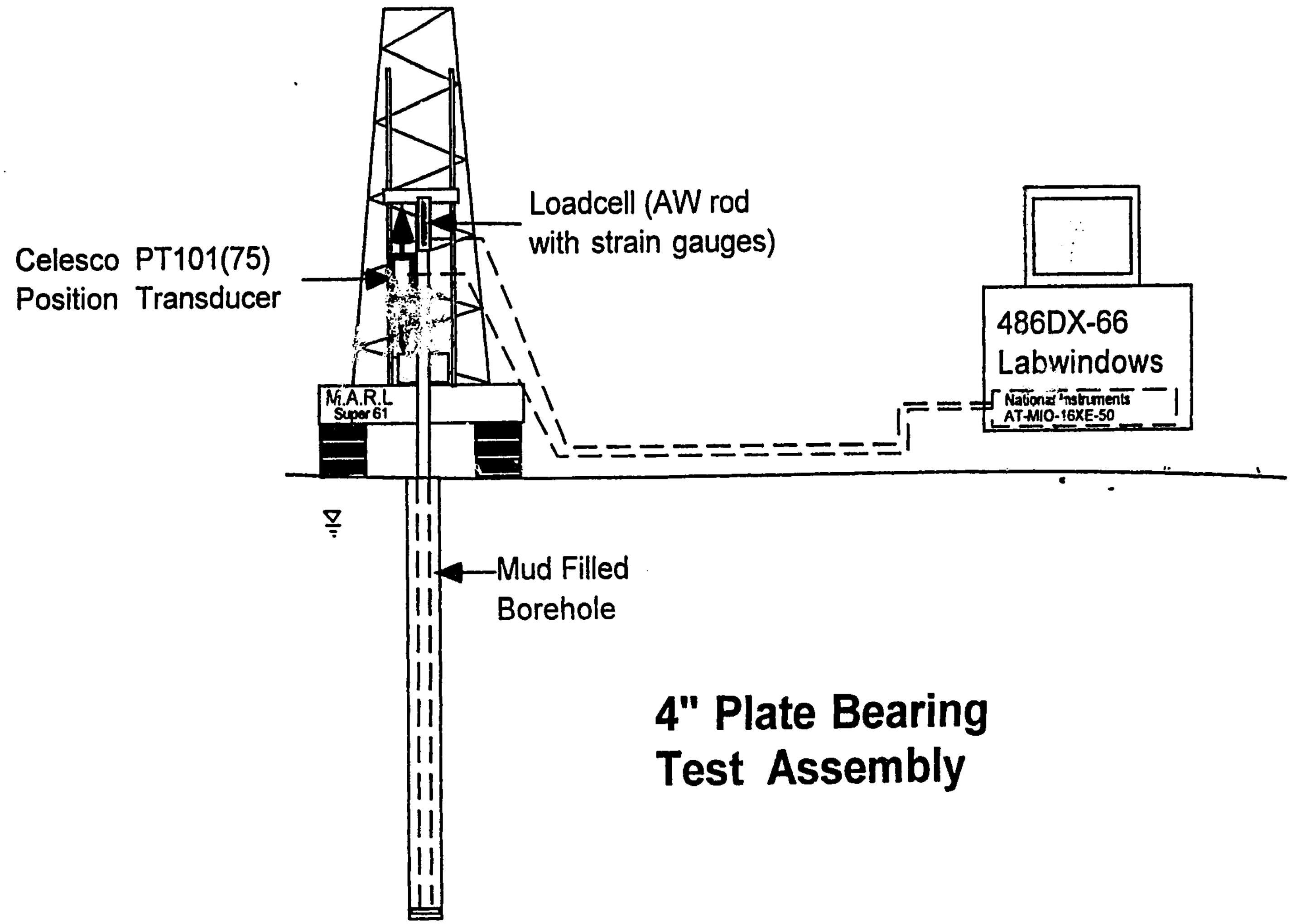

Figure 6-2 Configuration of the 4" (10 cm) diameter downhole plate load test setup.

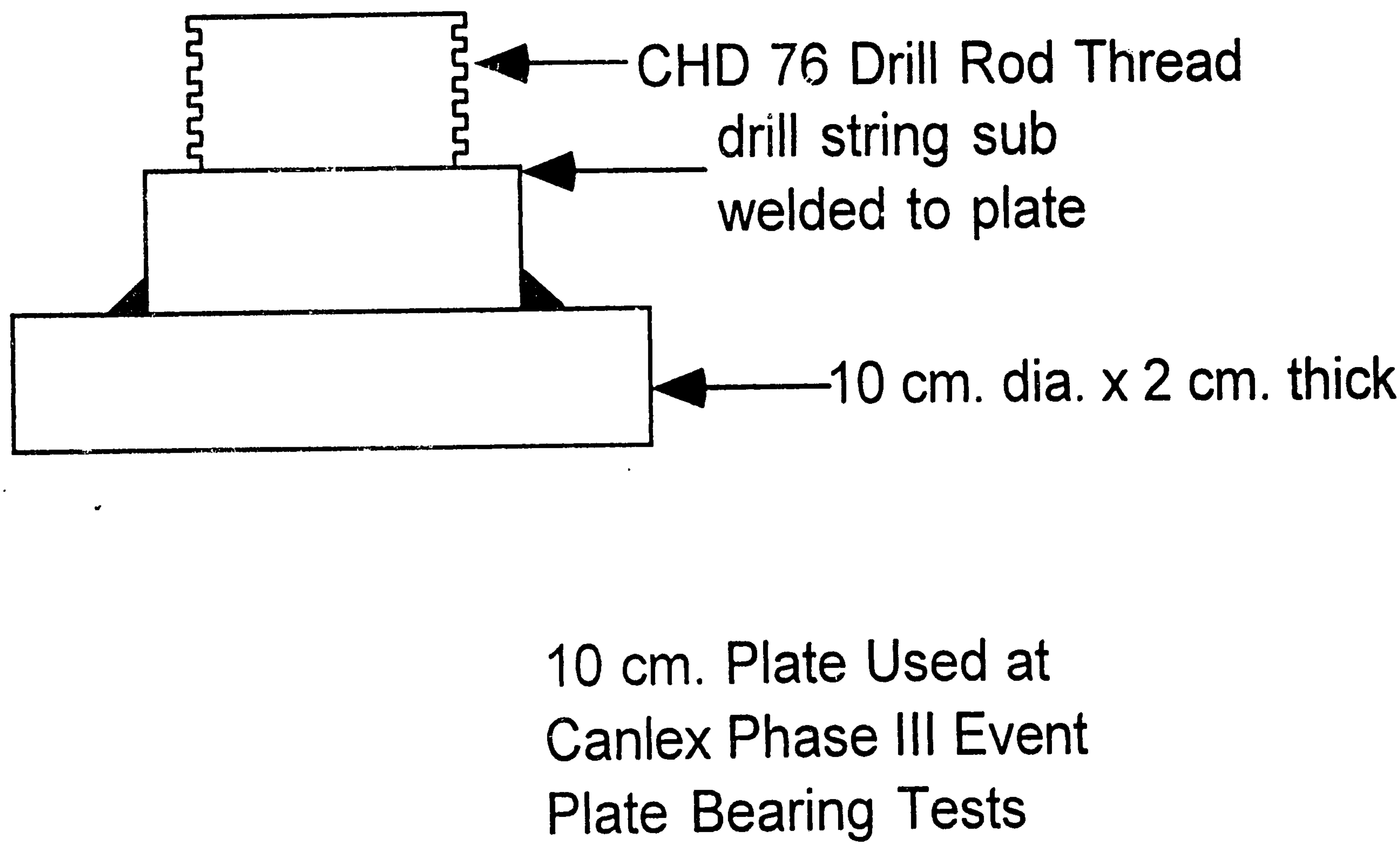

Figure 6-3 Schematic outlining the details of the 4" (10 cm) diameter downhole plate assembly.

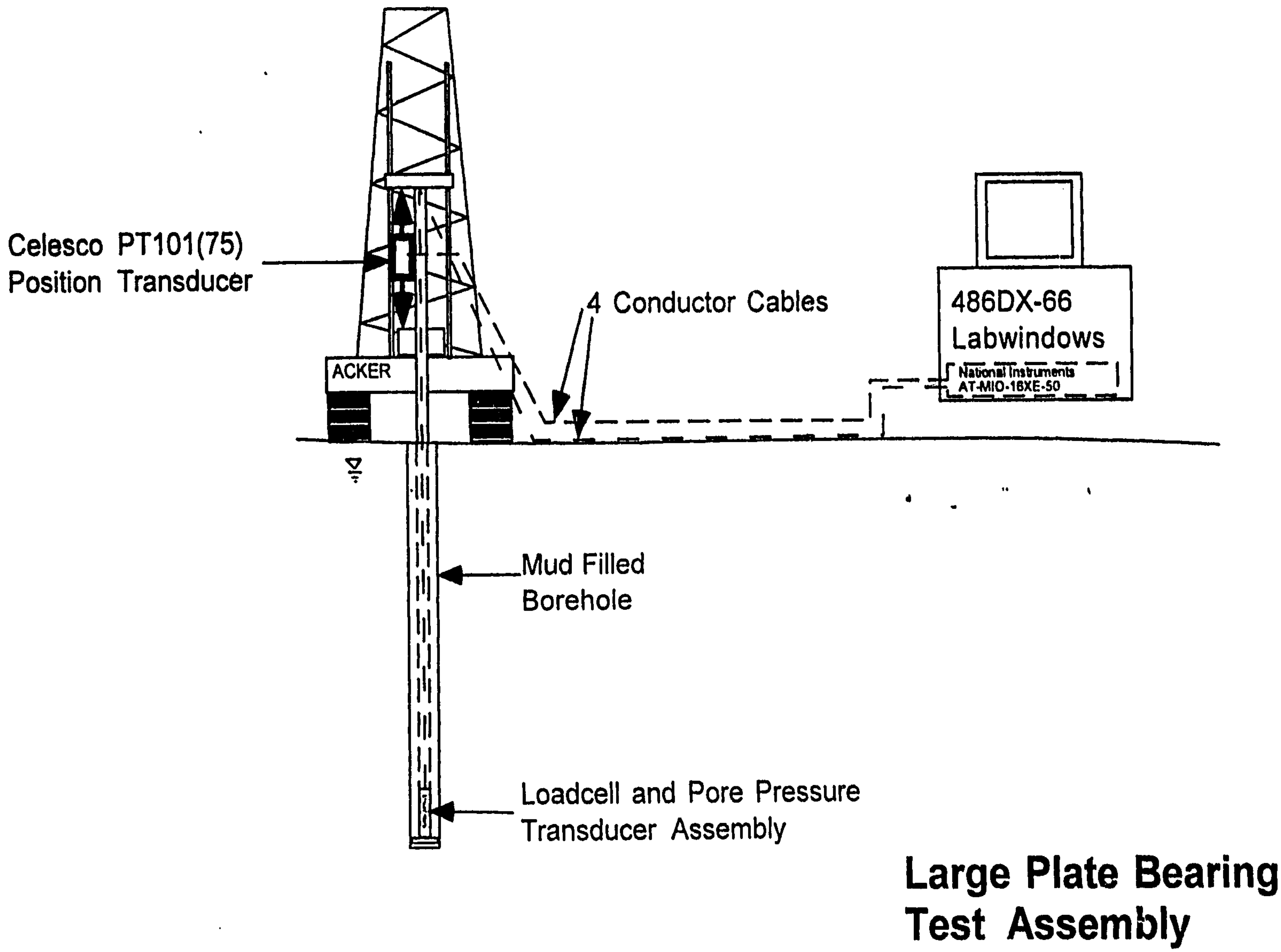

Figure 6-5 Configuration of the large diameter downhole plate load test setup, with downhole load cell and pore pressure transducer.

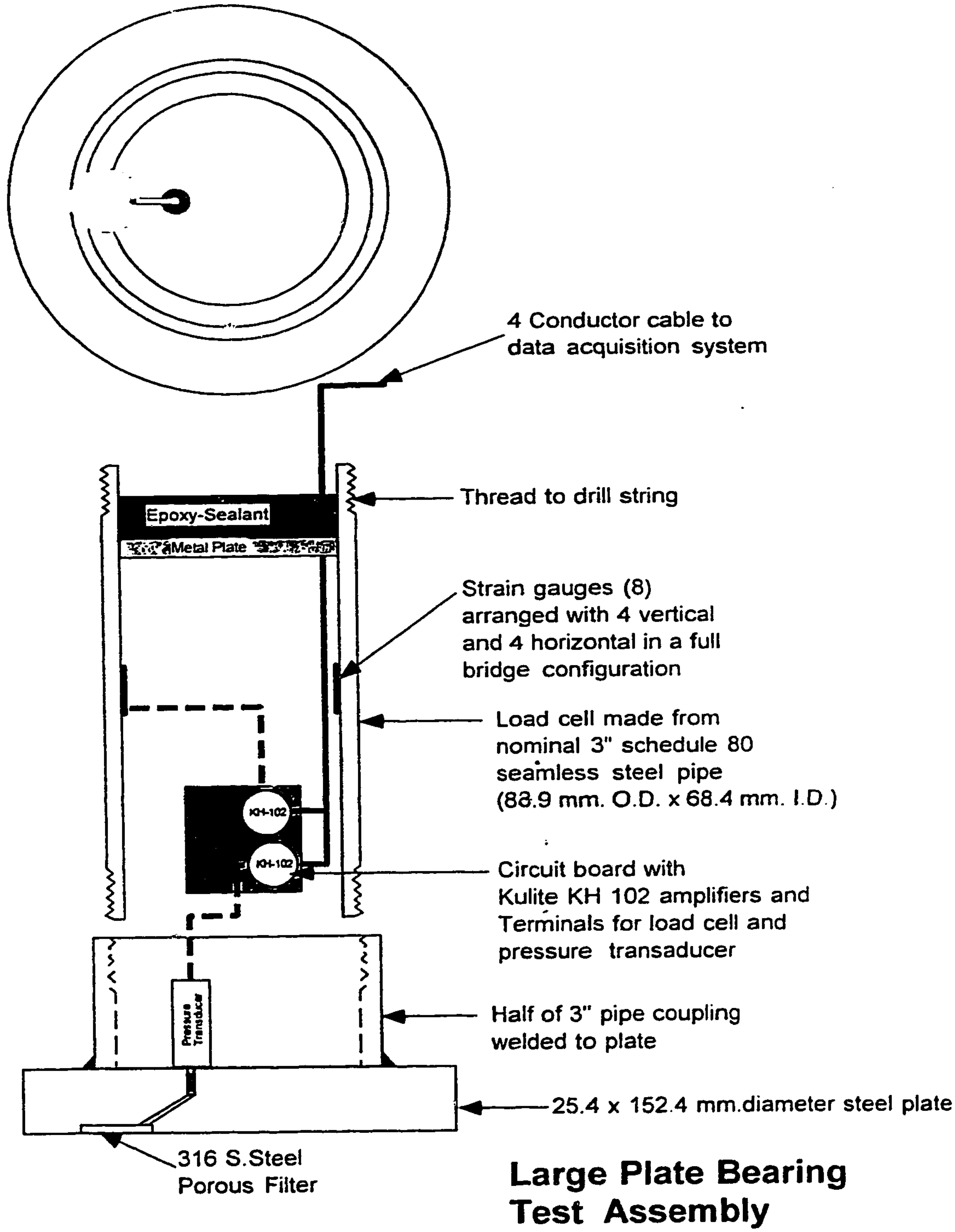

Figure 6-6 Schematic outlining the details of the large diameter downhole plate assembly, with built-in load cell and pore pressure transducer.

(a)

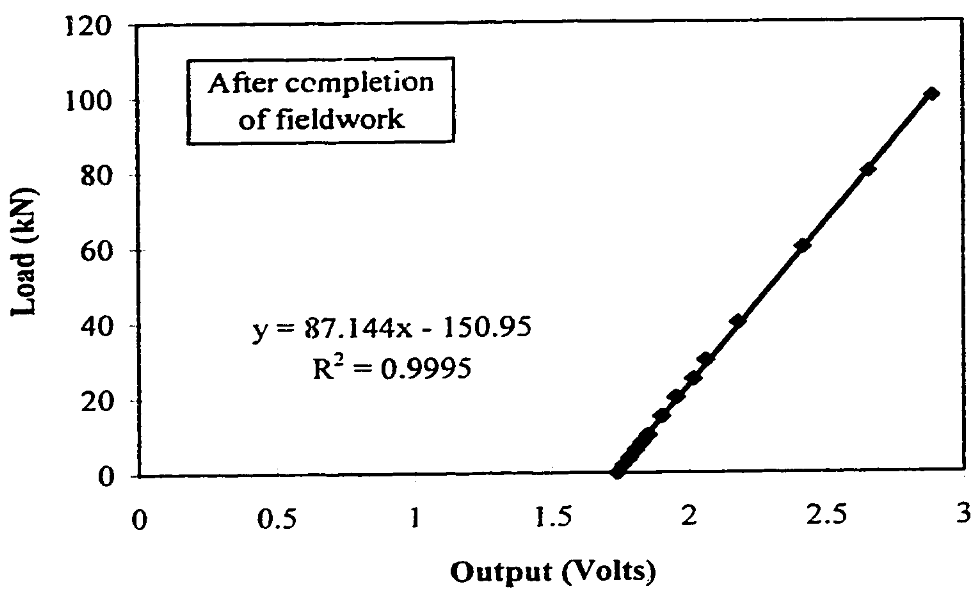

(b)

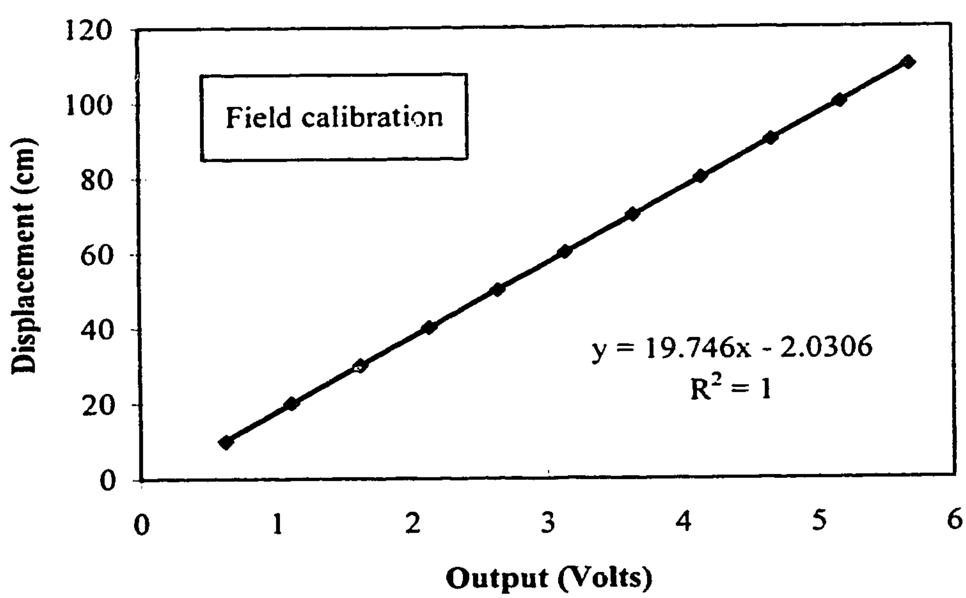

Figure 6-7 Calibration charts for the large diameter plate load tests for (a) the load cell and (b) the displacement cell.

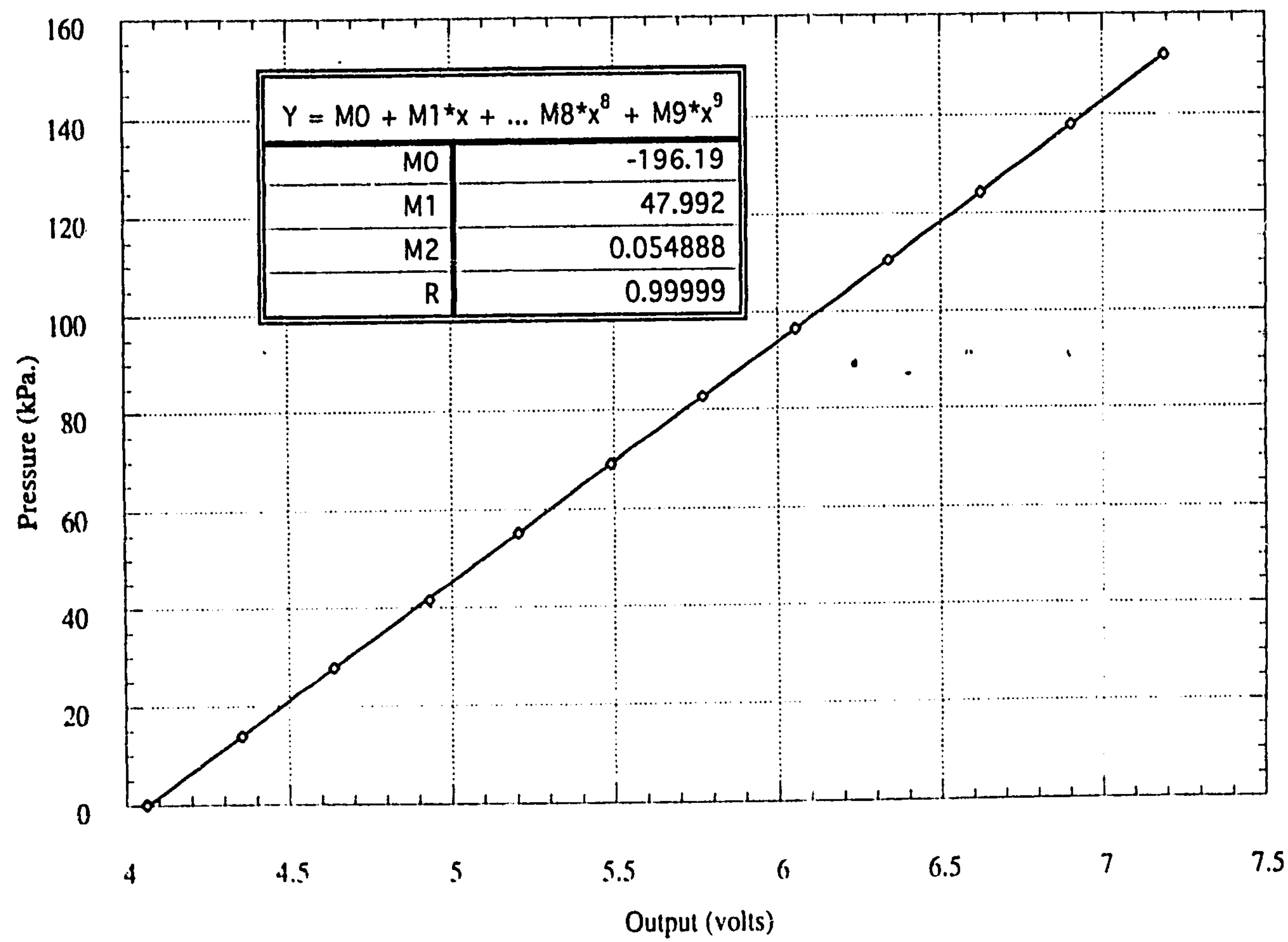

Figure 6-8 Calibration chart for the large diameter plate load tests for the pore pressure transducer.

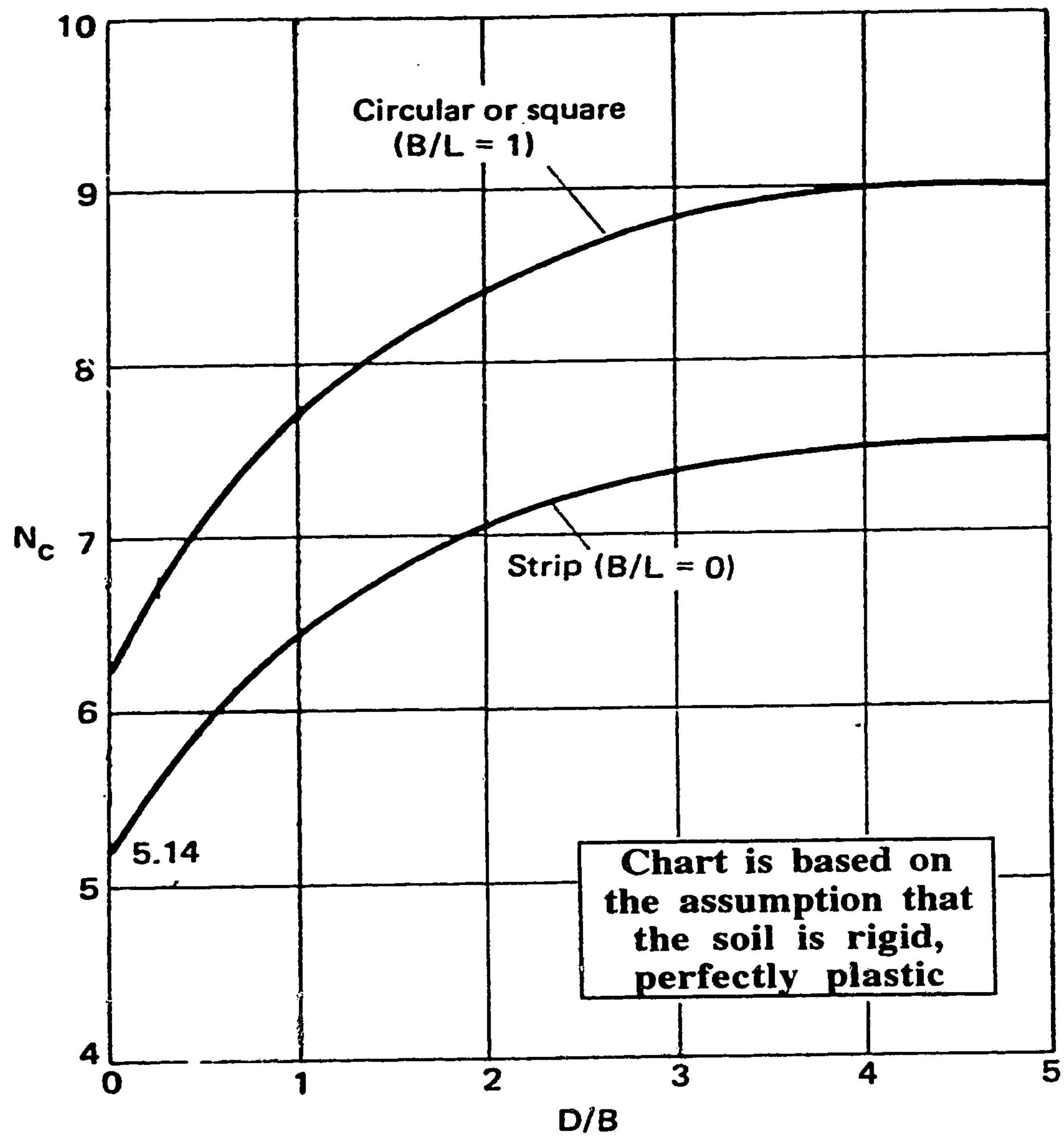

Figure 6-9 Recommended values of N_C for undrained loading in saturated clays (modified from Skempton, 1951).

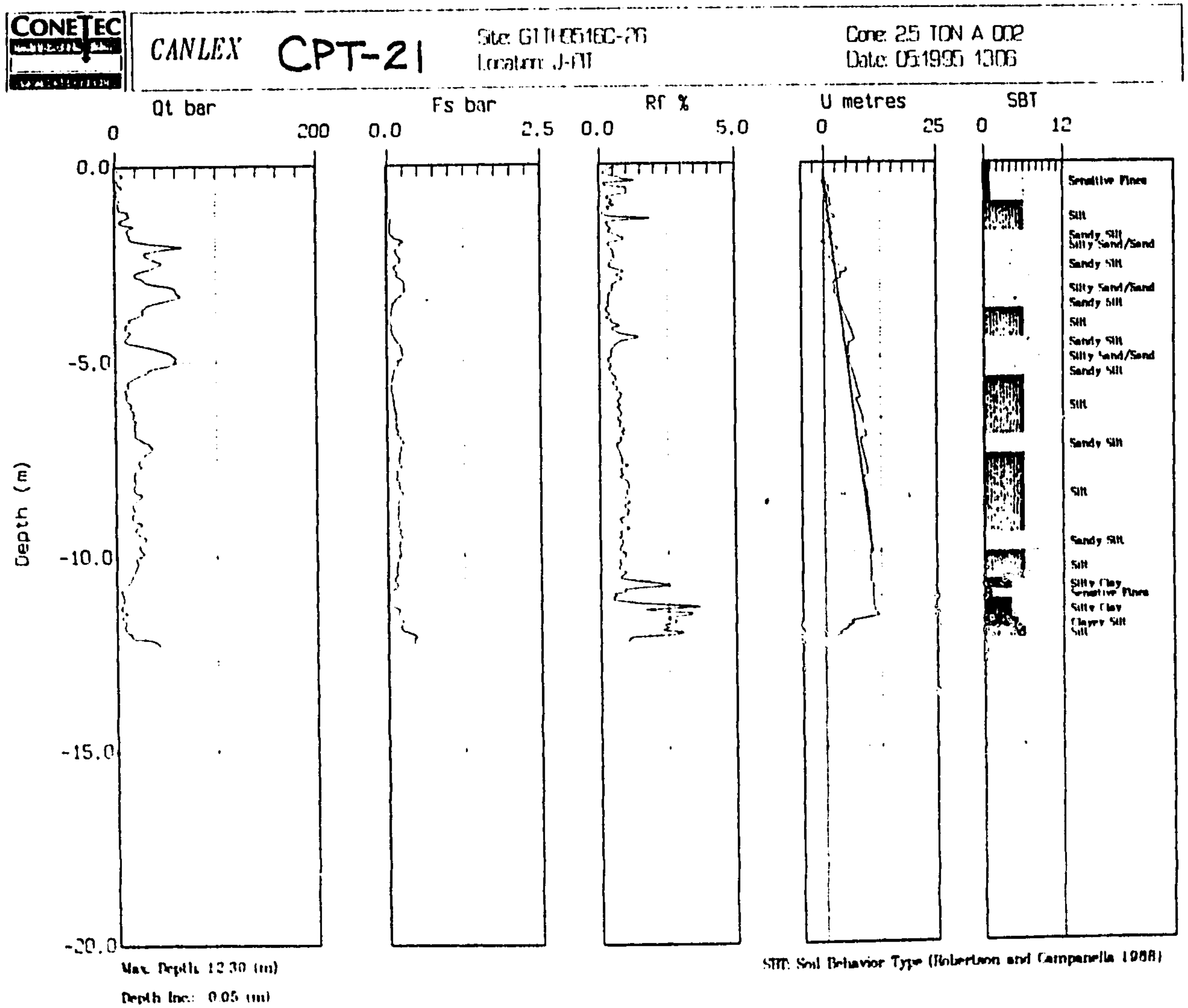

Figure 6-10 Typical CPT results (CPT-21) in the detailed test site area at the CANLEX Phase III site (J-pit) (modified from ConeTec, 1995).

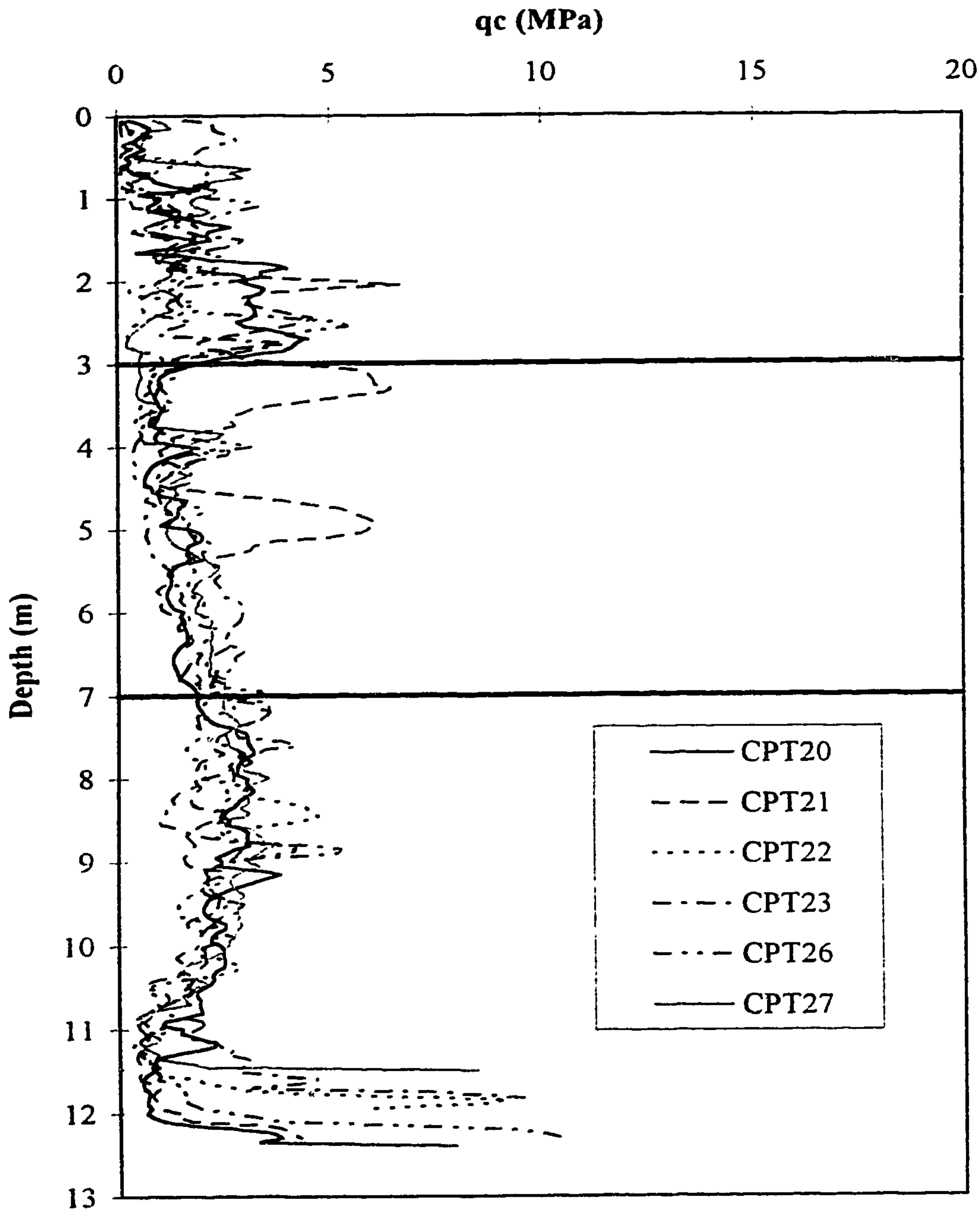

Figure 6-11 Summary of corrected CPT cone tip resistance profiles from all CPTs in and near the detailed test site area at the CANLEX Phase III site (J-pit); test site target zone for testing and sampling located from 3 m to 7 m, as indicated.

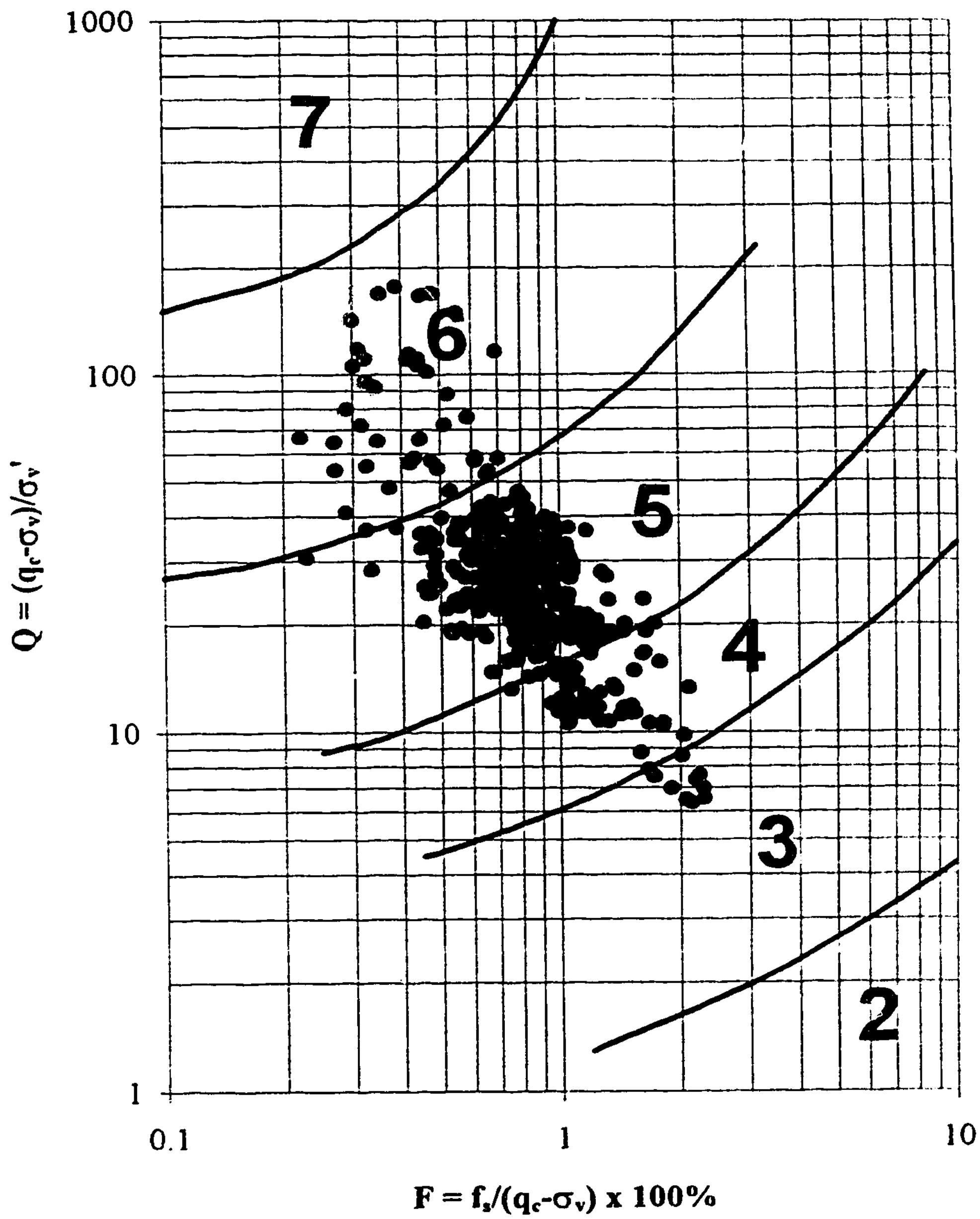

Figure 6-12 Plot of the CPT data in the target zone at CANLEX Phase III site (J-pit) on the soil behaviour type classification chart by Robertson (1990).

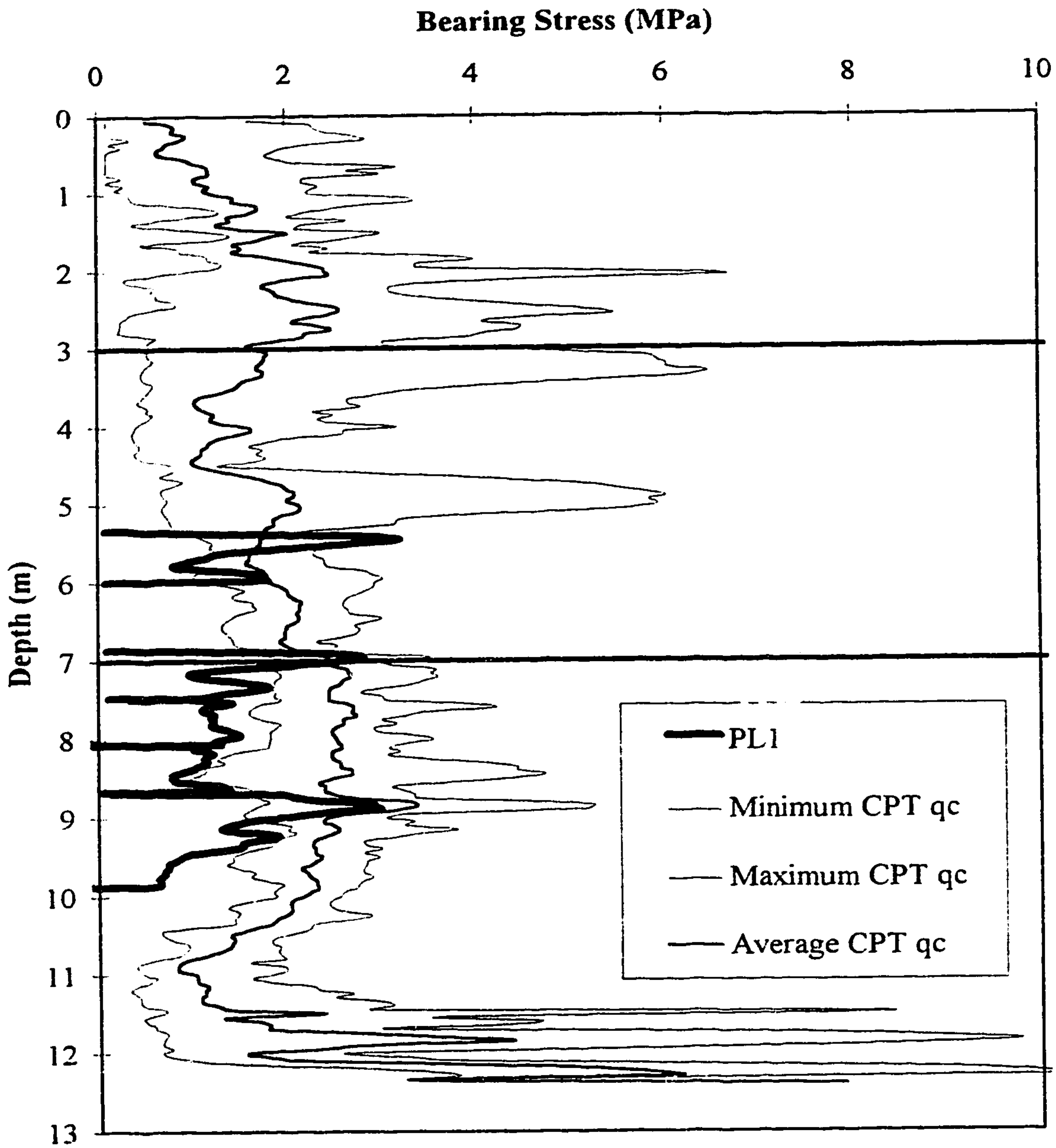

Figure 6-13 Bearing stress versus depth measured during 4" (10 cm) diameter plate load tests in borehole PL1.

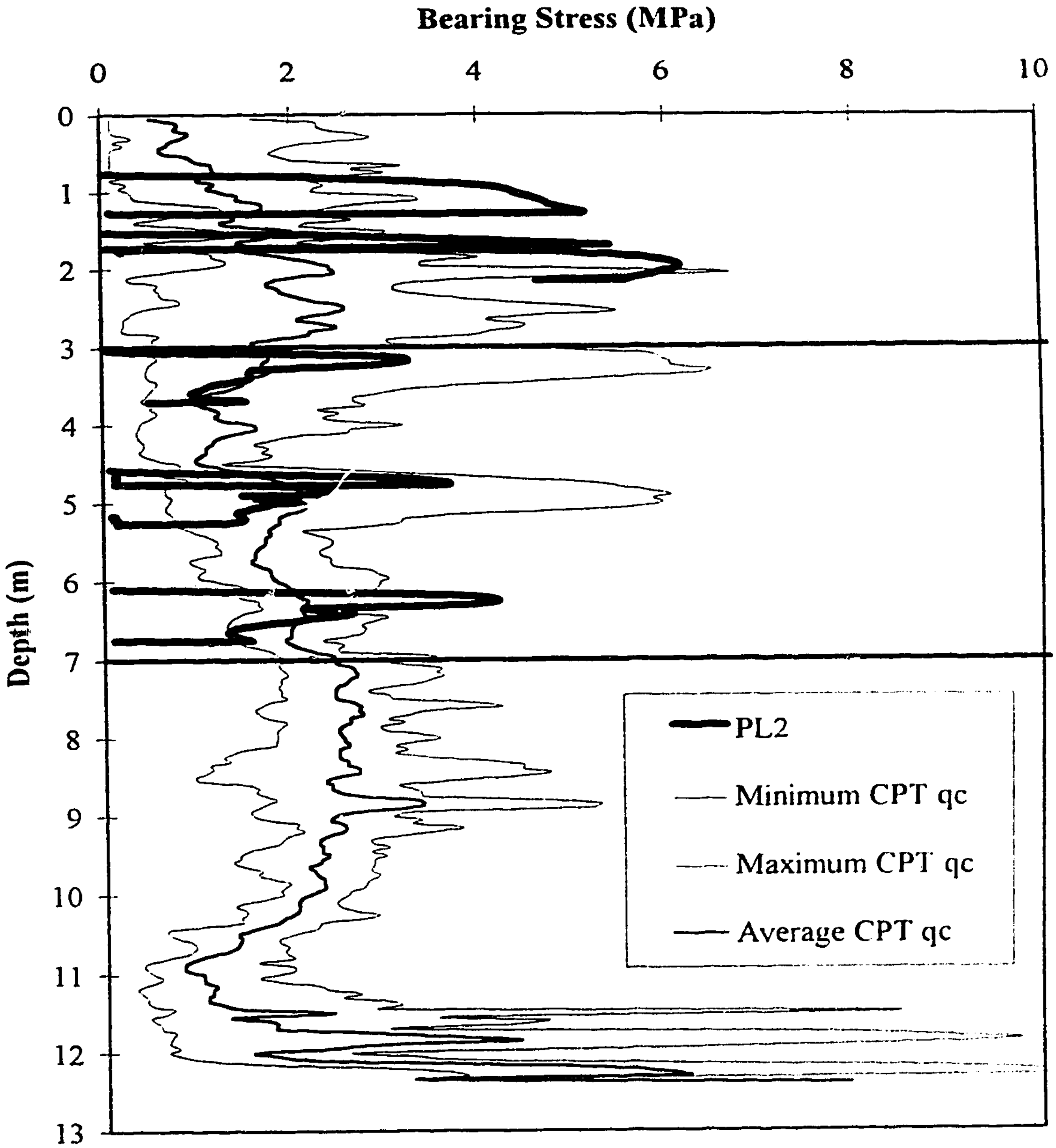

Figure 6-14 Bearing stress versus depth measured during 4" (10 cm) diameter plate load tests in borehole PL2.

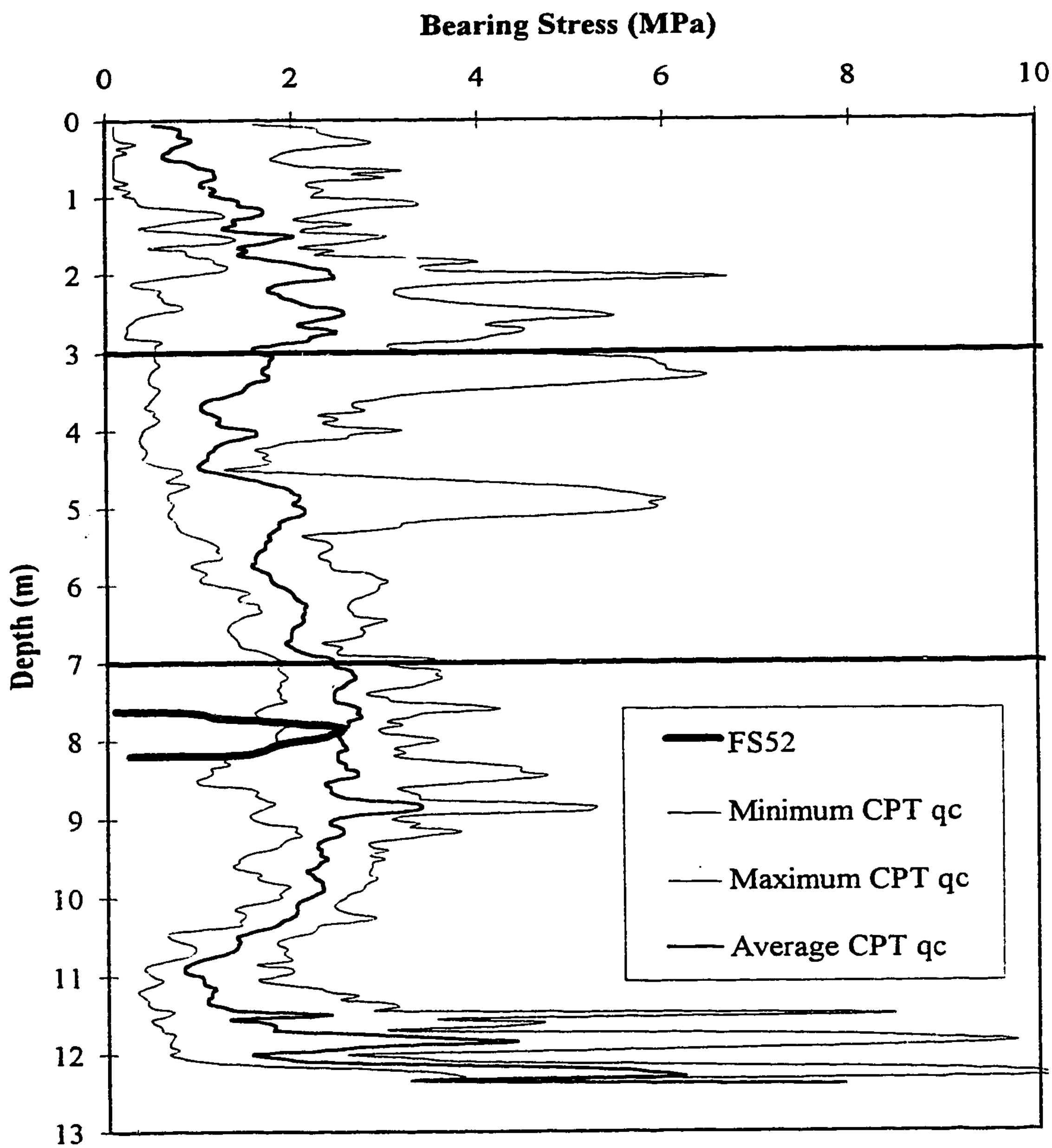

Figure 6-15 Bearing stress versus depth measured during 4" (10 cm) diameter plate load tests in borehole FS52.

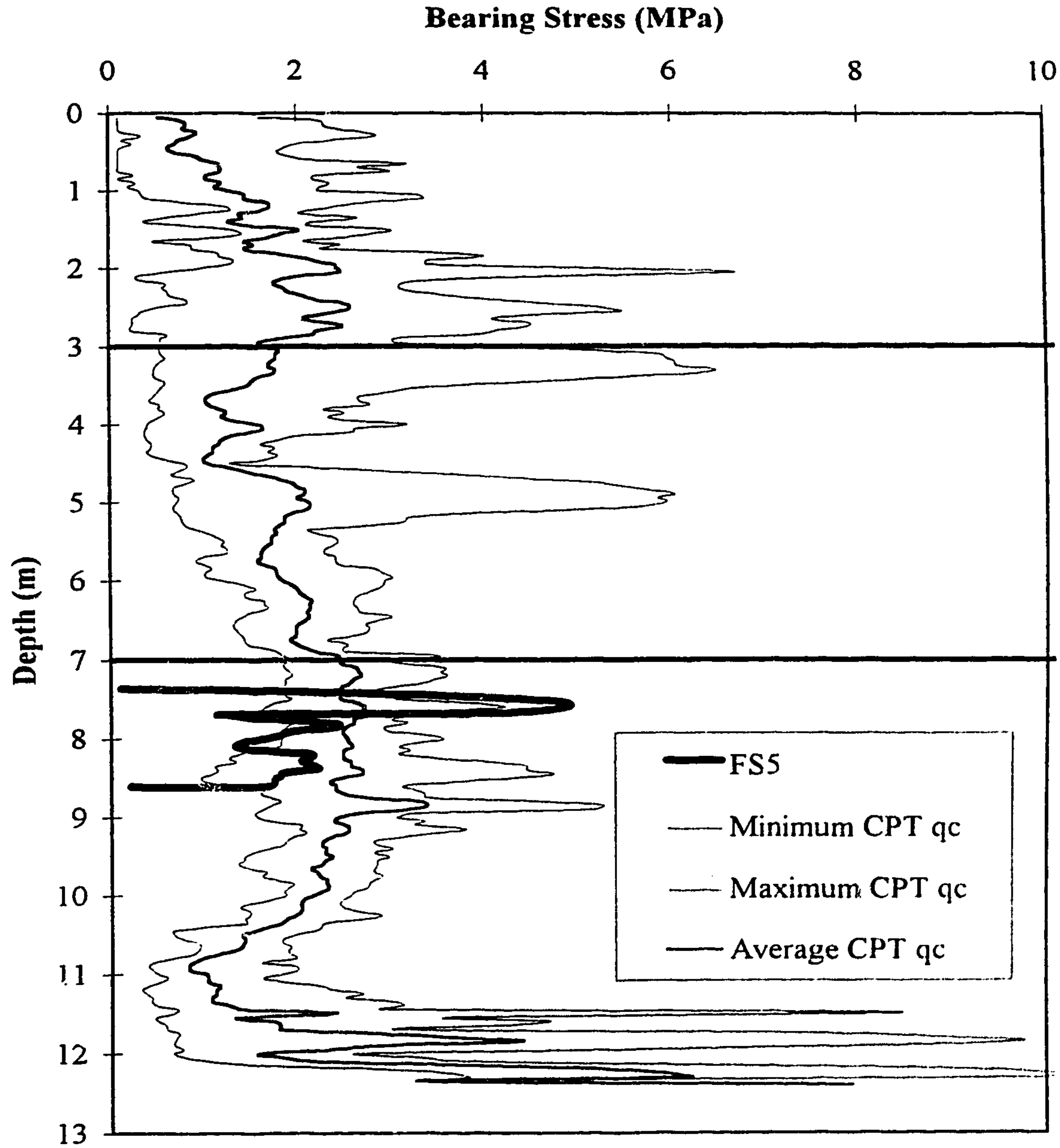

Figure 6-16 Bearing stress versus depth measured during 4" (10 cm) diameter plate load tests in borehole FS5.

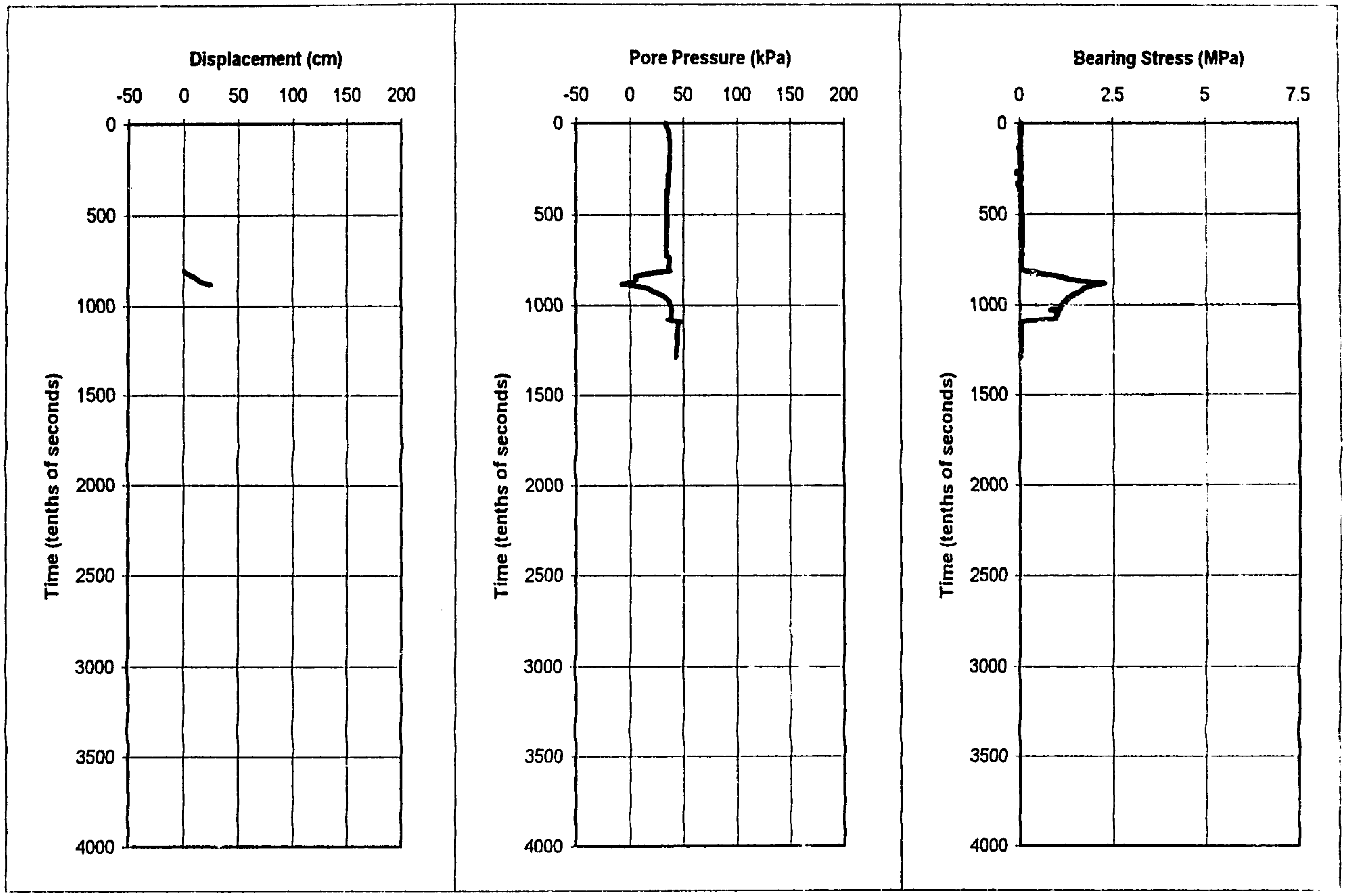

Figure 6-17 Results of 7" (18 cm) plate load test PL4-1 in terms of (a) displacement versus time, (b) pore pressure measurements versus time and (c) bearing stress measurements versus time.

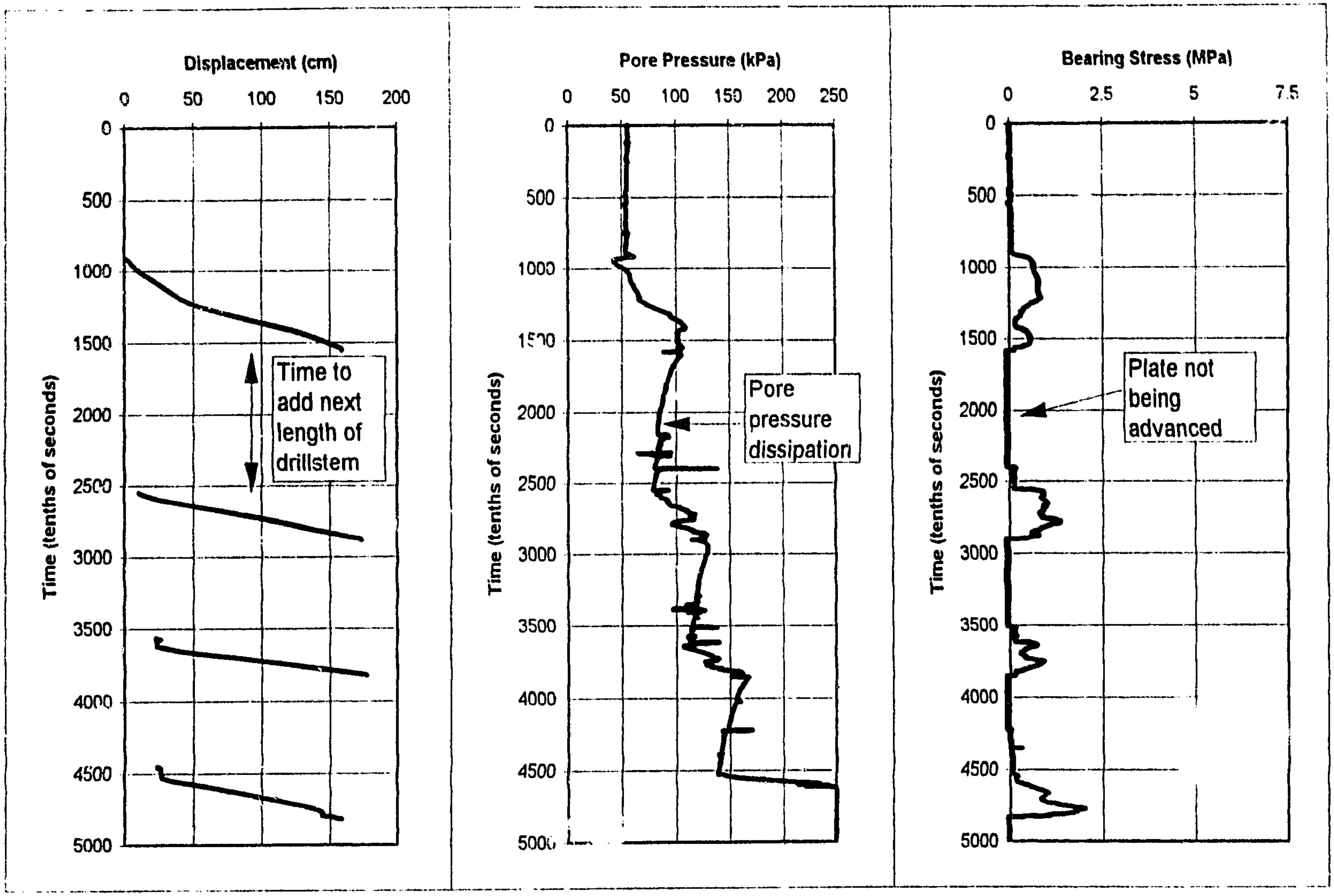

Figure 6-19 Results of 6" (15 cm) plate load test PL4-3 in terms of (a) displacement versus time, (b) pore pressure measurements versus time and (c) bearing stress measurements versus time.

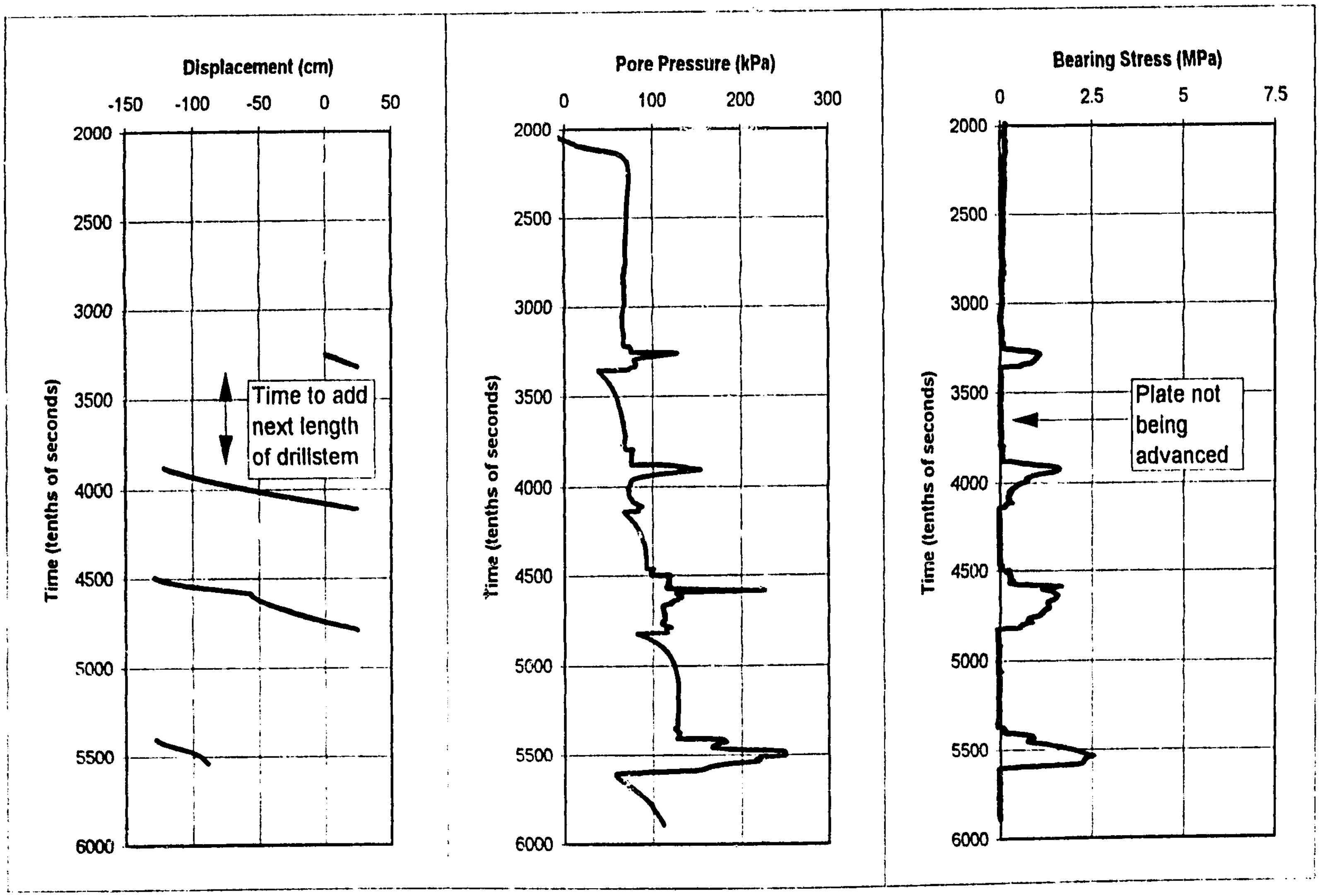

Figure 6-20 Results of 6" (15 cm) plate load test PL5-1 in terms of (a) displacement versus time, (b) pore pressure measurements versus time and (c) bearing stress measurements versus time.

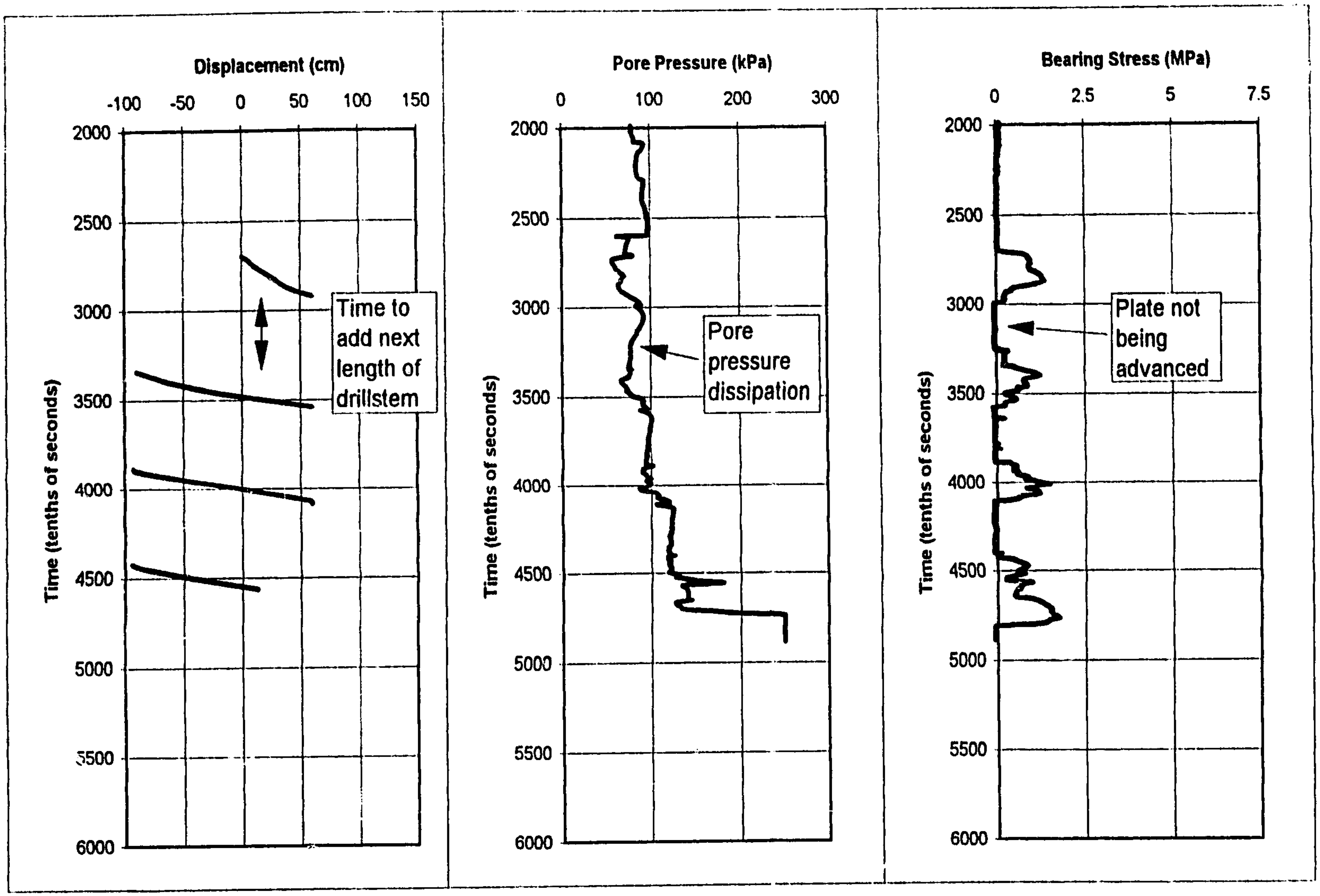

Figure 6-21 Results of 6" (15 cm) plate load test PL6-1 in terms of (a) displacement versus time, (b) pore pressure measurements versus time and (c) bearing stress measurements versus time.

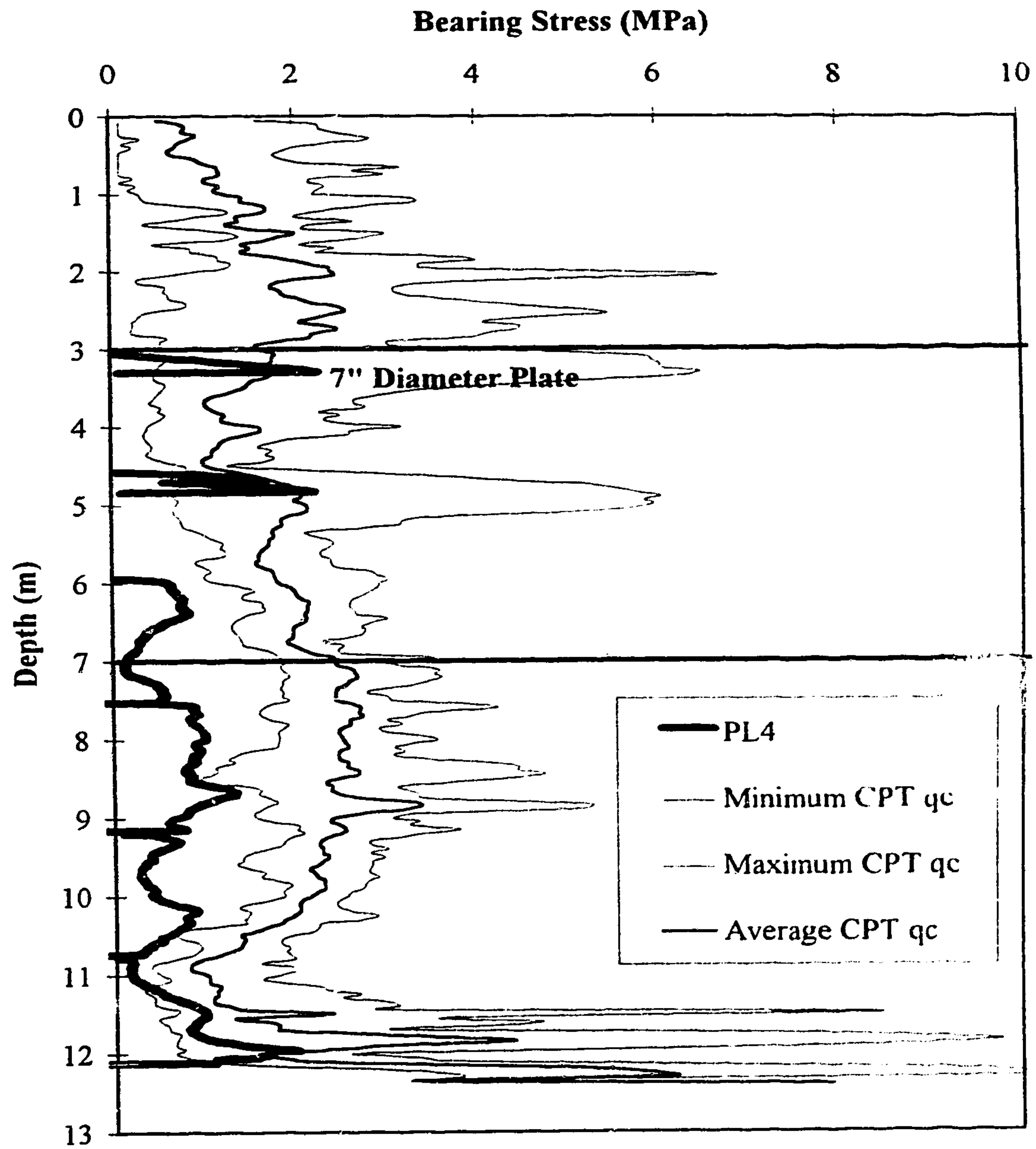

Figure 6-22 Bearing stress versus depth measured during 6" (15 cm) diameter plate load tests in borehole PL4; note the first test used a 7" (18 cm) diameter plate.

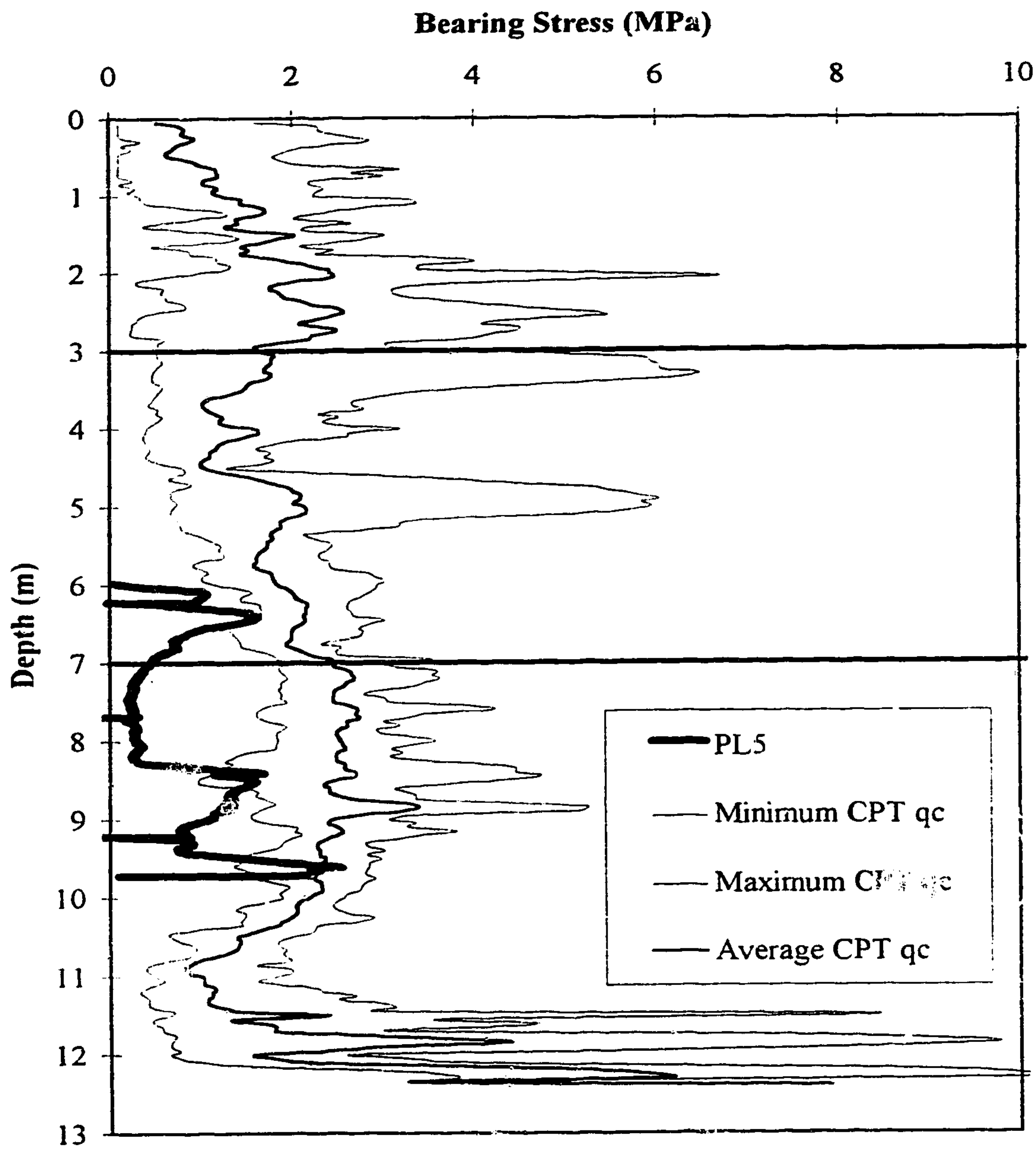

Figure 6-23 Bearing stress versus depth measured during 6" (15 cm) diameter plate load tests in borehole PL5.

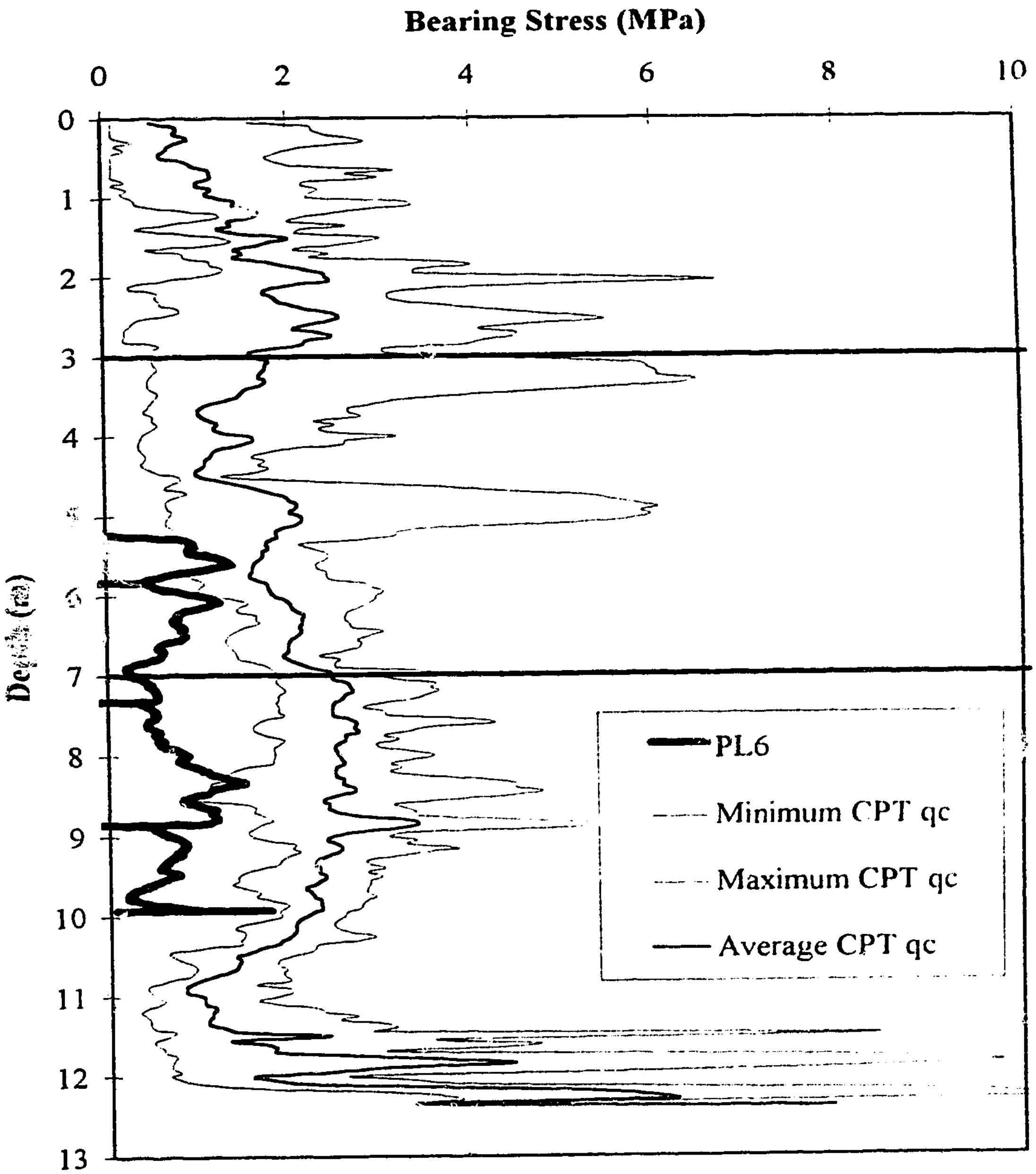

Figure 6-24 Bearing stress versus depth measured during 6" (15 cm) diameter plate load tests in borehole PL6.

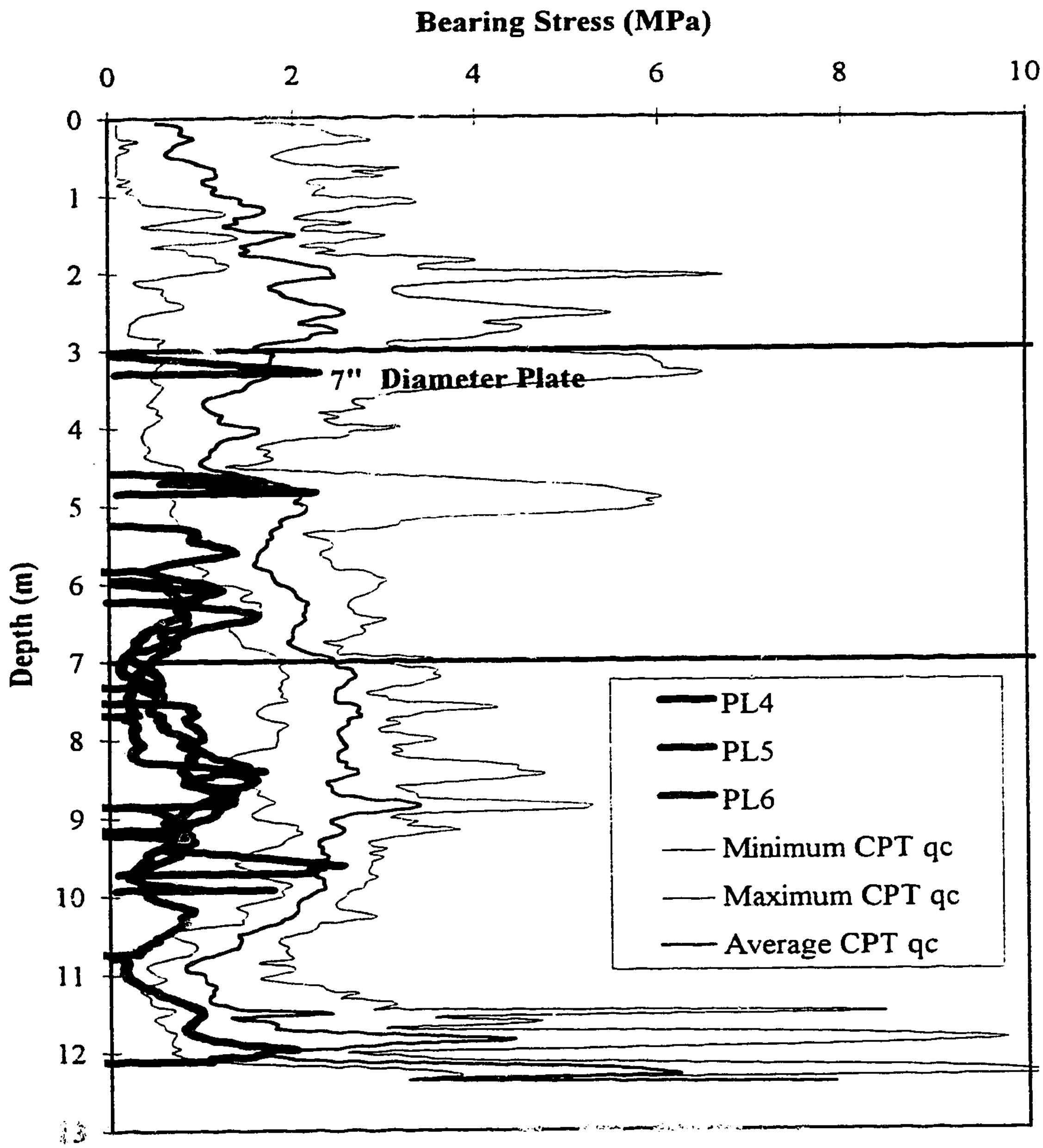

Figure 6-25 Summary of bearing stress versus depth measured during 6" (15 cm) diameter plate load tests in boreholes PL4, PL5 and PL6.

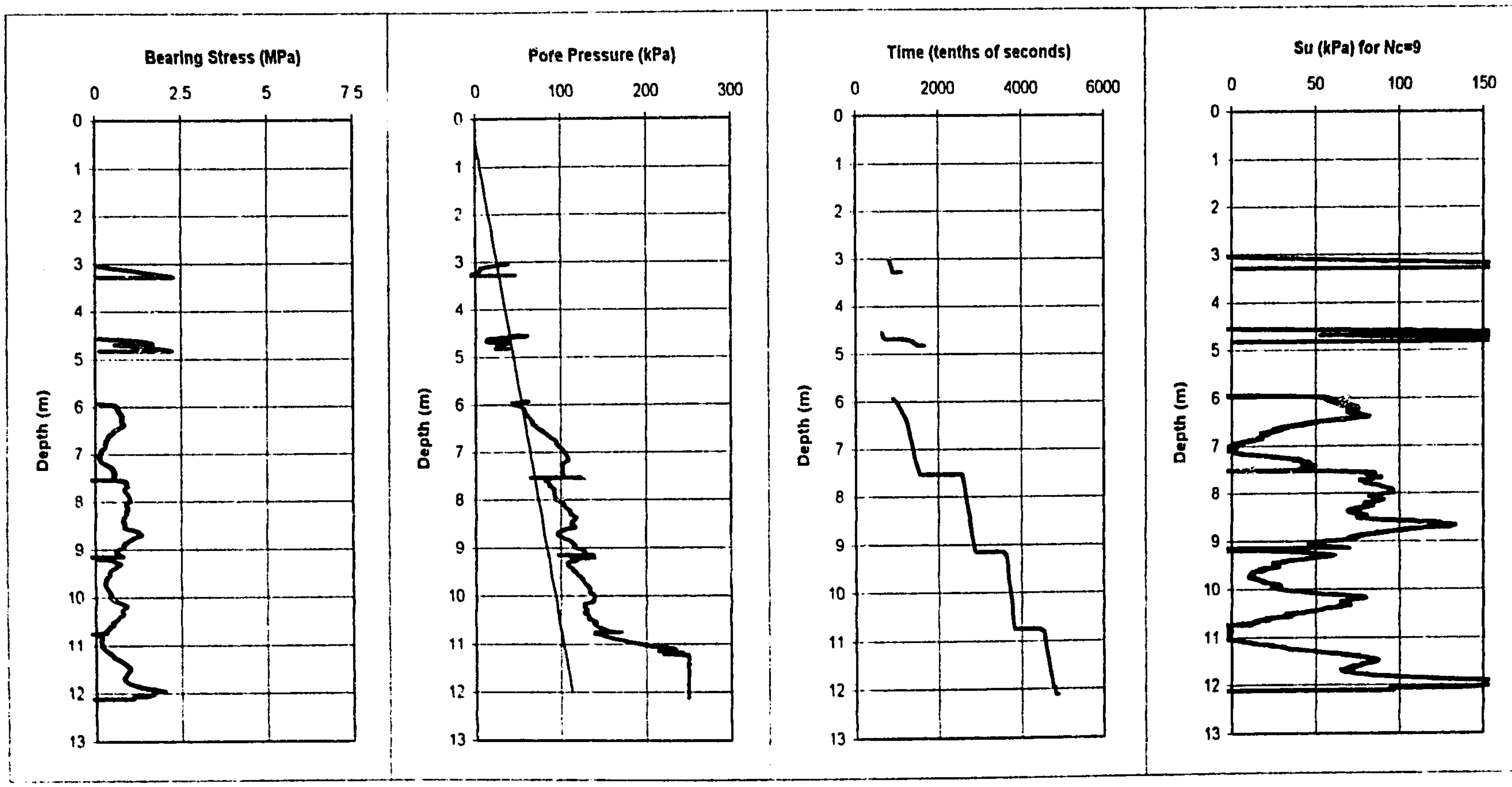

Figure 6-26 Profiles of 6" (15 cm) plate load test results versus depth in borehole PL4 in terms of (a) bearing stress, (b) pore pressure compared to hydrostatic, (c) time, and (d) estimated undrained shear strength (S_u) based on N_c=9.

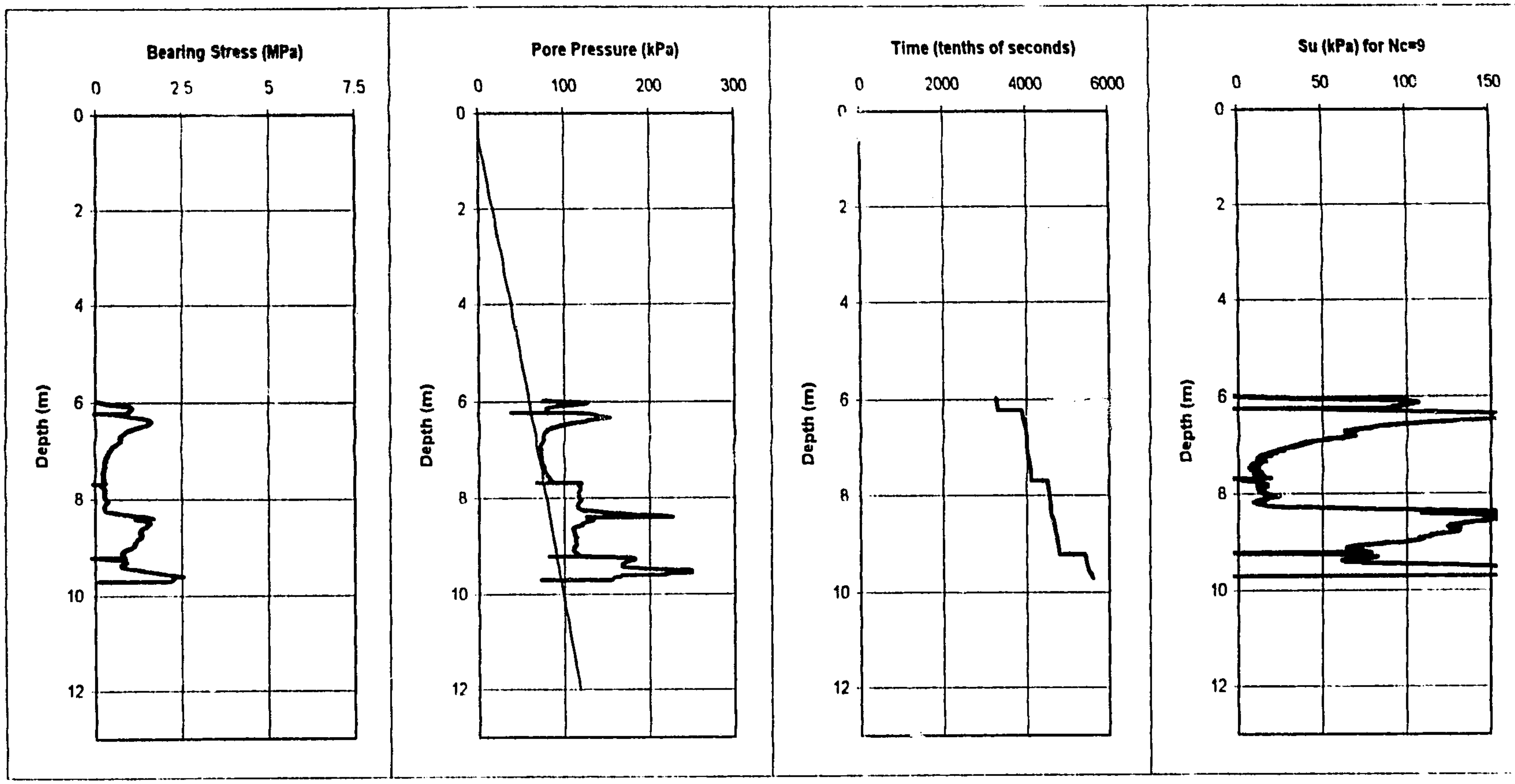

Figure 6-27 Profiles of 6" (15 cm) plate load test results versus depth in bo... 5 in terms of (a) bearing stress, (b) pore pressure compared to hydrostatic, (c) time, and (d) estimated undrained shear strength (S_u) based on N_c=9.

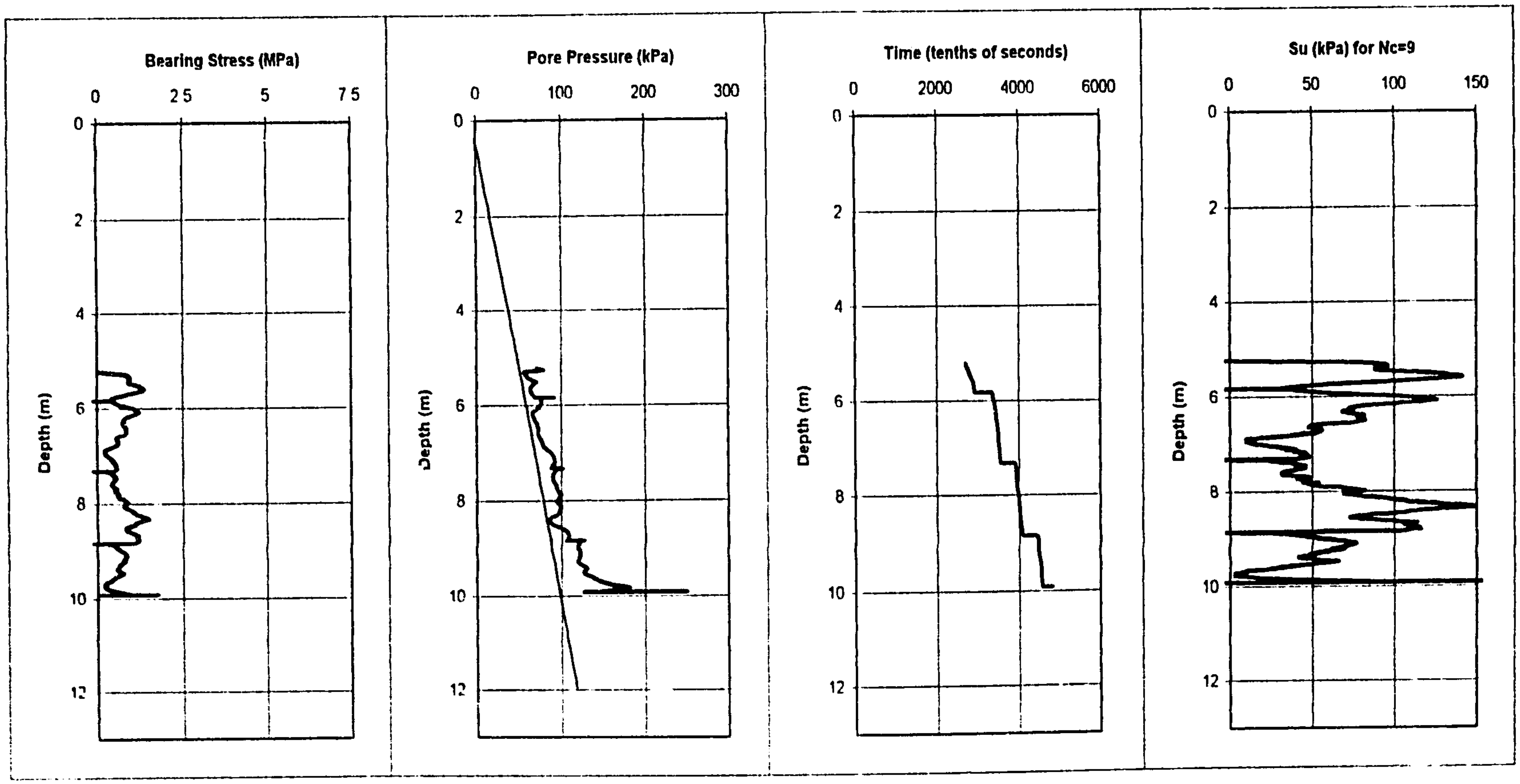

Figure 6-28 Profiles of 6" (15 cm) plate load test results versus depth in borehole PL6 in terms of (a) bearing stress, (b) pore pressure compared to hydrostatic, (c) time, and (d) estimated undrained shear strength (S_u) based on N_c=9.

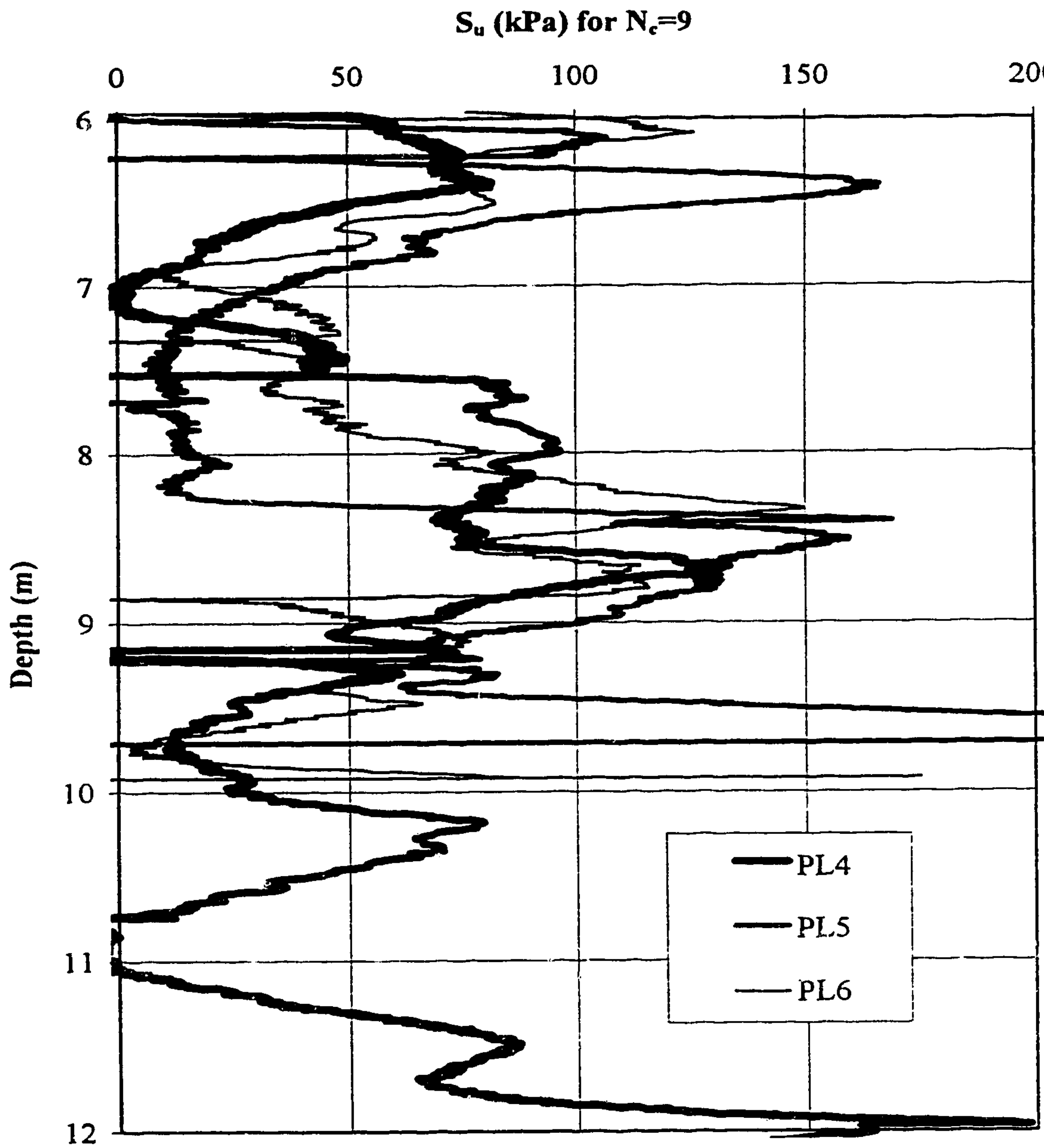

Figure 6-29 Summary of profiles of estimated undrained shear strength (S_u) based on N_c=9 for boreholes PL4, PL5 and PL6.

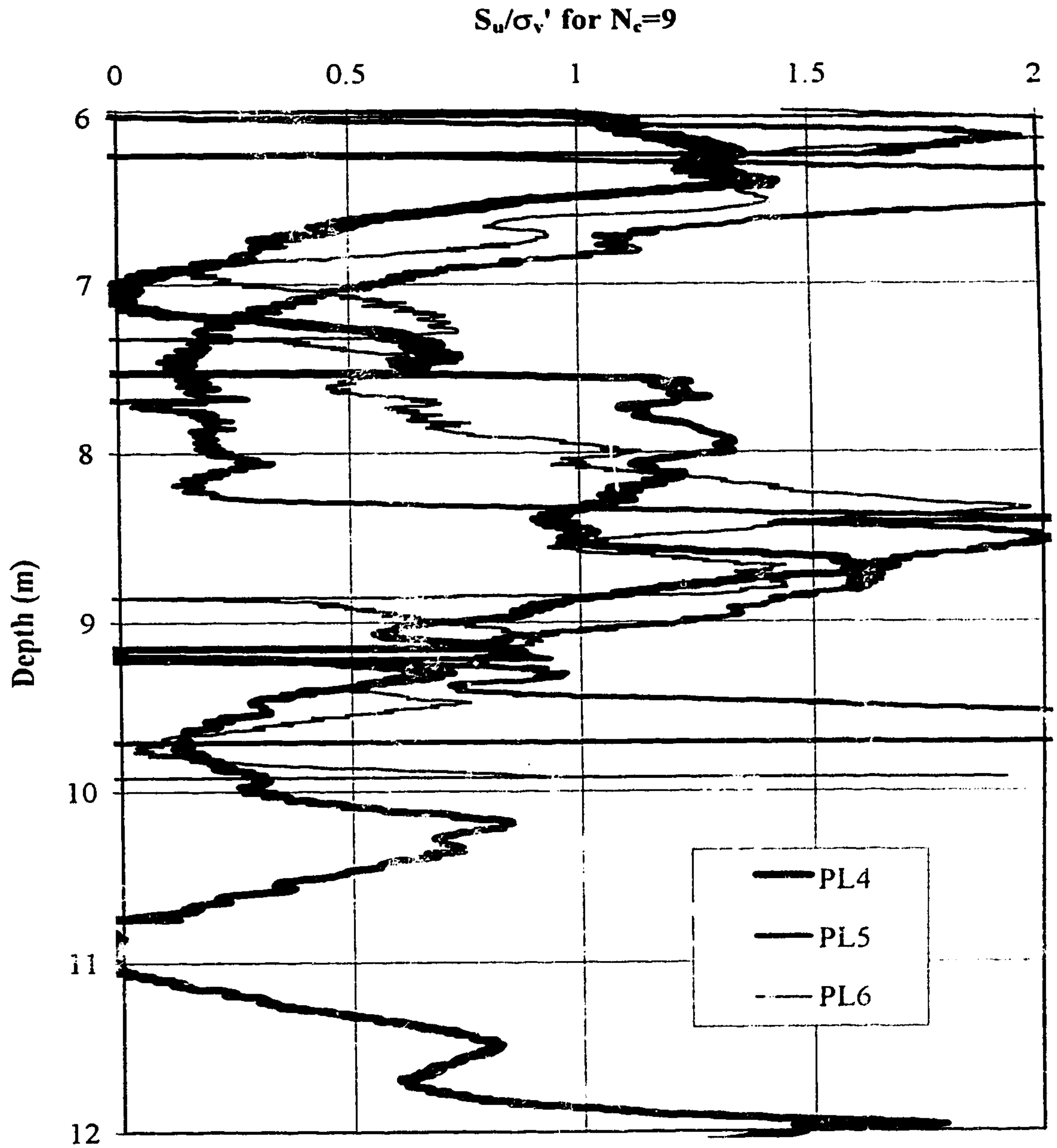

Figure 6-30 Summary of profiles of estimated ratio of undrained shear strength to vertical effective stress (S_u/σ_v') based on N_c=9 for boreholes PL4, PL5 and PL6.

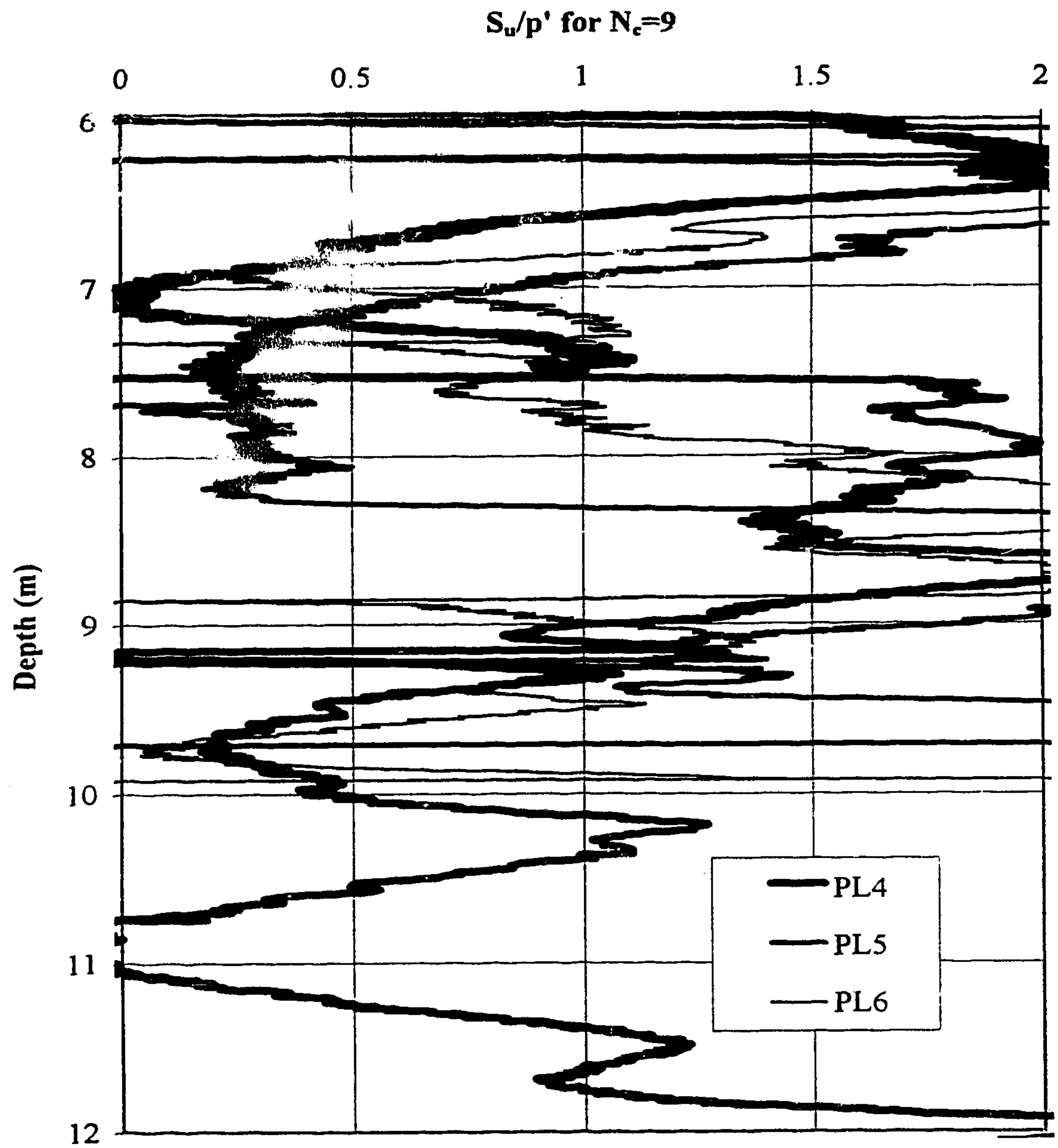

Figure 6-31 Summary of profiles of estimated ratio of undrained shear strength to mean normal effective stress (S_u/p') based on N_c=9 and K_0=0.5 for boreholes PL4, PL5 and PL6.

Equation 3-5 in Chapter 3, an average fines content of 6.8 % would be predicted, on average, in the target zone. Limited data is available at present regarding the grain size distributions of the undisturbed samples. A comparison can be made once this information becomes available. Preliminary information indicates that in-situ fines contents could be slightly smaller, in the order of 2% to 5%. The maximum, minimum and average predicted fines content profiles based on the CPT are shown in Figure 8-19b. It is interesting to note that these profiles predict a reasonably uniform fines content (indicating a reasonably uniform material) in the target zone.

Based on Equation 3-3 in Chapter 3, the average fines content of 6.8% would lead to, on average, a very small recommended correction of Δq_{c1}=0.3 MPa to the q_{c1} profile to produce a clean sand equivalent profile of cone tip resistance, $(q_{c1})_{cs}$. Combining the resulting clean sand equivalent profile with Equation 3-2 in Chapter 3, leads to the estimated CRR profile, as shown in Figure 8-19c. Again, the maximum, minimum and average profiles of estimated CRR are given. Superimposed on Figure 8-19c are solid dots representing the results of cyclic simple shear testing on undisturbed samples from the Massey site target zone. Both the estimated profile of CRR and the undisturbed sample CRR values are for Magnitude M=7.5 earthquakes (N=15 cycles). The estimated profile of CRR agrees well with the undisturbed samples tested to date, indicating a reasonably uniform average CRR of approximately 0.1 in the target zone. The standard deviation of 1.00 MPa for qc1 measurements in the target zone translates into a fairly small range in estimated CRR of approximately ± 0.01.

The soil classification data presented in Figure 8-9 can be compared with the soil classification chart methods of predicting CRR by Olsen and Koester (1995) and by Suzuki et al. (1995), as described in Chapter 3 (see Figures 3-14 and 3-15, respectively). Each of the three soil classification charts normalize cone tip resistance in a different manner, but for vertical effective stresses close to the reference atmospheric pressure of 100 kPa (as is the case at the Massey site), the three methods are very similar. The values on the cone tip resistance axis on the Robertson (1990) chart and the Olsen and Koester (1995) chart will be approximately equal (both axes are dimensionless). However, the values on the cone tip resistance axis on the Suzuki et al. (1995) will be approximately one tenth of the values on the Robertson (1990) chart, due to differences in units (the Suzuki et al. (1995) axis is in units of MPa, while the Robertson (1990) axis is dimensionless). The Olsen and Koester (1995) method would predict a similar average CRR of about 0.1 in the Massey site target zone. The Suzuki et al. (1995) method would probably also predict an average CRR of about 0.1 in the target zone (only contours of CRR=0.15 and CRR=0.25 are given on the Suzuki et al. (1995) plots, so some judgement is required).

For design purposes, the expected earthquake-induced cycle stress ratio (CSR) profile could be superimposed over Figure 8-19e. If there were large zones over which CSR is significantly larger than CRR, potential deformations could be estimated by predicting post cyclic liquefaction shear and volumetric strains using the method by Ishihara (1993), as described in Chapter 3 (see Figure 3-10). If there were only limited zones over which CSR>CRR, these zones should be investigated in greater detail because the CPT methods of predicting CRR likely contains some conservatism due to the selection of average values to produce the correlations.

The in-situ CRR can also be estimated from the SPT data in the target zone at the Massey site. The average $(N_1)_{60}$ in the target zone was 10.3 (SD=3.8). The estimated fines content at Massey of 6.8% is such that the sand is close to being classified as a clean sand (FC $\leq$ 5%) by the Seed et al. (1985) methodology (i.e. the recommended correction to $(N_1)_{60}$ would be small). The clean sand relationships between CRR and SPT $(N_1)_{60}$ by both Seed et al. (1985) and Fear and McRoberts (1995) described in Chapter 2 (see Figures 2-1 and 2-8, respectively) would predict an average CRR slightly greater than 0.10 based on the average $(N_1)_{60}$ of 10.3 in the target zone at Massey. However, the standard deviation of 3.8 for $(N_1)_{60}$ measurements in the target zone translates to a large range in predicted CRR of at least $\pm$ 0.05.

The shear wave velocity measurements in the target zone at the Massey site can also be used to estimate the in-situ CRR. The average V_{s1} in the target zone was 168 m/s (SD=6.4 m/s). The relationship between CRR and V_{s1} by Robertson et al. (1992) described in Chapter 3 (see Figure 3-17a) would predict an average CRR of approximately 0.19 based on the average V_{s1} of 168.2 m/s; this is significantly higher that the results of laboratory testing on undisturbed samples. However, the shear wave velocity correlation based on the recent NCEER Workshop (1996) discussions, as described in Chapter 3 (see Figure 3-17b), gives an estimated CRR of approximately 0.1, agreeing much better with the results of laboratory testing. The standard deviation of 6.4 m/s for V_{s1} measurements in the target zone translates into a much smaller range in predicted CRR (approximately $\pm$ 0.02) than the standard deviation in $(N_1)_{60}$ does.

8.7 Discussion

8.7.1 Data review results compared with other CANLEX sites

Table 8-6 compares the results of the data review at the Massey and Kidd sites with the data review that has been performed at Phase I and Phase III of the CANLEX project. Detailed descriptions of the Phase I and Phase III data reviews, as well as the detailed data review of the Kidd site will be contained in CANLEX Project final reports. All of the values in Table 8-6 are given as the overall average in the target zone at each site; for some parameters, the overall standard deviation is also given. Index parameters for the four sites were given in Table 8-1. Grain characteristic parameters for the four sites were given in Table 8-2.

Overall, the target zone at the Kidd site had higher average values of $(N_1)_{60}$, q_{c1}, and V_{s1} than the target zone at the Massey site. This is likely partially due to aging effects. The scatter in SPT, CPT and shear wave velocity data (as represented by the standard deviations) was similar at the two sites. The Massey and Kidd sites had similar average values of Y, while both the average X and the average qc1/(N1)60 were smaller at Kidd than at Massey. Similar average fines contents were predicted at each site using the integrated CPT method described in Chapter 3. Actual fines content data from undisturbed samples are still required to check the accuracy of these predictions. The average void ratio predicted by the geophysical logs is closer to the average of the undisturbed samples tested to date at the Massey site. At the Kidd site, the geophysical logging appears to significantly underpredict the average void ratio. However, as reported by Lawrence et al. (1995), the geophysical logs at Kidd were not of the same quality as at Massey. The average void ratio at Massey appears to be higher than the average void ratio at Kidd. However, additional undisturbed samples at both sites, particularly Kidd (at which only six sample void ratios are available to date) are required to confirm the average values. Since samples were initially selected with the goal of attempting to test the loosest samples first, the actual average void ratio at each site may be slightly less than the average value to date, as given in Table 8-6.

The data review results for the Phase I (Syncrude) site are also presented in Table 8-6. The target zone at the Phase I site was located at a much greater depth than the target zone at either of the Phase II sites. The average $(N_1)_{60}$ and q_{c1} were higher than either of the Phase II sites. However, the average V_{s1} was lower than either of the Phase II sites. The scatter in SPT and CPT data at the Phase I site was similar to the scatter at both of the

Phase II sites. The shear wave velocity data, however, was much more scattered than the shear wave velocity data at either of the Phase II sites, with the standard deviation being in the order of 20 m/s compared to 5 to 6 m/s at the Phase II sites (see Table 8-6). This suggests that the shear wave velocity measurements at the Phase I site either have more variation or are less reliable than at the Phase II sites. The fact that the standard deviations for the CPT are similar at both the Phase I and II sites suggests the latter. The average value of $q_{c1}/(N_1)_{60}$ at the Phase I site was similar to that at the Kidd site, while the average values of both Y and X at the Phase I site were much smaller than at either of the Phase II sites. In addition, the values of Y and X were more scattered at the Phase I site (indicated by the larger standard deviations). Both Y and X at the Phase I site were likely strongly influenced by the lower values of shear wave velocity which high a high degree of scatter. Geophysical logging at the Phase I site predicted a similar average void ratio to the average of the undisturbed samples available to date. As for the Phase II sites, the actual average void ratio at each site may be slightly less than the average value to date shown in Table 8-6, because samples were initially selected with the goal of attempting to test the loosest samples first. An average fines content of 12.4% was predicted at the Phase I site, using the integrated CPT method described in Chapter 3. To date, grain size distributions for undisturbed samples have indicated a smaller average fines content in the order of 5%. However, more data is required before any firm conclusions can be made. In addition, the method outlined in Chapter 3 proposed tentative relationships to estimate fines content. The method will be updated as additional data become available; in addition, Chapter 3 recommended that the equations given in the method were general and might require site specific modifications.

Table 8-6 also presents the summarized data review results available to date from the Phase III (J-pit) site. The target zone at the Phase III site is shallower than the target zones at the Phase I and II sites. The Phase III site is also the youngest deposit of the four sites, consisting of freshly placed (< 1 month old) Syncrude sand tailings. The results of the data review for the Phase III site suggest that this sand is unusual, as compared to the other sites. The average values of $(N_1)_{60}$, q_{c1} and V_{s1} are all significantly smaller than the values at the Phase I and Phase II sites. In general, the SPT, CPT and shear wave velocity measurements also appear to be more consistent (i.e. less scattered) that at the other sites. The average values of Y, X and $q_{c1}/(N_1)_{60}$ do not appear unusual and are in the same range as the values for the other sites. The integrated CPT method described in Chapter 3 predicts a higher fines content at the Phase III site than at the other sites. However, actual fines content data from undisturbed samples are required to check the accuracy of these predictions. Conventional or shear wave velocity based interpretations of the $(N_1)_{60}$, q_{c1} or V_{s1} profiles would predict significantly higher void ratios than suggested by the undisturbed samples available to date. However, geophysical logging predicts an average void ratio similar to the average void ratio of the undisturbed samples available to date.

A possible explanation for the discrepancy in results is that the SPT, CPT and shear wave velocity measurements were strongly influenced by the high fines content and, hence, possibly the skeletal void ratio at the Phase III site. The void ratios estimated for the undisturbed samples and predicted by the geophysical logging are total void ratios. When the undisturbed sample total void ratios were corrected to approximate equivalent skeletal void ratios based on the average fines content in the target zone, the void ratio interpretations of the SPT, CPT and shear wave velocity measurements had much better agreement with the undisturbed samples. Further details of this analysis will be provided the Phase III data review report. The results seem to indicate that skeletal void ratio may be a factor for sands with a high fines content. Scanning electron microscopy has also shown that at least some of the undisturbed samples from the Phase III site appear to have an unusual fabric due to the high fines content (Hofmann, 1995). It will be interesting to carefully examine the results of testing undisturbed samples to see if their response appears to be linked to skeletal or total void ratios.

8.7.2 Estimated response

a) Flow liquefaction

Table 8-7 summarizes the average state of Fraser River sand in the target zone at the Massey site, based on the undisturbed samples available to date. The average RSR of 0.29 was estimated by combining the average effective stresses at the mid-depth of the target zone at each site and the overall average void ratio of all undisturbed samples available to date, as summarized in Table 8-6. In general, as discussed previously, interpretation of the in-situ testing signatures appears to predict similar average states over most of the target zone at each site. However, both in-situ testing and undisturbed samples have indicated that there may be layers with the target zone having significantly higher values of RSR (i.e. looser). Based on the average predicted RSR at the Massey site, Table 8-7 presents the corresponding estimated values for the various components of response described in Chapter 4 (see Figures 4-15 and 4-16), for triaxial compression and extension, respectively.

Brittleness index (I_B) and axial strain at minimum strength (ε_a) were estimated based on Equations 8-1 and 8-2, respectively; i.e. the laboratory based relationships based on testing at the Massey site. The ultimate values of M were assumed to be approximately $(M_f)_C$=1.5 and $(M_f)_E$=1.0, for triaxial compression and extension, respectively, based on the results of the laboratory testing at the Massey site, discussed previously. Based on the limited testing to date on undisturbed samples of Fraser River sand, $I_B \approx 0$ for triaxial compression loading indicates that the material would strain-harden in triaxial compression. Consequently, S_{min}, S_p and S_f will all be equal and can be estimated by combining Equation 4-28 in Chapter 4, which estimates the theoretical S_f/p_i', with the average $(M_f)_C$ and p'_i. The value of p'_f can be estimated by combining S_f and M_f (see Equation 4-15 in Chapter 4) and will be equal to both p'_{min} and p'_p. Axial strain at minimum strength is not applicable for strain hardening material. In triaxial extension, S_{min} can be estimated by combining Equation 4-29 in Chapter 4, which estimates the theoretical S_{min}/p'_i, with the average p'_i. S_p can be estimated by combining the estimated I_B and S_{min} with the average S_i (=q_i/2) and the triaxial extension formula for brittleness index (see Equation 4-27a in Chapter 4). S_f can be estimated by combining Equation 4-28 in Chapter 4, which estimates the theoretical S_f/p_i', with the average $(M_f)_E$ and p'_i. The value of p'_{min} can be estimated by combining S_{min} and M_{min} (see Equation 4-16 in Chapter 4), assuming that M_{min}=M_f. The value of p'_p can be estimated by combining S_p and M_p. Using the plots of M_p versus RSR for Massey as a reference (see Figure 8-14c), an average M_p of 0.75 was selected for triaxial extension based on the average RSR values of 0.24 to 0.29 calculated for the Phase II sites. The value of p'_f can be estimated by combining S_f and M_f.

Included in Table 8-7 are the average corrected values of SPT and CPT penetration resistance and shear wave velocity measurements. The correlation parameters between the three tests (i.e. Y, X and $q_{c1}/(N_1)_{60}$) are also given. As a guide to estimating in-situ response to undrained monotonic loading, the average values of $(N_1)_{60}$, q_{c1} and V_{s1} can be linked to the average response in triaxial compression and triaxial extension at each site. The averaged values of $(N_1)_{60}$, q_{c1} and V_{s1} were all higher at Kidd than at Massey; this is likely partially a result of aging. The average RSR at the two sites are reasonably similar; consequently, the estimated components are somewhat similar, although higher strengths are predicted at Kidd because RSR is slightly smaller. The methods of estimating the undrained strength are sensitive to RSR, as is indicated by this comparison. However, the methods can be useful in estimating the overall average and general range in response at a given site.

Based on the summary presented in Table 8-7, Figure 8-20 illustrates how average q-p' stress paths and S_u-ε_a stress-strain curves for Fraser River sand in the target zone at each Phase II site can be back-calculated by combining the individual components of response estimated from the average state in the target zone at each site. Average stress paths and stress-strain curves are shown for both triaxial compression and triaxial extension directions of loading. The stress path curves were estimated by sketching a line through the points (p'_i, q_i), (p'_p, q_p), (p'_{min}, q_{min}), and (p'_f, q_f), as summarized in Table 8-7, using, as a reference, some of the actual stress paths plotted for undisturbed samples with similar values of RSR tested in the laboratory. Obviously some artistic licence has been used to create these figures and they are shown primarily for illustrative purposes. The stress-strain curves were estimated by sketching a line through the points (S_i, $(\varepsilon_a)_i$=0), (S_p, $(\varepsilon_a)_p$), (S_{min}, $(\varepsilon_a)_{min}$), and (S_f, $(\varepsilon_a)_f$), as summarized in Table 8-7. The triaxial compression stress-strain curves are shown to strain-harden directly to ultimate state; the shapes of the curves were drawn using, as a reference, some of the actual stress-strain curves plotted for undisturbed samples with similar values of RSR tested in the laboratory. For the triaxial extension stress-strain curves, $(\varepsilon_a)_p$ was estimated to have a value of approximately 0.25%, based on laboratory results. The value of $(\varepsilon_a)_{min}$ for the triaxial extension stress-strain curves was estimated by adding half of the axial strain estimated to occur while at minimum strength to the value of $(\varepsilon_a)_p$. For both triaxial compression and extension tests, $(\varepsilon_a)_f$ was set equal to 20%. This is typically the limit to which laboratory tests are taken; however, the actual ultimate strength likely occurs at larger strains, as indicated by the fact that many of the undisturbed samples were still strain-hardening towards their respective ultimate states when the triaxial tests were stopped.

b) Cyclic softening

Included in Table 8-7 is a summary of the integrated CPT method for estimating CRR, described in Chapter 3, as applied to the average CPT data in the target zone at each of the Phase II sites. The average I_c classifies the soil in the target zone at the Massey site as a sand (clean sand to silty sand) since $1.31 < I_c < 2.05$ (see Chapter 3, Table 3-1). The standard deviation is small, indicating a fairly uniform target zone, in terms of soil classification. Similar average fines contents of approximately 7% are predicted for the target zone at the Massey site. The resulting average recommended correction to CPT penetration resistance, Δq_{c1}, is very small. In the target zone, when the average Δq_{c1} is added to the average corrected q_{c1}, an average CRR of approximately 0.10 is estimated.

Since the Massey soil deposit is considered to be fairly uniform in the target zone, a fairly uniform average CRR of 0.10 would be expected throughout much of the target zone at each site. This was clearly shown in Figures 8-19.

Included in Table 8-7 are the average corrected values of SPT and CPT penetration resistance and shear wave velocity measurements. The correlation parameters between the three tests (i.e. Y, X and $q_{c1}/(N_1)_{60}$) are also given. As a guide to estimating in-situ response to undrained cyclic loading, the average values of $(N_1)_{60}$, q_{c1} and V_{s1} can be linked to the average estimated CRR at each site. It is of interest to compare the value of CRR that other existing methods would predict from the average in-situ testing with the average value estimated using the integrated CPT approach. The estimated fines content at Massey of 6.8% is such that the sand is close to being classified as a clean sand (FC ≤ 5%) by the Seed et al. (1985) methodology (i.e. the recommended correction to (N1)60 would be small). The clean sand relationships between CRR and SPT $(N_1)_{60}$ by both Seed et al. (1985) and Fear and McRoberts (1995), as described in Chapter 2 (see Figures 2-1 and 2-8), would predict an average CRR slightly greater than 0.10 based on the average $(N_1)_{60}$ of 10.3 in the target zone at Massey. However, the relationship between CRR and Vs1 by Robertson et al. (1992), described in Chapter 3 (see Figure 3-17a), would predict a higher average CRR of approximately 0.19 based on the average V_{s1} of 168.2 m/s. However, as discussed earlier, the shear wave velocity correlation based on the recent NCEER Workshop (1996) discussions, as described in Chapter 3 (see Figure 3-17b), gives an estimated CRR of approximately 0.1, agreeing much better with the results of laboratory testing. As previously discussed, for the average values of Q and F at both Phase II sites, the soil classification based method by Olsen and Koester (1995), described in Chapter 3 (see Figure 3-14), would predict an average CRR of approximately 0.075, similar to the value of 0.10 predicted by the integrated CPT method.

8.8 Summary and Conclusions

Consistent frameworks for evaluating the potential for both cyclic softening and flow liquefaction have been proposed in Chapters 3 and 4 as a means of interpreting and comparing various field and laboratory data and linking the observed response in the laboratory to in-situ test results. The suggested framework for evaluation of flow liquefaction potential is based on estimating values of RSR for laboratory samples and in-situ field conditions, relative to a reference USL established by laboratory testing, as described in Chapter 4. RSR provides the link between in-situ testing signatures and response to undrained monotonic loading observed in the laboratory. The suggested framework for evaluating cyclic softening potential is based on an integrated CPT approach described in Chapter 3.

Applying the two frameworks to the Massey site in this chapter has led to the general conclusion that in the target zone the site is, on average, essentially non-susceptible to flow liquefaction. If a suitable trigger resulted in undrained monotonic loading, most of the target zone at the site would respond in a non-brittle, strain-hardening manner in triaxial compression and could exhibit a temporary loss in strength with minimum associated axial strains in triaxial extension before strain-hardening. Some specific zones at the Massey site would require further investigation for design purposes to evaluate the continuity of the looser layers. When subjected to cyclic loading, the target zones at the Massey site would have an average M=7.5 equivalent CRR of approximately 0.1. Cyclic liquefaction and subsequent deformations [illegible] a problem if the earthquake induced CSR exceeded this resistance.

Table 8-1: Index parameters for CANLEX sites

Parameter	Phase I	Phase II (Fraser River Sand)		Phase III	Ticino Sand*
	Syncrude	Massey	Kidd	J-pit	
Approx. age of deposit	30 years	200 years **	4 000 years **	1 month	< 1 week
Target Zone Depth (m)	27 to 37 (Elev. 325 m to 315 m)	8 to 13	12 to 17	3 to 7	-
Depth to GWT (m)	21	1.5	1.5	0.5	-
γ (kN/m^3) above GWT below GWT	18.5 19.5	18.5 19.5	18.5 19.5	18.5 19.5	-
Mineralogy (of silt size fraction of soil)	90% quartz 5% feldspar 5% kaolinite	70% quartz 15 % feldspar 5% mica 5% kaolinite 5% chlorite & smectite	70% quartz 15 % feldspar 5% mica 5% kaolinite 5% chlorite & smectite	assumed to be the same as Phase I	95% quartz 5% feldspar
Grain Size Cu (D_{60}/D_{10})	2.22 (0.2/0.09)	2.14 (0.30/0.14)	2.5 (0.35/0.14)	not presently available	1.13 (0.65/0.40)
Average FC (%) from SPT	12	3	6.8	10	< 5%
e_{max}§	0.958	1.102	1.077	0.901 (FC=4%-10%) 0.986 (FC=10%-40%)	0.89
e_{min}§	0.668	0.715	0.715	0.579 (FC=4%-10%) 0.461 (FC=10%-40%)	0.52
G_s	2.66	2.68	2.72	2.62	2.67
K_o***	0.5	0.5	0.5	0.5	-

Notes:

* Calibration chamber studies (Baldi et al., 1986)

** Monahan et al. (1995)

*** estimated from pressuremeter testing results

§ all values of e_{max} and e_{min} were determined by U. of A., except those for Phase I which were determined by UBC

Table 8-2: Grain characteristic parameters for CANLEX sites

Parameter	Phase I	Phase II (Fraser River Sand)		Phase III
	Syncrude	Massey	Kidd	J-pit
Γ	0.919 (e>0.829) 1.920 (e<0.829)	1.071 (e>0.979) 1.80 (e<0.979)	1.071 (e>0.979) 1.80 (e<0.979)	0.919 (e>0.829) 1.920 (e<0.829)
λ_{ln}	0.015 (e>0.829) 0.182 (e<0.829)	0.0165 (e>0.979) 0.1477 (e<0.979)	0.0165 (e>0.979) 0.1477 (e<0.979)	0.015 (e>0.829) 0.182 (e<0.829)
A*	311 (311 + 0)	317 (295 + 22)	325 (295 + 30)	311 (311 + 0)
B	188	143	143	188

Notes:
* a (b + c), where a = estimated value for the deposit in-situ; b = value determined from testing young reconstituted samples in the laboratory; c = correction to account for aging effects in-situ, based on the work by Robertson et al. (1995)

Table 8-3: Summary of data for Massey frozen samples tested to date

Massey Tunnel		Pa	100	(kPa)		e>0.979	e<0.979	
Gs	2.68	γ water	9.8	(kPa)	Γ	1.071	1.8	
GWT (m)	1.5	γ dry	18.5	(kN/m3)	λ	0.0165	0.1477	
Ko	0.5	γ sat.	19.5	(kN/m3)	Breakpoint void ratio		0.979	

FROZEN SAMPLES Sample No.	Average Depth (m)	Average σv' (kPa)	Void Ratio	RSR	Source of e S=sent R=received	Lab sent to	T=triaxial (C,E) SS=simple shear CSS=cyclic SS	Fines Content (% passing No. 200 sieve)	Lab e	Lab RSR	IB	Smin/p1	% εa at Smin	S0p1	Mp	Mf	CRR (M=7.5)
M94F6 C2B	9.155	102.0	0.9788	0.262	S	UBC	TE - DRAINED										
M94F4 C4-2	10.425	114.3	0.9793	0.294	S	UBC	TE		0.982	0.333	0.106	0.050	8.0	0.273	1.47	0.92	
M94F6 C7A	11.85	128.1	0.9299	0.236	S	UBC	TE		0.914	0.205	0.000	0.181	3.3	0.665	0.99	0.94	
M94F2 C2B-1	9.005	100.5	0.9129	0.165	S	UBC	TE		0.910	0.158	0.021	0.135	2.3	0.683	0.68	1.01	
M94F2 C7B-1	10.685	116.8	0.9852	0.430	S	UBC	TC - DRAINED										
M94F4 C4-1	10.255	112.7	0.9928	0.657	S	UBC	TC		0.990	0.531	0.000	1.960	0.0	1.960	1.38	1.38	
M94F4 C4-3	10.605	116.1	0.9803	0.317	S	UBC	TC		0.983	0.360	0.000	2.133	0.0	2.133	1.55	1.55	
M94F6 C4-2	10.375	113.8	0.9473	0.236	S	UBC	TC		0.942	0.220	0.000	2.727	0.0	2.727	1.42	1.42	
M94F4 C3A	9.33	103.7	1.0188	2.922	S	UBC	SS										
M94F6 C3-1	9.31	103.5	1.0025	1.086	S	UBC	SS										
M94F6 C3-2	9.33	103.7	0.9855	0.388	S	UBC	SS										
M94F2 C7B-2	10.78	117.8	1.0319	7.341	S	UBC	SS										
M94F2 C7B-3	10.81	118.1	1.0189	3.347	S	UBC	SS										
M94F2 C2B-2	9.545	105.8	0.8788	0.136	S	UBC	CSS		0.809								0.144
M94F2 C2B-3	10.03	110.5	0.9041	0.171	S	UBC	CSS		0.862								0.099
M94F5 C3C-1	10.47	114.8	1.0327	7.509	S	UBC	CSS		1.005								0.098
M94F5 C3C-2	10.5	115.1	0.9854	0.428	S	UBC	CSS		0.969								0.080
M94F2 C11B-1	12.75	136.9	1.025	5.617	S	UBC	CSS		0.995								0.111
M94F2 C11B-2	12.78	137.2	1.0267	6.239	S	UBC	CSS		0.997								0.089
M94F6 C4B-1	10.53	115.3	1.0241	4.482	S	UBC	CSS		0.998								0.094
M94F6 C4B-2	10.55	115.5	1.0257	4.946	S	UBC	CSS		0.986								0.093
M94F6 C6-1	11.19	121.7	0.9766	0.308	S	UBC	CSS		0.958								0.112
M94F6 C6-2	11.22	122.0	0.9697	0.294	S	UBC	CSS		0.953								0.084
M94F6 C6-3	11.25	122.3	0.9705	0.297	S	UBC	CSS		0.957								0.111
M94F4 C2B	9.075	101.2	0.9065	0.159	S	Laval - VA01	TC		0.909	0.143	0	4.502	0	4.502	1.57	1.57	
M94F6 C2A	8.775	98.3	0.8708	0.121	S	Laval - VA02	TC		0.853	0.094	0	8.246	0	8.246	1.54	1.54	
M94F4 C4	10.2362	112.5	0.9733	0.278	S	Laval - VA12	TC		0.962	0.251	0	2.825	0	2.825	1.78	1.78	
M94F4 C4-4	10.73	117.3	0.9808	0.330	S	Laval - VA13	TC		1.043	14.293	0	1.370	0	1.370	1.47	1.47	
M94F2 C11B	12.62	135.6	1.0285	6.880	S	VA14 (M94F2C	TC		1.000	1.193	0	2.160	0	2.160	1.47	1.47	
M94F2 C7B-1	10.84	118.3	0.9146	0.197	S	Laval - VA15	TC		0.810	0.094	0	7.104	0	7.104	1.52	1.52	
M94F2 C7B-2	10.95	119.4	1.0149	2.657	S	Laval - VA16	TC		0.983	0.370	0	3.105	0	3.105	1.51	1.51	
M94F6 C4-1	10.5	115.1	0.9831	0.373	S	Laval-VA17	TC		0.968	0.268	0	3.146	0	3.146	1.52	1.52	
M94F4 C1B	7.87	89.5	1.0512	17.979	S	Laval											
M94F2 C3A-1	8.18	92.5	0.9379	0.180	S	Laval											
M94F2 C3A-2	8.29	93.6	0.9378	0.182	S	Laval											
M94F2 C10-1	12.19	131.4	0.9504	0.278	S	Laval											
M94F2 C10-2	12.3	132.5	0.976	0.334	S	Laval											
M94F4 C6-4	12.6	135.4			S	UofA											
LAVAL LARGE DIAMETER SAMPLES																	
MT 1-1 (Samp#1Tub	8.12	92.0	1.033	6.128	S	Laval - VA04											
MT 1-2 (Samp#1Tub	8.12	92.0	1.0376	8.099	S	Laval - VA05											
MT 3-1 (Samp#1Tub	8.12	92.0	1.0435	11.580	S	Laval - VA03											
MT 3-2 (Samp#1Tub	8.12	92.0	1.0141	1.949	S	Laval - VA06											
Tube#2 A-1	8.85	99.0	0.9515	0.211	S	Laval											
Tube#2 A-2	8.85	99.0	0.9426	0.199	S	Laval											
Tube#2 A-4	8.85	99.0	0.974	0.246	S	Laval											
Tube#2 B-1	8.95	100.0	0.9513	0.213	S	Laval											
Tube#2 B-2	8.95	100.0	0.9438	0.202	S	Laval											
Tube#2 B-3	9.01	100.6	0.9017	0.153	S	Laval											
Tube#2 B-4	9.01	100.6	0.891	0.142	S	Laval											
Tube#2 C-1	9.125	101.7	0.8909	0.144	S	Laval											
Tube#2 D-1	9.22	102.6	0.8015	0.079	S	Laval											
Tube#2 D-2	9.22	102.6	0.8162	0.088	S	Laval											

Table 8-4: Summary of undrained monotonic test results for Massey site

Lab.	Test No.	INITIAL STATE (e)c	σvi'	σhi'	p'i	qi	Si	ess	Ψ	Ψ/λ	RSR p'i-p'ss	PEAK or YIELD (q)p Δ	(q)p total	(S)p Δ	(S)p total	(p')p	Mp total q/p'	Peak φ'
UBC	M94 F4 C41 (TC)	0.99	108	54	72.0	54	27	1.000	-0.010	-0.632	0.531	228.3	282.3	114.2	141.2	204.8	1.38	34.1
UBC	M94 F4 C43 (TC)	0.983	112	56	74.7	56	28	1.000	-0.017	-1.020	0.360	262.5	318.5	131.3	159.3	206.1	1.55	37.9
UBC	M94 F6 C42 (TC)	0.942	110	55	73.3	55	27.5	1.166	-0.224	-1.514	0.220	345.0	400.0	172.5	200.0	282.2	1.42	35.0
U of A	FS-UT-TAC	0.963	135.6	76.2	96.0	59.4	29.7	1.126	-0.163	-1.103	0.332	92.6	152.0	46.3	76.0			
UBC	M94 F4 C42 (TE)	0.982	110	55	73.3	55	27.5	1.000	-0.018	-1.099	0.333	69.8	14.8	34.9	7.4	10.1	1.47	75.8
UBC	M94 F6 C7A (TE)	0.914	124	62	82.7	62	31	1.148	-0.234	-1.584	0.205	92.0	30.0	46.0	15.0	30.2	0.99	36.5
UBC	M94 F2 C2B1 (TE)	0.91	98	49	65.3	49	24.5	1.183	-0.273	-1.846	0.158	68.0	19.0	34.0	9.5	28.1	0.68	22.4
U of A	FS-MT-TAC (T1)	1.01	643.7	328.9	433.8	314.8	157.4	0.971	0.039	2.376	10.758	71.4	386.2	35.7	193.1	430.0	0.90	21.0
U of A	FS-MT-TAE (T4)	1.013	638.4	322.8	428.0	315.6	157.8	0.971	0.042	2.544	12.730	449.1	133.5	224.6	66.8	180.0	0.74	25.0
UBC - Thomas	FS-WP-TAC	0.934	791.0	409.0	536.3	382	191	0.872	0.062	0.421	1.524	84.2	466.2	42.1	233.1	465.5	1.00	25.4
UBC - Thomas	FS-WP-TAE	0.934	791.0	409.0	536.3	382	191	0.872	0.062	0.421	1.524	512.0	130.0	256.0	65.0	136.5	0.95	34.5
Laval - VA01	M94F4 C2B	0.909	87.47	43.57	58.2	43.90	21.95	1.200	-0.291	-1.969	0.140	480.1	524.0	240.1	262.0	332.8	1.57	38.6
Laval - VA02	M94F6 C2A	0.853	84.77	43.27	57.1	41.50	20.75	1.203	-0.350	-2.367	0.094	900.2	941.7	450.1	470.9	611.6	1.54	37.8
Laval - VA12	M94F4 C4	0.962	113.20	53.20	73.2	60.00	30.00	1.166	-0.204	-1.380	0.251	353.6	413.6	176.8	206.8	231.8	1.78	43.4
Laval - VA13	M94F4 C4-4	1.043	121.00	56.50	78.0	64.50	32.25	0.999	0.044	2.660	14.293	149.2	213.7	74.6	106.9	145.7	1.47	36.1
Laval - VA14	M94F2 C11B	1.000	131.27	66.67	88.2	64.60	32.30	0.997	0.003	0.177	1.193	316.5	381.1	158.3	190.6	260.1	1.47	36.1
Laval - VA15	M94F2 C7B-1	0.810	115.13	57.03	76.4	58.10	29.05	1.160	-0.350	-2.367	0.094	1027.4	1085.5	513.7	542.8	714.7	1.52	37.3
Laval - VA16	M94F2 C7B-2	0.983	114.57	57.77	76.7	56.80	28.40	0.999	-0.016	-0.993	0.370	419.5	476.3	209.8	238.2	316.4	1.51	37.0
Laval - VA17	M94F6 C4-1	0.968	112.53	55.93	74.8	56.60	28.30	1.163	-0.195	-1.318	0.268	414.1	470.7	207.1	235.4	309.1	1.52	37.4

Lab.	Test No.	MINIMUM (q)qss Δ	(q)qss total	(S)min Δ	(S)min total	Smin/p'o total	p'min	% axial strain at Smin	IB Δ	ULTIMATE (End of test) (q)uss Δ	(q)uss total	Sf Δ	Sf total	Sf/p'i total	p'f	Mf total q/p'	USS φ'
UBC	M94 F4 C41 (TC)	228.3	282.3	114.2	141.2	1.96	204.8	0	0.00	228.3	282.3	114.2	141.2	1.96	204.8	1.38	34.1
UBC	M94 F4 C43 (TC)	262.5	318.5	131.3	159.3	2.13	206.1	0	0.00	262.5	318.5	131.3	159.3	2.13	206.1	1.55	37.9
UBC	M94 F6 C42 (TC)	345.0	400.0	172.5	200.0	2.73	282.2	0	0.00	345.0	400.0	172.5	200.0	2.73	282.2	1.42	35.0
U of A	FS-UT-TAC	80.1	139.5	40.1	69.8	0.73		4	0.14								
UBC	M94 F4 C42 (TE)	62.4	7.4	31.2	3.7	0.05	10.1	8	0.11	95.0	40.0	47.5	20.0	0.27	43.4	0.92	33.0
UBC	M94 F6 C7A (TE)	92.0	30.0	46.0	15.0	0.18	30.2	3.3	0.00	172.0	110.0	86.0	55.0	0.67	117.5	0.94	33.7
UBC	M94 F2 C2B1 (TE)	66.6	17.6	33.3	8.8	0.13	16.1	2.3	0.02	138.2	89.2	69.1	44.6	0.68	88.1	1.01	37.5
U of A	FS-MT-TAC (T1)	-222.5	92.3	-111.3	46.2	0.11	60.0	23	4.12	-222.5	92.3	-111.3	46.2	0.11	60	1.54	37.7
U of A	FS-MT-TAE (T4)	422.9	107.3	211.4	53.6	0.13	80.0	11	0.06	430.6	115.0	215.3	57.5	0.13	90	1.28	54.3
UBC - Thomas	FS-WP-TAC	55.6	437.6	27.8	218.8	0.41	327.1	1.2	0.34	95.6	477.6	47.8	238.8	0.45	343.1	1.39	34.4
UBC - Thomas	FS-WP-TAE	469.6	87.6	234.8	43.8	0.08	82.1	5.5	0.08	515.3	133.3	257.7	66.7	0.12	136.5	0.98	35.7
Laval - VA01	M94F4 C2B	480.1	524.0	240.1	262.0	4.50	332.8	0	0.00	480.1	524.0	240.1	262.0	4.50	332.8	[illegible]	38.6
Laval - VA02	M94F6 C2A	900.2	941.7	450.1	470.9	8.25	611.6	0	0.00	900.2	941.7	450.1	470.9	8.25	611.6	[illegible]	37.8
Laval - VA12	M94F4 C4	353.6	413.6	[illegible]	206.8	2.83	231.8	0	0.00	353.6	413.6	176.8	206.8	2.83	231.8	[illegible]	43.4
Laval - VA13	M94F4 C4-4	149.2	[illegible]	[illegible]	106.9	1.37	145.7	0	0.00	149.2	213.7	74.6	106.9	1.37	145.7	1.47	36.1
Laval - VA14	M94F2 C11B	316.5	[illegible]	158.3	190.6	2.16	260.1	0	0.00	316.5	381.1	158.3	190.6	2.16	260.1	1.47	[illegible]
Laval - VA15	M94F2 C7B-1	1027.4	1085.5	[illegible]	542.8	[illegible]	714.7	0	0.00	1027.4	1085.5	513.7	542.8	7.10	714.7	[illegible]	[illegible]
Laval - VA16	M94F2 C7B-2	419.5	476.3	[illegible]	238.2	3.10	316.4	0	0.00	419.5	476.3	209.8	238.2	3.10	316.4	[illegible]	[illegible]
Laval - VA17	M94F6 C4-1	414.1	470.7	207.1	235.4	3.15	309.1	0	0.00	414.1	470.7	[illegible]	235.4	3.15	309.1	[illegible]	37.4

Notes: Tests are anisotropically consolidated triaxial compression and extension tests on Massey undisturbed and reconstituted sand; tests by Thomas are on reconstituted Fraser River sand

Table 8-5: Summary of undrained cyclic simple shear test results for Massey site

Depth (m)	Sample No.	e_c	τ_{cy}/σ'_{vc}	N	M	Correction $\frac{CRR_M}{CRR_{M=7.5}}$	CRR (M=7.5)
9.55	M94 F2 C2B2	0.809	0.123	30	8.61	0.854	0.144
10.02	M94 F2 C2B3	0.862	0.123	7	6.23	1.244	0.099
10.46	M94 F5 C3C1	1.005	0.09	20	8.07	0.920	0.098
10.49	M94 F5 C3C2	0.968	0.1	7	6.23	1.244	0.080
12.74	M94 F2 C11B1	0.995	0.095	31	8.62	0.853	0.111
12.77	M94 F2 C11B2	0.997	0.107	8	6.41	1.201	0.089
10.52	M94 F6 C4B1	0.998	0.109	9	6.59	1.162	0.094
10.54	M94 F6 C4B2	0.986	0.108	9	6.59	1.162	0.093
11.18	M94 F6 C61	0.958	0.098	25	8.43	0.874	0.112
11.21	M94 F6 C62	0.953	0.108	6	6.03	1.292	0.084
11.24	M94 F6 C63	0.957	0.105	18	7.87	0.946	0.111

Table 8-6: Summarized results of data review: average values of soil parameters in the target zone at CANLEX sites

Parameter	Phase I	Phase II		Phase III
	Syncrude	Massey	Kidd	J-pit
Target Zone Depth (m)	27 to 37 (Elev. 325-315)	8 to 13	12 to 17	3 to 7
In-situ testing results:				
$(N_1)_{60}$	18.2 (SD=3.0)	10.3 (SD=3.8)	17.2 (SD=4.8)	3.4 (SD=2.0)
q_{c1} (MPa)	7.46 (SD=1.69)	5.34 (SD=1.00)	6.53 (SD=1.82)	2.35 (SD=1.53)
V_{s1} (m/s)	156.4 (SD=20.1)	168.2 (SD=6.4)	177.4 (SD=5.4)	127.1 (SD=3.0)
Y	95.5 (SD=12.1)	110.2 (SD=4.6)	110.8 (SD=5.0)	101.1 (SD=5.9)
X	75.0 (SD=8.6)	94.7 (SD=7.7)	88.4 (SD=6.1)	88.0 (SD=5.6)
$q_{c1}/(N_1)_{60}$	0.42 (SD=0.15)	0.58 (SD=0.17)	0.45 (SD=0.07)	0.51 (SD=0.25)
e predicted by geophysical	0.787 (SD=0.052)	0.991 (SD=0.071)	0.776 (SD=0.064)	0.736 (SD=0.091)
FC (%) predicted by CPT	12.4	6.8	6.7	14.9
Frozen samples tested to date:				
FC (%)	5.1 (range: 1.8 to 11.1)	≈ 2 to 8	≈ 3 to 8	≈ 10 to 15
e	0.769 (SD=0.036)	0.976 (SD=0.046)	0.908 (SD=0.040)	0.761 (SD=0.059)
D_r (%) *	65	31	48	43
Ψ**	- 0.063	- 0.024	- 0.086	- 0.104
RSR***	0.59	0.29	0.24	0.06

Notes:
Values for parameters are shown as the average in the target zone (SD= standard deviation)
* calculated using e_{max} and e_{min} in Table I-3 (FC=10-40% used for Phase III)
** relative to the flat portion of the appropriate reference USL; see Table I-4
*** relative to the appropriate reference USL (see Table I-4); calculated from average e of frozen samples and average estimated p' in target zone

Table 8-7: Predicted average response at the Massey site based on average values of soil parameters in the target zone

Parameter	Average value at Massey Site	
Flow liquefaction		
Depth (m)	10.5	
GWT(m)	1.5	
Unit weight of soil (kN/m^3)	18.5 (above GWT) 19.5 (below GWT)	
in-situ σ'_{vi} (kPa)	115	
in-situ K_o	0.5	
in-situ σ'_{hi} (kPa)	57.5	
in-situ p'_i (kPa)	76.7	
in-situ q_i (kPa)	57.5	
in-situ e	0.976	
in-situ p'_{us}	264.8	
in-situ RSR	0.29	
Average Response	**Compression**	**Extension**
I_B	0.03	0.05
S_{min}/p'_i	2.6	0.02
ε_a (%) at S_{min}	N/A	4.8
S_f/p'_i	2.6	1.7
M_p	1.5	0.75
M_f	1.5	1.0
S_{min} (kPa)	199.4	1.5
p'_{min} (kPa)	265.9	3.0
S_p (kPa)	199.4	3.09
p'_p (kPa)	265.9	8.2
S_f (kPa)	199.4	130.4
p'_f (kPa)	265.9	260.8
In-situ Testing		
$(N_1)_{60}$	10.3 (SD=3.8)	
q_{c1} (MPa)	5.34 (SD=1.00)	
V_{s1} (m/s)	168.2 (SD=6.4)	
Y	110.2 (SD=4.6)	
X	94.7 (SD=7.7)	
$q_{c1}/(N_1)_{60}$	0.58 (SD=0.17)	
Cyclic liquefaction		
Q	49.4 (SD=9.9)	
F	0.398 (SD=0.089)	
I_c	1.962 (SD=0.085)	
Soil behaviour type	clean to silty sand	
FC (%)	6.8	
Δq_{c1} (MPa)	0.30	
CRR (M=7.5; N=15 cycles)	0.10	

Note:
Values for parameters are shown as the average in the target zone (SD=standard deviation)

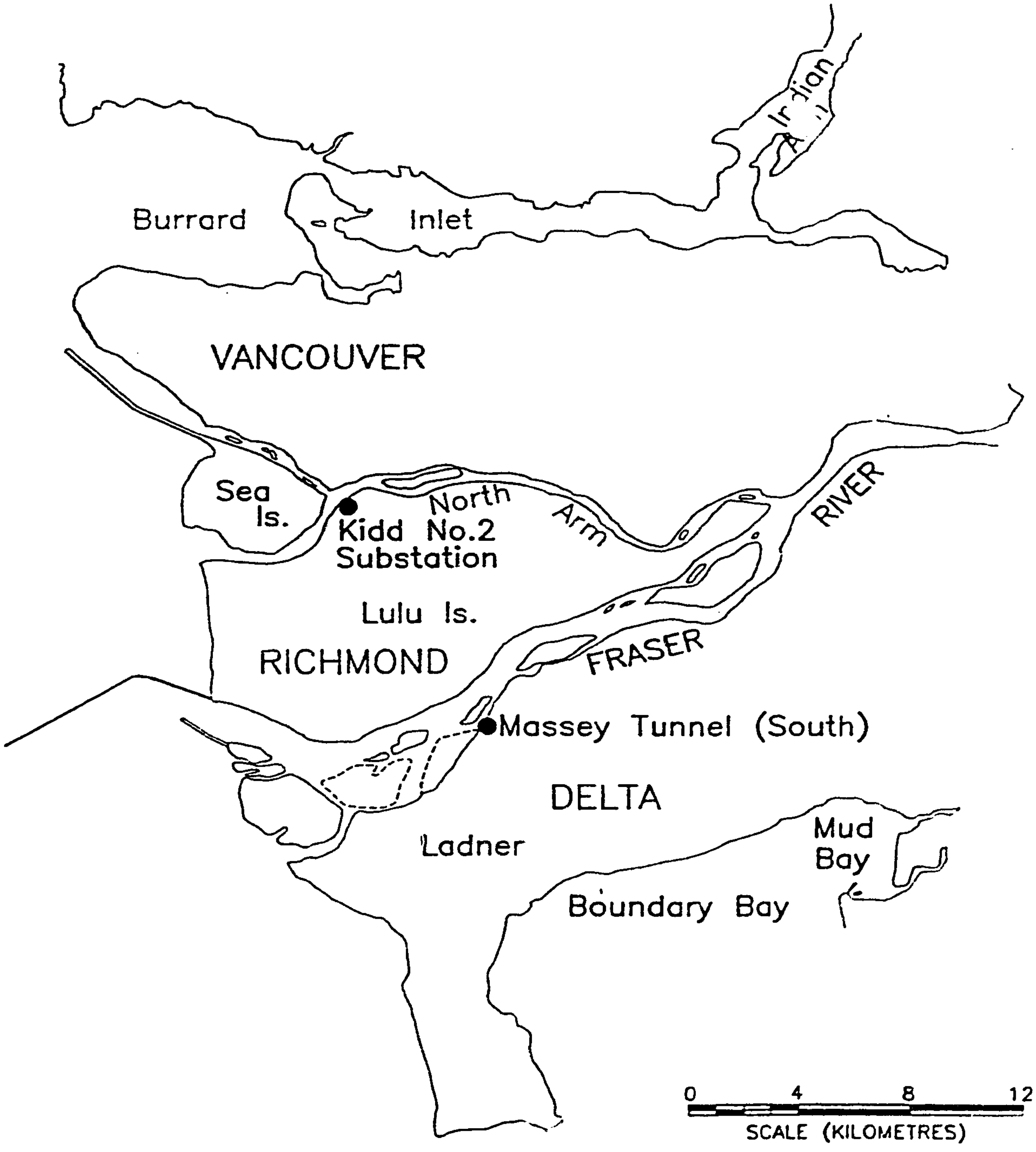

Figure 8-1 Location of CANLEX Phase II Massey and Kidd sites in the Fraser River Delta, B.C. (modified from Lawrence et al., 1995).

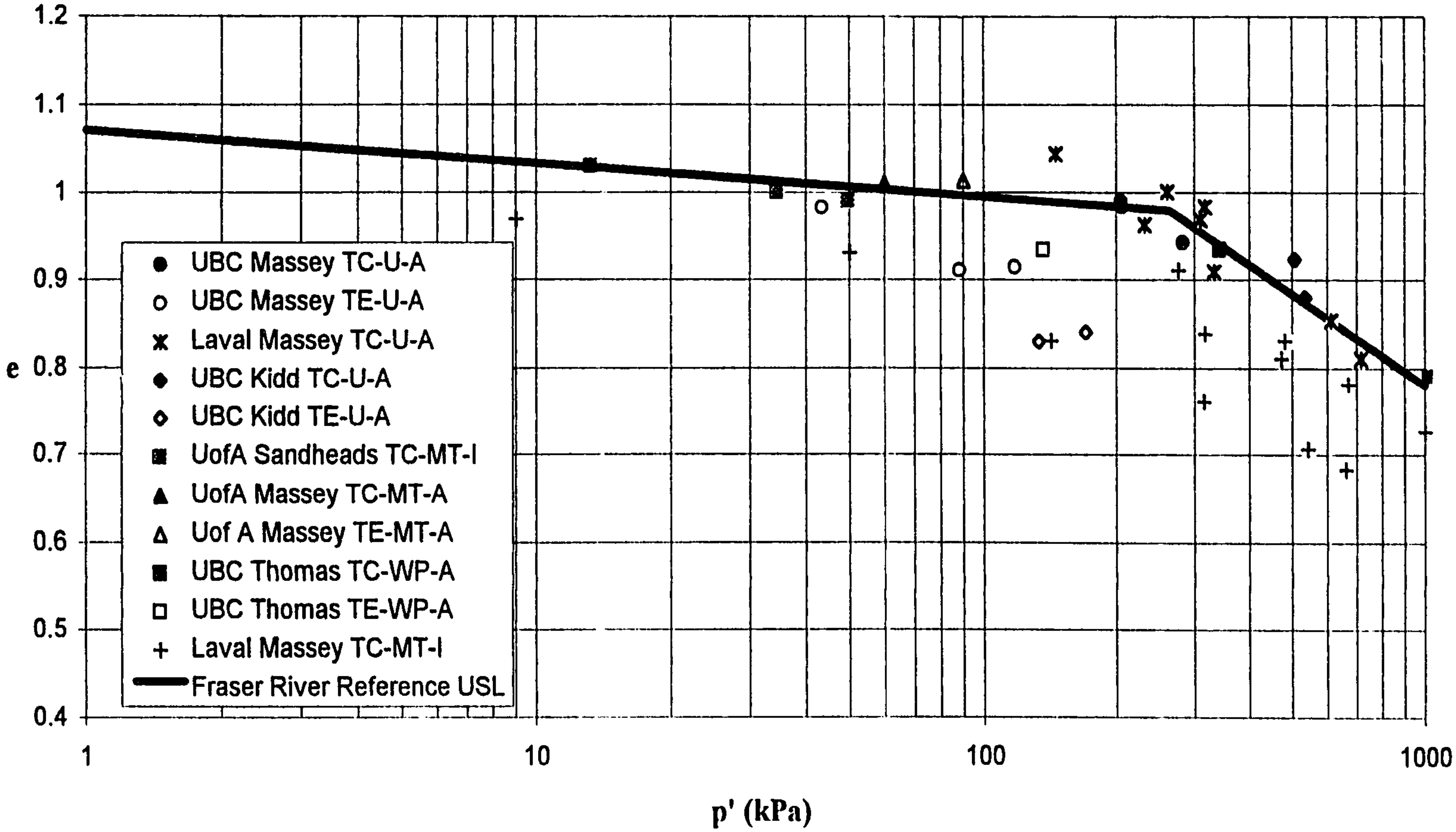

Figure 8-2 End of test conditions for all Fraser River reconstituted and undisturbed triaxial samples; selected reference ultimate state line (USL) for Fraser River sand is indicated.

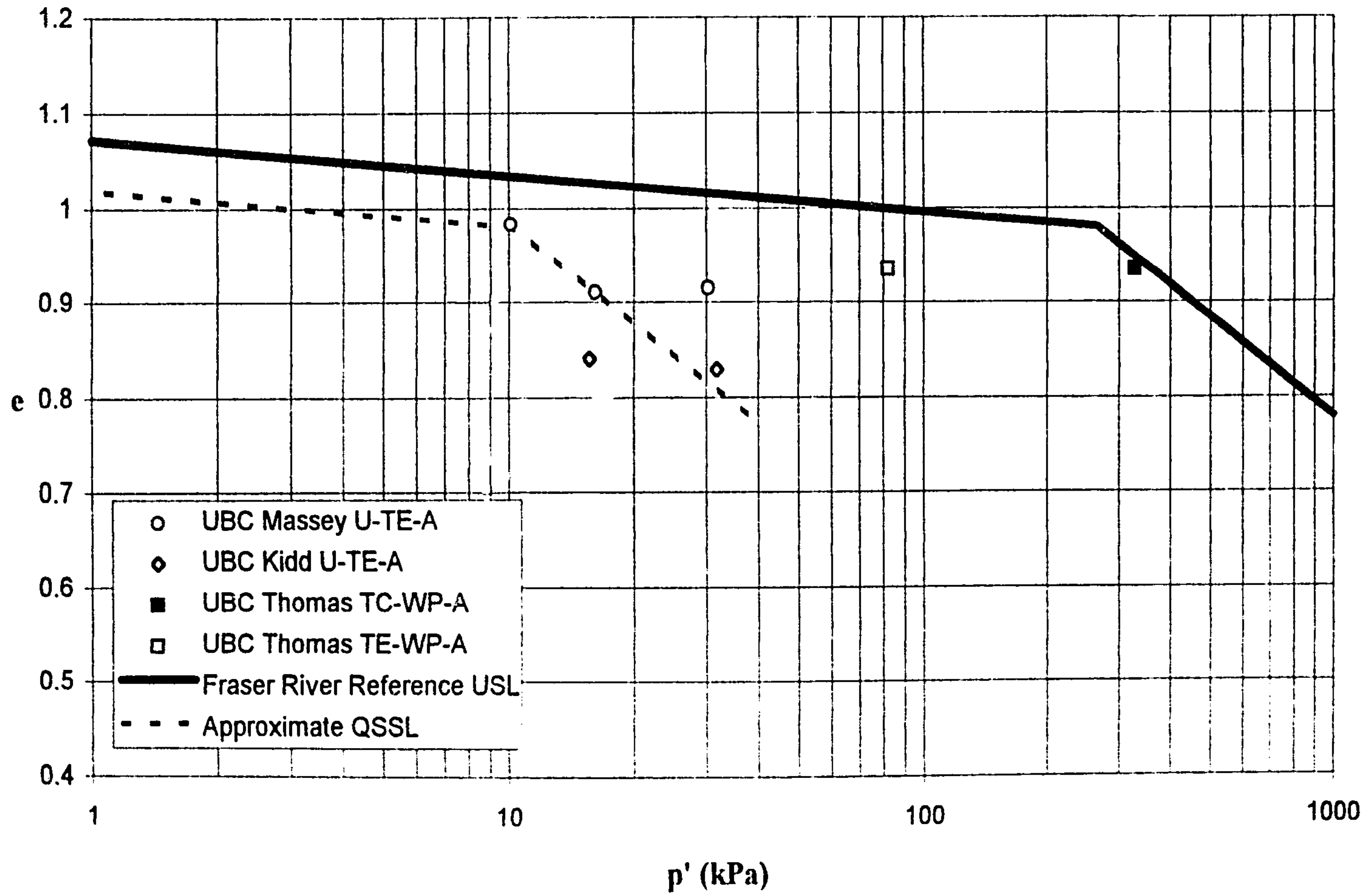

Figure 8-3 Quasi-steady state (QSS) conditions for any of the Fraser River samples in Figure 8-2 that had a QSS; selected approximate QSS line (QSSL) is indicated; selected reference USL is shown for comparison.

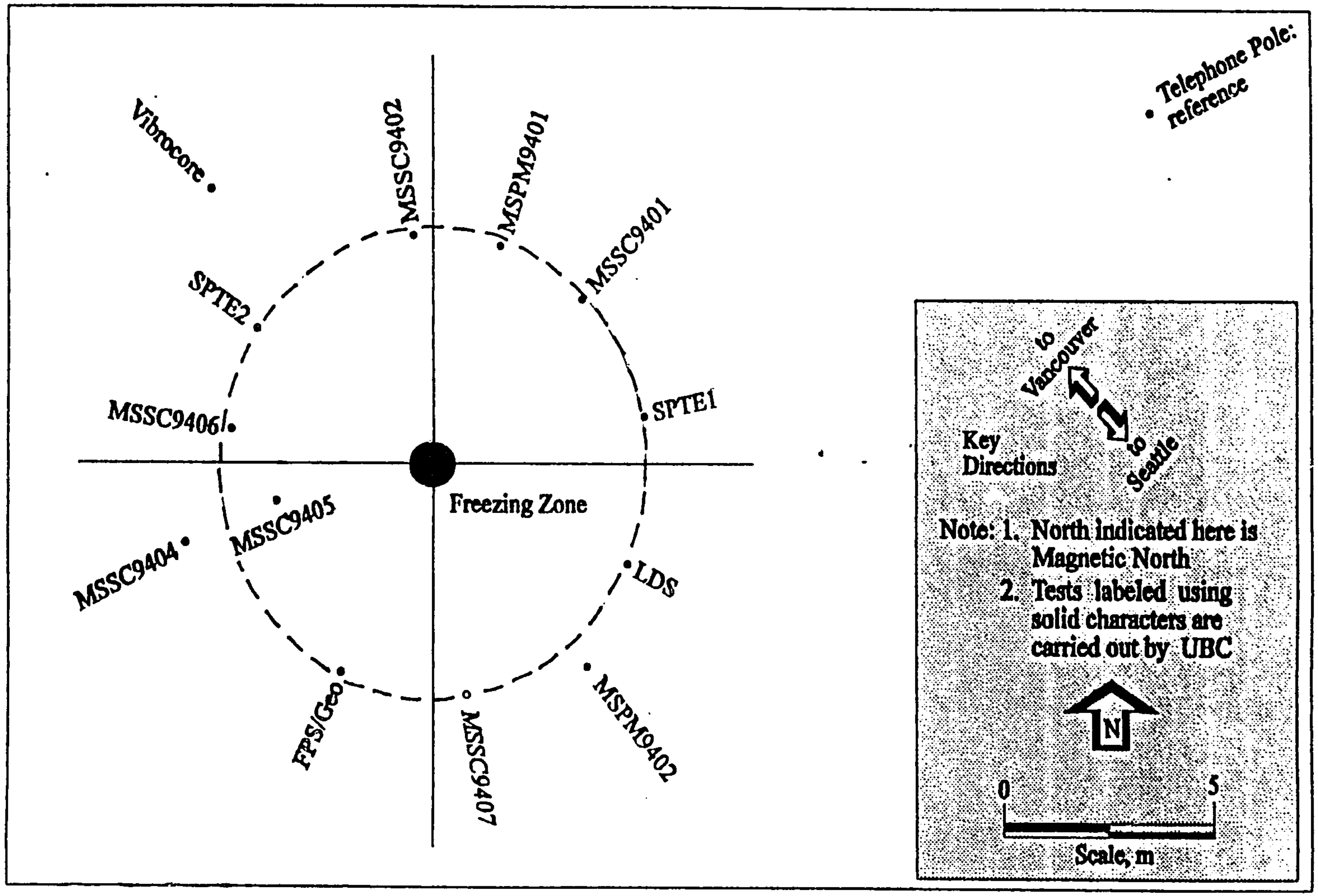

Figure 8-4 Plan of the detailed test site at the CANLEX Phase II Massey site (modified from Campanella, 1995).

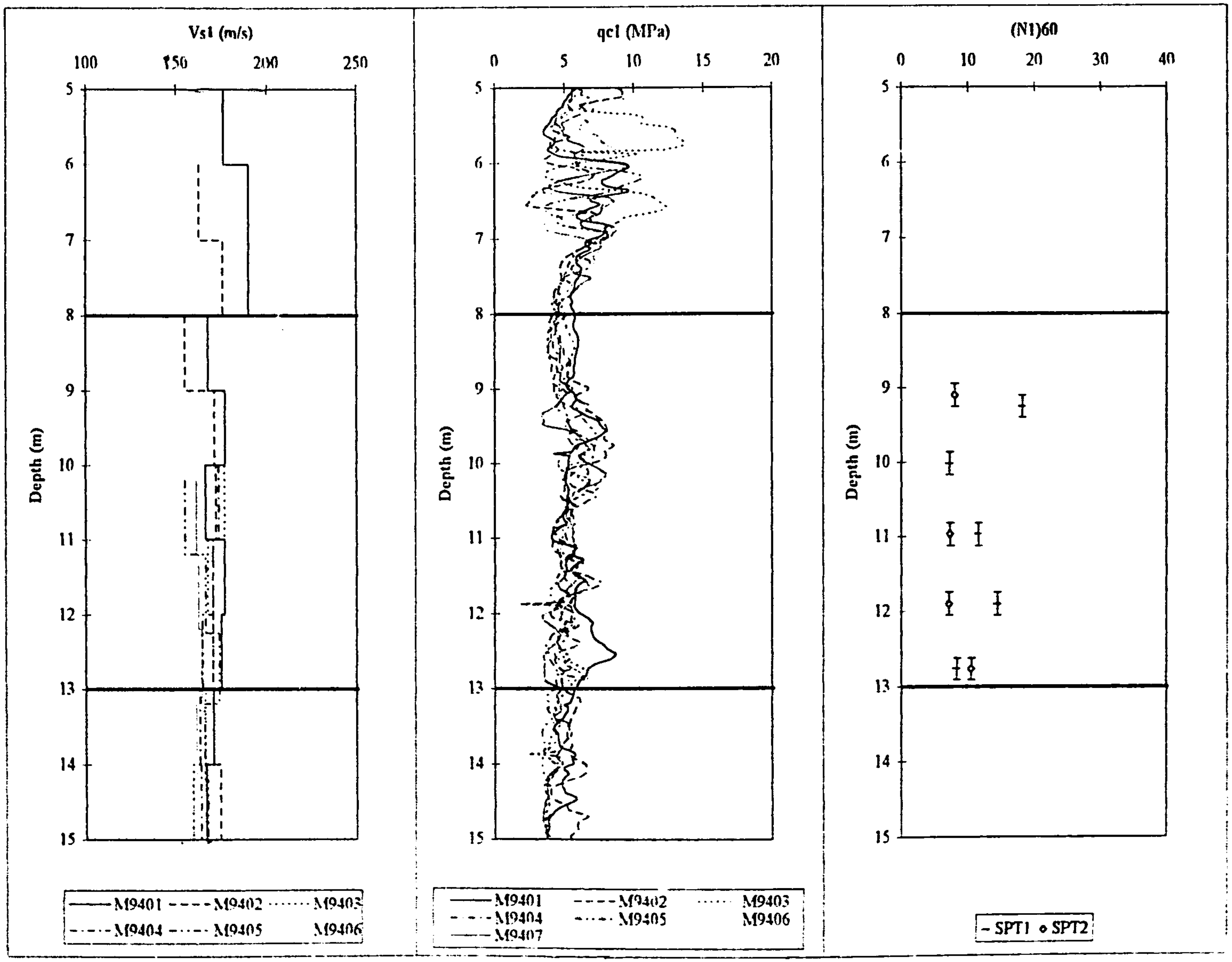

Figure 8-5 Corrected profiles of (a) shear wave velocity, V_{s1}, (b) CPT cone tip resistance, q_{c1}, and (c) SPT blowcount, $(N_1)_{60}$, at the Massey site; test site target zone for testing and sampling located from 8 m to 13 m, as indicated.

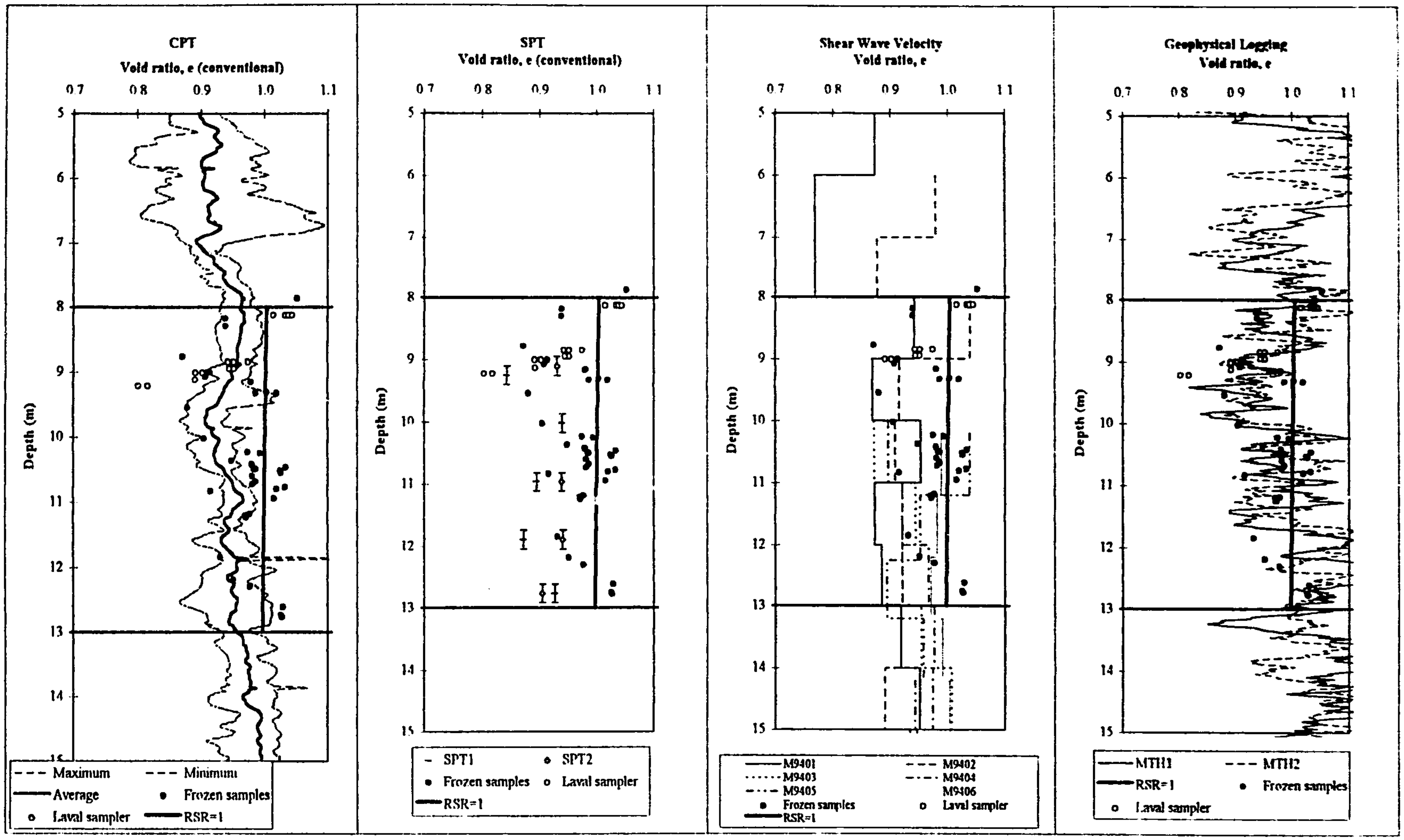

Figure 8-6 Conventional void ratio interpretations for (a) CPT, (b) SPT, (c) V_S measurements, and (d) geophysical logging; void ratios of frozen samples and Laval sampler samples are shown for comparison; RSR=1 line based on selected reference Fraser River USL is also shown.

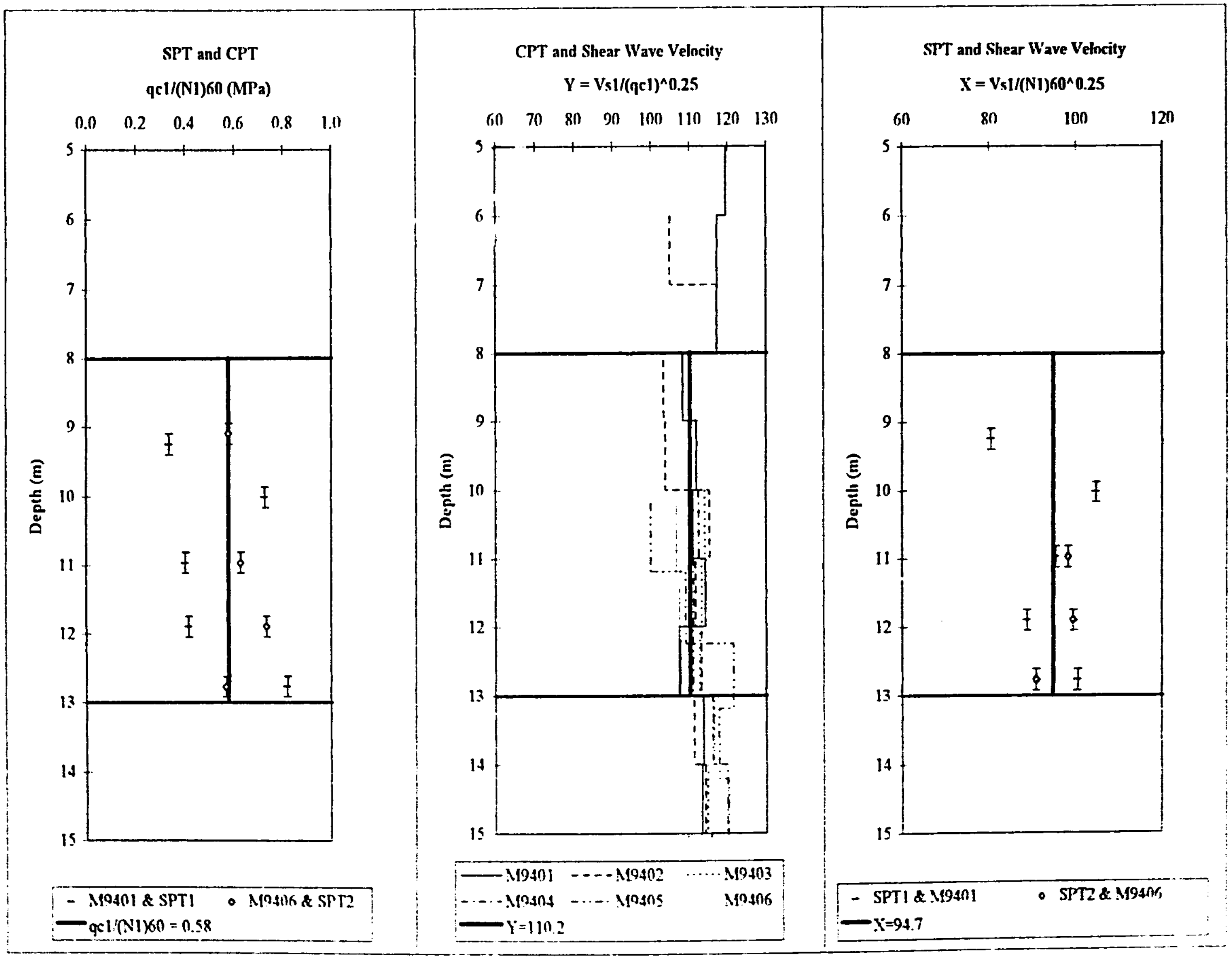

Figure 8-7 Correlations between in-situ tests: (a) comparison of CPT and SPT in terms of $q_{c1}/(N_1)_{60}$, (b) comparison of CPT and V_s in terms of Y, (c) comparison of SPT and shear wave velocity in terms of X.

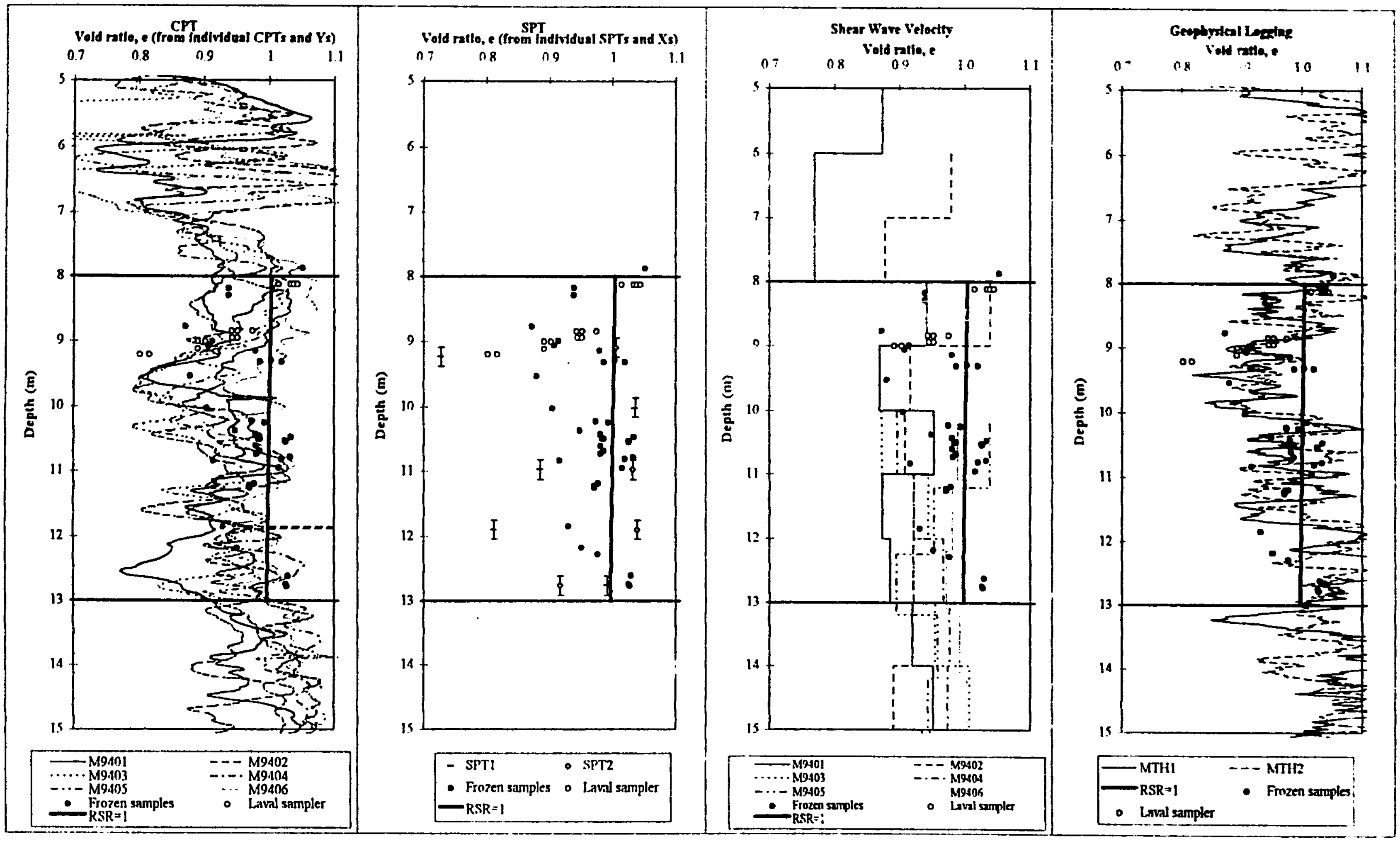

Figure 8-8 Direct void ratio interpretations for (a) CPT, (b) SPT, (c) V_S measurements, and (d) geophysical logging; void ratios of frozen samples and Laval sampler samples are shown for comparison; RSR=1 line based on selected reference Fraser River USL is also shown.

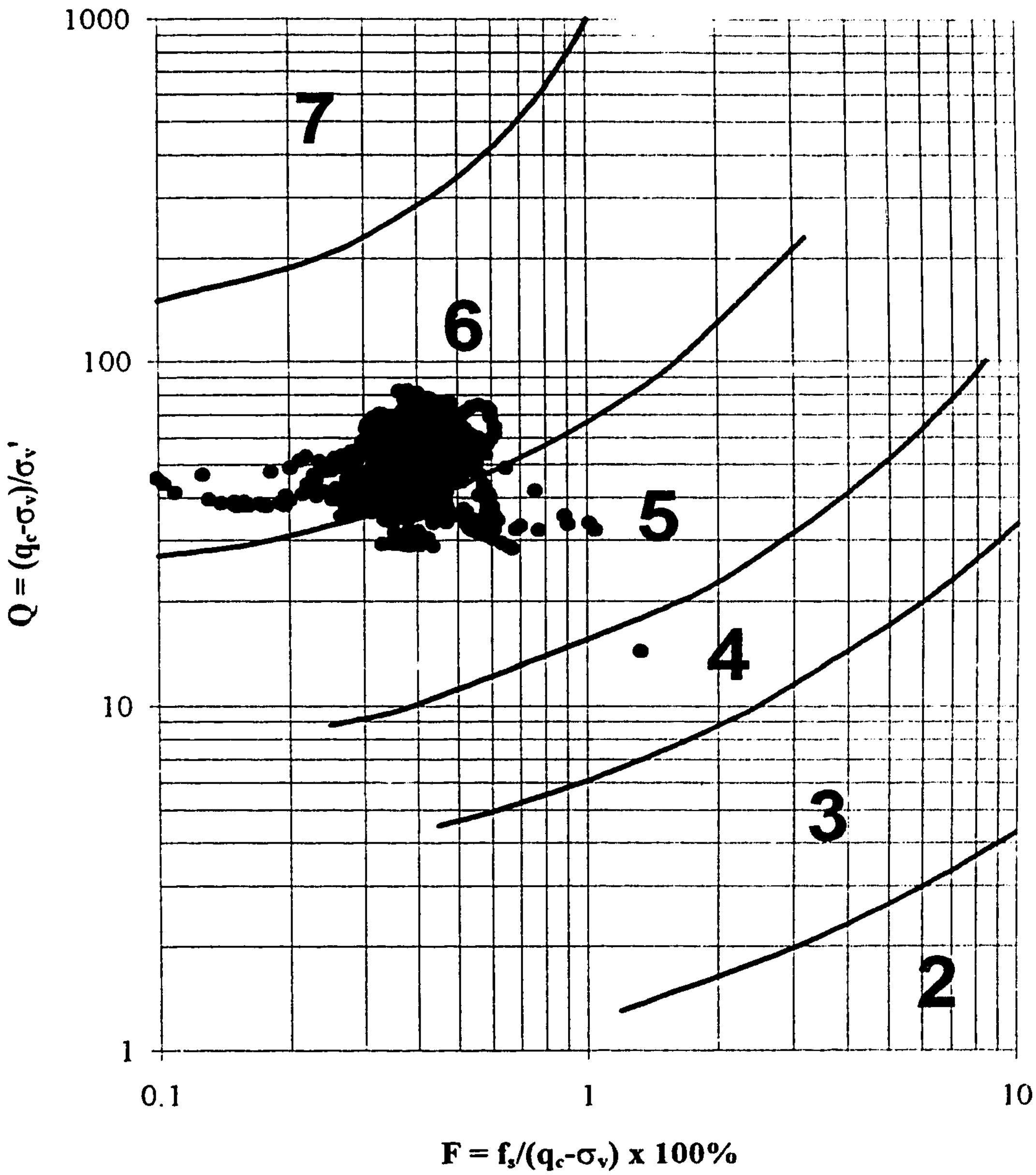

Figure 8-9 Plot of the CPT data in the target zone at the Massey site (8 m to 13 m) on the soil behaviour type classification chart by Robertson (1990).

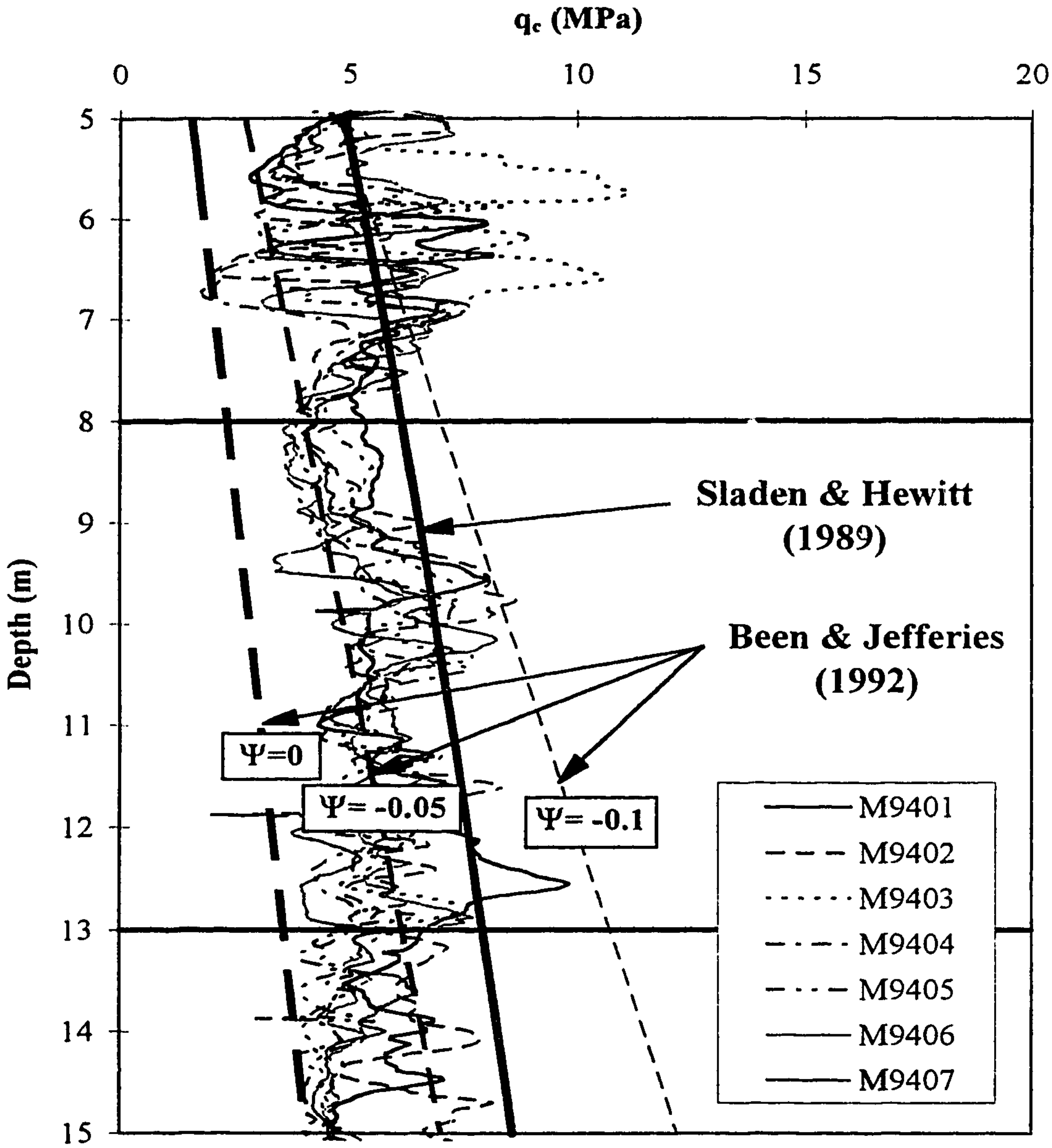

Figure 8-10 Comparison at the Massey site of the state parameter method by Been and Jefferies (1992) and the field observation method by Sladen and Hewitt (1989) for estimating flow liquefaction potential based on CPT results.

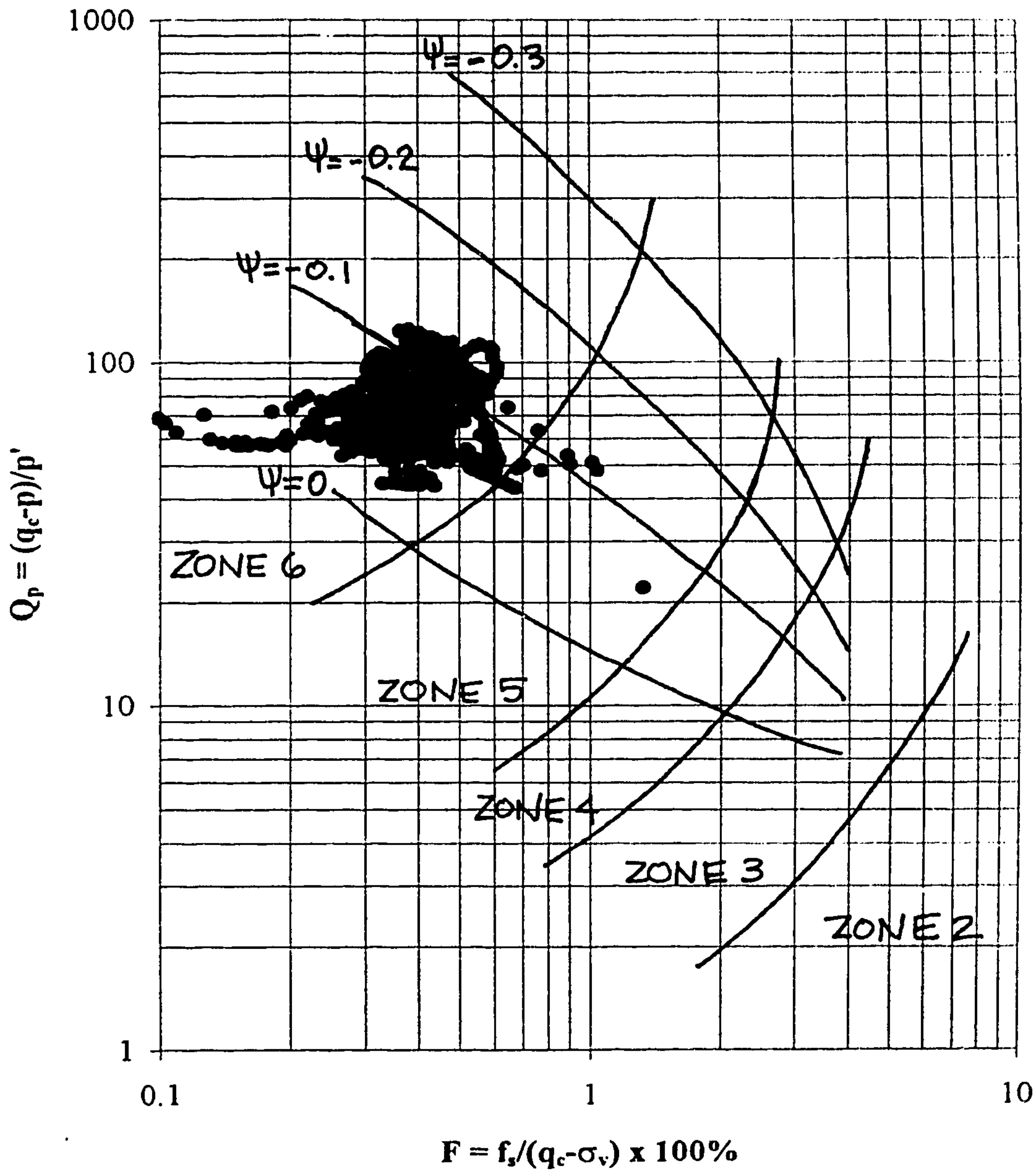

Figure 8-11 Estimation of state parameter in the target zone at the Massey site using the method by Plewes et al. (1992) based on estimated contours of state parameter on a soil behaviour type classification chart.

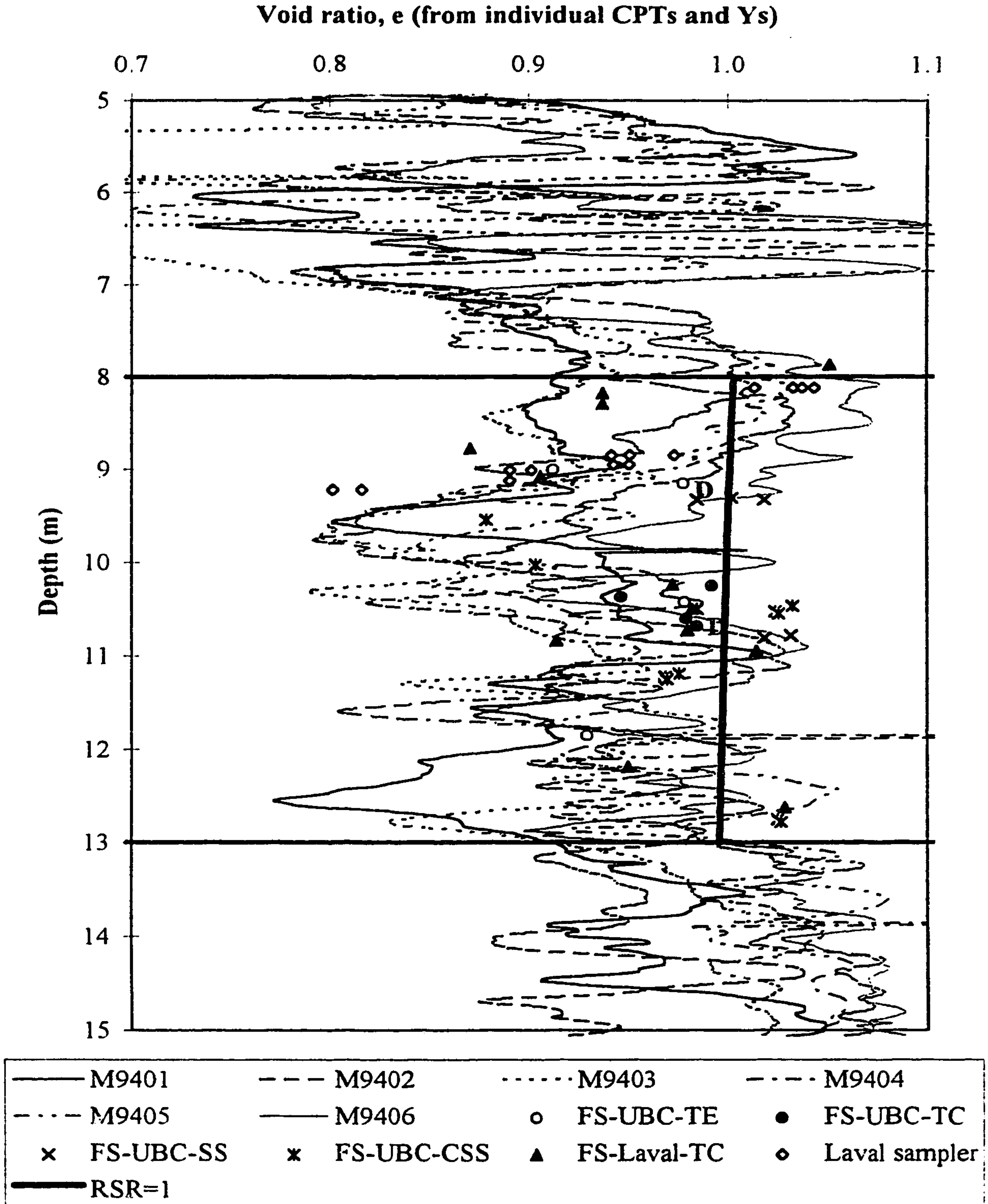

Figure 8-12 Enlarged plot of shear wave velocity based interpretation of void ratio from the CPT from Figure 8-8(a) illustrating the types of laboratory tests that were conducted on frozen samples from the Massey site (D=drained test).

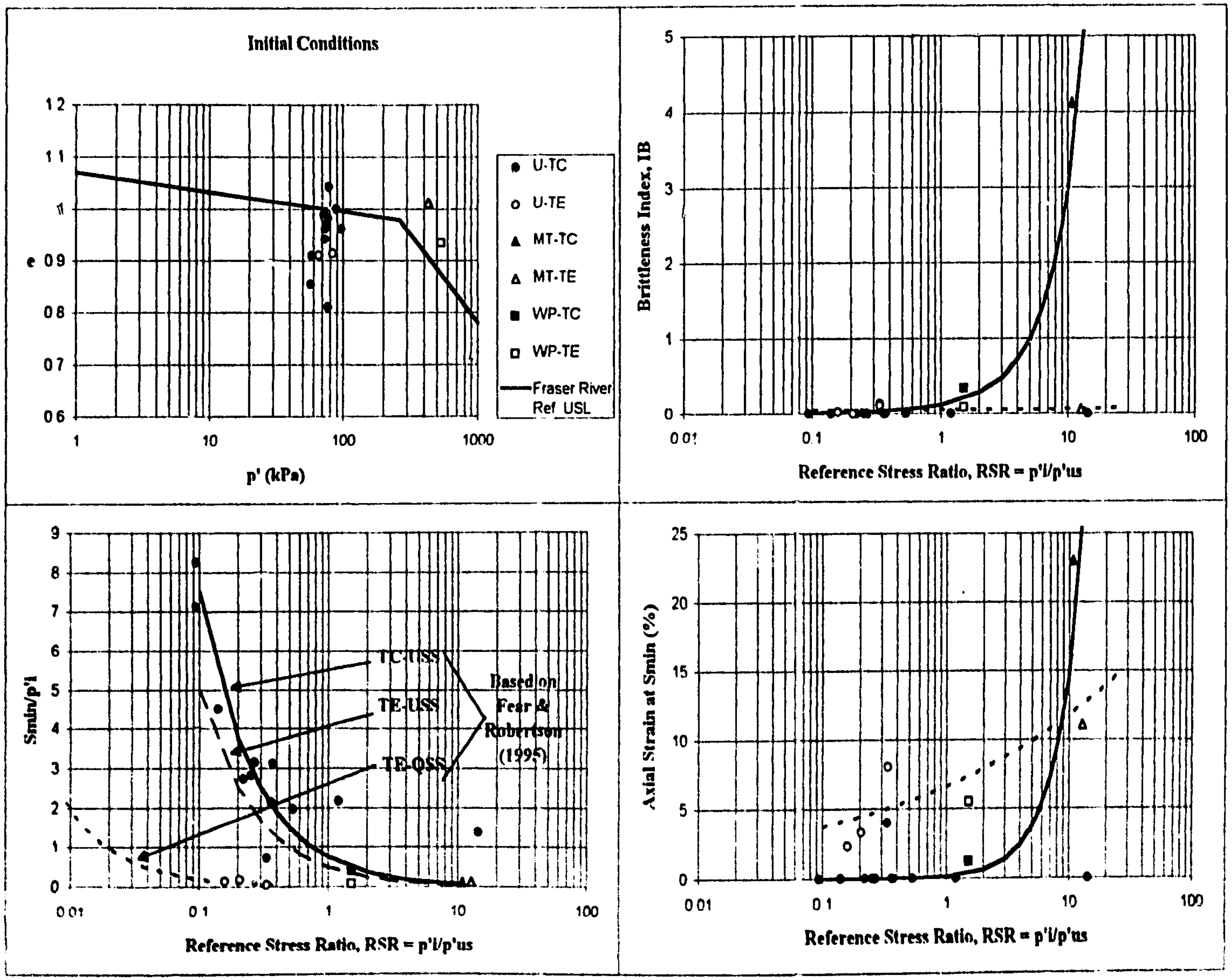

Figure 8-13 Undrained monotonic laboratory response of anisotropically consolidated Massey triaxial samples: (a) initial conditions, (b) brittleness index, I_B, (c) minimum strength ratio, S_{min}/p'_i, and (d) axial strain (ε_a) at S_{min}.

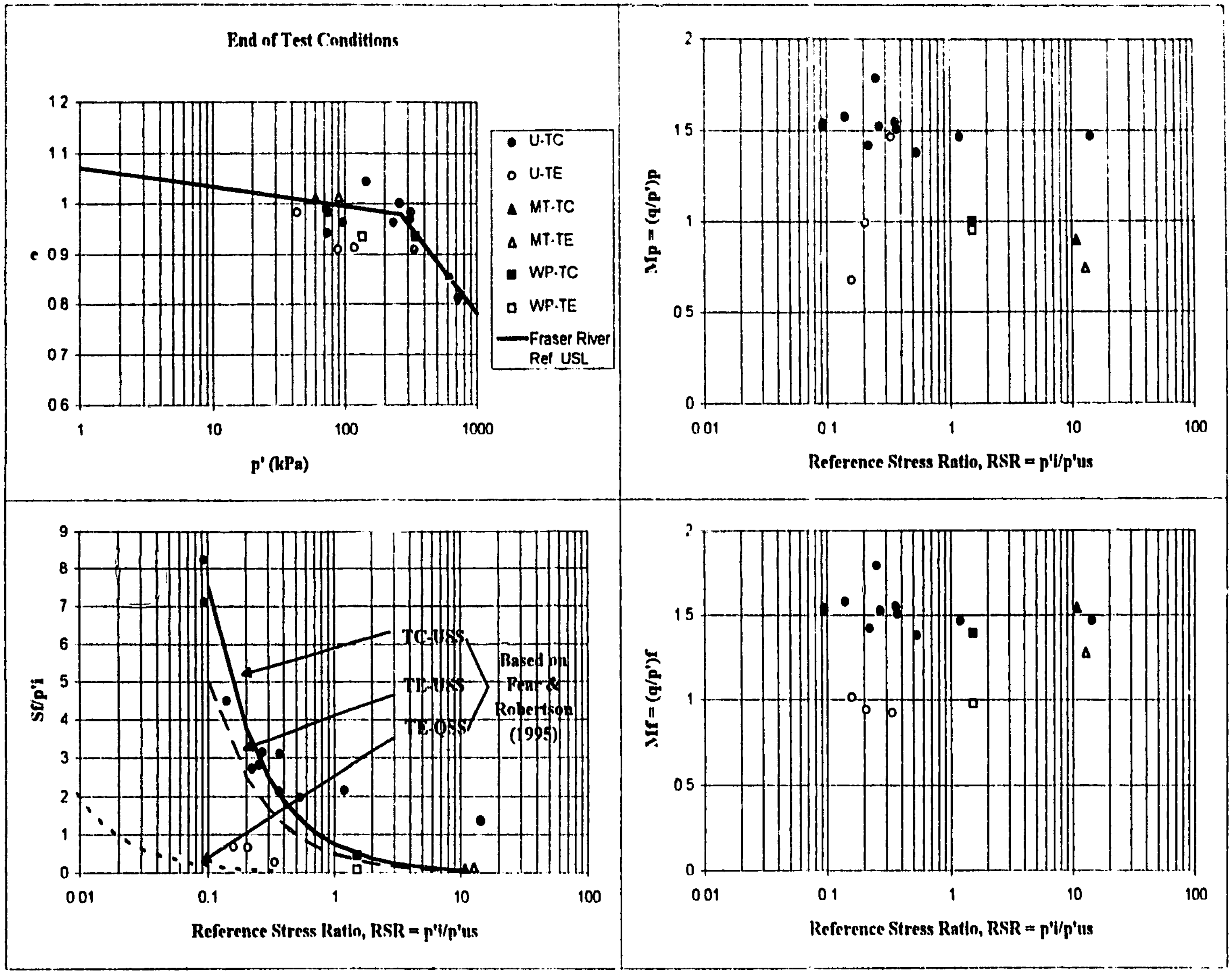

Figure 8-14 Undrained monotonic laboratory response of anisotropically consolidated Massey triaxial samples: (a) end-of-test conditions, (b) end-of-test strength ratio, S_f/p'_i, (c) peak stress ratio, M_p, and (d) end-of test stress ratio, M_f.

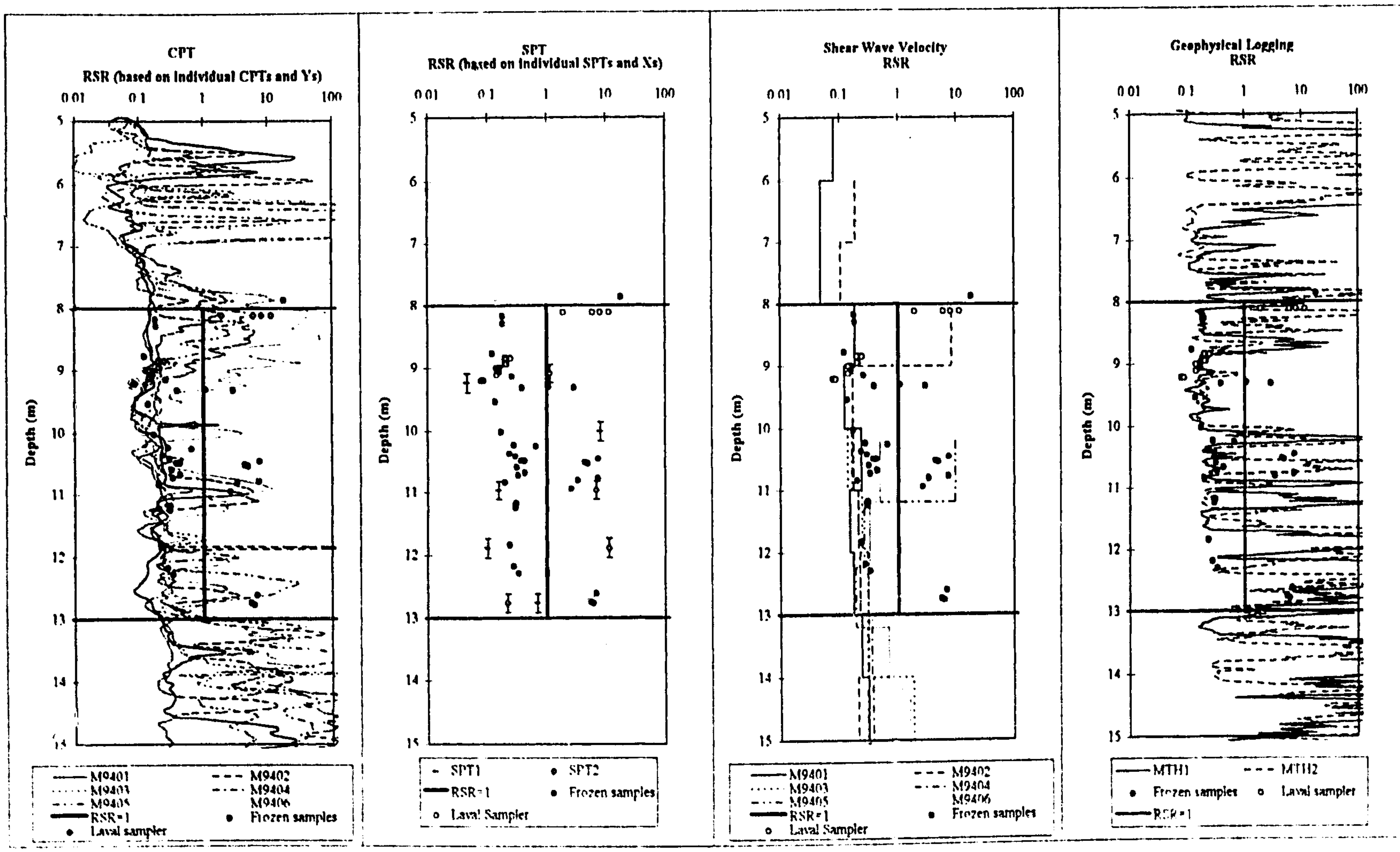

Figure 8-15 Profiles of estimated RSR in-situ at the Massey site relative to the reference Fraser River USL for (a) CPT, (b) SPT, (c) Vs, and (d) geophysical logging.

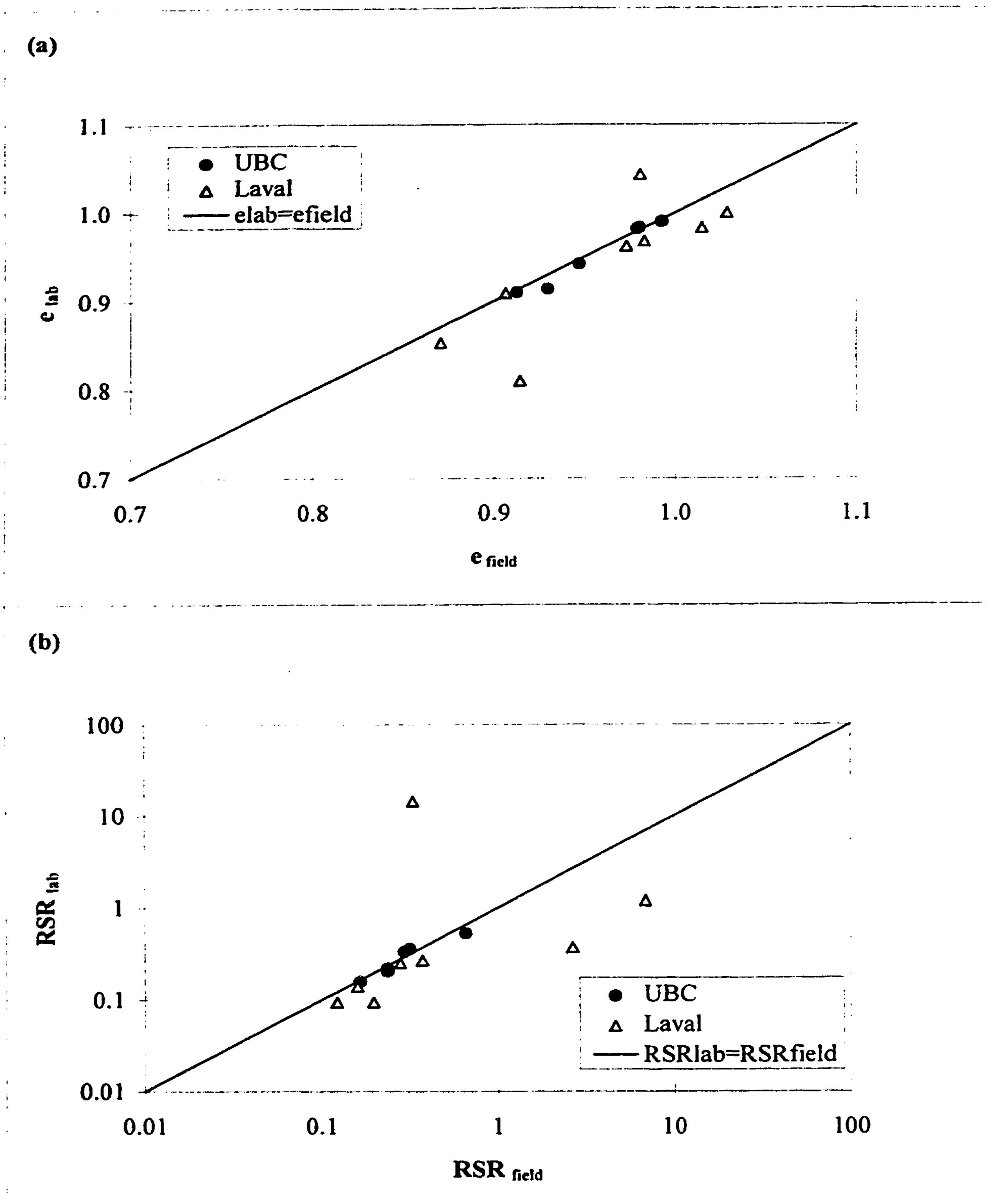

Figure 8-16 Comparison between laboratory conditions (termed lab) and estimated in-situ conditions (termed field) for frozen samples from the Massey site: (a) comparison of e_{lab} and e_{field}, (b) comparison of RSR_{lab} and RSR_{field}.

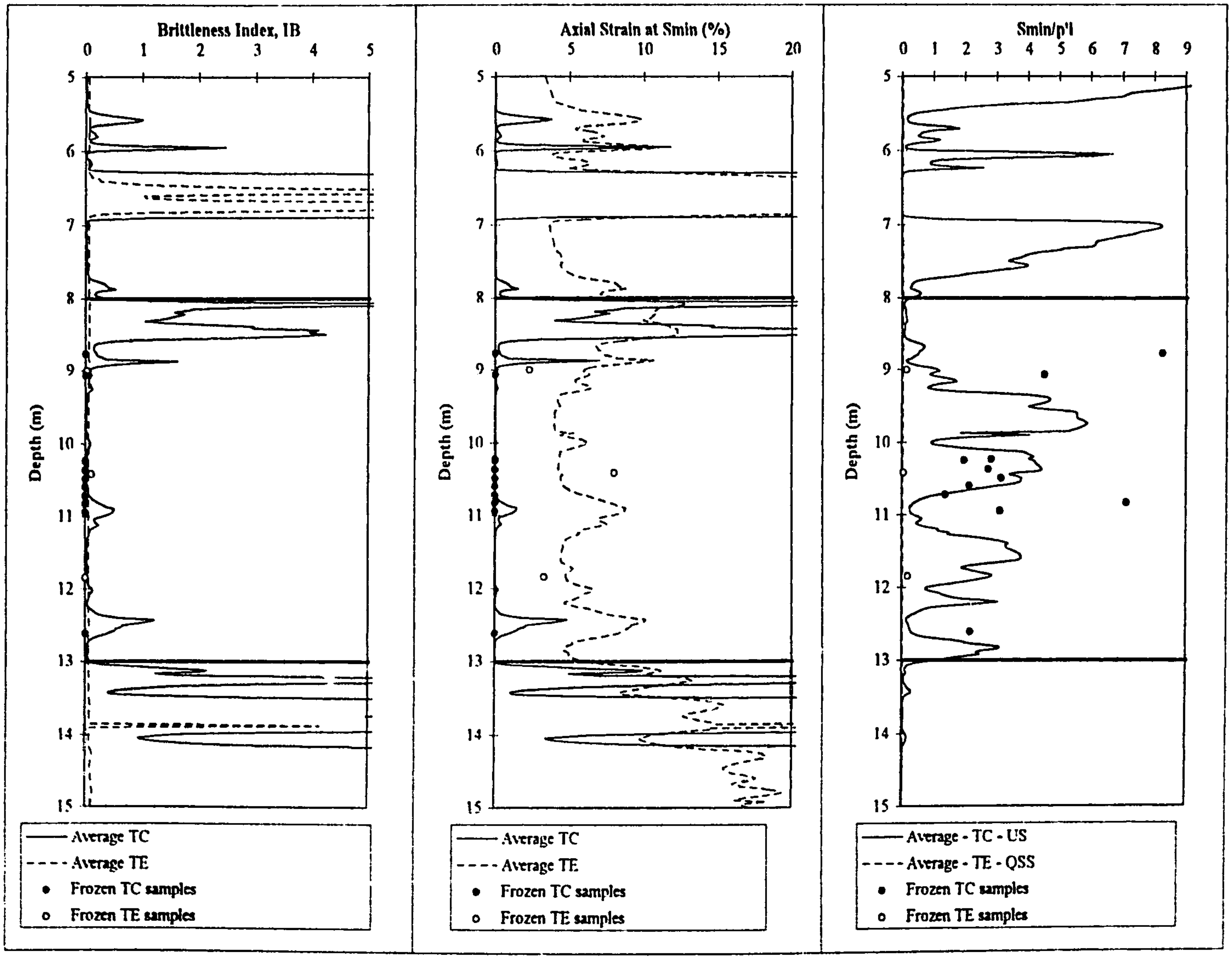

Figure 8-17 Estimated average profiles of undrained triaxial compression and extension response in-situ at the Massey site based on interpretation of the CPT compared with results of testing frozen samples: (a) brittleness index, I_B, (b) axial strain (ε_a) at minimum strength, and (c) minimum strength ratio, S_{min}/p'_i.

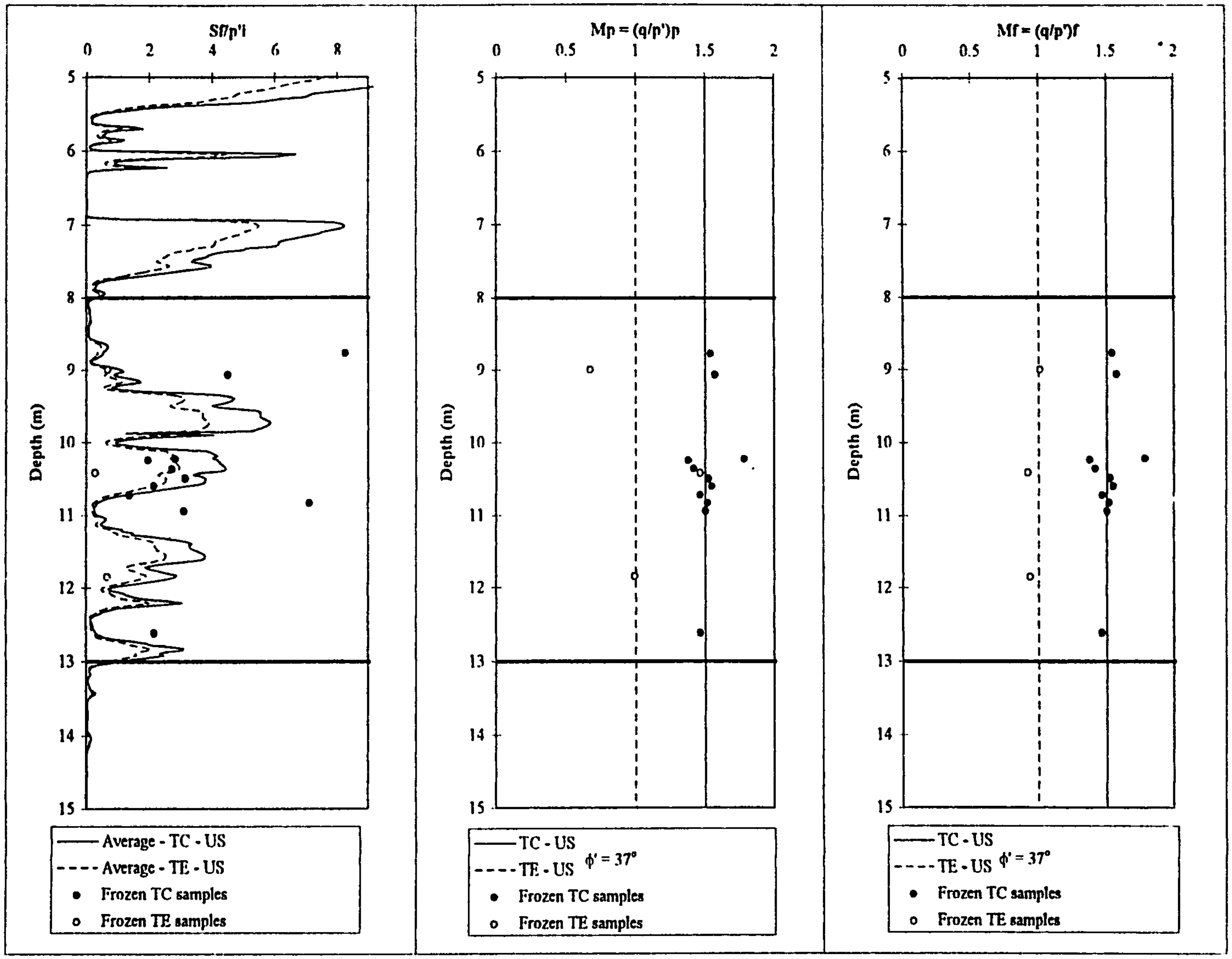

Figure 8-18 Estimated average profiles of undrained triaxial compression and extension response in-situ at the Massey site based on interpretation of the CPT compared with results of testing frozen samples: (a) end-of-test strength ratio, S_f/p'_i, (b) peak stress ratio, M_p, and (c) end-of-test stress ratio, M_f.

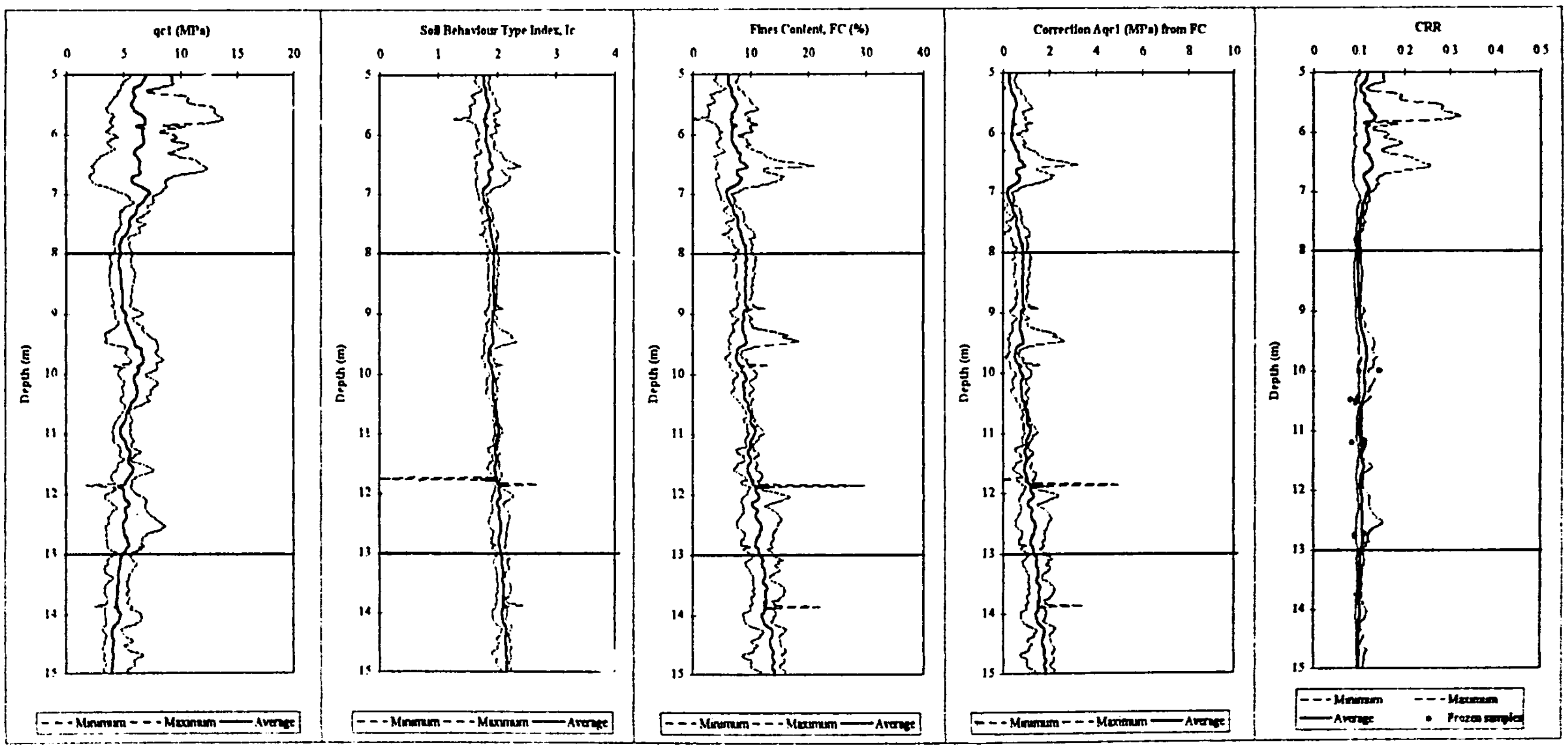

Figure 8-19 Application of the integrated CPT method to the Massey site: (a) CPT q_{c1} results, (b) interpreted soil behaviour type index, I_c, (c) estimated fines contents (FC), (d) recommended fines content based correction to q_{c1} to obtain clean sand equivalent value, and (e) estimated cyclic resistance ratio (CRR) profile compared with results of testing frozen samples.

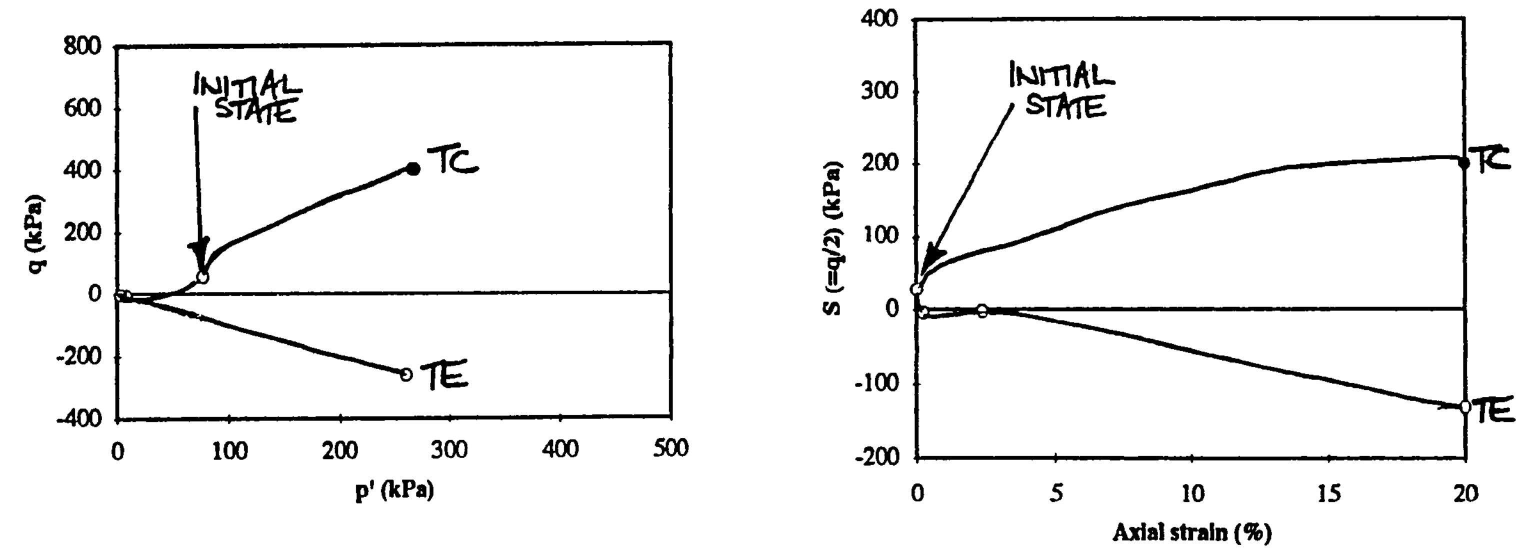

Figure 8-20 Illustration of how typical undrained triaxial compression and triaxial extension (a) stress paths and (b) stress strain curves can be estimated by combining individual estimated components of response corresponding to the average estimated RSR in the Massey site target zone (see Table 8-7).

References

Ayoubian, A. 1995. Triaxial testing on very loose sands for flow liquefaction analyses. *M.Sc. Thesis*, University of Alberta.

Baldi, G. et al. 1986. Interpretation of CPT's and CPTU's. II Part: Drained penetration on sands. *Proc. IV Int. Geotech. Seminar on Field Instrumentation and In Situ Measurements, Nanyang Tech. Inst.*, Singapore.

Been, K., and Jefferies, M.G. 1992. Towards systematic CPT interpretation. *Proceedings of the Wroth Symposium*, 44-55.

Campanella, R.G. 1995. General site characterization of Massey Tunnel north end at Deas Island, Highway 99, Ministry of Transportation and Highways right-of-way. *CANLEX Phase II Activity 3A Report*, In-situ Testing Group, The University of British Columbia.

Chillarige, A.R.V., Morgenstern, N.R., Robertson, P.K., and Christian, H. 1995. Characterization of Fraser River Delta sand. *Proceedings of the 48th Canadian Geotechnical Conference*, Vancouver, B.C., 2: 711-720.

Fear, C.E., and McRoberts, E.C. 1995. Reconsideration of initiation of liquefaction in sandy soils. *Journal of Geotechnical Engineering*, ASCE 121(3): 249-261.

Fear, C.E., and Robertson, P.K. 1996. CANLEX Phase II data review report. CANLEX Project Report, University of Alberta.

Hofmann, B.A. 1995. Personal communication.

Ishihara, K. 1993. Liquefaction and flow failure during earthquakes. The 33rd Rankine Lecture, *Géotechnique*, 43(3): 351-415.

Jefferies, M.G. and Davies, M.P. 1991. Discussion on soil classification by the cone penetration test. *Canadian Geotechnical Journal*, 28(1): 173-176.

Lawrence, M.S., Shelbourn, M.A.B., and Howie, J.A. 1995. Geophysical logging of Phase II sites. *CANLEX Phase II Activity 4A (Conventional Sampling and Logging) Report*, AGRA Earth & Environmental Limited.

Monahan, P.A., Luternauer, J.L., and Barrie, J.V. 1995. The geology of the CANLEX Phase II sites in Delta and Richmond British Columbia. *Proceedings of the 48th Canadian Geotechnical Conference*, Vancouver, B.C., 59-68.

NCEER Workshop 1996. Proceedings to be published at a subsequent date by Youd et al. (1996).

Olsen, R.S., and Koester, J.P. 1995. Prediction of liquefaction resistance using the CPT. *Proceedings of the International Symposium on Cone Penetration Testing, CPT '95*, Linkoping, Sweden.

Plewes, H.D., Davies, M.P, and Jefferies, M.G. 1992. CPT based screening procedure for evaluating liquefaction susceptibility. *Proceedings of the 45th Canadian Geotechnical Conference*, Toronto, Ontario, 4:1-4:9.

Pouliot, N. and Konrad, J.-M. 1995. Laboratory testing of reconstituted and of in-situ frozen specimens, Massey Tunnel Sand. *CANLEX Phase II Report*, Université Laval.

Robertson, P.K. 1990. Soil classification using the CPT. *Canadian Geotechnical Journal*, 27(1): 151-158.

Robertson, P.K., Fear, C.E., Woeller, D.J., and Weemees, I. 1995. Estimation of sand compressibility from seismic CPT. *Proceedings of the 48th Canadian Geotechnical Conference*, Vancouver, 1: 441-448.

Robertson, P.K., Woeller, D.J., and Finn, W.D.L. 1992. Seismic cone penetration test for evaluating liquefaction potential under cyclic loading. *Canadian Geotechnical Journal*, 29: 686-695.

Sasitharan, S., Robertson, P.K., Sego, D.C., and Morgenstern, N.R. 1994. State boundary surface for very loose sand and its practical implications. *Can. Geotech. J.*, 31(3): 321-334.

Seed, H.B., Tokimatsu, K., Harder, L.F., and Chung, R. 1985. Influence of SPT procedures in soil liquefaction resistance evaluations. *Journal of Geotechnical Engineering*, ASCE 111(12): 1425-1445.

Skempton, A.W. 1986. Standard penetration test procedures and the effects in sands of overburden pressure, relative density, particle size, ageing and overconsolidation. *Géotechnique*, 36(3): 425-447.

Sladen, J.A., and Hewitt, K.J. 1989. Influence of placement method on the in situ density of hydraulic sand fills. *Canadian Geotechnical Journal*, 26: 453-466.

Stewart, R.A. 1993. Site selection - Phase II. *CANLEX Phase I Activity 7 Report*, B.C. Hydro.

Suzuki, Y., Tokimatsu, K., Taye, Y. and Kubota, Y. 1995. Correlation between CPT data and dynamic properties of in-situ frozen samples. *Proceedings of the 3rd International Conference on Recent Advances in Geotechnical Earthquake Engineering and Soil Dynamics*, St. Louis, U.S.A., 1.

Thomas, J. 1992. Static, cyclic and post liquefaction undrained behaviour of Fraser River sand. *M.Sc. Thesis*, University of British Columbia.

Tokimatsu, K., and Yoshimi, Y. 1983. Empirical correlation of soil liquefaction based on SPT N-value and fines content. *Soils and Foundations*, 23(4): 56-74.

CHAPTER 9

GENERAL DISCUSSION AND CONCLUSIONS

9.1 Overview

As described in Chapter 1, liquefaction of sandy soils can have significant financial, environmental and human impacts. Observable surface features can range from sand boils to catastrophic flow failures, depending on the type and extent of liquefaction that occurs. Liquefaction phenomena have been divided into two main types, after Robertson (1994) and Robertson and Fear (1995), as defined in Chapter 1. Cyclic softening (liquefaction) generally occurs in level to gently sloping ground in which shear stress reversal can occur, but may also occur in and around soil structures and buildings. Deformations associated with cyclic softening occur only during the cyclic loading and accumulate with additional cycles of loading as a consequence of a loss in soil stiffness. Flow liquefaction occurs only in strain-softening soil, provided that a trigger mechanism (static or cyclic) causes the soil to strain-soften. Flow liquefaction generally occurs in sloping ground in which the driving stresses are larger than the resulting ultimate or minimum undrained shear strength of the soil. Deformations can be catastrophic (i.e. flow failures) if the soil structure contains sufficient strain-softening material relative to strain-hardening material and if the geometry is such that a kinematically admissible mechanism can develop.

9.2 Evaluation of Cyclic Softening Potential

The most reliable method of estimating cyclic resistance of sandy soils in the laboratory is by testing high quality undisturbed samples under the appropriate cyclic loading. In-situ ground freezing and subsequent coring has recently been successful in obtaining such samples at several sites as part of the CANLEX project (Hofmann et al., 1994; 1995). However, in-situ ground freezing technology is expensive and would typically be limited to high risk projects for which the consequences of failure can be enormous and large financial decisions must be made. Consequently, methods for estimating cyclic resistance based on less expensive in-situ tests are required. Conventionally, SPT-based methods have been used; recently, CPT and shear wave velocity based methods have been developed. Seismic CPT probes provide shear wave velocity measurements in addition to conventional CPT data. Thus, the seismic CPT provides a useful technique for evaluating cyclic softening (liquefaction) potential based on two independent profiles. If there is not consistency in the evaluation of cyclic softening (liquefaction) potential, soil samples should be obtained to evaluate grain characteristic parameters. Whether or not a sandy soil deposit is susceptible to cyclic softening (liquefaction) is a function of both the sand characteristics (such as density, stresses, amount of fines, plasticity of fines) and the size and duration of cyclic loading.

9.2.1 Simplified "Seed" methodology

The late Professor H.B. Seed and other researchers at the University of California, Berkeley, developed a simplified method for evaluating cyclic softening (liquefaction) potential of sandy soils based on SPT in-situ testing (Seed et al., 1985; Seed and Harder, 1990). The primary advantage of this method is that it is easy to understand and relatively easy to apply. At the time that the method was developed, there was a large database of SPT data and, hence, the SPT was the best in-situ test to use to estimate the cyclic resistance of a sandy soil. Various corrections were proposed by Seed (1987), Seed et al. (1985) and Seed and Harder (1990) for fines content, sloping ground conditions and high overburden stress stresses.

As illustrated in Chapter 2, the Seed methodology generally provides a conservative estimate of cyclic softening (liquefaction) potential because the case records in the database were generally assigned average representative $(N_1)_{60}$ values; however, the method is typically applied to the entire $(N_1)_{60}$ profile at a site. The revised database presented in Chapter 2, based on a minimum representative $(N_1)_{60}$ approach for each case record gives less conservative correlations, particularly at higher values of $(N_1)_{60}$. The resulting correlations (see Figure 2-8 in Chapter 2) are more similar to the limiting shear strain values associated with liquefaction, developed by Seed et al. (1985) and shown in Figure 2-11 in Chapter 2. A very important point to reiterate is that the database of case records was developed based on Holocene age deposits, level to gently sloping ground, equivalent magnitude M=7.5 earthquakes, and depths ranging from 1 to 14 m (3 to 47 ft), but generally (i.e. 90% of the case records) less than 10 m (32 ft). Hence, caution should be exercised when extrapolating the correlation to conditions outside of this range. Experience has shown that the corrections for sloping ground and high overburden stress conditions are not always reliable; e.g. at Duncan Dam (Byrne et al., 1994). In addition, the phenomenon of flow liquefaction is often of greater concern in large sloping structures and the resulting deformations can be more catastrophic. Therefore, extrapolation of the correlations based on cyclic softening (liquefaction) in level ground to the evaluation of large sloping structures does not seem appropriate.

For low risk, small scale projects in level to gently sloping ground, the SPT-based simplified Seed methodology is useful and generally conservative. The SPT sampler provides soil samples which can be used to estimate fines content and apply the fines content corrections recommended by Seed (1987). However, many factors can affect the measured SPT penetration resistance (Skempton, 1986; Robertson et al., 1983). The two most important factors are effective overburden stress and the energy delivered to the SPT sampler, expressed in terms of rod energy ratio (ER), in percent. A vertical effective stress of 100 kPa and an ER of 60% are generally accepted as the reference values to use to correct the measured blowcount to an $(N_1)_{60}$ value (Seed et al., 1985; Robertson and Fear, 1995). It is very important to carefully measure the ER during the actual site investigation, if possible, in order to obtain a reliable measure of corrected SPT penetration resistance. Global values of ER are available for various SPT hammer/anvil systems and methods of hammer release and ER at a site is often assumed based on these global values (Seed et al., 1985). However, these values are only a guide and site specific values may differ significantly from the global values.

9.2.2 Integrated CPT approach

The SPT has many inherent difficulties and often poor repeatability. Consequently, CPT-based methods of estimating cyclic resistance have been developed and the database of available case records is continually growing. The CPT has the advantage that, not only is it generally more repeatable and reliable than the SPT, but it also provides a continuous profile of soil stratigraphy. Chapter 3 presented a new, integrated CPT method for evaluating the cyclic softening (liquefaction) potential of a sandy soil deposit. Although the CPT does not provide soil samples like the SPT does, the integrated method demonstrates that grain characteristics such as fines content can be estimated from the CPT data in order to correct the measured penetration resistance for fines content. Increasing fines content is generally associated with increasing compressibility and, therefore, decreasing penetration resistance. Once the in-situ penetration resistance is corrected for overburden effects and fines content, the corrected clean sand equivalent penetration resistance can be used to estimate the cyclic resistance of a soil, based on the modified Robertson and Campanella (1985) correlation proposed by the recent NCEER Workshop (1996), as described in

Chapter 3.

The integrated CPT method proposed in Chapter 3 is broken down into its individual components such that site specific modifications can be made, if necessary. The integrated CPT method is easily applied to CPT results using a spreadsheet. The equations representing the various components of the method can be used and can be easily modified to suit any site specific conditions that differ from the recommended relationships. For high risk projects, both the fines content and cyclic resistance estimations can be checked on a site specific basis by obtaining and testing undisturbed samples under the appropriate cyclic loading. For moderate risk projects, the fines content estimations based on the CPT can be checked on a site specific basis from bulk samples. The various components of the integrated CPT method proposed here can be combined and summarized on a CPT based soil classification chart, as demonstrated in Chapter 3 (see Figure 3-16). Thus, for low risk projects, the method can be applied directly.

The integrated CPT method is also based around the simplified Seed methodology. The original Robertson and Campanella (1985) method of estimating cyclic resistance from the CPT was based on SPT-CPT conversions, although the proposed correlation is now based on extensive field observations. Thus, an important feature to recognize is that, as for the Seed et al. (1985) SPT method, the correlation given in Chapter 3 appears to be based on average values of q_{c1}. However, the correlation is often applied to the entire CPT profile at a site. Consequently, the integrated CPT method may provide a conservative estimate of cyclic softening (liquefaction) potential and caution should be applied in variable deposits in which a small part of the CPT data could indicate possible cyclic softening (liquefaction). Although not carried out in this study, it would be interesting to revisit the CPT case records in detail from a minimum q_{c1} approach similar to the review of the SPT case records presented in Chapter 2. Chapter 3 also illustrated a method for correcting the measured penetration resistance in thin sand layers embedded in thick soft clay layers. A very important point to reiterate is that, similar to the SPT database, the database of CPT case records was developed based on Holocene age deposits, level to gently sloping ground, equivalent magnitude M=7.5 earthquakes, and depths ranging from 1 to 15 m (3 to 45 ft), but generally (i.e. 84% of the case records) less than 10 m (32 ft). Hence, as for the SPT method, caution should be exercised when extrapolating the CPT correlations to conditions outside of this range. In addition, as for the SPT method, extrapolation of the CPT correlations based on cyclic softening (liquefaction) in level ground to the evaluation of large sloping structures does not seem appropriate.

9.3 Evaluation of Flow Liquefaction Potential and Subsequent Response

Flow liquefaction occurs in strain-softening soils if a suitable trigger mechanism can develop. The trigger mechanism can be static or cyclic and undrained or drained in nature. Once such material is triggered, undrained strain-softening occurs. Flow liquefaction can occur rapidly, with little warning, and if sufficient strain-softening material liquefies, catastrophic deformations can result. As for the evaluation of cyclic softening, the seismic CPT provides a useful technique for evaluating flow liquefaction potential based on two independent profiles. If there is not consistency in the evaluation of flow liquefaction potential, soil samples should be obtained to evaluate grain characteristic parameters. Whether or not a sand deposit is susceptible to flow liquefaction is a function of the sand characteristics in terms of density, stresses, grain characteristics and soil structure.

9.3.1 Empirical approach

Conventionally, the simplified Seed methodology described above has been used to predict liquefaction potential in general for a given cyclic (earthquake) loading. It has been used as a design tool in both level to gently sloping ground and in large, steeply sloping soil structures. However, as discussed previously, experience (e.g. Byrne et al, 1994) has shown that the correction factors to account for sloping ground and high overburden stresses (Seed and Harder, 1990) are questionable. In addition, flow liquefaction resulting from a static trigger can not be evaluated using the Seed methodology since it only incorporates cyclic (earthquake) loading conditions. Therefore, extrapolating the empirical methods for evaluating cyclic softening (liquefaction) potential to evaluating the potential of flow liquefaction resulting from either static or cyclic triggers is not appropriate. As outlined in Chapter 1, when describing the terminology adopted in this thesis, the two phenomena involve different physics; therefore, it is more logical to evaluate the potential of the two phenomena using different methods.

Sladen and Hewitt (1989), Been and Jefferies (1992) and Plewes et al. (1992) all developed various methods of estimating soil state (and therefore flow liquefaction potential) from CPT results. The Sladen and Hewitt (1989) method was based on field observations of cases of flow failures and cases of no failure in the Beaufort Sea for which CPT data was available. The Been and Jefferies (1992) and Plewes et al. (1992) methods involved estimating state parameter as a measure of flow liquefaction potential from the CPT based on calibration chamber studies.

9.3.2 Simplified reference stress ratio (RSR) approach

The conventional CPT empirical methods described above are suitable for evaluating flow liquefaction potential, but are not capable of estimating the undrained response of a sand over a large stress range or when comparing different sands. In addition, the state parameter method by Been and Jefferies (1992) is much less conservative than the Sladen and Hewitt (1989) field observation based method. Therefore, the geotechnical engineer may be uncertain if a soil deposit is susceptible to flow liquefaction if the two methods give conflicting predictions.

Chapter 4 proposed a new method of evaluating flow liquefaction potential based on the term reference stress ratio (RSR) which provides an alternate measure of soil state and is related to state parameter by the slope of the ultimate state line (USL). The framework incorporates critical state soil mechanics and provides a link between in-situ testing results and observed undrained response when soil samples are tested in the laboratory. Not only does the proposed framework provide an estimate of flow liquefaction potential, but it is capable of estimating undrained response under different directions of loading (i.e. triaxial compression or triaxial extension) over a range in RSR (i.e. a range in void ratio and initial stress conditions).

To apply the proposed framework directly requires various input parameters, in particular an estimate of the void ratio profile and the location and slope of the USL in e-p' space for a given soil deposit. The void ratio profile can be estimated from the SPT, CPT, shear wave velocity measurements or geophysical logging using any of the conventional or new methods discussed in Chapter 4. The shear wave velocity based method of interpreting seismic CPT results or direct interpretations of geophysical results appear to be best at capturing the range in void ratio on a continuous basis in a given soil deposit, at least for young, uncemented loose sands. If the project is of low risk in nature, the USL parameters can be estimated based on the results of testing other, but similar, sands. The database of USLs for various types of sands is growing and can be used as a reference. The seismic CPT is especially useful as it allows for estimations of the compressibility of a soil by comparing the measured cone tip resistance with the shear wave velocity measurements. Soil compressibility in turn can be used to estimate the slope of the USL, as proposed by

Robertson et al. (1995). It is also possible to estimate USL parameters (nai..ely, λ_{ln}) directly from CPT soil classification charts (Been and Jefferies, 1992).

By combining the estimated void ratio profile in a soil deposit with the estimated USL parameters, it is possible to make an estimation of RSR throughout the deposit. A profile of RSR can be used to estimate soil response to undrained loading, based on the type of RSR based laboratory response curves presented in Chapter 8 for the CANLEX Phase II Massey site. Although data are preliminary and, therefore, at present the resulting response curves are only applicable to Fraser River sand, they may prove to be general in nature as additional data becomes available from other CANLEX sites. The proposed framework illustrated that undrained response can be divided into various components. Once these components are estimated for a particular soil deposit, they can be combined to estimate stress-strain curves, as illustrated in Chapter 8.

The method for evaluating flow liquefaction potential proposed in Chapter 4 requires some knowledge or estimate of the USL. However, as a very preliminary site screening approach, single valued criteria in terms of $(N_1)_{60}$, q_{c1} or V_{s1} can be used as a guide to evaluate flow liquefaction potential. Typical values that are often used are $(N_1)_{60} \approx 10$, $q_{c1} \approx 5$ MPa and $V_{s1} \approx 150$ m/s. However, it is extremely important to note that these values are not applicable to all sandy soils. The values of $(N_1)_{60}$ and q_{c1}, in particular, are influenced by the compressibility of a soil (of which fines content can help provide a measure), whereas the value of V_{s1} is little affected. The method proposed by Plewes et al. (1992) recognizes this effect in that the value of the normalized cone tip resistance defining the Ψ=0 contour (i.e. the USL) is a function of friction ratio (see Figure 4-11 in Chapter 4). More compressible soils tend to have higher friction ratios for the same cone tip resistance.

9.3.3 Site specific approach

Clearly, the flow liquefaction framework proposed in Chapter 4 is best applied on a detailed site specific basis such that the individual parameters such as the location and slope of the USL can be determined with greater certainty. If the shear wave velocity based method is to be used to interpret void ratios, the parameters A and B (linking shear wave velocity to void ratio) and X and Y (linking shear wave velocity to the SPT and CPT, respecti ~ly) can be determined better on a site specific basis. Void ratio estimates based on the CPT or geophysical logging appear to be the most promising methods, particularly as they are capable of providing detailed continuous profiles through a given soil deposit.

A detailed site specific approach also allows for obtaining and testing undisturbed samples. The framework can then be fine-tuned and modified to link the in-situ test results with the laboratory results via RSR on a site specific basis. The worked example in Chapter 8 illustrates how the proposed framework can be applied to a specific site (the CANLEX Massey site), how site specific relationships between various components of response and RSR can be estimated, and how site specific methods of estimating RSR from in-situ tests can be developed.

9.4 Risk Assessment: A Family of Solutions

Various methods have been reviewed and proposed for evaluating both cyclic softening (liquefaction) and flow liquefaction in sandy soils, based on in-situ testing. Figure 9-1 provides a conceptual illustration of how, for a given in-situ test (e.g. the CPT), the described methods can be used to estimate a dividing line in terms of the test's measured parameter (e.g. cone tip resistance, q_c) for evaluating flow liquefaction potential or cyclic softening (liquefaction) potential. The dividing line for evaluating flow liquefaction potential is a function of sand characteristics, while the dividing line for evaluating cyclic softening (liquefaction) potential depends on both sand characteristics and the size and duration of the expected cyclic loading. In general, very loose, strain-softening sand will be susceptible to both flow liquefaction and cyclic softening, loose to medium dense sand may be susceptible to cyclic softening (depending on the size and duration of the cyclic loading), but not to flow liquefaction, and denser sands will not be susceptible to either type of liquefaction.

Figure 9-2 presents a flowchart summarizing the recommended procedure for evaluating the liquefaction potential of a sandy soil deposit. This chart can be used in conjunction with the flowchart explaining liquefaction terminology (modified from Robertson, 1994) presented in Chapter 1 (see Figure 1-1). Since flow liquefaction can generally lead to larger deformations and, thus, greater risk to human safety, the given soil deposit should first be evaluated for flow liquefaction potential. The framework proposed in Chapter 4 can be applied as illustrated in the worked example at the Massey site in Chapter 8. If some material is found to be susceptible to flow liquefaction, response to undrained loading should be estimated using the framework. A stability analysis should then be performed based on the estimated response to determine whether or not the combination of site geometry and type of soil are such that a kinematically admissible mechanism can form and lead to a flow failure. If the soil structure is found to be stable, a deformation analysis should be carried out. Deformations may arise if there is a mixture of strain-softening or limited strain-softening material and strain-hardening material present. The direction of loading that will occur in-situ must be carefully considered when performing such stability and deformation evaluations. Triaxial extension and triaxial compression loading, which appear to represent the two loading extremes (Vaid et al., 1995) may lead to very different responses to undrained loading. Undrained response in simple shear would be predicted to be somewhere in between the two extremes (Vaid et al., 1995).

If a material is not susceptible to flow liquefaction, it may still be susceptible to cyclic softening (liquefaction) depending on the sand characteristics and the size and duration of cyclic loading (typically associated with a design earthquake). The integrated CPT method proposed in Chapter 3 should be used to estimate the cyclic softening (liquefaction) potential of the soil. If the soil is found to be susceptible to this type of liquefaction, a deformation analysis should be performed. In level ground, for example, horizontal displacements and settlements can be estimated using methods proposed by Ishihara (1993), as described in Chapter 3 (see Figure 3-10). In gently sloping ground, methods such as that by Youd (1993) can be used to evaluate expected deformations associated with lateral spreading. More complex methods using finite element analysis, for example, may be required to evaluate the extent of deformations in sloping ground as a result of a loss in soil stiffness during cyclic loading. If a soil is found to be susceptible to cyclic softening and drainage paths are restricted by overlying less permeable layers, the soil should be re-evaluated for flow liquefaction potential because pore water redistribution may lead to loosening of the soil.

If the analyses described above indicate a stability problem or excessive deformations resulting from either flow liquefaction or cyclic softening, site remediation may be required. Depending on the type of liquefaction that is of concern, either the framework proposed for evaluating flow liquefaction or the integrated CPT method for evaluating cyclic softening (liquefaction) can be used as a quality control measure to evaluate the effectiveness of any site remediation that is performed.

Figures 9-3 and 9-4 present flowcharts outlining the recommended methods for evaluating cyclic softening (liquefaction) and flow liquefaction, respectively, based on in-situ testing in sandy soils. Each figure indicates that the recommended procedure is a function of the risk level associated with a particular project. Ideally, a complete field investigation and laboratory testing of undisturbed samples would be carried out at a given site. However, such a comprehensive method of evaluation of liquefaction potential is often beyond the budget and scope of many projects. The higher the risk level associated with a given project, the more important it is to strive towards the ideal comprehensive investigation. The following sections describe the recommended procedures for various levels of risk.

9.4.1 Low risk projects

In general terms, low risk projects are ones for which the consequences of failure will have an extremely low probability of impacting human safety, have little effect on the environment and for which the financial implications will not be significant. Consequently large financial decisions do not need to be made for these types of projects. As a result, the project scope and budget is often fairly restrictive in the amount of in-situ testing and laboratory testing that can be performed.

For such projects, cyclic softening (liquefaction) can be evaluated using penetration tests such as the SPT or CPT. Figure 9-3 indicates that the CPT is the preferred method because it is generally more reliable and provides a continuous profile of soil stratigraphy. The integrated CPT method proposed in Chapter 3 can be used directly to evaluate the cyclic softening (liquefaction) potential of low risk projects.

Figure 9-4 indicates that various types of in-situ testing to estimate soil state can be used to evaluate flow liquefaction potential for low risk projects. The CPT and geophysical logging are preferable because they generally give more reliable continuous profiles. The shear wave velocity based method of estimating void ratio from the seismic CPT appears to be better than conventional methods, at least for young, uncemented loose sands. Interpretations of void ratio from whatever type of in-situ testing is selected can be combined with an estimate of the USL for the soil (based on other similar soils or via compressibility estimated by the seismic CPT) to evaluate flow liquefaction potential.

9.4.2 Moderate risk projects

Moderate risk projects have higher probabilities of affecting human safety and the environment and have larger financial consequences associated with failure. For such projects, both Figures 9-3 and 9-4 illustrate that some site specific modifications to the simplified methods of evaluating either cyclic softening (liquefaction) or flow liquefaction should be made. In the case of cyclic softening (liquefaction) evaluation, Figure 9-3 indicates that components of the integrated CPT method can be modified based on site specific fines contents (from bulk samples) and measured cyclic resistance of reconstituted samples at similar void ratios and fabric to those in-situ. Shear wave velocity measurements can be used to check that the reconstituted samples are as similar as possible to the in-situ conditions (Tokimatsu and Hosaka, 1986). Additional in-situ testing such as geophysical logging or shear wave velocity measurements can be conducting to provide independent means of evaluating cyclic resistance.

In the case of flow liquefaction evaluation, Figure 9-4 indicates that laboratory testing of reconstituted samples can be used to better estimate a site specific USL in order to estimate RSR from in-situ tests. Conducting shear wave velocity measurements and determining parameters such as X and Y (linking shear wave velocity measurements to SPT and CPT penetration resistance, respectively) on a site specific basis allows for better interpretation of void ratio from either the SPT or CPT using the shear wave velocity based method of interpreting void ratio. Having shear wave velocity measurements and/or geophysical logging results in addition to CPT results provides independent means of estimating flow liquefaction potential at a given site.

9.4.3 High risk projects

High risk projects are those for which the consequences of failure can be enormous in terms of human safety, environmental impacts and/or financial implications. For such projects, it is essential to conduct a detailed site specific analysis. Both Figures 9-3 and 9-4 indicate that a preliminary site investigation can be carried out first, using the simplified methods of evaluating either cyclic softening (liquefaction) or flow liquefaction. Based on the results of such a preliminary site screening, a detailed investigation including obtaining and testing undisturbed soil samples can be initiated. Self boring pressuremeter testing is useful for estimating horizontal stress conditions and, hence, the value of Ko in-situ. The results of testing undisturbed samples in the laboratory can also be linked to the in-situ testing in order to extrapolate the results from the detailed (frozen) sampling area across the site. Figure 9-3 indicates that for evaluating cyclic softening (liquefaction), this can be done by modifying the integrated CPT method at the site to match the cyclic resistance of undisturbed samples when tested in the laboratory. For evaluating flow liquefaction,

Figure 9-4 indicates that RSR, relative to the site specific USL, can be used to link the undrained laboratory response of undisturbed samples to in-situ testing across the site.

9.5 Cautionary Notes and Limitations of the Proposed Methods

The proposed methods for evaluating cyclic softening (liquefaction) or flow liquefaction potential are still somewhat preliminary in nature, but confidence in applying the methods should increase as the methods are applied at additional sites and modified as necessary.

9.5.1 Cyclic softening evaluation

a) Loose clean sand versus sand with fines

Referring to the soil classification chart by Robertson (1990) in Chapter 3 (see Figure 3-6), it is clear that, based on CPT results, loose clean sands may sometimes be confused with somewhat denser sands containing fines. Both materials would have low cone tip penetration resistances. Since the integrated CPT method applies a fines content correction based on fines content, if a loose clean sand is interpreted as having an apparent fines content, the resulting prediction of CRR could be unconservative. However, the friction ratio should increase in the denser sand containing fines. A site specific check of the fines content that the integrated CPT method predicts is useful to avoid this confusion.

b) Minimum versus average design approach

Chapter 2 illustrated the effect of consistently selecting a minimum SPT $(N_1)_{60}$ to represent each case record. If this method is applied to the entire SPT profile, any low points would definitely be considered to be susceptible to cyclic softening (liquefaction). The conventional SPT, CPT and shear wave velocity based methods of evaluating cyclic softening (liquefaction) potential all consist of case records for which the average penetration resistance or measurement was generally used as the representative value. However, when applied in practice, the resulting correlations are often applied quite literally to every point in the in-situ test profile, including low points. Thus, these methods may be overly conservative in some soil deposits.

9.5.2 Flow liquefaction evaluation

a) Grain characteristic and site specific input parameters

The estimation of various aspects of response using the framework proposed in Chapter 4 can be sensitive to some of the input parameters, particularly the parameters defining the reference USL for a particular soil. Site specific testing allows for better estimates of such input parameters. When shear wave velocity measurements are used to interpret void ratio, the parameters A and B must be carefully selected. If SPT or CPT measurements are interpreted using the shear wave velocity based method, site specific values for the parameters X and Y can result in better estimates of void ratio.

b) Total void ratio versus skeletal void ratio effects on response

As briefly outlined in Chapter 8, when comparing the data review of the Massey site to the results of the data reviews at the other CANLEX sites to date, the Phase III site appeared unusual and suggested that skeletal void ratio may have a dominating effect on penetration resistance or shear wave velocity measurements in sands with high fines contents (FC $\geq$ 10%). It remains unclear at this point whether skeletal void ratio also dominates the undrained response of undisturbed soil samples when tested in the laboratory. Further studies on the Phase III site samples will allow this factor to be investigated further. If skeletal void ratio is found to be a controlling factor at sites with high fines contents, the proposed framework for investigating flow liquefaction potential could still be applied by combining profiles of skeletal void ratio with an USL based on skeletal void ratios. Additional studies would have to be performed to determine whether or not further modifications would have to be made to components of the integrated CPT method for evaluating cyclic softening (liquefaction) potential at such sites.

c) Using undisturbed samples as a reference

Throughout this thesis undisturbed samples are required as a reference for detailed evaluations of both cyclic softening (liquefaction) and flow liquefaction potential and response. Ground freezing and subsequent coring appear to be capable of providing undisturbed samples at a variety of sites (Hofmann, 1994 and 1995). Once undisturbed samples are obtained, changes in void ratio and stresses (i.e. changes in RSR) must be minimized if samples are to be tested and the results compared directly with predictions of undrained response based on in-situ testing and the methods proposed here. Testing undisturbed samples under anisotropic stress states to mimic the in-situ conditions is an essential factor for observing a relevant undrained response in the laboratory. If samples experience small changes in state (ΔRSR) due to disturbance in sampling, handling, thawing, or consolidation, it may be possible to correct the response using the general response curves shown in Chapter 8.

9.6 Recommendations for Future Work

The work presented here serves to illustrate that liquefaction of sandy soils is a complex process. The methods presented in this thesis provide a step in the right direction, but clearly much more research is necessary to better understand how to characterize sandy soils and evaluate liquefaction potential.

9.6.1 Investigating proposed methods of evaluation at other sites

As the CANLEX project continues to process field and laboratory data from other sites, the methods proposed here for evaluating cyclic softening (liquefaction) and flow liquefaction can be further evaluated. Modifications to the methods can be made as necessary and, as the volume of data grows, more definite conclusions can be made about the possible global nature of the proposed methods and correlations.

a) Cyclic softening

Application of the integrated CPT method to a variety of sites (e.g. all of the CANLEX sites) will confirm or help modify the individual components discussed in Chapter 3. In particular, the relationship between soil behaviour type index, I_c, and fines content can be investigated and the resulting estimates of CRR can be compared with the results of testing undisturbed samples at each site.

An additional useful exercise would be to review the database of case histories forming the CRR-CPT correlation to investigate the choice of representative q_{c1} for each case record, similar to the review of the SPT database carried out in Chapter 2. However, this review should include all aspects of the CPT profile, including friction ratio and pore pressure measurements, where available.

b) Flow liquefaction

The issue of quasi-steady state (QSS) is something that needs to be pursued further in future studies. QSS is currently a topic of debate amongst researchers. The framework proposed in this study incorporates QSS; however, in addition to RSR, QSS depends on soil fabric (Ishihara, 1993) and thus may be difficult to estimate in a global manner. Ultimate state, however, may be linked with RSR in a global manner because it is not dependent on soil fabric since the soil becomes completely remoulded by the time ultimate state is reached. The phenomenon of QSS is observed in the laboratory, particularly in triaxial extension tests (see laboratory stress strain curves for the Massey site in Appendix B). Further studies should investigate if QSS actually occurs in the field and if not, if there are mechanisms such as shear banding and internal void ratio changes within the soil sample while being tested in undrained monotonic loading that create a QSS in the laboratory.

The implications of any such findings will be significant because undrained strengths associated with the QSS can be much lower than those associated with ultimate state. To be conservative, many geotechnical engineers may use the QSS strengths rather than ultimate strengths to analyze stability. This can have large financial implications. If a soil has limited strain-softening behaviour, it will demonstrate a QSS. However, after limited straining associated with the point of QSS, the soil will strain-harden to ultimate state. In analyzing a slope stability problem, the question arises as to whether the material will have gained enough momentum during the point of QSS that it cannot stop itself when it would be expected to strain-harden and become stronger.

Further studies are needed to investigate the triaxial extension direction of loading. First to investigate the phenomenon of QSS, as discussed above, but secondly, to investigate when, where and the extent to which a soil actually becomes loaded in triaxial extension in the field. The much lower undrained strengths for soil tested in triaxial extension in the laboratory (as compared to triaxial compression) only apply if a soil becomes loaded to failure in this direction of loading. As Chapter 4 indicated, K_o (K_o<1.0) conditions in-situ will preload elements of soil in compression. As a result, sufficient unloading is first required before an element will become loaded in extension. Extensional loading is typically associated with the toe of a slope. However, additional studies would be useful to examine the extent of possible in-situ extensional loading in greater detail.

9.6.2 Development of a continuous seismic CPT

Chapters 4 and 8 illustrated that shear wave velocity measurements may provide a good method of estimating void ratio (and hence, RSR) in-situ because shear wave velocity measurements are much less affected by factors such as soil compressibility than either SPT or CPT penetration resistance. However, shear wave velocity measurements are typically averaged over 1 m intervals providing a step function rather than a continuous profile. A useful research project would be to develop the technology to perform continuous shear wave velocity measurements in order to obtain a continuous shear wave velocity profile.

Current technology for measuring shear wave velocity that is commonly used consists of stopping the CPT every 1 m, hitting a seismic beam with a sledge hammer at the ground surface and measuring the time the seismic wave takes to reach the geophone located in the CPT probe at depth. Measurements are recorded electronically and the operator checks that a good signal has been obtained. A method of differences is used to average the shear wave velocity over every 1 m interval of depth. In order to continuously record shear wave velocities, a source at the ground surface would provide seismic waves and the interval difference over which the measurements are averaged would need to be decreased to a few centimetres. The electronics and computer system would have to be modified to record measurements continuously together with the CPT measurements, rather than stopping every time a shear wave velocity measurement is required.

Further studies using bender elements to measure shear wave velocities in soil samples of different states in the laboratory should also be carried out to further investigate the relationship between shear wave velocity and void ratio described in Chapter 4. The method outlined in Chapter 4 (see Equation 4-4) is sensitive to the value of the parameters A and B. Additional studies may be able to confirm or modify the relationship between shear wave velocity and void ratio for various sands in an attempt to improve the accuracy of estimating void ratio from shear wave velocity measurements. This could lead to better interpretations of in-situ shear wave velocity profiles. When combined with the possibility of obtaining continuous shear wave velocity profiles, the resulting method may be able to provide fairly accurate detailed estimates of void ratio.

9.6.3 Further testing of downhole plate load tests in loose sand

Using a simple interpretation method, Chapter 6 served to illustrate the promising potential of rapid downhole plate load tests in loose sand for estimating undrained strengths. The experimental program was clearly preliminary in nature and only limited data are available. Further studies would be useful and would need to place more consideration on how the test results are interpreted. Once a sufficient number of undisturbed samples from the site where the plate load tests were performed are tested, comparisons can be made between the interpretation of the plate load tests and the undrained strength of the soil in the laboratory. Due to factors such as soil squeezing around the plate while the plate is being advanced which may complicate the interpretation of the tests, rapid large diameter cone tests may be a better alternative. However, practical difficulties may arise with respect to the load capacity of the drill rig required to push a large cone, particularly in ground conditions having variable soil states.

9.7 Final Remarks

Liquefaction of sandy soils is a complex process which can be affected by a variety of factors including sand characteristics, site geometry and the nature of the undrained loading. A distinction has been made here between cyclic softening and flow liquefaction. However, as illustrated in Chapter 8, after a "liquefaction" induced soil failure has occurred, it is often difficult to establish which phenomenon controlled the observed deformations. Both in-situ testing and laboratory testing are often part of any site investigation. However, this thesis has proposed a framework by which to link the two types of testing together in a meaningful way to better understand the undrained response of sand to both static and cyclic loading.

The integrated CPT method proposed for evaluating cyclic softening potential is an empirical method, whereas the framework for evaluating flow liquefaction potential and response combines both theoretical and empirical aspects. The concept of RSR to characterize the state of a sand for considerations of flow liquefaction has advantages over the state parameter approach as it is more global in nature, relates better to undrained response and is related to OCR which is traditionally used to evaluate clay, it may allow for all soils to be considered in a similar manner. The recommended procedure to follow at any site is a function of the level of risk associated with a particular project. Thus, a family of solutions exist for evaluating either cyclic softening or flow liquefaction, ranging from simple, conservative, empirical methods to fully comprehensive, site specific field and laboratory investigations.

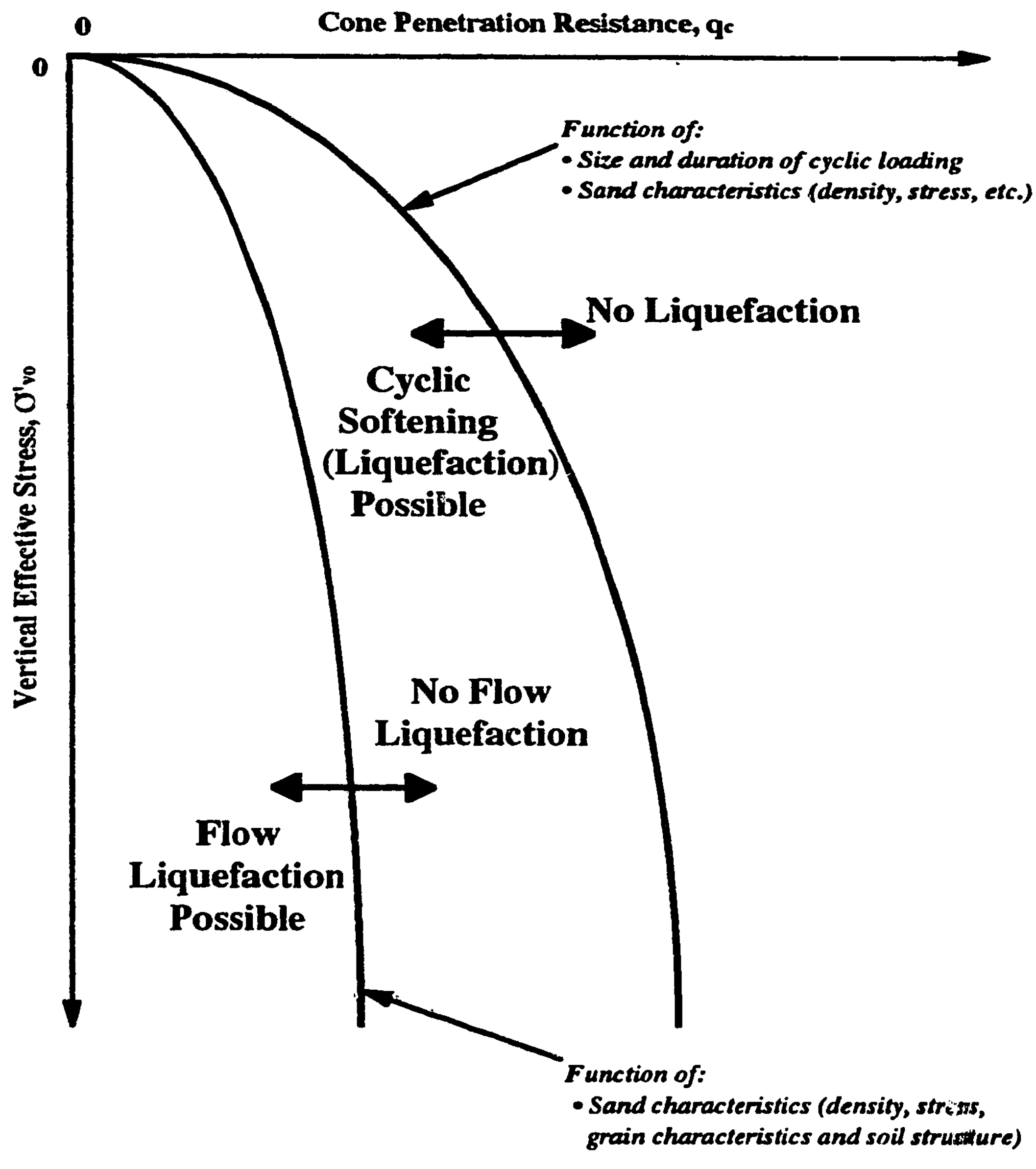

Figure 9-1 Schematic illustrating the concept of dividing lines in terms of CPT penetration resistance, q_c, for both flow liquefaction potential and cyclic softening (liquefaction) potential.

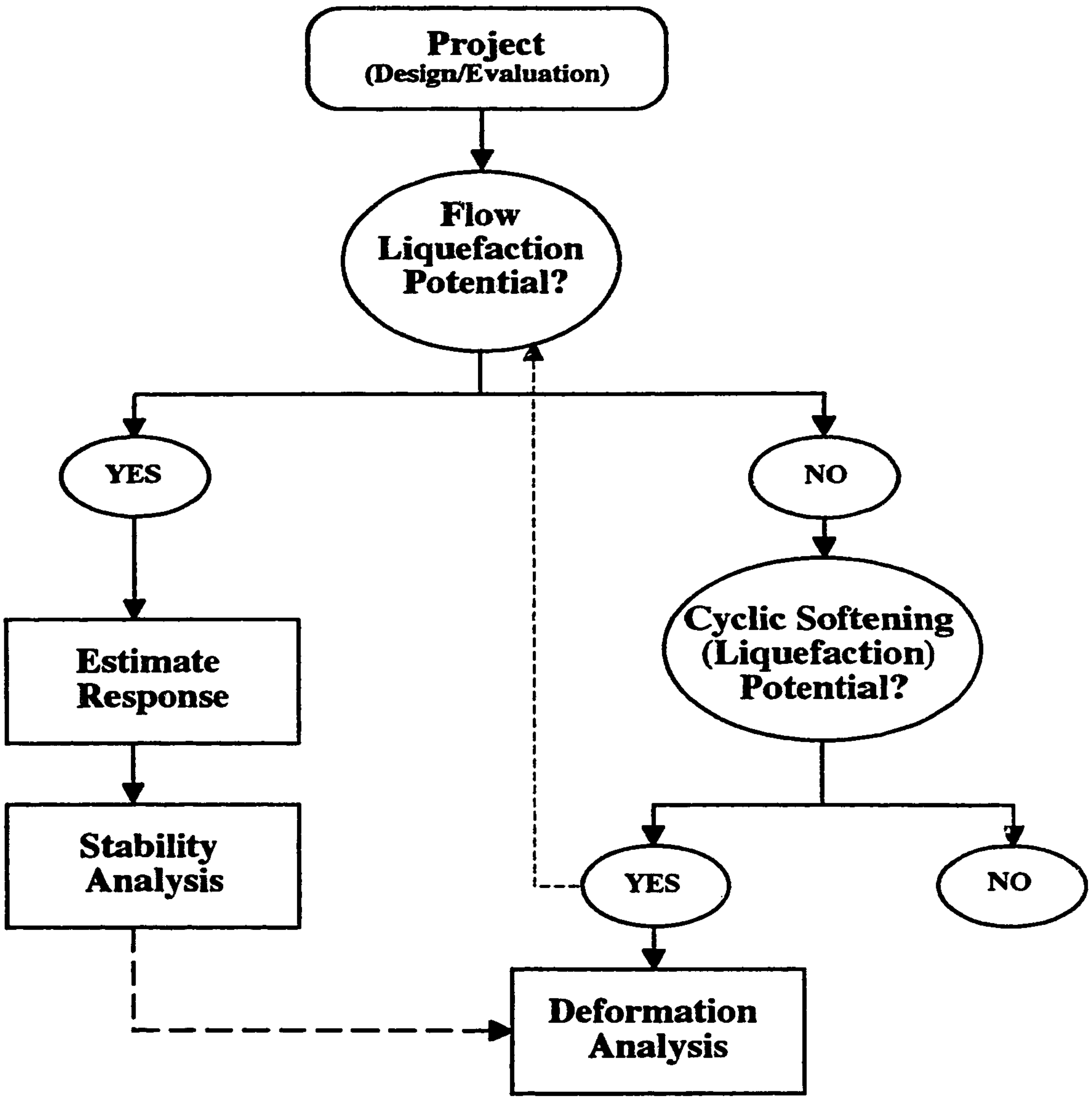

Figure 9-2 General flowchart for evaluating liquefaction potential at a site.

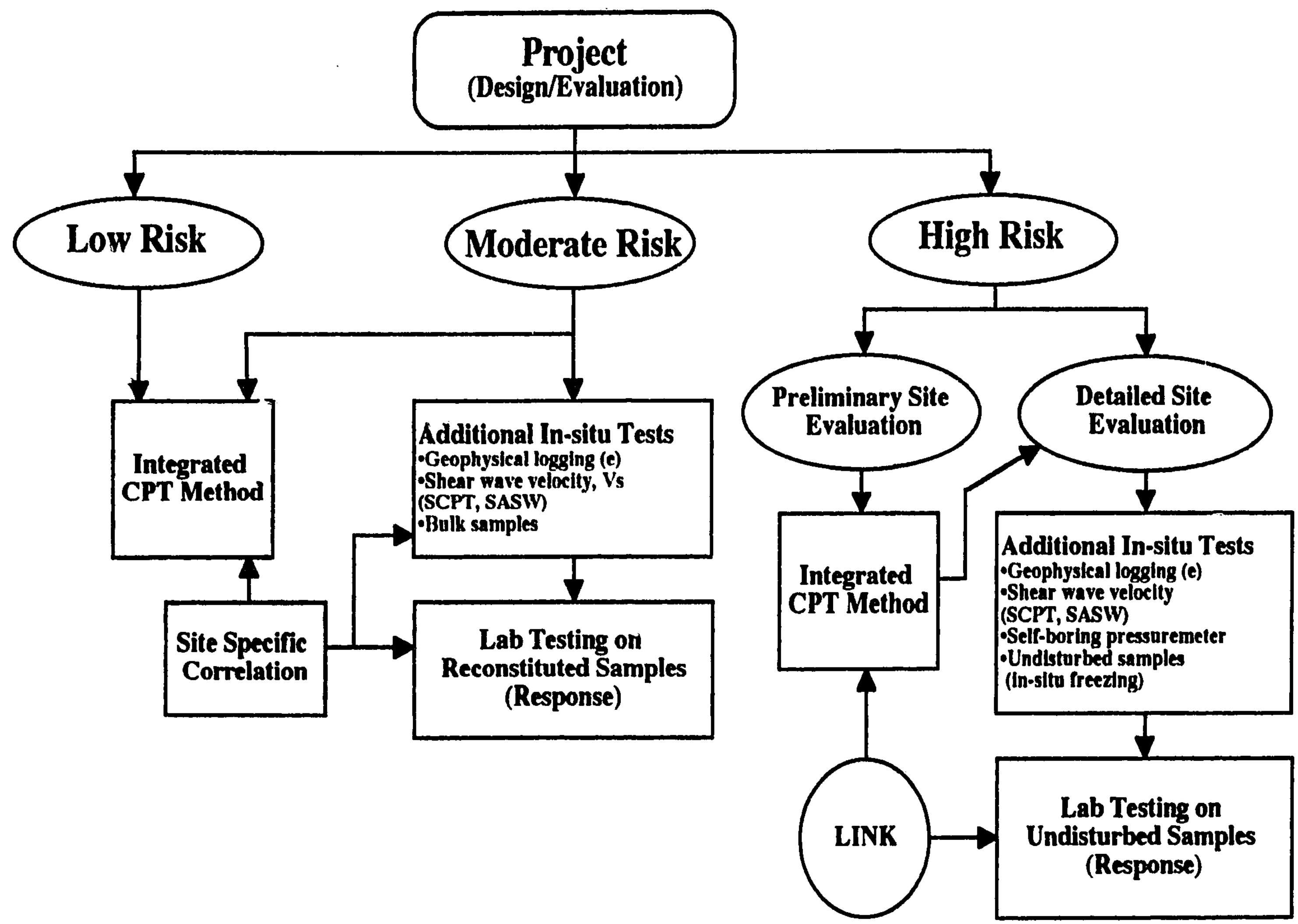

Figure 9-3 Recommended family of solutions for evaluating cyclic softening (liquefaction) potential based on the risk level (i.e. consequences of failure) associated with a particular project.

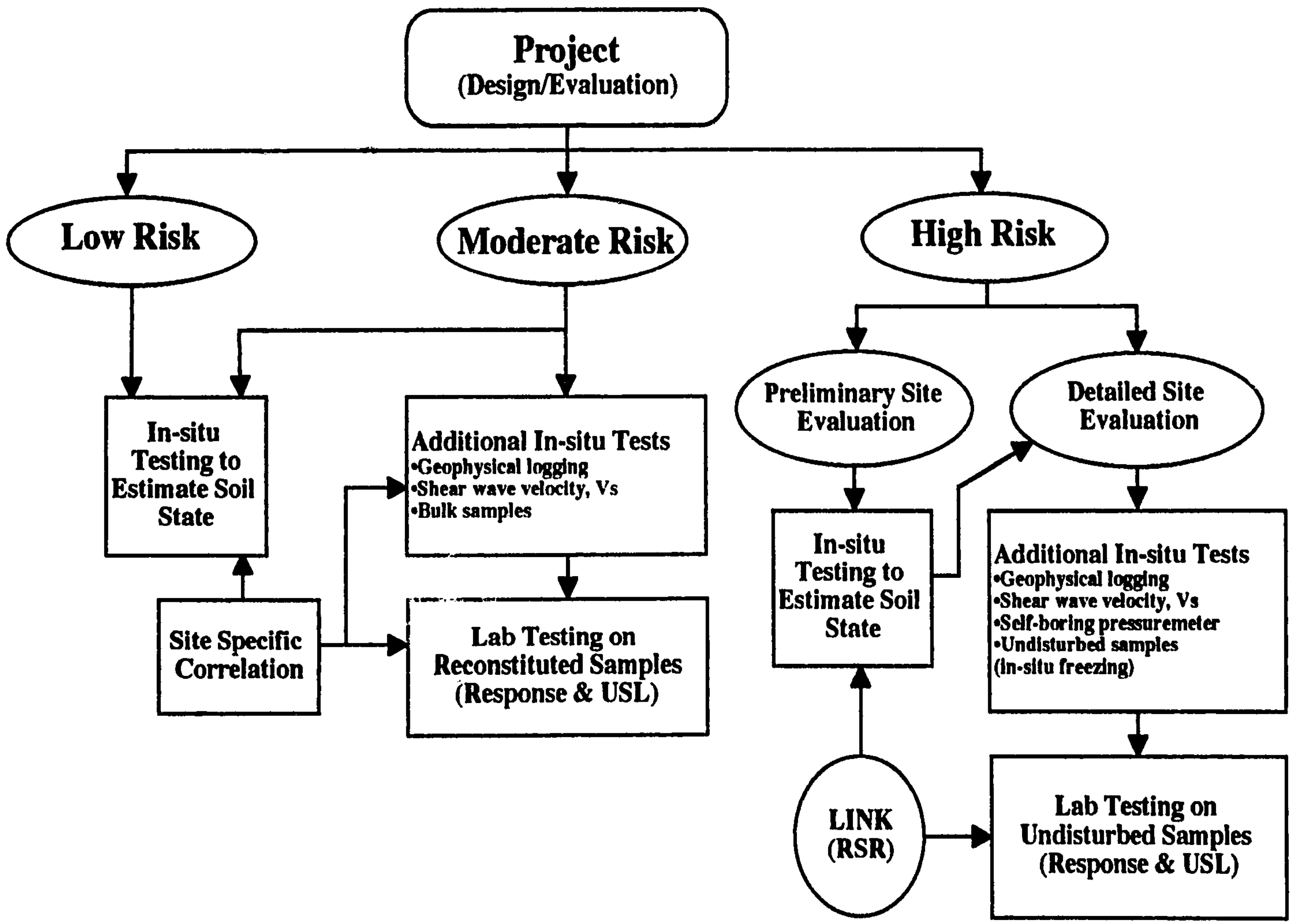

Figure 9-4 Recommended family of solutions for evaluating flow liquefaction potential based on the risk level (i.e. consequences of failure) associated with a particular project.

References

Been, K., and Jefferies, M.G. 1992. Towards systematic CPT interpretation. *Proceedings of the Wroth Symposium*, 44-55.

Byrne, P.M., Imrie, A.L., and Morgenstern, N.R. 1994. Results and implications of seismic performance studies for Duncan Dam. *Canadian Geotechnical Journal*, 31: 979-988.

Hofmann, B.A., Sego, D.C., and Robertson, P.K. 1994. Undisturbed sampling of a deep loose sand deposit using ground freezing. *Proceedings of the 47th Canadian Geotechnical Conference*, Halifax, Nova Scotia, 287-296.

Hofmann, B.A., and Sego, D.C. 1995. In-situ ground freezing for undisturbed samples of loose sand - Phase II. *Proceedings of the 48th Canadian Geotechnical Conference*, Vancouver, B.C., 197-212.

Ishihara, K. 1993. Liquefaction and flow failure during earthquakes. The 33rd Rankine Lecture, *Géotechnique*, 43(3): 351-415.

NCEER Workshop 1996. Proceedings to be published at a subsequent date by Youd et al. (1996).

Plewes, H.D., Davies, M.P, and Jefferies, M.G. 1992. CPT based screening procedure for evaluating liquefaction susceptibility. *Proceedings of the 45th Canadian Geotechnical Conference*, Toronto, Ontario, 4:1-4:9.

Robertson, P.K. 1990. Soil classification using the CPT. *Canadian Geotechnical Journal*, 27(1): 151-158.

Robertson, P.K. 1994. Suggested terminology for liquefaction. *Proceedings of the 47th Canadian Geotechnical Conference*, Halifax, Nova Scotia, 277-286.

Robertson, P.K. and Fear, C.E. 1995. Liquefaction of sands and its evaluation. *IS Tokyo '95, First International Conference on Earthquake Geotechnical Engineering*, Keynote Lecture.

Robertson, P.K., Campanella, R.G., and Wightman, A. 1983. SPT-CPT correlations. *Journal of Geotechnical Division of ASCE*, 109: 1449-1459.

Robertson, P.K., Fear, C.E., Woeller, D.J., and Weemees, I. 1995. Estimation of sand compressibility from seismic CPT. *Proceedings of the 48th Canadian Geotechnical Conference*, Vancouver, 1, 441-448.

Robertson, P.K. and Campanella, R.G. 1985. Liquefaction potential of sands using the cone penetration test. *Journal of Geotechnical Division of ASCE*, 22(3): 298-307.

Seed, H.B. 1987. Design problems in soil liquefaction. *Journal of Geotechnical Engineering*, ASCE 113(8): 827-845.

Seed, H. B., Tokimatsu, K., Harder, L. F., and Chung, R. 1985. Influence of SPT procedures in soil liquefaction resistance evaluations. *J. Geotech. Engrg.*, ASCE 111(12): 1425-1445.

Seed, R.B., and Harder, L.F. 1990. SPT-based analysis of cyclic pore pressure generation and undrained residual strength. *Proceedings of the H. Bolton Seed Memorial Symposium*, 2: 351-376.

Skempton, A. W. 1986. Standard penetration test procedures and the effects in sands of overburden pressure, relative density, particle size, ageing and overconsolidation. *Geotechnique*, 36(3): 425-447.

Sladen, J.A., and Hewitt, K.J. 1989. Influence of placement method on the in situ density of hydraulic sand fills. *Canadian Geotechnical Journal*, 26: 453-466.

Tokimatsu, K., and Hosaka, Y. 1986. Effects of sample disturbance on dynamic properties of sand. *Soils and Foundations*, 26(1): 53-64.

Vaid, Y.P., Sivathayalan, S., Uthayakumar, M., and Eliadorani, A. 1995. Liquefaction potential of reconstituted Syncrude sand. *Proceedings of the 48th Canadian Geotechnical Conference*, Vancouver, B.C., 1: 319-330.

Youd, T. L. 1993. Liquefaction-induced lateral spread displacement. *Technical Note N-1862*, Naval Civil Engineering Laboratory, Port Hueneme, California.